Dipl.-Ing. Elias Karabelas

Space-Time Discontinuous Galerkin Methods for Cardiac Electro-Mechanics

DISSERTATION

zur Erlangung des akademischen Grades

Doktor der technischen Wissenschaften

eingereicht an der

Technischen Universität Graz

Betreuer:
Univ.-Prof. Dipl.-Math. Dr.rer.nat. Olaf Steinbach
Technische Universität Graz
Institut für Numerische Mathematik

Begutachter:
Univ.-Prof. Dipl.-Ing. Dr. Ulrich Langer
Johannes Kepler Universität Linz
Insitut für Numerische Mathemaik

Assoz. Prof. Priv.-Doz. Dipl.-Ing. Dr.techn. Gernot Plank
Medizinische Universität Graz
Institut für Biophysik

Graz, Jänner 2015

EIDESSTATTLICHE ERKLÄRUNG

Ich erkläre an Eides statt, dass ich die vorliegende Arbeit selbstständig verfasst, andere als die angegebenen Quellen/Hilfsmittel nicht benutzt, und die den benutzten Quellen wörtlich und inhaltlich entnommenen Stellen als solche kenntlich gemacht habe. Das in TUGRAZ-online hochgeladene Textdokument ist mit der vorliegenden Dissertation identisch.

Datum	Unterschrift

This document is set in Latin Modern, compiled with pdfLaTeX2e and `Biber`.

The LaTeX template from Karl Voit is based on KOMA script and can be found online: https://github.com/novoid/LaTeX-KOMA-template

Acknowledgement

I would like to thank my advisor Prof. Olaf Steinbach for his support and guidance throughout the research. He gave me the opportunity to visit a lot of workshops and conferences which helped and motivated me a lot. Special thanks should be payed to my reviewers Prof. Ulrich Langer and Assoc. Prof. Gernot Plank. I would also like to thank Ass. Prof. Günther Of for the fruitful discussions and help throughout my PhD.

Furthermore, I would like to express my gratitude to my former colleague Martin Neumüller for providing me his software package NESHMET. It would have been much harder without it. Also I would like to thank Christoph Augustin for providing me support in the development of assembling routines for nonlinear elasticity. Finally I would like to thank my friend and co-worker Arno Kimeswenger always having an sympathetic ear for my questions and ideas.

Special thanks goes to the SFB research center "Mathematical Optimization and Applications in Biomedical Sciences" and the austrian science fund FWF which provided me with financial aid.

I would like to thank my whole family and friends, for their support throughout my studies. Especially I would like to thank my mother Renate and her spouse Harald. Finally I would like to thank my girlfriend Eva for her patience and good advice.

Abstract

In this work numerical methods for solving non-linear time dependent partial differential equations arising in the modeling of cardiac electro-mechanics. The models of cardiac electro-mechanics will be introduced and discussed. For the discretization a discontinuous Galerkin method will be applied in space and time, by decomposing the space-time domain into finite elements. An error analysis for the discretization of the models of the electric activity of the human heart will be given and numerical examples confirming the proven estimates will be shown. Furthermore, a discontinuous Galerkin method for the passive mechanic behavior of human heart tissue will be given and confirming convergence studies will be presented. Eventually, both methods will be coupled and the theses concludes with some numerical examples for coupled problems.

Zusammenfassung

In dieser Arbeit werden numerische Lösungsverfahren für nichtlineare zeitabhängige partielle Differentialgleichungen besprochen. Insbesondere liegt der Fokus auf den Modellen der gekoppelten elektromechanischen Aktivität des menschlichen Herzens. Für die Diskretisierung solcher Probleme wird ein "discontinuous Galerkin"-Verfahren in Raum und Zeit angewendet, indem der gesamte Raumzeitzylinder in finite Elemente zerlegt wird. Eine numerische Analysis wiewohl auch Konvergenzstudien für die Diskretisierung der Modelle der elektrischen Aktivität des menschlichen Herzens werden präsentiert. Weiters wird ein "discontinuous Galerkin"-Verfahren für die passive mechanische Aktivität des menschlichen Herzens vorgestellt und mit numerischen Beispielen untermauert. Am Ende der Arbeit werden numerische Beispiele zu gekoppelten Problemen präsentiert.

Contents

1 Introduction

Motivation

The human heart has played an important role for understanding the body since antiquity. In the fourth century B. C., the Greek philosopher Aristotle identified the heart as the most important organ of the body. He characterized it as the seat of many human abilities, such as intelligence, motion and sensation.

During the last millennium, the pursuit of knowledge of the human heart has gained more importance, not only by a desire to understand the mechanical and electrochemical processes, but also by the increasing clinical importance. According to the World Health Organization (WHO) heart diseases are one of the top ten causes of death in western society, see [137]. Thus, improving the understanding of the function of the human heart may lead to new techniques for the diagnosis and treatment of heart problems.

Over the last decades, the amount of information about the mechanisms of the human heart has rapidly increased. Now one is in the position to observe cellular and even sub-cellular processes. Nevertheless there remain several unanswered questions. For example, it is still not clear what happens in a human heart during defibrillation.

The most prominent and standard tool in cardiology is the electrocardiogram, abbreviated ECG. It dates back to Wilhem Einthoven, see [59]. However, in the ECG one deals with the human heart as a black-box and tries to reconstruct some dipole distribution. This is known as the inverse problem of electrocardiography, see [93, 94, 174]. Furthermore, one has no possibility to study complex arrhythmias in the human heart, by just using an ECG. Nowadays one tries to model the human heart more detailed with sub-cellular to macroscopic models as well as their coupled interaction. This reflects and

is based upon the increasing physiological knowledge about the human heart. These days it is known that changes in the macroscopic scale of the heart, for example high blood pressure, acts down to the sub-cellular and the genetic level but also vice versa. This is a quite new research field know as epigenetics. For more information about epigenetics we refer to [132].

The newly developed models give the possibility for *in silico* simulations and enable studies of heart diseases without harming a human patient. However, very few attention has been payed to a strict mathematical formulation and to a numerical analysis. This marks the starting point of this thesis. Our considerations will start with the state-of-the-art models describing the electro-mechanical behavior of human heart tissue. Thus one arrives at time-dependent essentially non-linear coupled systems of partial differential equations. This serves us as motivation to consider space-time methods.

Space-Time Methods

A classic way of discretizing time-dependent problems is to discretize first in space with finite elements and afterwards use suitable time stepping techniques. Seeing this procedure in a space-time setting one obtains tensor product space-time elements. A schematic view of such a discretization is depicted in Figure 1.1. Such kind of methods have been widely used, see for example [34, 51, 52, 54, 91, 153, 154, 176, 184].

In this thesis we will use a different approach. Based on ideas developed in [129] we will use a **full space-time discontinuous Galerkin finite element method**, abbreviated **DGFEM**. Space-time discontinuous Galerkin finite element methods have already been used, see for example [7, 31, 75, 87, 99, 130, 173, 181]. The origin of discontinuous Galerkin finite element methods can be traced back to [148].

The idea behind the space-time methods is to think of the time variable t as an additional spatial coordinate. This allows for rather general almost arbitrary discretizations of space-time geometries, see Figure 1.2 for a schematic view. Thus one obtains, for example, a four dimensional object for a time dependent problem over a three dimensional computational geometry.

One major advantage of this space-time discretization is the possibility to rather easily apply adaptive algorithms to resolve physical properties better in space and time simultaneously. This idea has already been exploited in [2, 16, 53, 117, 149, 164]. Furthermore one can apply ideas from domain decomposition, resulting in parallel space-time methods. This has been already used in [129, Chapter 3].

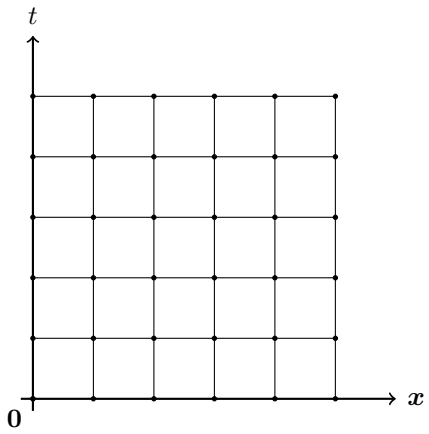

Figure 1.1: A schematic space-time discretization of a one dimensional problem corresponding to a time-stepping procedure.

Outline

Following on from this introduction, we give a brief overview of the relevant modeling aspects for human heart tissue. This includes the modeling of cardiac electric activity, passive mechanical behavior as well as the coupling of these two aspects. The first model will be governed by the well-known **Bidomain equations**, while the second one will be described by Cauchy's equation of motion. Worth mentioning in this context is the strong anisotropic nature of biological materials as well as their nearly incompressibility. One needs to account for those. Finally we will describe the possibilities of coupling the electric part of the models with the passive mechanic part.

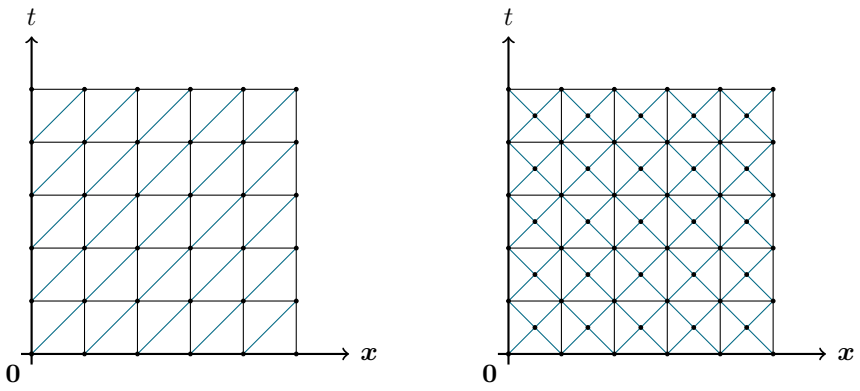

Figure 1.2: Schematic view of possible arbitrary space-time discretizations of a one dimensional problem.

In the subsequent Chapter 3 we will recollect the basic mathematical tools needed to develop a space-time discontinuous Galerkin method. This includes function spaces, abstract non-conforming stability and error analysis as well as triangulations.

Continuing, in Chapter 4 we will apply the tools developed so far and derive a full space-time formulation for the Bidomain equations. Consecutively, we will give a numerical analysis based on a simpler linear problem. We will show boundedness and stability of the resulting discretized problems and present convergence studies. After that we will expand our results to the non-linear case and present convergence studies, too.

In Chapter 5 we will present a discontinuous Galerkin finite element formulation based on [138]. An overview of existing literature and a summary of the numerical analysis is given and, furthermore, we will give details on the implementational aspects of DGFEM for nonlinear elasticity and close this chapter with some convergence studies.

Eventually, in Chapter 6 we will combine the two earlier developed building blocks and apply them to a coupled problem of cardiac electro-mechanics. We will present the discretization with DGFEM as well as some numerical aspects and close this chapter with numerical experiments.

We conclude in the last chapter with a short overview and an outlook to upcoming perspectives and open questions.

2 Modeling

In this introductory chapter the basic facts about the underlying physiological and physical problems will be recited. This part is inspired by and excerpted from [84, 93, 94, 166].

2.1 Physiological Background

The most studied organ in human physiology appears to be the heart, although its function seems quite simple: it pumps blood through our body by contracting and expanding about 2.5 billion times during a normal lifetime of a human being. As a fact, heart failure, either electrical or mechanical, is one of the most common causes of death in the Western world, see [137].

The human heart is a muscular organ, weighing about 250 to 350 grams with a size comparable to a fist, which, as denoted above, pumps the blood through the blood vessels, delivering nutrients and removing waste from each organ, by repeated, rhythmic contractions. This process, where the oxygen rich blood is delivered to the organs is called the **systemic circulation**. Furthermore the human heart drives de-oxygenated blood through our lungs for re-oxygenation (the so called **pulmonary circulation**). Figure 2.1 shows a schematic view of the heart.

The coordination of the mechanical activity of the human heart is closely related to the signal transportation in it. In order to develop the models one needs to understand the basic underlying physiological principles. That is the goal of this section.

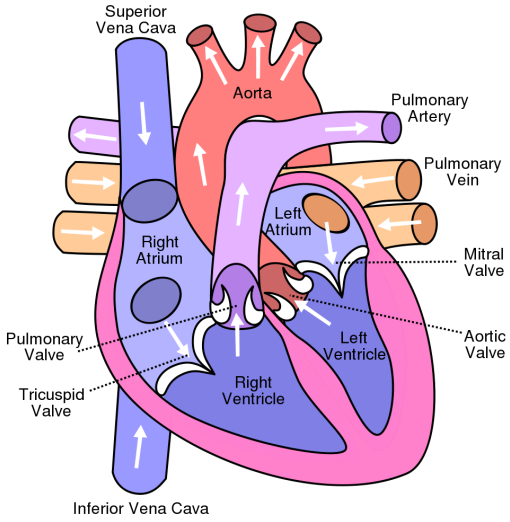

Figure 2.1: Schematic view of the human heart [189]

2.1.1 Facts & Figures

The location of the human heart is anterior to the vertebral column, i.e. the spine, and posterior to the sternum, i.e. the chest. As one can see in Figure 2.1, the human heart consists of four chambers: the right and left **atria**, which receive the blood from the body acting as a large-volume low-pressure reservoir, and the left and right **ventricles**, which actually do the predominant pumping of the blood through our body.

The mantle of the human heart consists of three layers. The outermost is referred to as **epicardium**, which mainly consists of collagen fibers and serves as a protective layer. The middle one is called the **myocardium**, consisting of muscle cells, called **myocytes**, which do the actual contraction of the heart, and innermost the **endocardium**, like the epicardium consisting of mainly collagen which serves as an interface between the heart wall and the human blood. For more details on the physiological background of contractile myocytes we refer to [94, Chap. 15] or [166, p. 60ff].

The thickness of the epicardium, about 100 μm, and of the endocardium, about 100 μm, is much less than the one of the myocardium. Although it is not uniform but it is always many magnitudes thicker than the epi and endocardium. Epi-

and endocardium being considered as mere protective respectively interfacing layers it is justified to restrict one's attention and model to the myocardium itself. Following [84] we adopt the assumption, that the myocardium can be described as a continuum composed of laminar sheets of parallel myocytes arranged in fibers, see [72] for a discussion. Figure 2.2 shows the basic structure of the left ventricle. It was extracted from [84]. As one can see the fiber direction of these muscles rotates, in a mathematical positive sense, throughout the wall thickness from 50° to 70° near the epicardium to −50° to −70° near the endocardium. The organization of the myocardial layers is characterized best by a right-handed orthonormal set of basis vectors $(\boldsymbol{f}_0, \boldsymbol{s}_0, \boldsymbol{n}_0)$, denoted **fiber direction**, **sheet direction** and **sheet normal direction** respectively. According to [84] we shall use the local index set $\{f, s, n\}$ for referring to fiber, sheet and normal direction. The idea behind this will be explained in Section 2.2.5. Furthermore we will use the pairs fs, fn and sn when referring to the fiber-sheet, fiber-normal and sheet-normal planes respectively. For a detailed overview on the structure of the myocardium we refer to [68, 84, 108, 109, 110, 158] as a starting point. The passive mechanical model of the myocardium is presented in Section 2.3.8.

The mechanical response of the human heart relies on a very complex electrochemical signal conduction system which will be discussed in the next section.

2.1.2 Signal Conduction & Overview of the Cardiac Cycle

For a more detailed description about the signal conduction of the human heart the reader is referred to [114, 166].

Cardiac tissue is called a **functional syncytium** of myocytes. This means that cells are separated morphologically but connected through so-called **gap junctions**. Gap junctions enable the cells to exchange different ions and molecules, like e.g. Na^+ or adenosine triphosphate (ATP), with each other. See [102] for more details on the role of ATP. This transfer between cells is one of the reasons why the heart muscle can contract so fast. For more details on gap junctions refer to [166].

Myocytes have two very important abilities, namely they are excitable and contractile. The first means, that they can transport electric potentials and

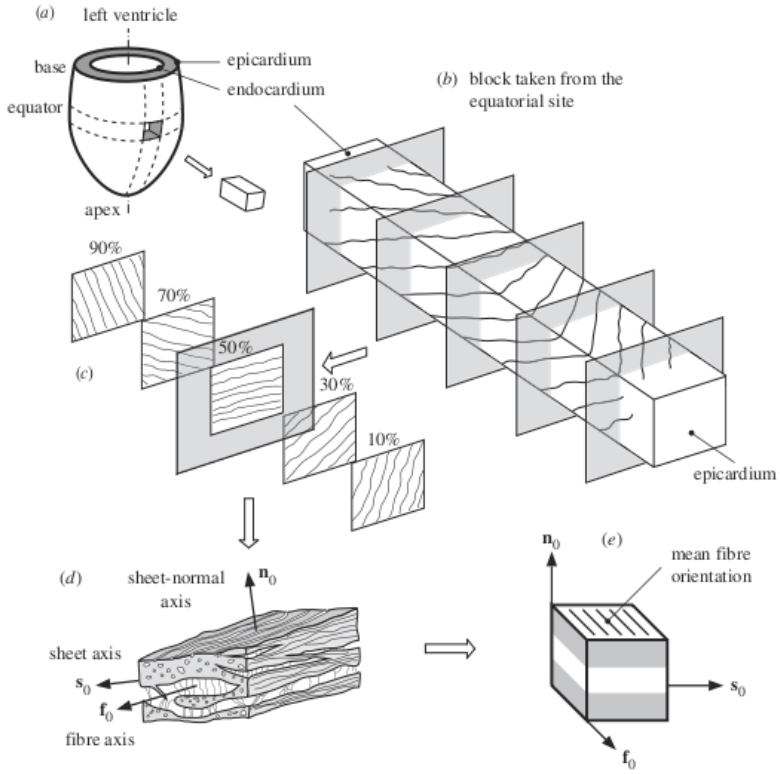

Figure 2.2: Schematic view of the muscle structure in the human heart [84, p. 3448 Fig. 1.].

(a) shows an schematic view of the left ventricle where a small block of myocardial tissue has been cut out.
(b) shows the structure of the muscle from the endocardium to the epicardium.
(c) shows five special longitudinal-circumferential layers at varying thickness of the myocardium, from 10 to 90 per cent of the wall thickness.
(d) shows the make-up of myocytes, with embedded collagen fibers and the local right-handed orthonormal fiber coordinate system with the fiber axis $\boldsymbol{f}_0$, sheet axis $\boldsymbol{s}_0$ and sheet-normal axis $\boldsymbol{n}_0$.
(e) shows a cube of layered tissue with local coordinates (X_1, X_2, X_3) which is used to develop the mechanical models in [84].

these potentials cause the cells to actually contract. For a detailed physiological overview the interested reader may refer to [166, p. 60] and also [69, 79, 88] and for a detailed mathematical modeling overview one should refer to [94, Chap. 15]. The excitability of the myocytes is fundamental for understanding the functionality of the human heart and will be addressed in Section 2.2.5. However, to ensure correctness of the complex process of pumping blood through our body, there is an intense communication and synchronization between the cells, which is controlled by the **signal conduction system** of the heart as depicted in Figure 2.3. The electrical activity of the human heart starts in a bunch

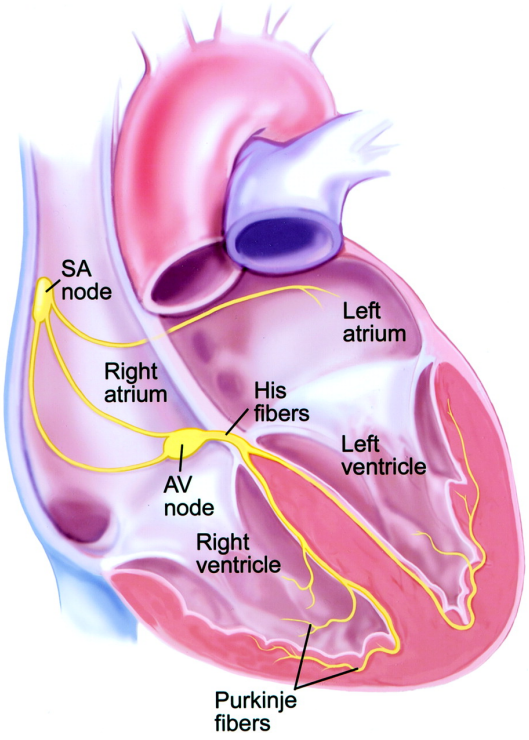

Figure 2.3: Schematic view of the signal conduction system of the human heart [185].

of cells known as the **sinoatrial node**, short SA node, which is found just below the superior **vena cava** of the right atrium. The cells in the SA node are very special cells, as they work as autonomous oscillators, meaning that they can alter their electric potential without effects from outside. This change of electric potential (known as **action potential**) is then mitigated through

the heart, starting by the atria. The atria and the ventricles are separated by a wall which consists of non-excitable cells. Thus the action potential cannot pass directly this barrier. However there exists one pathway through this barrier: another bunch of specialized cells, known as the **atrioventricular node**, or short AV node, located at the bottom of the atria. An important property of the AV node is, that its conductivity is much smaller than in usual heart cells, so these action potentials travel quite slow through these cells. This happens not without ulterior motive. If the signal would pass the AV node as fast as it travels through other cells, the ventricles would start to contract before the atria have ejected all of the stored blood into the ventricles. After the signal has passed the AV node it branches out through a specialized collection of cells known as the **bundle of His**, which is composed of **Purkinje fibers**. This Purkinje fiber network spreads out in a tree-like way into the left and right **bundle branches** all over the inside of the ventricles. The Purkinje fibers are connected to the ventricular muscle cells through junctions. When an action potential reaches a muscle cell from a Purkinje fiber it causes it to contract, and so the whole ventricle starts to contract. The end of the propagation of the action potential lies in the epicardial surface. After the signal has reached this point, the whole contraction is reversed and starts again from the SA node.

Summary

This was a very brief, and by no means complete, overview of the cardiac cycle in a human heart. It should be evident from the above paragraph, that there is a multitude of features of the myocardium to study. First of all one needs to know how the electric potentials of cells can be altered and how the "communication" of cells works, the latter leading to the so-called **ionic currents**. Bearing in mind the goal, of describing the myocardium as a whole (provided it can be modeled as a continuum), it is also of great interest how one can describe the propagation of action potentials in the whole human heart without focusing on the cellular structure. This will lead to the well-known **Bidomain** equations. Apart from the electric propagation in the human heart one wants to take a glance at the mechanic contraction of the heart. As said before, the contractile properties of myocytes are out of the scope of this thesis. We will stick to a pure formulation of the mechanical models from a continuum mechanical point of view. However, the mechanical and the electrical activities are not

self-contained. They depend on each other, thus one needs to account for that too, which will lead to a coupled multi-physics problem.

2.2 Cardiac Electric Activity

The electric activation of the human heart is a very complex procedure and relies on various different aspects. This chapter is by no means complete and many of the physiological and physical topics will just be touched on. A very good and detailed physiological overview of the electric activation in the human heart is found in [98, 146, 166, 174]. The mathematical modeling in this chapter is largely taken from [93, 94]. To be able to understand the processes of the electrical activation one needs to start at the cellular level. Nevertheless, it occurred many times in history of science that a simple approach used to describe the electrical activity of the human heart, was very successive. This was the electrocardiogram dating back to 1877. This shall serve as a motivation for the time being.

2.2.1 Modeling the Human Heart as a Dipole

This part is derived from [94, Chap. 12]. One of the oldest attempts to model the myocardial activity dates back to 1877, when the first electrocardiogram was recorded by Einthoven. For a more detailed view on the historical background we refer to [19, 59]. It has been known since than that the **action potential** — this is the potential difference across the cardiac cell membrane and it is the actual signal in the human heart which is transported — of the human heart generates an electrical potential field that could be measured on the body surface. In a first approach, the human body was modeled as a volume conductor. This means, when there is a current source somewhere in the body, currents will spread out throughout the body. With those currents flowing, one can measure the potential differences between any two points of the body's surface, given a voltmeter which is sensitive enough. Potential differences are observed whenever the current sources are sufficiently strong. There are three of such occurrences. When the action potential is spreading across the atria, there is a measurable signal, called the **P-wave**. When the action potential

is propagating through the wall of the ventricles, there is the largest of all deflections, called the **QRS-complex**. A schematic view of a single ECG recording is depicted in Figure 2.4.

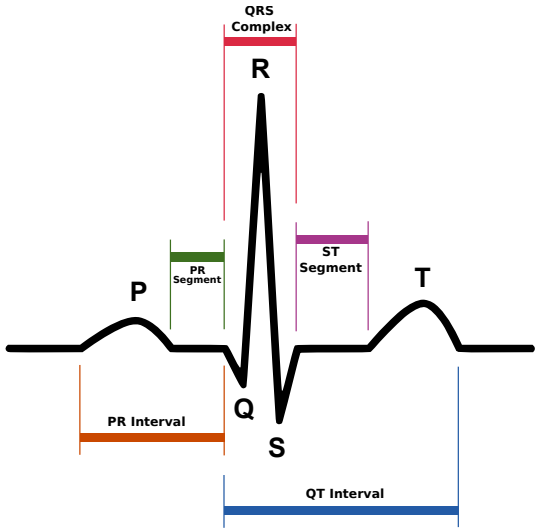

Figure 2.4: Schematic view of the sinus rhythm of the heart [190].

2.2.2 Cardiac Cells, Action Potentials and Ionic Currents

The volume conductor model, although very simple, is still the basis for the electrocardiography in modern medicine. However, to get a more profound understanding of the electric activation of the human heart, and because of the evolving knowledge about epigenetics, as mentioned in the introduction, one needs to take account of some physiological details. First of all one needs to understand how cardiac cells can transport electric signals.

The Cell Membrane

From an electrical point of view, the most important part of a cell is its membrane. Therefore details about the structure of a human cell will not be discussed here. The interested reader may refer to [166]. For our end it

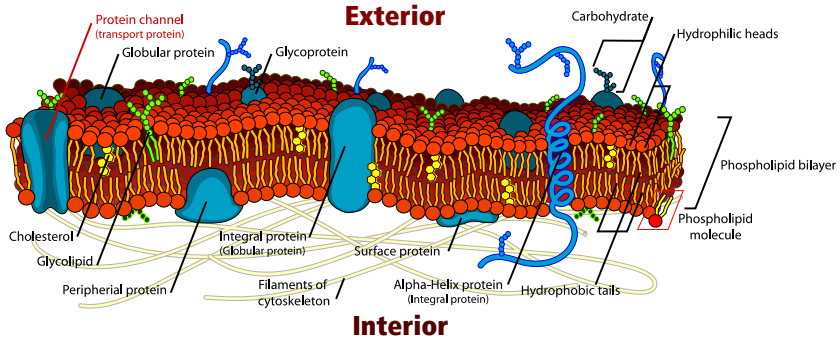

Figure 2.5: Schematic view of the cell membrane [188]. For the thesis, the most important part of the cell membrane are the channel proteins which have been marked red.

is sufficient to know, that a human cell consists of a cell membrane and the interior. Both the **intracellular** and **extracellular** space consist of, among many other things, a dilute aqueous solution of dissolved salts, primarily NaCl and KCl, which dissociate into Na^+, K^+ and Cl^- ions. Outside the cell in the extracellular space one also finds ions in a different concentration. Thus there is an electric imbalance and so cells possess an electric potential, whose idle state is referred to as **resting potential**. Inside the cell the electrical potential is denoted by u_i outside with u_e. The difference is denoted by $V_{\text{tm}} := u_e - u_i$ and is called the **trans-membrane potential**.

The cell membrane acts as a boundary separating the interior of the cell from its exterior. More important, it is selectively permeable, meaning that it allows particles, among also ions, to pass into and out the cell. It is composed of a double layer, or **bi-layer**, of phospho-lipid — where **lipid** is specified by a category of water-insoluble, energy rich macromolecules, like fats, waxes, and oils — molecules about 7.5nm thick. Figure 2.5 shows a schematic view of a cell membrane.

We will focus on a specific part of the cell membrane: the **channel proteins**, marked red in Figure 2.5. These are protein-lined pores which actual regulate the passage of ions through the cell membrane, thus maintaining concentration differences between the interior and the exterior of a cell.

There are two possibilities to transport molecules through the cell membrane. The first one is the so-called **passive transport**, by which a passive process

which is solely driven by concentration gradients is meant. The second possibility to transport molecules through the cell membrane is by a so-called **active transport**. An active transportation process involves the transportation of ions against their concentration gradient and thus is an energy consuming action. The whole maintenance of the concentration differences are set up by the active mechanisms of the cell. Also much of the metabolism of our body works due to such transports. In literature it is also quite common to refer to those active processes as **pumps**.

The most important of those pumps is the Na^+–K^+ ATPase, see [166], which uses the energy stored in ATP molecules to pump Na^+ out of the cell and K^+ in. There are much more of these pumps, many of them use Calcium Ca^{2+}. However, neither of these processes will be discussed here in detail as this would go beyond the scope of this thesis, the interested reader may refer to [166] for the physiological details and [93, 94] for the modeling details. We will stick to the fact, that the active transport together with the passive transport are essential for the health of a cell itself and for the regulation of the concentration differences.

2.2.3 Electric Circuit Model of the Cell Membrane

Since the cell membrane separates charges, it can be viewed as a capacitor, see [92] for details. The capacitance of any insulator is defined as the ratio of the charge across the capacitor to the voltage potential necessary to hold that charge, and it is denoted by

$$C_m = \frac{Q}{V}. \tag{2.1}$$

From standard electrostatics, e.g. Coulomb's law, see [92], one can derive the fact that for two parallel conducting plates separated by an insulator of thickness d, the capacitance is found to be

$$C_m = \frac{k\varepsilon_0}{d},$$

where k is the dielectric constant for the insulator and ε_0 is the permittivity of free space. The capacitance of the cell membrane is typically $1.0\,\mu\mathrm{F}/\mathrm{cm}^2$. Taking

that $\varepsilon_0 = \frac{10^{-9}}{36\pi}\,\mathrm{F/m}$ one calculates the dielectric constant of the cell membrane to be about 8.5.

We can think of the cell membrane as an electric circuit, as shown in Figure 2.6. It is assumed that the membrane acts like a capacitor in parallel with a,

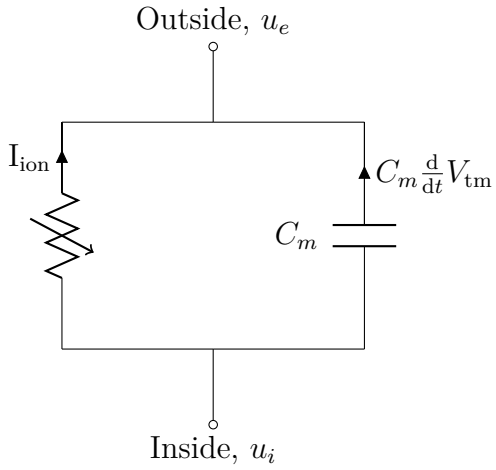

Figure 2.6: A simple circuit model of the cell membrane.

not necessarily ohmic, resistor. One knows that the current is $\frac{\mathrm{d}}{\mathrm{d}t}Q$, thus from (2.1) it follows that the current flowing over the capacitor is given by $C_m \frac{\mathrm{d}}{\mathrm{d}t} V_{\mathrm{tm}}$, provided that C_m is constant. Finally using Kirchoff's law one obtains

$$C_m \frac{\mathrm{d}}{\mathrm{d}t} V_{\mathrm{tm}} + I_{\mathrm{ion}} = 0.$$

The function I_{ion}, called the **ionic current**, describes the current flowing through the resistor depicted in Figure 2.6. Further, some external current sources are assumed to be applied either on the inside, which are then called s_i, or on the outside of a cell which then are named s_e. So one obtains the following two equations:

$$\begin{aligned} C_m \frac{\mathrm{d}}{\mathrm{d}t} V_{\mathrm{tm}} + I_{\mathrm{ion}} &= s_e, \\ C_m \frac{\mathrm{d}}{\mathrm{d}t} V_{\mathrm{tm}} + I_{\mathrm{ion}} &= -s_i. \end{aligned}$$

2.2.4 Functional Dependence of I_{ion}

As written above the differences in ionic concentrations between the inside and outside of a cell create a potential difference along the cell membrane. The trans-membrane potential V_{tm} in particular drives a current flux between the interior and the exterior of a cell which was denoted above as ionic current I_{ion}. The physical details of the ionic currents are not to be discussed here. The interested reader may refer to [94, Chapt. 2, 3 and 5]. The most important aspect for modeling is that the ionic current has a functional dependence on the action potential V_{tm}, i.e. $I_{\text{ion}} = I_{\text{ion}}(V_{\text{tm}})$. The difficulties arise, when one tries to figure out how this dependence may look like. In [94] one finds two possibilities how to describe the functional dependence of the ionic current, a quasi-linear one reading

$$I_{\text{ion}}(V_{\text{tm}}) = \sum_{\text{ions}} g_{\text{ions}}(V_{\text{tm}})(V_{\text{tm}} - V_{\text{ions}}),$$

where ions stands for a list of ions of interest (like Na^+, K^+ and so on). The values g_{ions} represent not necessarily constant conductivities. For each ion, V_{ions} denotes the **Nernst potential**, see [94, Chapt. 3] for details. This model is quite popular, as one can divide the dependence of the ionic current up to different ionic currents for each ion and then lump all together to a so-called **leakage current**. The second possibility is to use a similar decomposition of the ionic current into a current for each ion using the Goldman-Hodgkin-Katz current equation reading

$$I_{\text{S}} = P_S \frac{z^2 F^2}{RT} V_{\text{tm}} \frac{c_i - c_e \exp\left(-\frac{zFV_{\text{tm}}}{RT}\right)}{1 - \exp\left(-\frac{zFV_{\text{tm}}}{RT}\right)},$$

where S stands for the type of ion, z is the valence of the ion S, c_i and c_e are the respective concentrations in the intra and extra cellular regions, R is the universal gas constant, T is the absolute temperature, P_S is the permeability of the cell membrane to the specific ion S and F is Faraday's constant. In the next section we will see how we can describe the evolution of the ionic current.

2.2.5 Excitability of Myocytes

Section 2.2.4 was devoted onto how the trans-membrane potential V_{tm} causes ionic currents I_{ion} to flow through the membrane. Regulation of this membrane potential by control of the ionic channels is one of the most important cellular functions. Myocytes, especially, use this membrane potential, as discussed in Section 2.1 as a signal to control the contraction of the myocardium. Thus, the contraction is dependent on the generation of electric signals. As aforementioned, heart cells belong to a class of very special cells: they are excitable. This means, that if a sufficiently strong current is applied, the membrane potential performs a pronounced oscillation before eventually returning to the resting potential value. Figure 2.7 shows a schematic view of an action potential typical for ventricular heart cells. It should be mentioned at this point that the shape

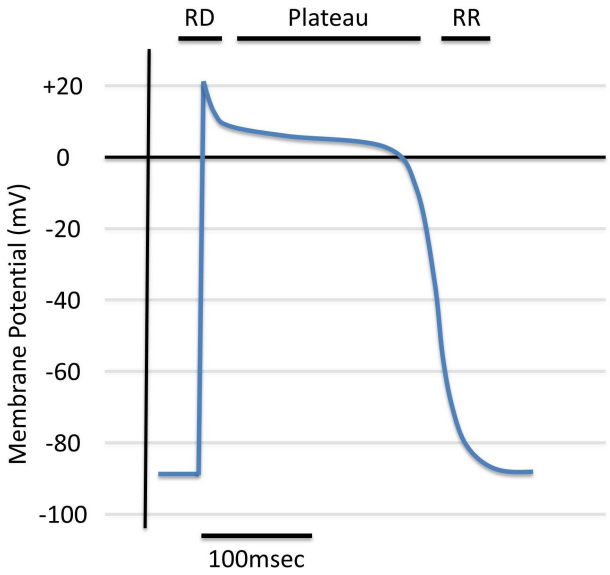

Figure 2.7: Typical curve of an ventricular cell action potential [116].

of the action potentials differs from cell to cell in the heart. This means, the models for the SA node will not be adequate for describing the potential of the AV node and the other cell types in the myocardium respectively.

In Section 2.1 this change of potential was referred to as action potential. The most obvious advantage of excitability is that an excitable cell either responds

in full to a stimulus or not at all, and thus a stimulus of sufficient amplitude may be reliably distinguished from background noise. In this way, noise is filtered out, and a signal is reliably transmitted.

The studies on the generation and propagation of those signals have been made for nearly a hundred years. Although the generation and propagation of signals have been extensively studied by physiologists for at least the past hundred years, the most important landmark in these studies is the work of Alan Hodgkin and Andrew Huxley, see [83], who developed the first quantitative model for the propagation of an electrical signal along a squid giant axon. Their model was originally used to explain the action potential in the long giant axon of a squid nerve cell, but the ideas have since been extended and applied to a wide variety of excitable cells.

In the spirit of Hodgkin and Huxley many models have been developed. All those models do share a common structure, see [120]. They are called **Hodgkin-Huxley-type models**, since they are all based, mathematically, on the original model from Hodgkin and Huxley [83]. In [120] one finds a very good summary of the various models for ionic currents. The models are based on viewing the cell membrane as an electrical circuit and applying Kirchoff's law to it. This means that the membrane current model consists of a capacitive current term and a variety of ionic current terms appropriate for a specific type of cell. The general form of the spatially-independent model with n ionic currents is

$$C_m \frac{\mathrm{d}}{\mathrm{d}t} V_{\mathrm{tm}} = -\sum_{i=1}^{n} \bar{g}_i a_i^p b_i^q (V_{\mathrm{tm}} - V_i) + I_{\mathrm{app}}(t), \tag{2.2}$$

$$\frac{\mathrm{d}}{\mathrm{d}t} a_i = \frac{a_i^\infty(V_{\mathrm{tm}}) - a_i}{\tau_{a_i}(V_{\mathrm{tm}})}, \qquad i = 1, 2, \ldots, n, \tag{2.3}$$

$$\frac{\mathrm{d}}{\mathrm{d}t} b_i = \frac{b_i^\infty(V_{\mathrm{tm}}) - b_i}{\tau_{b_i}(V_{\mathrm{tm}})}, \qquad i = 1, 2, \ldots, n, \tag{2.4}$$

where C_m is the capacitance of the cell membrane, V_{tm} is the trans-membrane potential, $\bar{g}_i$ is the maximal conductance of the channel for ion i, a_i and b_i are the gating variables taking values between 0 and 1, V_i is the Nernst potential for the i^{th} ion, I_{appl} is the applied stimulus current. The latter may consist of a signal coming from an adjacent cell or from an external applied current. Further, a_i^∞ and b_i^∞ are the steady state values of the gating variables at potential V_{tm}, τ_{a_i} and τ_{b_i} are the relaxation time constants at potential V_{tm} and finally p, q

denote some arbitrary real exponents. Many of the excitability models known throughout the literature can be written in this form. There is a huge collection of those models available for simulation through the CellML-project, see [118]. Taking note, we write the evolution equation for the ionic current I_{ion} in the following abstract way as a system of nonlinear ordinary differential equations:

$$\begin{aligned} I_{\text{ion}} &= g(V_{\text{tm}}, \boldsymbol{v}), \\ \frac{\mathrm{d}}{\mathrm{d}t}\boldsymbol{v} &= -\boldsymbol{H}(V_{\text{tm}}, \boldsymbol{v}), \qquad (2.5) \\ \boldsymbol{v}(t=0) &= \boldsymbol{v}_0. \qquad (2.6) \end{aligned}$$

With this notation one covers almost any possible shape of the ionic current appearing in the literature.

2.2.6 Phenomenological Models

The complexity of ionic current models can be a challenge for numerical simulations and also for mathematical analysis. Therefore many simplified models have been developed. Although neglecting the physiological details, these models are capable of approximately reproducing action potentials.

FitzHugh-Nagumo Model

The most simple phenomenological model is the FitzHugh-Nagumo model, see [66, 123]. The model is governed by the relations

$$\begin{aligned} \mathrm{I}_{\text{ion}}(V_{\text{tm}}, v) &:= c_1 V_{\text{tm}}(V_{\text{tm}} - V_{\text{th}})(1 - V_{\text{tm}}) + c_2 v, \qquad (2.7) \\ H(V_{\text{tm}}, v) &:= b(dv - V_{\text{tm}}). \qquad (2.8) \end{aligned}$$

For this specific model the value of V_{tm} has been rescaled to the interval $[0, 1]$. The constants $c_1, c_2, V_{\text{th}}, b, d$ can be looked up in [157, Figure 1].

Rogers-McCulloch Model

The second model we want to present is the Rogers-McCulloch model, see [157]. This model is a modification of the original FitzHugh-Nagumo model. In this case we have

$$\mathrm{I}_{\mathrm{ion}}(V_{\mathrm{tm}}, v) := c_1 V_{\mathrm{tm}}(V_{\mathrm{tm}} - V_{\mathrm{th}})(1 - V_{\mathrm{tm}}) + c_2 V_{\mathrm{tm}} v, \tag{2.9}$$

$$H(V_{\mathrm{tm}}, v) := b(dv - V_{\mathrm{tm}}). \tag{2.10}$$

For this specific model the value of V_{tm} has been rescaled to the interval $[0, 1]$. The constants $c_1, c_2, V_{\mathrm{th}}, b, d$ can be looked up in [157, Figure 1].

Aliev-Panfilov Model

The third model we want to mention is the Aliev-Panfilov model, see [4]. The difference to the Rogers-McCulloch model is the nonlinear behavior in the second equation. The model reads as

$$\mathrm{I}_{\mathrm{ion}}(V_{\mathrm{tm}}, v) := c_1 V_{\mathrm{tm}}(V_{\mathrm{tm}} - V_{\mathrm{th}})(1 - V_{\mathrm{tm}}) + c_2 V_{\mathrm{tm}} v, \tag{2.11}$$

$$H(V_{\mathrm{tm}}, v) := \left(\varepsilon_0 + \frac{\mu_1 v}{\mu_2 + V_{\mathrm{tm}}}\right)\left(v + kV_{\mathrm{tm}}\left(V_{\mathrm{tm}} - V_{\mathrm{th}} - 1\right)\right). \tag{2.12}$$

Again, this model works with a rescaled trans-membrane potential V_{tm} in the range of $[0, 1]$. The constants $c_1, c_2, V_{\mathrm{th}}, \varepsilon_0, \mu_1, \mu_2, k$ can be looked up in [4, Page 294].

There are many more phenomenological models. The interested reader may look up [65, 119]. Proceeding, the readers attention is switched to the mathematical modeling of macroscopic signal propagation in the human heart.

2.2.7 The Bidomain Equations

It would be possible to model the whole human heart on a cellular basis. However, this would be computational very expensive. Furthermore one would need to develop a very detailed cell model which would have to be applied to each cell and then coupled among each other. The latter is for being able to describe the

propagation of signals through the cells. This coupling is complicated by the fact, that the signal which is transported is in fact the trans-membrane potential V_{tm}, and thus the intra and extra cellular spaces have to be continuously connected and intertwined, so that one can move continuously between any two points within one space without traversing through the complementary space.

As aforementioned, it is yet not possible to write and solve equations that account for the cellular structure and the details of the geometry of the human heart. In a first step, see Section 2.2.1, it was described that modeling the human heart in a macroscopic sense as a dipole suffices for some medical application but is not adequate for a complete description of the electrical activation of the human heart. A more accurate description will be obtained by the **Bidomain model** first introduced by L. Tung, see [178], as well as [82, 114] for details.

For deriving an accurate model for the electric activation of the myocardium one applies procedures from continuum mechanics, known as **homogenization**. With this one can write equations in an averaged, or smoothed, sense which are adequate for the many computational situations. In continuum mechanics, it is quite common to study averaged quantities, to avoid modeling the molecular structure of solids and fluids, see e.g. [70, 90] but also [143] and [94, Chap. 7,12] for mathematical details and a justification. In the setting of myocardial tissue one starts from a microscopic description and with a homogenization argument derives averaged equations. This are known as the Bidomain equations. For details on the homogenization approach and a precise derivation of the equations we refer to [38, 128].

The Bidomain equations can be stated in different forms. We will use the **parabolic-elliptic** form reading as: Find $(V_{\mathrm{tm}}, u_e, \boldsymbol{v})$ such that

$$\chi C_m \frac{\partial}{\partial t} V_{\mathrm{tm}} + \chi \mathrm{I}_{\mathrm{ion}}(V_{\mathrm{tm}}) - \operatorname{div}\left(\mathbf{M}_i \operatorname{grad} V_{\mathrm{tm}}\right) - \operatorname{div}\left(\mathbf{M}_i \operatorname{grad} u_e\right) = s_i, \tag{2.13}$$

$$- \operatorname{div}\left(\mathbf{M}_i \operatorname{grad} V_{\mathrm{tm}}\right) - \operatorname{div}\left((\mathbf{M}_i + \mathbf{M}_e) \operatorname{grad} u_e\right) = s_i + s_e, \tag{2.14}$$

$$\frac{\partial}{\partial t} \boldsymbol{v} + \boldsymbol{H}(V_{\mathrm{tm}}, \boldsymbol{v}) = \mathbf{0} \tag{2.15}$$

in $\Omega \times (0,T)$. The boundary conditions are assumed to be of Robin type and read as

$$\boldsymbol{n} \cdot (\mathbf{M}_i \operatorname{grad} V_{\mathrm{tm}} + \mathbf{M}_i \operatorname{grad} u_e) + \alpha_i (V_{\mathrm{tm}} + u_e) = g_{R,i}, \tag{2.16}$$

$$\boldsymbol{n} \cdot (\mathbf{M}_e \operatorname{grad} u_e) + \alpha_e u_e = g_{R,e} \tag{2.17}$$

on $\partial\Omega \times (0,T)$. Finally we impose initial conditions on V_{tm} and $\boldsymbol{v}$ of the form

$$V_{\mathrm{tm}}(0,\boldsymbol{x}) = V_{\mathrm{tm}}^0(\boldsymbol{x}), \tag{2.18}$$

$$\boldsymbol{v}(0,\boldsymbol{x}) = \boldsymbol{v}^0(\boldsymbol{x}). \tag{2.19}$$

The constant χ is the **surface-to-volume ratio** and results from the homogenization procedure. The constant C_m is the capacitance of the cell membrane. The values for χ, C_m can be looked up in Table 2.1. Next some basic facts about the conductivity tensors $\mathbf{M}_i$ and $\mathbf{M}_e$ will be recited.

Conductivity and Fiber Orientation

It is known, that the myocardium is the most important part, when describing the pumping process of the human heart. For the electrochemical modeling the Bidomain model (2.13)–(2.17) has been derived. Now one needs to establish the conductive properties of the myocardium. One important fact is, that the conduction in the human heart is highly anisotropic, and as said above, the quantities $\mathbf{M}_i$ and $\mathbf{M}_e$ are tensor-valued functions. This specific anisotropy comes from the structure of the myocardium as discussed in Section 2.1.1. There a local coordinate system spanned by $\boldsymbol{f}_0, \boldsymbol{s}_0$ and $\boldsymbol{n}_0$ was introduced. It is well known that the conductivity along the fiber axis $\boldsymbol{f}_0$ is much higher than along $\boldsymbol{s}_0, \boldsymbol{n}_0$. This means one may assume the conductivity tensor of the form

$$\mathbf{M}(\boldsymbol{x}) = m_f \boldsymbol{f}_0(\boldsymbol{x}) \otimes \boldsymbol{f}_0(\boldsymbol{x}) + m_s \boldsymbol{s}_0(\boldsymbol{x}) \otimes \boldsymbol{s}_0(\boldsymbol{x}) + m_n \boldsymbol{n}_0(\boldsymbol{x}) \otimes \boldsymbol{n}_0(\boldsymbol{x}).$$

In real-life applications the distribution of the basis $\{\boldsymbol{f}_0, \boldsymbol{s}_0, \boldsymbol{n}_0\}$ is derived with **diffusive tensor imaging**, see [97, 145] for details.

For orthonormal $\boldsymbol{f}_0, \boldsymbol{s}_0, \boldsymbol{n}_0$ one may interpret m_f, m_s, m_n as the eigenvalues of $\mathbf{M}$. Furthermore for orthonormal $\boldsymbol{f}_0, \boldsymbol{s}_0, \boldsymbol{n}_0$ one may eliminate one axis and write

$$\mathbf{M}(\boldsymbol{x}) = m_n \mathbf{I} + (m_f - m_n) \boldsymbol{f}_0(\boldsymbol{x}) \otimes \boldsymbol{f}_0(\boldsymbol{x}) + (m_s - m_n) \boldsymbol{s}_0(\boldsymbol{x}) \otimes \boldsymbol{s}_0(\boldsymbol{x})$$

The values are given in Table 2.1.

Parameter	Value	Unit
C_m	1.0000E−2	$\mathrm{F/m^2}$
χ	2.0000E+5	$\mathrm{1/m}$
m_f^i	3.0000E−1	$\mathrm{S/m}$
m_s^i	1.0000E−1	$\mathrm{S/m}$
m_n^i	3.1525E−2	$\mathrm{S/m}$
m_f^e	2.0000E−1	$\mathrm{S/m}$
m_s^e	1.6500E−1	$\mathrm{S/m}$
m_n^e	1.3514E−1	$\mathrm{S/m}$

Table 2.1: Values of the parameters for the Bidomain model: the conductivity values, the value for χ and the value for C_m are taken from [101],[81] and [147].

Summary

In this chapter the basic models for the electric part of the cardiac cycle have been developed which eventually lead to the Bidomain equations. Furthermore the conductive properties of the human heart with tensor-valued functions were described and the ionic currents were taken account of, by modeling them in the most abstract way. Summarizing the complete electronic model of the human heart in dimensional form reads to find $(V_{\mathrm{tm}}, u_e, \boldsymbol{v})$ such that:

$$\chi C_m \frac{\partial V_{\mathrm{tm}}}{\partial t} + \chi \mathrm{I}_{\mathrm{ion}}(V_{\mathrm{tm}}, \boldsymbol{v}) - \mathrm{div}(\mathbf{M}_i \,\mathrm{grad}\, V_{\mathrm{tm}}) - \mathrm{div}\,(\mathbf{M}_i \,\mathrm{grad}\, u_e) = s_i, \quad (2.20)$$

$$- \mathrm{div}(\mathbf{M}_i \,\mathrm{grad}\, V_{\mathrm{tm}}) - \mathrm{div}((\mathbf{M}_i + \mathbf{M}_e) \,\mathrm{grad}\, u_e) = s_i + s_e, \quad (2.21)$$

$$\frac{\partial \boldsymbol{v}}{\partial t} + \boldsymbol{H}(V_{\mathrm{tm}}, \boldsymbol{v}) = 0 \quad (2.22)$$

in $\Omega \times (0, T)$ and completed by the boundary and initial conditions

$$(\mathbf{M}_i \,\mathrm{grad}(V_{\mathrm{tm}} + u_e), \boldsymbol{n}) + \alpha_i (V_{\mathrm{tm}} + u_e) = g_{R.i} \quad \text{on } \partial\Omega \times (0, T], \quad (2.23)$$

$$(\mathbf{M}_e \,\mathrm{grad}\, u_e, \boldsymbol{n}) + \alpha_e u_e = g_{R,e} \quad \text{on } \partial\Omega \times (0, T], \quad (2.24)$$

$$V_{\mathrm{tm}}(0, \boldsymbol{x}) = V_{\mathrm{tm}}^0 \quad \text{in } \Omega, \quad (2.25)$$

$$\boldsymbol{v}(0, \boldsymbol{x}) = \boldsymbol{v}_0 \quad \text{in } \Omega. \quad (2.26)$$

Remark 2.1. *Usually, one assumes that $s_e = -s_i$ so that the right hand side of equation* (2.21) *vanishes.*

2.3 Passive Mechanical Behavior of Heart Tissue

In this section the models covering the pure mechanical deformation of human heart tissue will be summarized. In contrast to modeling the electric activation of the human heart, mechanic models are already established and well understood. Thus one can describe the passive deformation of the human heart with standard tools from continuum mechanics. For an introduction to continuum mechanics we refer to [35, 85, 135, 177] as well as [11, Chapter 3]. For sake of completeness the most important facts from continuum mechanics will subsequently be recited.

2.3.1 Bodies and Configurations

Definition 2.2 (Body)**.** *A **body** $\mathcal{B}$ is a set whose elements can be put into a one-to-one correspondence with points of a region Ω in a three-dimensional Euclidean point space. The elements of $\mathcal{B}$ are called **particles**, or **material points**, and Ω is called a **configuration** of $\mathcal{B}$.*

As a body moves the configuration B will change in time.

Definition 2.3. *Let $t \in I \subset \mathbb{R}^+$. The family $\{\Omega(t) : t \in I\}$ of unique configurations of $\mathcal{B}$ at time time t is called the **motion** of $\mathcal{B}$.*

Remark 2.4. *It is assumed, that as $\mathcal{B}$ moves continuously also $\Omega(t)$ evolves continuously.*

Further, it is quite convenient to identify a so-called **reference configuration**, Ω_r say, which is an arbitrarily chosen fixed configuration. Then any particle P of $\mathcal{B}$ may be labeled by its position vector $\boldsymbol{X} \in \Omega_r$, relative to a chosen origin $\boldsymbol{O}$. It should be noted that the reference configuration need not be a configuration which is actually occupied by the body $\mathcal{B}$. Let further $\boldsymbol{x}$ be the position vector of P in the configuration $\Omega(t)$ at time t relative to another

chosen origin $\boldsymbol{o}$. Again for sake of simplicity one may choose $\boldsymbol{O} = \boldsymbol{o}$. Similar to that one says that $\mathcal{B}$ occupies the configuration $\Omega(t)$ at time t and call $\Omega(t)$ the **current configuration**. Here we will choose $\Omega_r = \Omega(0)$. Since Ω_r and $\Omega(t)$ are configurations of $\mathcal{B}$ there exists a bijective mapping $\boldsymbol{\chi}\colon \Omega_r \to \Omega(t)$ such that

$$\boldsymbol{x} = \boldsymbol{\chi}(\boldsymbol{X}, t) \qquad \text{for all } \boldsymbol{X} \in \Omega_r, \tag{2.27}$$

$$\boldsymbol{X} = \boldsymbol{\chi}^{-1}(\boldsymbol{x}, t) \qquad \text{for all } \boldsymbol{x} \in \Omega(t). \tag{2.28}$$

It can be seen from (2.27), that one can characterize either of the coordinates with its counterpart. Figure 2.8 shows a schematic summary.

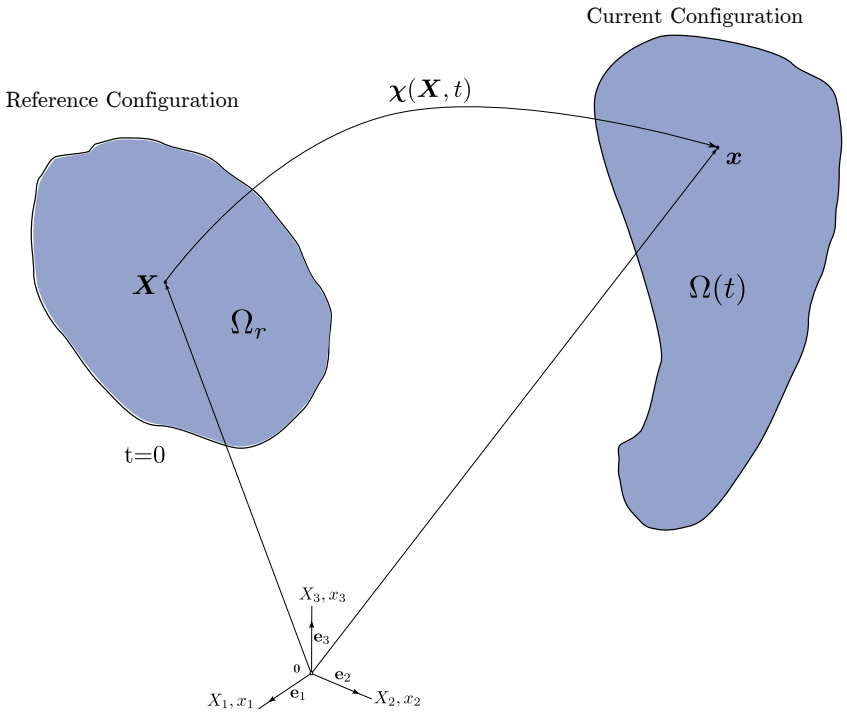

Figure 2.8: Reference configuration Ω_r and current configuration Ω_t with the position vectors $\boldsymbol{X}$ and $\boldsymbol{x}$ of a material point P and the motion $\boldsymbol{\chi}(\boldsymbol{X}, t)$. The coordinate system is spanned by an orthonormal basis $\{\boldsymbol{e}_i\}_{i=1}^3$

.

2.3.2 Material and Spatial Descriptions

In the development of the basic principles of continuum mechanics a body $\mathcal{B}$ is assigned to various physical properties which are represented by scalar, vector and tensor fields defined on **either** Ω_r **or** $\Omega(t)$. In case of Ω_r both the position vector $\boldsymbol{X}$ and the time t serve as independent variables, the fields are said to be defined in **referential, material or Lagrangian** description then. Alternatively, in the case of $\Omega(t)$, $\boldsymbol{x}$ and t serve as independent variables. Here, one refers to the **spatial or Eulerian** description. The distinction between these two descriptions is crucial. To make things more clear: In material description attention is paid to a particle, and one observes what happens to the particle as it moves. Spatial description puts attention to a specific point in space, and one studies what happens at the point as time changes.

For studying solid mechanics one needs to work with derivatives in Eulerian or Lagrangian configurations and relate them to each other. Henceforth the Einstein summation convention applies.

Definition 2.5 (Material Gradient, Spatial Gradient)**.** *The* ***material gradient*** *of a sufficiently smooth material field* $\Phi(\boldsymbol{X}, t)$ *is defined by*

$$\operatorname{Grad} \Phi(\boldsymbol{X}, t) := \frac{\partial}{\partial X_i} \Phi(\boldsymbol{X}, t) \boldsymbol{e}_i.$$

The ***spatial gradient*** *of a sufficiently smooth spatial field* $\phi(\boldsymbol{x}, t)$ *is defined as*

$$\operatorname{grad} \phi(\boldsymbol{x}, t) := \frac{\partial}{\partial x_i} \phi(\boldsymbol{x}, t) \boldsymbol{e}_i.$$

In case of a vector-valued function $\boldsymbol{u}$ *we define the material or spatial gradient as*

$$\operatorname{grad} \boldsymbol{u}(\boldsymbol{x}, t) := \nabla_{\boldsymbol{x}} \otimes \boldsymbol{u} = \frac{\partial}{\partial x_q} \boldsymbol{u} \otimes \boldsymbol{e}_q = \frac{\partial}{\partial x_q} u_p \boldsymbol{e}_p \otimes \boldsymbol{e}_q,$$
$$\operatorname{Grad} \boldsymbol{U}(\boldsymbol{X}, t) := \nabla_{\boldsymbol{X}} \otimes \boldsymbol{U} = \frac{\partial}{\partial X_q} \boldsymbol{U} \otimes \boldsymbol{e}_q = \frac{\partial}{\partial X_q} U_p \boldsymbol{e}_p \otimes \boldsymbol{e}_q.$$

Definition 2.6 (Material Divergence, Spatial Divergence)**.** *The* ***material divergence*** *of a sufficiently smooth material field* $\boldsymbol{\Phi}(\boldsymbol{X}, t)$ *is defined as*

$$\operatorname{Div} \boldsymbol{\Phi}(\boldsymbol{X}, t) := \frac{\partial}{\partial X_i} \Phi_i(\boldsymbol{X}, t).$$

The ***spatial divergence*** *of a sufficiently smooth spatial field* $\boldsymbol{\phi}(\boldsymbol{x}, t)$ *is defined as*

$$\operatorname{div} \boldsymbol{\phi}(\boldsymbol{x}, t) := \frac{\partial}{\partial x_i} \phi_i(\boldsymbol{x}, t).$$

In case of tensor-valued functions $\mathbf{a}, \mathbf{A}$ *we define the spatial and material divergence as*

$$\operatorname{div} \mathbf{a}(\boldsymbol{x}, t) := \frac{\partial}{\partial x_p} a_{pq}(\boldsymbol{x}, t) \boldsymbol{e}_q,$$
$$\operatorname{Div} \mathbf{A}(\boldsymbol{X}, t) := \frac{\partial}{\partial X_p} A_{pq}(\boldsymbol{x}, t) \boldsymbol{e}_q.$$

Definition 2.7 (Material Time Derivative of a Material Field)**.** *The* ***material time derivative*** *of a material field* $\Phi(\boldsymbol{X}, t)$*, either scalar or vector-valued, is defined as*

$$\dot{\Phi}(\boldsymbol{X}, t) = \frac{\partial}{\partial t} \Phi(\boldsymbol{X}, t) := \left(\frac{\partial}{\partial t} \Phi(\boldsymbol{Y}, t) \right) \Big|_{\boldsymbol{Y} = \boldsymbol{X}}.$$

When dealing with multi-physics problems one often needs to switch between the Eulerian and the Lagrangian description of a function. For example: Let ϕ be a scalar spatial field, this means $\phi = \phi(\boldsymbol{x}, t)$. Since $\boldsymbol{x} = \boldsymbol{\chi}(\boldsymbol{X}, t)$ one may define $\Phi(\boldsymbol{X}, t) := \phi(\boldsymbol{\chi}(\boldsymbol{X}, t), t)$ and thus one can switch between the two descriptions, provided $\boldsymbol{\chi}$ is known. When one wants to calculate the material time derivative of a spatial field one needs to be cautious. The connection of the two descriptions is given by

Lemma 2.8. *Let* $\phi(\boldsymbol{x}, t)$ *be a given sufficiently smooth function in spatial coordinates and* $\Phi(\boldsymbol{X}, t) := \phi(\boldsymbol{\chi}^{-1}(\boldsymbol{x}, t), t)$*. Then it holds:*

$$\frac{\partial}{\partial t} \Phi(\boldsymbol{X}, t) = \frac{d}{dt} \phi(\boldsymbol{x}, t) = \frac{\partial}{\partial t} \phi(\boldsymbol{x}, t) + (\operatorname{grad} \phi(\boldsymbol{x}, t), \boldsymbol{v}(\boldsymbol{x}, t)).$$

Proof. The proof follows by taking the total derivative $\frac{\mathrm{d}}{\mathrm{d}t}$ of the equation $\Phi(\boldsymbol{X}, t) = \phi(\boldsymbol{\chi}^{-1}(\boldsymbol{x}, t), t) = \phi(\boldsymbol{x}, t)$ and apply the chain rule. □

Remark 2.9. *An analogous result holds for vector-valued functions $\boldsymbol{\phi}(\boldsymbol{x}, t)$:*

$$\frac{\partial}{\partial t}\boldsymbol{\Phi}(\boldsymbol{X}, t) = \frac{d}{dt}\boldsymbol{\phi}(\boldsymbol{x}, t) = \frac{\partial}{\partial t}\boldsymbol{\phi}(\boldsymbol{x}, t) + \operatorname{grad}(\boldsymbol{\phi}(\boldsymbol{x}, t))\boldsymbol{v}(\boldsymbol{x}, t).$$

2.3.3 Deformation Gradient and Displacement

The **deformation gradient** $\mathbf{F}$ is defined as

$$\mathbf{F}(\boldsymbol{X}, t) := \operatorname{Grad} \boldsymbol{x}(\boldsymbol{X}, t) = \operatorname{Grad} \boldsymbol{\chi}(\boldsymbol{X}, t).$$

This special gradient is a Cartesian tensor of order two and can be expressed as

$$\mathbf{F} = \frac{\partial}{\partial X_A} x_b \boldsymbol{e}_b \otimes \boldsymbol{e}_A,$$

or in component form as

$$F_{bA} = \frac{\partial}{\partial X_A} x_b$$

with $x_b = \chi_b(\boldsymbol{X}, t)$. Let us also define the **Jacobian** J as

$$J(\boldsymbol{X}, t) := \det \mathbf{F}(\boldsymbol{X}, t).$$

From a physical point of view it is reasonable to assume that $J \neq 0$ which is justified by the following: Consider the equation $\mathbf{F}\Delta\boldsymbol{X} = \mathbf{0}$ for a small line element $\Delta\boldsymbol{X}$. Provided $\Delta\boldsymbol{X} \neq \mathbf{0}$ $J = 0$ would imply that there is at least one line element whose length is reduced to zero by the deformation, in other words, annihilated. This is physically unrealistic and so one can exclude this from one's consideration. Having that one can ensure that $\mathbf{F}$ is nonsingular and so there exists the inverse $\mathbf{F}^{-1}$ given by

$$\mathbf{F}^{-1}(\boldsymbol{x}, t) = \operatorname{grad} \boldsymbol{X}(\boldsymbol{x}, t),$$

with the components

$$(\mathsf{F}^{-1})_{Ba} = \frac{\partial X_B}{\partial x_a}.$$

From a numerical point of view it is convenient to introduce the **displacement** $\boldsymbol{U}(\boldsymbol{X}, t)$ as

$$\boldsymbol{U}(\boldsymbol{X}, t) := \boldsymbol{x}(\boldsymbol{X}, t) - \boldsymbol{X}.$$

This field relates the position $\boldsymbol{X}$ of a particle P in the undeformed configuration to its position $\boldsymbol{x}$ in the deformed configuration at time t. The displacement $\boldsymbol{U}$ is a function of the material coordinates $\boldsymbol{X}$. One can also define the displacement field in spatial coordinates as

$$\boldsymbol{u}(\boldsymbol{x}, t) = \boldsymbol{x} - \boldsymbol{X}(\boldsymbol{x}, t).$$

Here the position $\boldsymbol{x}$ of a particle P at time t is specified by its position $\boldsymbol{X}(\boldsymbol{x}, t)$ in the reference configuration Ω_r plus its displacement $\boldsymbol{u}(\boldsymbol{x}, t)$ from that position. Due to the correspondence between the reference and current configuration the two descriptions $\boldsymbol{U}$ and $\boldsymbol{u}$ are related by

$$\boldsymbol{u}(\boldsymbol{x}, t) : = \boldsymbol{U}(\boldsymbol{\chi}^{-1}(\boldsymbol{x}, t), t).$$

It should be noted that $\boldsymbol{U}$ and $\boldsymbol{u}$ need to have the same values. Further, when choosing the reference configuration Ω_r to coincide with the initial configuration $\Omega(0)$ one sees that the displacement has to vanish in the reference configuration. This can be expressed as

$$\boldsymbol{U}(\boldsymbol{X}, t = 0) = \boldsymbol{u}(\boldsymbol{x}, t = 0) = \boldsymbol{0}.$$

Having defined the displacement $\boldsymbol{U}$ one immediately sees that

$$\boldsymbol{\chi}(\boldsymbol{X}, t) = \boldsymbol{x}(\boldsymbol{X}, t) = \boldsymbol{X} + \boldsymbol{U}(\boldsymbol{X}, t)$$

and

$$\mathsf{F}(\boldsymbol{X}, t) = \mathsf{I} + \operatorname{Grad} \boldsymbol{U}(\boldsymbol{X}, t),$$

where $\operatorname{Grad} \boldsymbol{u}$ is the **displacement gradient**. Similarly one obtains in spatial coordinates that

$$\operatorname{grad} \boldsymbol{u}(\boldsymbol{x}, t) = \mathsf{I} - \mathsf{F}^{-1}(\boldsymbol{x}, t).$$

Furthermore the **left** and **right Cauchy tensors** are introduced as

$$\mathbf{b} := \mathbf{F}\mathbf{F}^\top,$$
$$\mathbf{C} := \mathbf{F}^\top\mathbf{F}.$$

Subsequent, some basic results about the connection between spatial and material gradients will be established. One can show quite elementarily the following:

Lemma 2.10. *Let $\phi, \boldsymbol{u}$ denote sufficiently smooth scalar and vector valued functions. Then there holds*

$$\operatorname{grad}\phi = \mathbf{F}^{-\top}\operatorname{Grad}\Phi, \tag{2.29}$$
$$\operatorname{grad}\boldsymbol{u} = \operatorname{Grad}(\boldsymbol{U})\mathbf{F}^{-1}. \tag{2.30}$$

Furthermore one can easily show:

Lemma 2.11. *There holds:*

$$\operatorname{Div}(J\mathbf{F}^{-\top}) = \mathbf{0}.$$

This results imply the following

Corollary 2.12 (Nanson's Formula)**.** *Let $\boldsymbol{N}$ be the almost everywhere defined normal vector of $\partial\Omega(0)$ and $\boldsymbol{n}$ the respective normal vector to $\partial\Omega(t)$. Then there holds:*

$$\boldsymbol{n} = J\mathbf{F}^{-\top}\boldsymbol{N}.$$

Finally we want to mention the following lemma.

Lemma 2.13. *Let $\boldsymbol{u}$ be a sufficiently smooth vector field. Then there holds:*

$$\operatorname{div}(\boldsymbol{u}) = \operatorname{Div}(J\mathbf{F}^{-1}\boldsymbol{U}), \tag{2.31}$$
$$\operatorname{Div}(\boldsymbol{U}) = \operatorname{div}(J^{-1}\mathbf{F}^\top\boldsymbol{u}). \tag{2.32}$$

2.3.4 Governing Equations for Nonlinear Elasticity

The governing equations are consequences of the fundamental physical principles of mass conservation and the balance of momentum. From these basic principles one can derive the well know **Cauchy's equation of motion** see [135, Chapter 3] for a precise derivation. Briefly, the theorem states the existence and symmetry of the **stress tensor** $\boldsymbol{\sigma}$ and the balance law

$$\begin{aligned}
\rho(t,\boldsymbol{x})\frac{\mathrm{d}^2}{\mathrm{d}t^2}\boldsymbol{u}(t,\boldsymbol{x}) - \operatorname{div}\boldsymbol{\sigma}(t,\boldsymbol{x}) &= \rho(t,\boldsymbol{x})\boldsymbol{f}(t,\boldsymbol{x}) && \text{in } \Omega(t)\times(0,T),\\
\frac{\mathrm{d}}{\mathrm{d}t}\rho(t,\boldsymbol{x}) + \rho(t,\boldsymbol{x})\operatorname{div}\left(\frac{\mathrm{d}}{\mathrm{d}t}\boldsymbol{u}(t,\boldsymbol{x})\right) &= 0 && \text{in } \Omega(t)\times(0,T),\\
\boldsymbol{\sigma}(t,\boldsymbol{x}) &= (\boldsymbol{\sigma}(t,\boldsymbol{x}))^\top,\\
\boldsymbol{\sigma}(t,\boldsymbol{x})\boldsymbol{n} &= \boldsymbol{g}_N(t,\boldsymbol{x}) && \text{on } \partial\Omega(t)\times(0,T).
\end{aligned}$$

Here ρ is the mass density of $\Omega(t)$, $\boldsymbol{f}$ are the body forces and $\boldsymbol{g}_N$ are the surface traction forces.

With the introduction of the **second Piola-Kirchoff stress tensor**

$$\mathbf{S} := J\mathbf{F}^{-1}\boldsymbol{\sigma}\mathbf{F}^{-\top}$$

one can derive the balance equations of nonlinear elasticity in material coordinates:

$$\begin{aligned}
\rho_0(\boldsymbol{X})\frac{\partial^2}{\partial t^2}\boldsymbol{U}(t,\boldsymbol{X}) - \operatorname{Div}(\mathbf{F}(t,\boldsymbol{X})\mathbf{S}(t,\boldsymbol{X})) &= \rho_0(\boldsymbol{X})\boldsymbol{f}(t,\boldsymbol{X}) && \text{in } \Omega_r\times(0,T),\\
\rho &= \rho_0(\boldsymbol{X})J(t,\boldsymbol{X}),\\
\mathbf{F}(t,\boldsymbol{X})\mathbf{S}(t,\boldsymbol{X})\boldsymbol{N} &= \boldsymbol{G}_N(t,\boldsymbol{X}) && \text{on } \partial\Omega_r\times(0,T).
\end{aligned}$$

The material and spatial formulations are equivalent.

Remark 2.14. *One needs to be careful with traction forces in material coordinates. Consider the case of a pure constant pressure load*

$$\boldsymbol{\sigma}\boldsymbol{n} = -p\boldsymbol{n}.$$

with a constant value $p > 0$. Then in material coordinates this transforms to

$$\mathbf{F}\mathbf{S}\boldsymbol{N} = -pJ\mathbf{F}^{-\top}\boldsymbol{N}.$$

Thus the boundary condition enters the system in a nonlinear way. See [35, Section 2.6 and 5.1] as well as [165] for more details.

The equations given above are not complete. To complete the system one needs to impose initial conditions of the form

$$\begin{aligned} \boldsymbol{u}(0,\boldsymbol{x}) &= \mathbf{0}, \\ \left(\frac{\mathrm{d}}{\mathrm{d}t}\boldsymbol{u}(t,\boldsymbol{x})\right)|_{t=0} &= \boldsymbol{u}_1(\boldsymbol{x}) \end{aligned}$$

or

$$\begin{aligned} \boldsymbol{U}(0,\boldsymbol{X}) &= \mathbf{0}, \\ \frac{\partial}{\partial t}\boldsymbol{U}(0,\boldsymbol{X}) &= \boldsymbol{U}_1(\boldsymbol{X}). \end{aligned}$$

Remark 2.15. *Following [186] one may neglect the terms $\rho\frac{d^2}{dt^2}\boldsymbol{u}$ and $\rho_0\frac{\partial^2}{\partial t^2}\boldsymbol{U}$ as well as body forces when modeling biological tissues. Then one obtains the* ***quasi-stationary*** *balance laws*

$$\begin{aligned} -\operatorname{div}\boldsymbol{\sigma}(t,\boldsymbol{x}) &= \mathbf{0} && \text{in } \Omega(t)\times(0,T), \\ \frac{d}{dt}\rho(t,\boldsymbol{x}) + \rho(t,\boldsymbol{x})\operatorname{div}\left(\frac{d}{dt}\boldsymbol{u}(t,\boldsymbol{x})\right) &= 0 && \text{in } \Omega(t)\times(0,T), \\ \boldsymbol{\sigma}(t,\boldsymbol{x}) &= (\boldsymbol{\sigma}(t,\boldsymbol{x}))^\top, \\ \boldsymbol{\sigma}(t,\boldsymbol{x})\boldsymbol{n} &= \boldsymbol{g}_N(t,\boldsymbol{x}) && \text{on } \partial\Omega(t)\times(0,T). \end{aligned}$$

and

$$\begin{aligned} -\operatorname{Div}(\mathbf{F}(t,\boldsymbol{X})\mathbf{S}(t,\boldsymbol{X})) &= \mathbf{0} && \text{in } \Omega_r\times(0,T), \\ \rho &= \rho_0(\boldsymbol{X})J(t,\boldsymbol{X}), \\ \mathbf{F}(t,\boldsymbol{X})\mathbf{S}(t,\boldsymbol{X})\boldsymbol{N} &= \boldsymbol{G}_N(t,\boldsymbol{X}) && \text{on } \partial\Omega_r\times(0,T). \end{aligned}$$

Furthermore one needs to establish a connection between the tensor $\boldsymbol{\sigma}$ and the displacement $\boldsymbol{u}$ and between $\mathbf{S}$ and $\boldsymbol{U}$ respectively. This is accomplished with **constitutive equations**.

2.3.5 Constitutive Equations

The aim of this part is to link the displacement (or deformation) of a body to the stress. A general treatment is out of the scope of this thesis so only

perfectly hyper-elastic materials will be considered. This excludes plastic deformations as well as damaging or viscous mechanisms. See [11, 18, 85, 135, 177] for a more comprehensive introduction. For a hyper-elastic material one has the existence of the **Helmholtz free-energy function** $W = W(\mathbf{F})$. In addition, provided the material is perfectly elastic one has the relation

$$\mathbf{S} = \mathbf{F}^{-1}\frac{\partial W}{\partial \mathbf{F}}.$$

This equation links the displacement $\boldsymbol{U}$ to the stress $\mathbf{S}$. Furthermore it is common to assume a **normalization condition**, i.e.:

$$W(\mathbf{I}) = 0.$$

If the normalization conditions are not satisfied one needs to account for **residual stresses**, see [3, 40, 76, 136, 156] for more details in the context of myocardial tissue. Moreover, from physical observations it is convenient to assert the following conditions:

$$W(\mathbf{F}) \geq 0, \tag{2.33}$$

$$W(\mathbf{F}(\boldsymbol{U})) < \infty \qquad \text{provided } |\boldsymbol{U}| < \infty, \tag{2.34}$$

$$\lim_{|\boldsymbol{U}|\to\infty} W(\mathbf{F}(\boldsymbol{U})) = \infty. \tag{2.35}$$

If one assumes that the strain energy function should be invariant under translation and rotation of the body $\mathcal{B}$ one obtains that

$$W(\mathbf{F}) = \Psi(\mathbf{C}).$$

Thus one in fact needs to find a constitutive relation that depends only on $\mathbf{C}$. Together with all the above stated assumptions one can conclude the following relations

$$\mathbf{S} = 2\frac{\partial \Psi(\mathbf{C})}{\partial \mathbf{C}},$$
$$\boldsymbol{\sigma} = 2J^{-1}\mathbf{F}\frac{\partial \Psi(\mathbf{C})}{\partial \mathbf{C}}\mathbf{F}^{\top}.$$

In the numerical treatment of nonlinear elastic materials one also needs the **elasticity tensor** in material coordinates $\mathbb{C}$ defined by

$$\mathbb{C} := 2\frac{\partial \mathbf{S}(\mathbf{C})}{\partial \mathbf{C}} = 4\frac{\partial^2 \Psi(\mathbf{C})}{\partial \mathbf{C}\partial \mathbf{C}}.$$

This is a tensor of order four. One can show, see [85, Chapter 6.6], that this tensor possess **minor** and **major** symmetries, i.e.

$$C_{ijkl} = C_{jikl} = C_{ijlk},$$
$$C_{ijkl} = C_{klij}.$$

In spatial coordinates the elasticity tensor is defined by

$$\mathbb{c}(a,b,c,d) := J^{-1} F_{aA} F_{bB} F_{cC} F_{dD} C_{ABCD}.$$

The spatial elasticity tensor inherits the properties of $\mathbb{C}$.

Remark 2.16. *The elasticity tensor $\mathbb{C}$ is convenient from a numerical point of view. Due to its symmetry properties one can use **Voigt's notation** and write $\mathbb{C}$ as a symmetric $\frac{d(d+1)}{2} \times \frac{d(d+1)}{2}$ matrix for example ($d = 3$)*

$$\mathsf{C}^V := \begin{pmatrix} C_{1111} & C_{1122} & C_{1133} & C_{1112} & C_{1123} & C_{1113} \\ & C_{2222} & C_{2233} & C_{2212} & C_{2223} & C_{2213} \\ & & C_{3333} & C_{3312} & C_{3323} & C_{3313} \\ & & & C_{1212} & C_{1223} & C_{1213} \\ & & & & C_{2323} & C_{2313} \\ & sym. & & & & C_{1313} \end{pmatrix}.$$

A symmetric second order tensor can also be written in Voigt notation ($d = 3$)as

$$\boldsymbol{S}^V := (S_{11}, S_{22}, S_{33}, 2S_{12}, 2S_{23}, 2S_{13})^\top.$$

With this convention it holds that

$$\mathsf{C}^V \boldsymbol{S}^V = (\mathbb{C} : \mathsf{S})^V.$$

However the following does not hold

$$\left(\mathsf{C}^V \boldsymbol{S}_1^V, \boldsymbol{S}_2^V\right) \neq \mathsf{S}_2 : \mathbb{C} : \mathsf{S}_1.$$

*A remedy is to use the **Mandel notation**. Here one defines*

$$\mathsf{C}^M := \begin{pmatrix} C_{1111} & C_{1122} & C_{1133} & \sqrt{2}C_{1112} & \sqrt{2}C_{1123} & \sqrt{2}C_{1113} \\ & C_{2222} & C_{2233} & \sqrt{2}C_{2212} & \sqrt{2}C_{2223} & \sqrt{2}C_{2213} \\ & & C_{3333} & \sqrt{2}C_{3312} & \sqrt{2}C_{3323} & \sqrt{2}C_{3313} \\ & & & 2C_{1212} & 2C_{1223} & 2C_{1213} \\ & & & & 2C_{2323} & 2C_{2313} \\ & sym. & & & & 2C_{1313} \end{pmatrix}$$

and

$$\boldsymbol{S}^M := (S_{11}, S_{22}, S_{33}, \sqrt{2}S_{12}, \sqrt{2}S_{23}, \sqrt{2}S_{13})^\top.$$

In this notation one has

$$\left(\mathbf{C}^M \boldsymbol{S}_1^M, \boldsymbol{S}_2^M\right) = \mathbf{S}_2 : \mathbb{C} : \mathbf{S}_1.$$

For more details on this topic we refer to [80].

2.3.6 Almost Incompressible Materials

Biological materials are treated as slightly incompressible materials. This means that $\det(\mathbf{F}) \approx 1$, see [183]. To account for this behavior one needs to adapt the constitutive equations. An approach to handle nearly incompressible materials, with $J = \det \mathbf{F}$ close to one, is the decoupling of the deformation into a **volumetric** (i.e. volume changing) and an **isochoric** (i.e. volume preserving) part, see [67, 85] for more details. This means that one decomposes

$$\mathbf{F} = (J^{\frac{1}{3}}\mathbf{I})\overline{\mathbf{F}}$$

where $\det \overline{\mathbf{F}} = 1$. This is called the **Flory split**. Thus one also has the splitting

$$\mathbf{C} = (J^{\frac{2}{3}}\mathbf{I})\overline{\mathbf{C}}$$

The Flory split allows to postulate an additive splitting of the strain energy function

$$\Psi(\mathbf{C}) = U(J) + \overline{\Psi}(\overline{\mathbf{C}}) \tag{2.36}$$

where $U(J)$ is a strictly convex function called **volumetric response function** and attains its unique minimum for $J = 1$. The function $\overline{\Psi}(\overline{\mathbf{C}})$ is called **isochoric response function**. It is required that

$$U(J) = 0 \Leftrightarrow J = 1,$$
$$\overline{\Psi}(\overline{\mathbf{C}}) = 0 \Leftrightarrow \overline{\mathbf{C}} = \mathbf{I}.$$

for fulfilling the normalization conditions.

Remark 2.17 (Specific volumetric response functions)**.** *The function $U(J)$ can be interpreted as a penalization for the constraint* $\det \mathbf{F} = 1$*, see [24, Chapter 6]. There exist a variety of possible choices for $U(J)$. We will consider the choice*

$$U(J) := \frac{\kappa}{2}(J-1)^2$$

or

$$U(J) := \frac{\kappa}{2}(\ln J)^2$$

with $\kappa \in \mathbb{R}^+$.

Example 2.18 (Almost incompressible neo-Hookean material)**.** The simplest nonlinear model is the so called **almost incompressible neo-Hookean material model**. There one has

$$\Psi(\mathbf{C}) := U(J) + \frac{\mu}{2}\left(\operatorname{tr}(\overline{\mathbf{C}}) - 3\right),$$

where the material parameter μ may be interpreted as the shear modulus. By definition this value is positive, i.e. $\mu > 0$. For more examples we refer to [11, Page 33].

Before continuing, the deviatoric operators in material and spatial coordinates will be introduced.

Definition 2.19 (Deviatoric operators)**.** *Let* $\mathbf{a}$ *and* $\mathbf{A}$ *be two tensor-valued functions in spatial and material coordinates. Then the* ***deviatoric operators*** *are defined as*

$$\operatorname{dev}(\mathbf{a}) := \mathbf{a} - \frac{1}{3}\operatorname{tr}(\mathbf{a})\mathbf{I},$$
$$\operatorname{Dev}(\mathbf{A}) := \mathbf{A} - \frac{1}{3}\left[\mathbf{A} : \mathbf{C}\right]\mathbf{C}^{-1}.$$

Further the following result is needed:

Lemma 2.20. *There holds:*

$$\frac{\partial J}{\partial \mathbf{C}} = \frac{J}{2}\mathbf{C}^{-1},$$
$$\frac{\partial J^{-\frac{2}{3}}}{\partial \mathbf{C}} = -\frac{1}{3}J^{-\frac{2}{3}}\mathbf{C}^{-1}.$$

Proof. See [85, Page 228]. □

With the help of these results one can prove that the Flory split (2.36) results in an additive split of the stress tensor $\mathbf{S}$ as well as the elasticity tensor $\mathbb{C}$

$$\begin{aligned}\mathbf{S} &= \mathbf{S}_{\text{vol}} + \mathbf{S}_{\text{iso}},\\ \mathbb{C} &= \mathbb{C}_{\text{vol}} + \mathbb{C}_{\text{iso}}.\end{aligned}$$

see [85, Chapter 6.4] and [11, Page 29 and Page 45]. Here one has

$$\begin{aligned}\mathbf{S}_{\text{vol}} &:= Jp\mathbf{C}^{-1},\\ \mathbf{S}_{\text{iso}} &:= 2J^{-\frac{2}{3}}\text{Dev}\left(\frac{\partial\overline{\Psi}(\overline{\mathbf{C}})}{\partial\overline{\mathbf{C}}}\right),\\ \mathbb{C}_{\text{vol}} &:= J\left(p + J\frac{\mathrm{d}^2U(J)}{\mathrm{d}J^2}\right)\mathbf{C}^{-1}\otimes\mathbf{C}^{-1} - 2Jp\mathbf{C}^{-1}\odot\mathbf{C}^{-1},\\ \mathbb{C}_{\text{iso}} &:= 2\frac{\partial\mathbf{S}_{\text{iso}}}{\partial\mathbf{C}}\end{aligned}$$

where the **hydrostatic pressure** p is defined as

$$p := \frac{\mathrm{d}U(J)}{\mathrm{d}J}.$$

and the relation "$\odot$" is defined for a symmetric tensor $\mathbf{A}$ as

$$(\mathbf{A}\odot\mathbf{A})_{ijkl} := \frac{1}{2}\left(A_{ik}A_{jl} + A_{il}A_{jk}\right)$$

see [85, Equation (6.164)]. The same procedure can be applied in spatial coordinates and one obtains

$$\begin{aligned}\boldsymbol{\sigma} &= \boldsymbol{\sigma}_{\text{vol}} + \boldsymbol{\sigma}_{\text{iso}},\\ \boldsymbol{\sigma}_{\text{vol}} &:= p\mathbf{I},\\ \boldsymbol{\sigma}_{\text{iso}} &:= 2J^{-1}\text{dev}\left(\overline{\mathbf{F}}\frac{\partial\overline{\Psi}(\overline{\mathbf{C}})}{\partial\overline{\mathbf{C}}}\overline{\mathbf{F}}^{\top}\right),\\ \mathfrak{c}_{\text{vol}} &:= \left(p + J\frac{\mathrm{d}^2U(J)}{\mathrm{d}J^2}\right)\mathbf{I}\otimes\mathbf{I} - 2p\mathbb{I}.\end{aligned}$$

The decoupling of the stress tensors applied to the quasi-stationary equations of nonlinear elasticity mentioned in Remark 2.15 leads to nonlinear saddle-point problems of the form

$$-\operatorname{div}\left(\boldsymbol{\sigma}_{\text{iso}}(\boldsymbol{u}(t,\boldsymbol{x})) + \boldsymbol{\sigma}_{\text{vol}}(p(t,\boldsymbol{x}),\boldsymbol{u}(t,\boldsymbol{x}))\right) = 0, \qquad \text{in } \Omega(t), \tag{2.37}$$

$$\frac{\mathrm{d}U(J(\boldsymbol{u}(t,\boldsymbol{x}))}{\mathrm{d}J} - p(t,\boldsymbol{x}) = 0 \qquad \text{in } \Omega(t), \tag{2.38}$$

and equivalently

$$-\operatorname{Div}\left(\mathbf{F}(\boldsymbol{U}(t,\boldsymbol{X})\left(\mathbf{S}_{\text{iso}}(\boldsymbol{U}(t,\boldsymbol{X})) + \mathbf{S}_{\text{vol}}(P(t,\boldsymbol{X}),\boldsymbol{U}(t,\boldsymbol{X}))\right)\right) = 0, \quad \text{in } \Omega_r, \tag{2.39}$$

$$\frac{\mathrm{d}U(J(\boldsymbol{U}(t,\boldsymbol{X}))}{\mathrm{d}J} - P(t,\boldsymbol{X}) = 0 \quad \text{in } \Omega_r. \tag{2.40}$$

The discretization of such a system may still suffer from locking phenomena, see [24, Chapter 6]. One possible remedy is to interpret $(\boldsymbol{U}, J, P)$ as independent variables and modify the system to

$$-\operatorname{Div}\left(\mathbf{F}(\boldsymbol{U})\left(\mathbf{S}_{\text{iso}}(\boldsymbol{U},J) + \mathbf{S}_{\text{vol}}(\boldsymbol{U},P,J)\right)\right) = 0, \qquad \text{in } \Omega_r, \tag{2.41}$$

$$\frac{\mathrm{d}U(D)}{\mathrm{d}D}\Big|_{D=J} - P = 0 \qquad \text{in } \Omega_r, \tag{2.42}$$

$$J - \det \mathbf{F}(\boldsymbol{U}) = 0 \qquad \text{in } \Omega_r. \tag{2.43}$$

A discretization of such a three-field approach will lead to the **mean dilatation technique**, see [24, Chapter 6].

2.3.7 Plain Strain Elasticity

In some cases it is justified to consider two-dimensional problems in elasticity. With the help of an example the differences to the three dimensional case will be sketched. For a detailed discussion we refer to [135, Section 5.2.6]. For the plain strain elastic case one has three important assumptions. The first one is that the geometry has the shape $\Omega_r = \Omega_r^{\text{2D}} \times [-Z, Z]$ with $Z \gg \operatorname{diam}(\Omega_r^{\text{2D}})$. The second assumption is that all exterior forces are orthogonal to the z-axis

and depend only on x and y. Finally it is assumed that the displacement has the form $\boldsymbol{U}(\boldsymbol{X}) = (U_1(X,Y), U_2(X,Y), C)$ with $C \in \mathbb{R}$. With this one has that the deformation gradient is of the form

$$\mathbf{F} = \begin{pmatrix} 1+\frac{\partial U_1}{\partial X} & \frac{\partial U_1}{\partial Y} & 0 \\ \frac{\partial U_2}{\partial X} & 1+\frac{\partial U_2}{\partial Y} & 0 \\ 0 & 0 & 1 \end{pmatrix} = \begin{pmatrix} \underline{\mathbf{F}} & \mathbf{0} \\ \mathbf{0}^\top & 1 \end{pmatrix}.$$

This implies first that $\det(\mathbf{F}) = \det(\underline{\mathbf{F}})$ and that $\mathbf{C} = \mathbf{F}^\top\mathbf{F}$ and $\mathbf{C}^{-1} = \mathbf{F}^{-1}\mathbf{F}^{-\top}$ have the same structure, i.e.

$$\mathbf{C} = \begin{pmatrix} \underline{\mathbf{C}} & \mathbf{0} \\ \mathbf{0}^\top & 1 \end{pmatrix}, \qquad \mathbf{C}^{-1} = \begin{pmatrix} \underline{\mathbf{C}}^{-1} & \mathbf{0} \\ \mathbf{0}^\top & 1 \end{pmatrix}$$

Now, consider the free energy function for an almost incompressible neo-Hookean solid

$$\Psi(\mathbf{C}) = \frac{\kappa}{2}(\ln J)^2 + \frac{\mu}{2}\left(\operatorname{tr}(\overline{\mathbf{C}}) - 3\right)$$

where $J = \det \mathbf{F}$ and $\overline{\mathbf{C}} = J^{-\frac{2}{3}}\mathbf{C}$. One may calculate the second Piola-Kirchoff tensor $\mathbf{S}$ as $\mathbf{S} = 2\frac{\partial \Psi(\mathbf{C})}{\partial \mathbf{C}}$ and obtain

$$\mathbf{S} = \kappa \ln(J)\mathbf{C}^{-1} + \mu J^{-\frac{2}{3}}\left(\mathbf{I} - \frac{1}{3}(\operatorname{tr}\mathbf{C})\mathbf{C}^{-1}\right).$$

Inserting the special form of $J = \det \underline{\mathbf{F}}$, $\mathbf{C}$ and $\mathbf{C}^{-1}$ one obtains

$$\mathbf{S} = \begin{pmatrix} \underline{\mathbf{S}} & \mathbf{0} \\ \mathbf{0}^\top & S_{33} \end{pmatrix}$$

where

$$\begin{aligned} \underline{\mathbf{S}} &= \kappa \ln(J)\underline{\mathbf{C}}^{-1} + \mu J^{-\frac{2}{3}}\left(\mathbf{I} - \frac{1}{3}(\operatorname{tr}(\underline{\mathbf{C}}) + 1)\underline{\mathbf{C}}^{-1}\right), \\ S_{33} &= \kappa \ln(J) + \mu J^{-\frac{2}{3}}\left(\frac{2}{3} - \frac{1}{3}\operatorname{tr}(\underline{\mathbf{C}})\right). \end{aligned}$$

Note that in general $S_{33} \neq 0$ but $S_{33} = S_{33}(X,Y)$. Plugging this into the equilibrium equations one gets that

$$-\operatorname{Div}(\underline{\mathbf{F}}(\boldsymbol{U}(X,Y))\underline{\mathbf{S}}(\boldsymbol{U}(X,Y)) = 0$$

where the divergence is taken only with respect to X and Y.

2.3.8 Constitutive Equations for Passive Myocardial Tissue

As discussed in Section 2.1.1, myocardial tissue is a strong anisotropic material. Hence an appropriate constitutive equation needs to account for the specific anisotropy of the underlying material. There have been several attempts to model myocardial tissue, we refer to [41, 77, 89, 162, 163, 192] for more details. We will use a model recently introduced in [55, 56, 84]. This model is based on an invariant-type formulation. For more details about invariant type strain energy functions we refer to [85, 135, 170]. The strain energy function is given by

$$\begin{aligned}\Psi(\mathbf{C}) = U(J) + \frac{a}{2b}\left(\exp\left[b(\overline{I}_1 - d)\right] - 1\right) + \frac{a_f}{2b_f}\left(\exp\left[b_f(\overline{I}_{4f} - 1)^2\right] - 1\right) \\ + \frac{a_s}{2b_s}\left(\exp\left[b_s(\overline{I}_{4s} - 1)^2\right] - 1\right) + \frac{a_{fs}}{2b_{fs}}\left(\exp\left[b_{fs}\overline{I}_{8fs}^2\right] - 1\right).\end{aligned}$$

The invariants are defined by

$$\begin{aligned}\overline{I}_1(\overline{\mathbf{C}}) &:= \operatorname{tr}\left(\overline{\mathbf{C}}\right), \\ \overline{I}_{4f}(\overline{\mathbf{C}}) &:= \left(\overline{\mathbf{C}}\boldsymbol{f}_0, \boldsymbol{f}_0\right), \qquad \overline{I}_{4s}(\overline{\mathbf{C}}) := \left(\overline{\mathbf{C}}\boldsymbol{s}_0, \boldsymbol{s}_0\right), \\ \overline{I}_{8fs}(\overline{\mathbf{C}}) &:= \left(\overline{\mathbf{C}}\boldsymbol{f}_0, \boldsymbol{s}_0\right).\end{aligned}$$

It needs to be mentioned that the terms involving $\overline{I}_{4f}, \overline{I}_{4s}$ are only active if $\overline{I}_{4f} > 1$ and $\overline{I}_{4s} > 1$. All occurring parameters are assumed to be positive. We refer to [55, Section 4.2.4] and [11, Section 3.15] for a specific choice of parameters and the explicit calculation of the stress tensors $\mathbf{S}_{\text{iso}}$ and $\mathbb{C}_{\text{iso}}$.

2.4 Models for Coupled Electro-Mechanics

In this chapter the presented models for the electrical and mechanical response of the human heart will be merged. This leads to a coupled multi-physics problem. There are different approaches to couple the electrical and mechanical response in the human heart, hence we try to give a summary on the models known in literature, see [43, 131, 134, 139, 186] and the bibliography found in these articles for more details.

2.4.1 Mechano-electric Feedback

We start with coupling the Bidomain equations to the mechanical response. In literature this is called the **mechano-electric feedback** (MEF), see [5, 6, 33, 104, 124, 126, 144]. As a matter of fact, one has a moving body in the coupled setting. Thus one first needs to specify the material and spatial description of these equations. From a physical point of view one should state the Bidomain equations in a spatial description. Thus one needs to remodel the equations with respect to moving domains. This includes the application of Reynold's transport theorem see [78, Page 78] and an energy balance equation. For more details we refer to [5, 151, 152]. The Bidomain equations in spatial coordinates can be stated as

$$\begin{aligned}\frac{\partial V_{\mathrm{tm}}}{\partial t} + \operatorname{div}(\dot{\boldsymbol{u}} V_{\mathrm{tm}}) + \mathrm{I}_{\mathrm{ion}}(V_{\mathrm{tm}}, \boldsymbol{v}) - \operatorname{div}(\mathbf{M}_i \operatorname{grad} V_{\mathrm{tm}}) - \operatorname{div}(\mathbf{M}_i \operatorname{grad} u_e) &= s_i,\\ - \operatorname{div}(\mathbf{M}_i \operatorname{grad} V_{\mathrm{tm}}) - \operatorname{div}((\mathbf{M}_i + \mathbf{M}_e) \operatorname{grad} u_e) &= 0,\\ \frac{\partial \boldsymbol{v}}{\partial t} + \operatorname{div}(\dot{\boldsymbol{u}} \otimes \boldsymbol{v}) + \boldsymbol{H}(V_{\mathrm{tm}}, \boldsymbol{v}) &= \mathbf{0}.\end{aligned}$$

For the subsequent considerations we will restrict ourselves to ionic models where $\boldsymbol{v} = v$ i.e. only one ionic variable. The mechanical coupling can be accomplished by two parts. First one may consider the coupling induced by the change of geometry. The equations of nonlinear elasticity are better suited for a material description so one transforms the spatial formulation of the Bidomain equations to material coordinates.

Lemma 2.21. *There holds:*

$$\frac{\partial J}{\partial t} = J \operatorname{div}(\dot{\boldsymbol{u}}).$$

Proof. See [78, Page 77 (2)]. □

Lemma 2.22. *There holds:*

$$\frac{\partial V_{\mathrm{tm}}}{\partial t} + \operatorname{div}(\dot{\boldsymbol{u}} V_{\mathrm{tm}}) = J^{-1} \frac{\partial}{\partial t}(J V_{\mathrm{tm}}).$$

Proof. The proof follows by direct calculation and application of Lemma 2.21:

$$\begin{aligned}\frac{\partial}{\partial t}(J(t,\boldsymbol{X})V_{\mathrm{tm}}(t,\boldsymbol{x}(t,\boldsymbol{X}))) &= \frac{\partial J}{\partial t}V_{\mathrm{tm}}(t,\boldsymbol{x}) + J\left[\left(\frac{\partial V_{\mathrm{tm}}}{\partial \boldsymbol{x}},\frac{\partial \boldsymbol{x}}{\partial t}\right)+\frac{\partial V_{\mathrm{tm}}}{\partial t}\right]\\ &= J\,\mathrm{div}(\dot{\boldsymbol{u}}) + J\left[\left(\mathrm{grad}\,V_{\mathrm{tm}},\frac{\partial \boldsymbol{x}}{\partial t}\right)+\frac{\partial V_{\mathrm{tm}}}{\partial t}\right]\\ &= J\left(\mathrm{div}(\dot{\boldsymbol{u}}V_{\mathrm{tm}})+\frac{\partial V_{\mathrm{tm}}}{\partial t}\right).\end{aligned}$$

□

Together with Lemmata 2.13 and 2.10 one obtains the Bidomain equations in material coordinates as

$$\begin{aligned}&\frac{\partial}{\partial t}(JV_{\mathrm{tm}}) + J\mathrm{I}_{\mathrm{ion}}(V_{\mathrm{tm}},v)\\ &\quad - J\,\mathrm{Div}\left(J\mathbf{F}^{-1}\mathbf{M}_i\mathbf{F}^{-\top}\,\mathrm{Grad}\,V_{\mathrm{tm}}\right) - J\,\mathrm{Div}\left(J\mathbf{F}^{-1}\mathbf{M}_i\mathbf{F}^{-\top}\,\mathrm{Grad}\,u_e\right) = Js_i,\\ &\quad - J\,\mathrm{Div}\left(J\mathbf{F}^{-1}\mathbf{M}_i\mathbf{F}^{-\top}\,\mathrm{Grad}\,V_{\mathrm{tm}}\right) - J\,\mathrm{Div}\left(J\mathbf{F}^{-1}\mathbf{M}_{i+e}\mathbf{F}^{-\top}\,\mathrm{Grad}\,u_e\right) = 0\end{aligned}$$

and the equations for the ionic variables in material coordinates

$$\frac{\partial}{\partial t}(J\boldsymbol{v}) + J\boldsymbol{H}(V_{\mathrm{tm}},\boldsymbol{v}) = \mathbf{0}.$$

In literature one usually sees that the term $\mathrm{Div}\left(J\mathbf{F}^{-1}\mathbf{M}_i\mathbf{F}^{-\top}\,\mathrm{Grad}\,V_{\mathrm{tm}}\right)$ is replaced by $\mathrm{Div}\left(J\mathbf{M}_i\mathbf{C}^{-1}\,\mathrm{Grad}\,V_{\mathrm{tm}}\right)$. To justify this one needs to pose an assumption on the tensors $\mathbf{M}_i, \mathbf{M}_e$.

Lemma 2.23. *Provided $\mathbf{M}_i$ is symmetric, $\mathbf{M}_i(\boldsymbol{x})\boldsymbol{n} = \alpha\boldsymbol{n}$ and $\mathbf{M}_i(\boldsymbol{X})\boldsymbol{N} = \alpha\boldsymbol{N}$ where $\boldsymbol{n}$ and $\boldsymbol{N}$ are the respective normal vectors to $\partial\Omega(t)$ and $\partial\Omega_r$, there holds:*

$$\int_{\Omega(t)} \mathrm{div}(\mathbf{M}_i\,\mathrm{grad}\,u)\;\mathrm{d}\boldsymbol{x} = \int_{\Omega_r}\mathrm{Div}(J\mathbf{M}_i\mathbf{C}^{-1}\,\mathrm{Grad}\,U)\;\mathrm{d}\boldsymbol{x}\,.$$

Proof. The proof follows by direct calculation:

$$\begin{aligned}
\int_{\Omega(t)} \operatorname{div}(\mathbf{M}_i \operatorname{grad} u)\ \mathrm{d}\boldsymbol{x} &= \int_{\partial\Omega(t)} (\mathbf{M}_i \operatorname{grad} u, \boldsymbol{n})\ \mathrm{ds}_{\boldsymbol{x}} = \int_{\partial\Omega(t)} (\operatorname{grad} u, \mathbf{M}_i \boldsymbol{n})\ \mathrm{ds}_{\boldsymbol{x}} \\
&= \alpha \int_{\partial\Omega(t)} (\operatorname{grad} u, \boldsymbol{n})\, \mathrm{ds}_{\boldsymbol{x}} = \alpha \int_{\partial\Omega_r} \left(\mathbf{F}^{-\top} \operatorname{Grad} U, J\mathbf{F}^{-\top}\boldsymbol{N}\right) \mathrm{ds}_{\boldsymbol{x}} \\
&= \alpha \int_{\partial\Omega_r} \left(J\mathbf{F}^{-1}\mathbf{F}^{-\top} \operatorname{Grad} U, \boldsymbol{N}\right) \mathrm{ds}_{\boldsymbol{x}} \\
&= \int_{\partial\Omega_r} \left(J\mathbf{C}^{-1} \operatorname{Grad} U, \mathbf{M}_i\boldsymbol{N}\right) \mathrm{ds}_{\boldsymbol{x}} \\
&= \int_{\Omega_r} \operatorname{Div}(J\mathbf{M}_i\mathbf{C}^{-1} \operatorname{Grad} U)\ \mathrm{d}\boldsymbol{x}
\end{aligned}$$

□

It still remains to represent the tensors $\mathbf{M}_i, \mathbf{M}_e$ in spatial and material coordinates. To the best of the authors knowledge there is no consensus in the existing literature about the interplay between diffusion and deformation and it is an actual research topic. See [5, 6, 23, 44, 103, 126, 186] and references therein for an overview on the ongoing discussion. We will assume that the orthonormal coordinate system $\{\boldsymbol{f}_0, \boldsymbol{s}_0, \boldsymbol{n}_0\}$ is given and fixed in material coordinates. Therefore we may assume that the conductivity tensor in material coordinates is given as

$$\mathbf{M}_i^{\mathrm{mat}} := m_i^f \boldsymbol{f}_0(\boldsymbol{X}) \otimes \boldsymbol{f}_0(\boldsymbol{X}) + m_i^s \boldsymbol{s}_0(\boldsymbol{X}) \otimes \boldsymbol{s}_0(\boldsymbol{X}) + m_i^n \boldsymbol{n}_0(\boldsymbol{X}) \otimes \boldsymbol{n}_0(\boldsymbol{X}).$$

If we take a smooth scalar function of material coordinates Φ we see that

$$\mathbf{M}_i^{\mathrm{mat}} \operatorname{Grad}\Phi = m_i^f(\boldsymbol{f}_0, \operatorname{Grad}\Phi)\boldsymbol{f}_0 + m_i^s(\boldsymbol{s}_0, \operatorname{Grad}\Phi)\boldsymbol{s}_0 + m_i^n(\boldsymbol{n}_0, \operatorname{Grad}\Phi)\boldsymbol{n}_0.$$

This means we get a transport of $m_i^f(\boldsymbol{f}_0, \operatorname{Grad}\Phi)$ in the direction of $\boldsymbol{f}_0$ and respectively for the other vectors. This motivates the definition of the spatial diffusion tensor as

$$\mathbf{M}_i^{\mathrm{space}} := m_i^f \mathbf{F}\boldsymbol{f}_0 \otimes \mathbf{F}\boldsymbol{f}_0 + m_i^s \mathbf{F}\boldsymbol{s}_0 \otimes \mathbf{F}\boldsymbol{s}_0 + m_i^n \mathbf{F}\boldsymbol{n}_0 \otimes \mathbf{F}\boldsymbol{n}_0.$$

After applying basic rules for the "$\otimes$"-product we obtain

$$\mathbf{M}_i^{\text{space}} = \mathbf{F}\mathbf{M}_i^{\text{mat}}\mathbf{F}^\top. \tag{2.44}$$

The above transformation is referred to as a **push-forward operation** for a **contravariant second-order tensor**. For a more detailed discussion on co- and contravariant tensors we refer to [85, 115, 135]. For more on the contravariant nature of a conductivity tensor we refer to [74]. Having fixed the relation between spatial and material form of the conductivity tensors $\mathbf{M}_i$, $\mathbf{M}_e$ as in (2.44) one sees that

$$J \operatorname{Div}\left(J\mathbf{F}^{-1}\mathbf{M}_i^{\text{space}}\mathbf{F}^{-\top} \operatorname{Grad} V_{\text{tm}}\right) = J \operatorname{Div}\left(J\mathbf{M}_i^{\text{mat}} \operatorname{Grad} V_{\text{tm}}\right).$$

A different kind of coupling is achieved by modifying the ionic currents and include deformation dependent variables. In general this means that one gets a new ionic current

$$\overline{\mathrm{I}_{\text{ion}}} = \mathrm{I}_{\text{ion}}(V_{\text{tm}}, \boldsymbol{v}) + \mathrm{I}_{\text{MEF}}(V_{\text{tm}}, \boldsymbol{w}, \boldsymbol{U}).$$

Here $\boldsymbol{w}$ is a new set of additional ionic variables which are sensitive to deformation. There are several models known in literature, for example [139, 140, 141, 150] and a lot more to be found in the CellML database. To specify the explicit dependence on $\boldsymbol{U}$ one usually assumes that the ionic current depends only on the stretch $\lambda_f := (\mathbf{C}\boldsymbol{f}_0, \boldsymbol{f}_0)$ in the fiber direction and on the stretch ratio $\frac{\partial}{\partial t}\lambda_f$. Two examples of models which are dependent on the stretch can be found in [33] and [95]. The first one is given by

$$\mathrm{I}_{\text{MEF}} := \begin{cases} g_s(V_{\text{tm}} - V_s)(\lambda_f - 1) & \text{if } \lambda_f > 1, \\ 0 & \text{else}, \end{cases}$$

with defined constants g_s, V_s. The second example is given by

$$\mathrm{I}_{\text{MEF}} := g_s(V_{\text{tm}} - V_s)\frac{1}{1 + \exp\left(-\delta(\lambda_f - 1)\right)}.$$

It is convenient to summarize such models in the form

$$\mathrm{I}_{\text{MEF}} := g_s(V_{\text{tm}} - V_s)g(\lambda_f). \tag{2.45}$$

2.4.2 Coupling Electrics to Mechanics

After discussing the coupling of the mechanical behavior to the electrical behavior we are interested in the other direction. In literature, see for example [6] and references therein, one may distinguish two popular approaches the **active strain**, see [5, 33, 124, 125, 175], and the **active stress** approach, see [73, 95, 141, 169]. The first approach is based on a splitting of the deformation gradient $\mathbf{F}$

$$\mathbf{F} = \mathbf{F}_{\text{pass}}\mathbf{F}_{\text{act}}$$

into an purely passive and an active deformation. In this case one obtains different governing equations and needs to provide a suitable constitutive relation for the active deformation $\mathbf{F}_{\text{act}}$. For the second approach one fixes the macroscopic passive constitutive behavior of the elastic material and then add a suitable active stress term

$$\mathbf{S} = \mathbf{S}_{\text{pass}} + \mathbf{S}_{\text{act}}.$$

We will focus on the active stress approach since it can be incorporated into existing solvers for nonlinear elasticity without major recoding. We will use the active stress model proposed in [6, (4.10)]. There one has

$$\mathbf{S}_{\text{act}} := T_a(V_{\text{tm}}, \boldsymbol{w}) I_{4f}(\mathbf{C})^{-\frac{1}{2}}(\boldsymbol{f}_0 \otimes \boldsymbol{f}_0). \tag{2.46}$$

Here $T_a(V_{\text{tm}}, \boldsymbol{w})$ is a function which describes the strength of active tension generated in the direction of the fibers $\boldsymbol{f}_0$. It may depend on additional internal variables $\boldsymbol{w}$ (for example the internal calcium concentration). We will use the following form taken from [73, Page 329]:

$$\begin{aligned}
\frac{\partial}{\partial t} T_a &= \epsilon(V_{\text{tm}}) \left(k_a(V_{\text{tm}} - V_r) - T_a\right), \\
\epsilon(V_{\text{tm}}) &:= \epsilon_0 + (\epsilon_\infty - \epsilon_0) \exp\left(-\exp\left(-\xi\left(V_{\text{tm}} - \overline{V}\right)\right)\right).
\end{aligned}$$

The function $\epsilon(V_{\text{tm}})$ is a smooth approximation of the Heaviside-function used in [126, Page 511]. It is used to account for the delay of mechanical response to electric potentials. An example of the function $\epsilon(V_{\text{tm}})$ is depicted in Figure 2.9.

Remark 2.24. *The elasticity tensor $\mathbb{C}_{act}$ can be calculated as*

$$\mathbb{C}_{act} = 2\frac{\partial \mathbf{S}_{act}}{\partial \mathbf{C}} = -T_a(V_{\text{tm}}, \boldsymbol{w}) I_{4f}(\mathbf{C})^{-\frac{3}{2}} \boldsymbol{f}_0 \otimes \boldsymbol{f}_0 \otimes \boldsymbol{f}_0 \otimes \boldsymbol{f}_0.$$

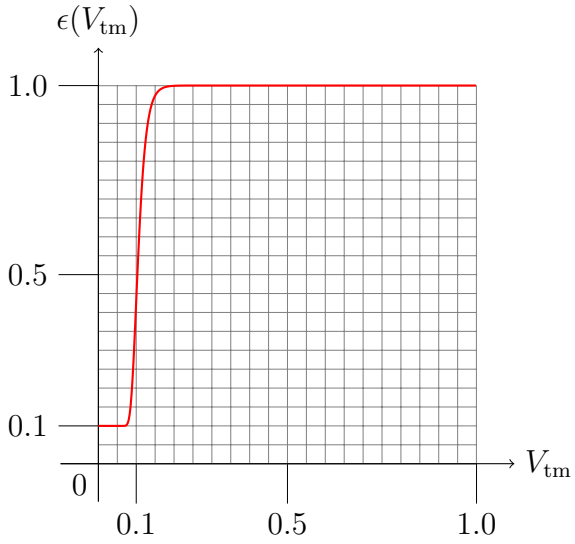

Figure 2.9: An example for the function $\epsilon(V_{\text{tm}})$. The parameters have been set to $\epsilon_0 = 0.1$, $\epsilon_\infty = 1.0$, $\xi = 70$ and $\overline{V} = 0.1$.

Summary

Summarizing all the results from before one arrives at the following fully coupled system of cardiac electro-mechanics written in material coordinates.

Find $(V_{\text{tm}}, u_e, \boldsymbol{v}, T_a, \boldsymbol{U})$ *such that*

$$\begin{aligned}
\frac{\partial}{\partial t}(JV_{\text{tm}}) + J\overline{\text{I}_{\text{ion}}} - J\,\text{Div}(J\mathbf{M}_i\,\text{Grad}\,V_{\text{tm}}) - J\,\text{Div}(J\mathbf{M}_i\,\text{Grad}\,u_e) &= Js_i,\\
-J\,\text{Div}(J\mathbf{M}_i\,\text{Grad}\,V_{\text{tm}}) - J\,\text{Div}(J\mathbf{M}_{i+e}\,\text{Grad}\,u_e) &= 0,\\
\frac{\partial}{\partial t}(J\boldsymbol{v}) + J\boldsymbol{H}(V_{\text{tm}}, \boldsymbol{v}) &= \mathbf{0},\\
\frac{\partial}{\partial t}(JT_a) + J\epsilon(V_{\text{tm}})\,(T_a - k_a(V_{\text{tm}} - V_r)) &= 0,\\
-\,\text{Div}(\mathbf{F}\,(\mathbf{S}_{pas} + \mathbf{S}_{act})) &= 0
\end{aligned}$$

in $\Omega_r \times (0,T)$ *and the boundary and initial conditions*

$$\begin{aligned}
\boldsymbol{N} \cdot (\mathbf{M}_i \operatorname{Grad} V_{\mathrm{tm}} + \mathbf{M}_i \operatorname{Grad} u_e) + \alpha_i (V_{\mathrm{tm}} + u_e) &= G_{R,i}, \\
\boldsymbol{N} \cdot (\mathbf{M}_e \operatorname{Grad} u_e) + \alpha_e u_e &= G_{R,e}, \\
\mathbf{F}(\mathbf{S}_{pas} + \mathbf{S}_{act})\boldsymbol{N} &= \mathbf{0}, \\
V_{\mathrm{tm}}(0, \boldsymbol{X}) &= V_{\mathrm{tm}}^0(\boldsymbol{X}), \\
\boldsymbol{v}(0, \boldsymbol{X}) &= \boldsymbol{v}^0(\boldsymbol{X}), \\
T_a(0, \boldsymbol{X}) &= T_a^0(\boldsymbol{X}),
\end{aligned}$$

on $\partial\Omega_r \times (0,T)$ *and* Ω_r.

Formulation 2.1: System of coupled cardiac electro-mechanics

3 Mathematical Preliminaries

In this chapter the mathematical tools needed for studying space-time methods will be summarized.

3.1 Anisotropic Sobolev Spaces

In this section function spaces used in the studies of time-dependent partial differential equations will be introduced. This part is mainly excerpted from [39, 111, 112]. Let $\Omega \subset \mathbb{R}^d$ be bounded with Lipschitz boundary $\partial\Omega$. One assumes additionally that the domain Ω does not change in time. For a given positive real number T one defines $I := (0, T)$, the **space-time cylinder** $Q := \Omega \times I$ and the **space-time surface** $\Sigma := \partial\Omega \times I$. Further one defines the **initial** and **end surfaces** as $\Sigma_0 := \Omega \times \{0\}$, $\Sigma_T := \Omega \times \{T\}$. With this one has that $\partial Q = \Sigma \cup \Sigma_0 \cup \Sigma_T$. Subsequently, the most important definitions in the context of Bochner integrable functions will be recited.

Definition 3.1. *Let X be a Banach space. Then a mapping $f\colon \overline{I} \to X$ is called* ***strongly measurable*** *iff there is a sequence $\{f_n\}_{n\in\mathbb{N}}$ of mappings of the form $f_n(t) := \sum_{k=1}^{K} \mathbb{1}_{A_k}(t)x_k$ with $x_k \in X$ and $A_k \subseteq \overline{I}$ Lebesgue-measurable sets such that*

$$\lim_{n\to\infty} \|f_n(t) - f(t)\|_X = 0 \qquad \text{for almost all } t \in \overline{I}.$$

Definition 3.2 (Bochner function spaces)**.** *Let X be a Banach space. Let $p \in [1, \infty]$. The following function spaces will be defined:*

1. *The space* $\mathrm{L}^p(I;X)$ *consists of all strongly measurable functions* $f\colon \overline{I} \to X$ *such that*

$$\|f\|_{\mathrm{L}^p(I;X)} := \left(\int_0^T \|f(t)\|_X^p \, \mathrm{d}t \right)^{\frac{1}{p}} < \infty.$$

2. *In the case* $p = \infty$ $\mathrm{L}^\infty(I;X)$ *is defined as the space of all strongly measurable functions* $f\colon \overline{I} \to X$ *such that*

$$\|f\|_{\mathrm{L}^\infty(I;X)} := \operatorname*{ess\,sup}_{t\in\overline{I}} \|f(t)\|_X < \infty.$$

3. *The space* $W^{k,p}(I;X)$ *consists of all strongly measurable functions* $f\colon \overline{I} \to X$ *admitting weak derivatives* $\frac{d^k f}{dt^k}$ *up to the order* k *which are elements of* $\mathrm{L}^p(I;X)$.
4. *The space* $\mathcal{C}(I;X)$ *consists of all continuous mappings* $f\colon \overline{I} \to X$ *with*

$$\|f\|_{\mathcal{C}(I;X)} := \max_{t\in\overline{I}} \|f(t)\|_X < \infty.$$

The next class of spaces is important in the study of linear parabolic partial differential equations.

Definition 3.3. *Let* $r, s \geq 0$. *Following [111] the* ***anisotropic Bochner-Sobolev*** *spaces are defined as*

$$\mathrm{H}^{r,s}(\mathbb{R}^d \times \mathbb{R}) := \mathrm{L}^2(\mathbb{R}; \mathrm{H}^r(\mathbb{R}^d)) \cap \mathrm{H}^s(\mathbb{R}; \mathrm{L}^2(\mathbb{R}^d)).$$

Using the Fourier transform

$$\hat{u}(\tau, \boldsymbol{x}) := \frac{1}{\sqrt{2\pi}} \int_{\mathbb{R}} e^{-it\tau} u(t, \boldsymbol{x}) \, \mathrm{d}t$$

the space $\mathrm{H}^{r,s}(\mathbb{R}^d \times \mathbb{R})$ *is equipped with the norm*

$$\|u\|^2_{\mathrm{H}^{r,s}(\mathbb{R}^d\times\mathbb{R})} := \int_{\mathbb{R}} \left(\|\hat{u}(\tau,\cdot)\|^2_{\mathrm{H}^r(\mathbb{R}^d)} + (1+|\tau|^2)^s \|\hat{u}(\tau,\cdot)\|^2_{\mathrm{L}^2(\mathbb{R}^d)} \right) \mathrm{d}\tau.$$

For $r, s < 0$ *one can define by duality* $\mathrm{H}^{r,s}(\mathbb{R}^d \times \mathbb{R}) := (\mathrm{H}^{-r,-s}(\mathbb{R}^d \times \mathbb{R}))'$.

One also needs to define the space

$$\mathrm{H}^{r,s}(Q) := \left\{ u|_Q : u \in \mathrm{H}^{r,s}(\mathbb{R}^d \times \mathbb{R}) \right\}$$

with the norm

$$\|u\|_{\mathrm{H}^{r,s}(Q)} := \inf_{\substack{w \in \mathrm{H}^{r,s}(\mathbb{R}^d \times \mathbb{R}) \\ w|_Q = u}} \|w\|_{\mathrm{H}^{r,s}(\mathbb{R}^d \times \mathbb{R})}.$$

3.2 Tools from Functional Analysis

In this section the main tools needed for studying partial differential equations in a functional analytical setting will be summarized. For more details on this topic we refer to [29, 36, 111, 171]. Let X and Y denote two Hilbert spaces. Many linear partial differential equations can be recast into operator equations over Hilbert spaces. The prototype for such problems looks like, given $f \in Y'$ find $u \in X$ such that

$$a(u, v) = \langle f, v \rangle \qquad \text{for all } v \in Y. \tag{3.1}$$

Here $a(\cdot, \cdot) \colon X \times Y \to \mathbb{R}$ denotes a bilinear form and $\langle \cdot, \cdot \rangle$ denotes the duality pairing between Y and its dual space Y'. The bilinear form $a(\cdot, \cdot)$ is said to be **bounded** if

$$|a(u, v)| \leq c_2^A \|u\|_X \|v\|_Y \qquad \text{for all } u \in X,\ v \in Y.$$

Upon defining an operator,

$$A \colon X \to Y'$$

by

$$\langle Au, v \rangle := a(u, v)$$

which is possible due to the Fréchet-Riesz representation theorem see [171, Theorem 3.3], Problem (3.1) is equivalent to the operator equation, find $u \in X$ such that

$$Au = f \qquad \text{in } Y', \tag{3.2}$$

see for example [171, Chapter 3]. Of course one wants to know whether such problems are (uniquely) solvable. The problems (3.1) or (3.2) are said to be **well-posed** if they admit a unique solution $u \in X$ or equivalently the operator A is an isomorphism. The key ingredient for checking well-posedness of an linear operator equation is the following theorem dating back to [14, 15, 127].

Theorem 3.4 (Aziz-Babuška-Nečas)**.** *Let X, Y be Hilbert spaces and let*

$$a(\cdot,\cdot)\colon X \times Y \to \mathbb{R}$$

be a bounded bilinear form and $f \in Y'$. Then the problem (3.1) *is well-posed iff*

1. *There is a $c_S > 0$ such that*

$$\sup_{\substack{v \in Y \\ \|v\|_Y \neq 0}} \frac{a(u,v)}{\|v\|_Y} \geq c_S \|u\|_X \qquad \text{for all } u \in X. \tag{3.3}$$

2. *For each $v \in Y$, $\|v\|_Y \neq 0$ there exists a $u \in X$ such that*

$$a(u,v) \neq 0.$$

Equivalently, problem (3.2) *is well-posed iff*

1. *There is a $c_S > 0$ such that*

$$\|Au\|_{Y'} \geq c_S \|u\|_X \qquad \text{for all } u \in X.$$

2. *The adjoint of A, $A'\colon Y \to X'$ is injective.*

Moreover there holds the stability result

$$\|u\|_X \leq \frac{1}{c_S} \|f\|_{Y'}.$$

Proof. See for example [27, Theorem 3.6]. □

Remark 3.5. *Condition* (3.3) *is called the* ***inf-sup-condition****. The name stems from the following equivalent formulation:*

$$\inf_{\substack{u \in X \\ \|u\|_X \neq 0}} \sup_{\substack{v \in Y \\ \|v\|_Y \neq 0}} \frac{a(u,v)}{\|u\|_X \|v\|_Y} \geq c_S.$$

For more on the inf-sup-condition see for example [159] and references therein.

In the case of $X = Y$ being a Hilbert space one can also rely on the well-known Lemma of Lax-Milgram, see [107].

Theorem 3.6 (Lemma of Lax-Milgram)**.** *Let X be a Hilbert space. Let*

$$a(\cdot,\cdot)\colon X \times X \to \mathbb{R}$$

be a bounded bilinear form and $f \in X'$. Suppose that $a(\cdot,\cdot)$ is X-elliptic, i.e.: there exists a $c_1^A > 0$ such that for all $v \in X$

$$a(v,v) \geq c_1^A \|v\|_X^2. \tag{3.4}$$

Then problem (3.1) *is well-posed. Moreover the following stability result holds:*

$$\|u\|_X \leq \frac{1}{c_1^A}\|f\|_{X'}.$$

Proof. For a proof consider [171, Theorem 3.4]. □

3.3 Newton's Method

In many physical problems one has to deal with nonlinear partial differential equations. This leads to nonlinear operator equations which can be stated very generally as find $u \in D \subset X$ such that

$$F(u) = 0.$$

Here $F\colon D \subseteq X \to Y$ is a nonlinear operator between Banach spaces X, Y. To solve such problems one may use the technique of successive linearization. Given a starting value $u_0 \in D$ one solves

$$F'(u^k)\delta u = -F(u^k)$$

with the **Fréchet-Derivative** F'. Then the next iterate is obtained as

$$u^{k+1} = u^k + \delta u.$$

This algorithm is also called **Newton's method**. For more details on Newton's method in general we refer to [46, 49, 50]. The convergence of Newton's method over Banach spaces is governed by the following theorem:

Theorem 3.7 (Newton-Kantorovich)**.** *Let X, Y be Banach spaces and $D \subset X$ open and convex. Let $F\colon D \to Y$ be a continuously Fréchet-differentiable operator and let $u^0 \in D$ be such that $F'(u^0)$ is invertible. Provided*

$$\left\|F'(u^0)^{-1}F(u^0)\right\|_X \leq \alpha, \qquad \left\|F'(u^0)(F'(u) - F'(v))\right\| \leq \omega_0\|u - v\|_X,$$

the sequence u^k obtained from Newton's method is well-defined and converges to u^* with $F(u^*) = 0$. The convergence is of second order for $h_0 := \alpha\omega_0 < \frac{1}{2}$ and the sequence u^k stays in the ball $B(u^0, r^0)$ where $r_0 := \frac{1}{\omega_0}(1 - \sqrt{1 - 2h_0})$.

Proof. See [46, Theorem 2.1]. □

3.4 Nonconforming Approximation Methods

In the previous section it was described how one can deal with operator equations over Banach spaces. In general it is not possible to solve operator equations over Banach spaces directly. Hence one relies on approximation methods to solve such kind of problems. Usually one introduces finite dimensional subspaces $X_h \subseteq X$ and $Y_h \subseteq Y$ and considers the discrete variational problem to find $u_h \in X_h$ such that

$$a(u_h, v_h) = \langle f, v_h \rangle \tag{3.5}$$

for all $v_h \in Y_h$. If $X = Y$ and $X_h = Y_h$ this is called a **conforming Galerkin-Bubnov method** otherwise **conforming Galerkin-Petrov method**. Due to conformity one also has the **Galerkin orthogonality**

$$a(u - u_h, v_h) = 0$$

for all $v_h \in Y_h$. Since one deals with finite-dimensional spaces, any $u_h \in X_h$ can be expanded into basis functions ϕ_l spanning X_h

$$u_h = \sum_{l=1}^{M} u_l \phi_l$$

where $M = |X_h|$. Using the linearity of the bilinear form $a(\cdot, \cdot)$ one obtains

$$\sum_{l=1}^{M} u_l a(\phi_l, \psi_k) = \langle f, \psi_k \rangle$$

for all $k = 1, \ldots, N := |Y_h|$. Upon defining

$$\mathbf{A}_h[k, l] := a(\phi_l, \psi_k)$$

one sees, that an equivalent linear system can be obtained reading as

$$\mathbf{A}_h \boldsymbol{u} = \boldsymbol{f}.$$

with the coefficient vector $\boldsymbol{u} = (u_1, \ldots, u_M)^\top \in \mathbb{R}^M$. Conversely, for each $\boldsymbol{w} \in \mathbb{R}^M$ one can construct a $w_h \in X_h$ by

$$w_h := \sum_{l=1}^{M} w_l \phi_l.$$

This is called the **Galerkin isomorphism**. In the case of a Galerkin-Bubnov method one obtains a square matrix $\mathbf{A}_h$. The unique solvability of the finite dimensional problem is covered by the following theorem.

Theorem 3.8. *Let $a(\cdot, \cdot) \colon X \times Y \to \mathbb{R}$ fulfill the assumptions of Theorem 3.4. Let $X_h \subseteq X$ and $Y_h \subseteq Y$ additionally fulfill a discrete inf-sup condition. Then there exists a unique solution $u_h \in X_h$ of the finite dimensional problem* (3.5) *and there holds the quasi-optimality estimate*

$$\|u - u_h\|_X \leq \left(1 + \frac{c_2^A}{c_S}\right) \inf_{w_h \in X_h} \|u - w_h\|_X.$$

Proof. See [27, Page 120, Satz 3.7], [171, Theorem 8.4] or [7, Theorem 4.1.4]. □

Sometimes it is more convenient to relax the conformity conditions and consider $X_h \nsubseteq X$ and $Y_h \nsubseteq Y$. Salient examples are the treatment of convection diffusion equations with dominant convection, see [37] and the numerical solution of compressible Navier-Stokes equations, see [20]. The discontinuous Galerkin method is a typical example of an nonconforming method. For more details on nonconforming methods in general we refer to [27, Chapter III] or [29, Chapter

10]. In the following the main tools for proving discrete well-posedness (existence and uniqueness) as well as abstract error estimates will be summarized, see [47, Chapter 1.3], [172] and [57, Section 2.3] for more details. The three main properties are:

1. Discrete (inf-sup-)stability (also called the **Ladyzhenskaja-Babuška-Brezzi-condition** short **LBB-condition**),
2. Consistency,
3. Boundedness.

For sake of brevity we will now specify that $f \in \mathrm{L}^2(Q)$. Let us consider a finite-dimensional subspace $V_h \subset \mathrm{L}^2(Q)$ but $V_h \nsubseteq X$. The aim is to investigate the discrete problem, given $f \in \mathrm{L}^2(Q)$ find $u_h \in V_h$ s.t.:

$$a_h(u_h, v_h) = (f, v_h)_{\mathrm{L}^2(\Omega)} \qquad \text{for all } v_h \in V_h. \tag{3.6}$$

Here the bilinear form $a_h \colon V_h \times V_h \to \mathbb{R}$. Since test and trial space are the same this variational formulation is of Galerkin-Bubnov type. One can rewrite (3.6) as an operator equation by introducing the linear operator $A_h \colon V_h \to V_h$

$$(A_h u_h, v_h)_{\mathrm{L}^2(\Omega)} := a_h(u_h, v_h)$$

and the right hand side as the $\mathrm{L}^2(Q)$-projection Q_h onto V_h. This leads to the equivalent discrete operator equation, given $f \in \mathrm{L}^2(Q)$ find $u_h \in V_h$ s.t.:

$$A_h u_h = Q_h f \qquad \text{in } V_h.$$

Remark 3.9. *It is common for discontinuous Galerkin methods in space to assume $f \in \mathrm{L}^2(\Omega)$. Thus one is able to define the right hand side of (3.6) with the $\mathrm{L}^2(\Omega)$-scalar product. In the case $f \in Y'$ but $f \notin \mathrm{L}^2(\Omega)$ one may use other techniques for defining the right hand side, see [47, Remark 4.9].*

The next step is to formulate the concept of discrete stability. To this end the space V_h is equipped with some norm $|||\cdot|||$.

Definition 3.10 (Discrete stability)**.** *The bilinear form $a_h \colon V_h \times V_h \to \mathbb{R}$ is called **discrete stable** on V_h if there is a $c_S > 0$ not depending on V_h such that*

$$c_S |||u_h||| \leq \sup_{\substack{v_h \in V_h \\ |||v_h||| \neq 0}} \frac{a_h(u_h, v_h)}{|||v_h|||} \qquad \text{for all } u_h \in V_h. \tag{3.7}$$

Remark 3.11. *Condition* (3.7) *is an discrete* inf-sup*-condition. This can be seen by rewriting it as*

$$c_S \leq \inf_{\substack{u_h \in V_h \\ |||v_h||| \neq 0}} \sup_{\substack{v_h \in V_h \\ |||v_h||| \neq 0}} \frac{a_h(u_h, v_h)}{|||u_h||| \, |||v_h|||}.$$

The concept of discrete stability ensures the discrete well-posedness of (3.6):

Lemma 3.12. *Let $f \in \mathrm{L}^2(Q)$. Then the discrete variational problem* (3.6) *is well-posed iff the bilinear form $a_h \colon V_h \times V_h \to \mathbb{R}$ is discrete stable on V_h.*

Proof. See [47, Lemma 1.30]. □

Remark 3.13. *A sufficient condition for discrete stability is* ***discrete ellipticity****, i.e.: there exists a $c_1^A > 0$ such that*

$$c_1^A |||v_h|||^2 \leq a_h(v_h, v_h) \qquad \text{for all } v_h \in V_h. \tag{3.8}$$

Up to now one has only considered the discrete setting. However, the goal is to link the continuous problem (3.1) to the discrete problem. In conforming finite element analysis one has $V_h \subset X$ and thus may plug in the exact solution u into the discrete bilinear form $a_h(\cdot, \cdot)$. However, in the nonconforming setting this may not be possible in general since $a_h(\cdot, \cdot)$ is only defined on $V_h \times V_h$. Therefore one assumes that there exists a subspace $X_* \subset X$ such that $u \in X_*$ and such that the bilinear form $a_h(\cdot, \cdot)$ can be extended to $X_* \times V_h$.

Definition 3.14 (Consistency)**.** *Let $u \in X_*$ be the exact solution to problem* (3.1)*. The bilinear form $a_h \colon V_h \times V_h \to \mathbb{R}$ is called* ***consistent*** *if it can be extended to $X_* \times V_h$ and*

$$a_h(u, v_h) = (f, v_h)_{\mathrm{L}^2(\Omega)} \qquad \text{for all } v_h \in V_h. \tag{3.9}$$

Remark 3.15. *Condition* (3.9) *is equivalent to the* ***Galerkin-orthogonality****:*

$$a_h(u - u_h, v_h) = 0 \qquad \text{for all } v_h \in V_h. \tag{3.10}$$

The last property needed is boundedness of the bilinear form. To this end one introduces the space

$$X_{*h} := X_* + V_h.$$

This is motivated by the fact that the approximation error $u - u_h$ is an element of this space. In general it is not possible to extend the norm $|||\cdot|||$ used in the discrete stability to the space X_{*h}. Therefore one introduces a second norm $|||\cdot|||_*$.

Definition 3.16 (Boundedness)**.** *The bilinear form $a_h \colon V_h \times V_h \to \mathbb{R}$ is called **bounded** in $X_{*h} \times V_h$ if there exists a constant $c_2^B > 0$ not depending on h such that*

$$|a_h(u, v_h)| \leq c_2^B |||u|||_* |||v_h|||, \tag{3.11}$$

where $|||\cdot|||_*$ is a norm defined on X_{*h} such that for all $u \in X_{*h}$ there holds $|||u||| \leq |||u|||_*$.

With these three properties one is in the position to state an abstract nonconforming error estimate [47, Theorem 1.35].

Theorem 3.17 (Abstract error estimate)**.** *Let u be the unique exact solution to (3.1) with $f \in \mathrm{L}^2(\Omega)$. Let u_h be the unique solution to (3.6). Let $X_* \subset X$ and assume that $u \in X_*$. Let $X_{*h} := X_* + V_h$ and assume that the bilinear form $a_h(\cdot, \cdot) \colon V_h \times V_h \to \mathbb{R}$ can be extended to $X_{*h} \times V_h$ and enjoys the properties of discrete stability, consistency and boundedness. Further let there be two norms $|||\cdot|||$, $|||\cdot|||_*$ defined on X_{*h} such that for all $v \in X_{*h}$ there holds $|||v||| \leq |||v|||_*$. Then*

$$|||u - u_h||| \leq \left(1 + \frac{c_2^B}{c_S}\right) \inf_{z_h \in V_h} |||u - z_h|||_*.$$

Proof. Take any $z_h \in V_h$. Then thanks to discrete stability we have

$$c_S |||u_h - z_h||| \leq \sup_{\substack{v_h \in V_h \\ |||v_h||| \neq 0}} \frac{a_h(u_h - z_h, v_h)}{|||v_h|||}.$$

Next we observe that

$$\sup_{\substack{v_h \in V_h \\ |||v_h||| \neq 0}} \frac{a_h(u_h - z_h, v_h)}{|||v_h|||} = \sup_{\substack{v_h \in V_h \\ |||v_h||| \neq 0}} \frac{a_h(u_h - u - (z_h - u), v_h)}{|||v_h|||}$$
$$= \sup_{\substack{v_h \in V_h \\ |||v_h||| \neq 0}} \frac{a_h(u - z_h, v_h)}{|||v_h|||}$$

due to consistency. Now we use the boundedness and obtain

$$\sup_{\substack{v_h \in V_h \\ |||v_h||| \neq 0}} \frac{a_h(u - z_h, v_h)}{|||v_h|||} \leq c_2^A \sup_{\substack{v_h \in V_h \\ |||v_h||| \neq 0}} \frac{|||u - z_h|||_* |||v_h|||}{|||v_h|||} = c_2^A |||u - z_h|||_*.$$

Hence we know that

$$|||u_h - z_h||| \leq \frac{c_2^A}{c_S} |||u - z_h|||_*.$$

Finally we conclude the proof with the help of the triangle inequality

$$|||u - u_h||| = |||u - z_h + z_h - u_h||| \leq |||u - z_h||| + |||u_h - z_h|||$$
$$\leq |||u - z_h|||_* + \frac{c_2^A}{c_S} |||u - z_h|||_*.$$

□

3.5 Tools for Discontinuous Galerkin Methods

For defining the discontinuous Galerkin finite element method one needs to introduce a few basic concepts. This part is mainly taken from [47, Chapter 1] and also [129, Chapter 2]. We start by defining the space-time dimension $d_T := d + 1$, where d is the dimension of the space domain Ω. For simplification it is assumed that the computational domain $Q \subset \mathbb{R}^{d_T}$ is a d_T-polytope.

Definition 3.18 (Boundary and Outer Normal)**.** *The boundary of $Q \subset \mathbb{R}^{d+1}$ is denoted by ∂Q. The almost everywhere defined outer normal is denoted by $\boldsymbol{n}$. Furthermore the normal vector admits the representation $\boldsymbol{n} = (\boldsymbol{n}_{\boldsymbol{x}}, n_t)$.*

Definition 3.19 (Simplex)**.** *Given $d_T + 1$ vectors $\boldsymbol{x}_1, \ldots, \boldsymbol{x}_{d_T+1} \in \mathbb{R}^{d_T}$ such that*

$$\{\boldsymbol{x}_2 - \boldsymbol{x}_1, \boldsymbol{x}_3 - \boldsymbol{x}_1, \ldots, \boldsymbol{x}_{d_T+1} - \boldsymbol{x}_1\}$$

are linear independent. Then the set

$$\tau := \operatorname{conv}\{\boldsymbol{x}_1, \ldots, \boldsymbol{x}_{d_T+1}\}$$

*is called a d_T-**simplex**. The vectors $\boldsymbol{x}_1, \ldots, \boldsymbol{x}_{d_T+1}$ are called **vertices** of τ.*

Remark 3.20. *For more information about triangulations of domains with dimension $d_T \geq 4$ we refer to [129, 130]. For non-polygonal domains one needs to take care of the approximation of the boundary curve $\partial Q \subset \mathbb{R}^{d_T-1}$, see for example [29, Chapter 4.7] and [36, Chapter 4.3].*

Definition 3.21 (Simplicial Mesh)**.** *Let $Q \subset \mathbb{R}^{d_T}$. Further, let there be given a set of $N \in \mathbb{N}$ d_T-dimensional non-overlapping simplex elements*

$$\mathcal{T} = \{\tau_1, \tau_2, \ldots, \tau_N\}, \qquad \tau_i \cap \tau_j = \emptyset \qquad \text{for all } \tau_i, \tau_j \in \mathcal{T}.$$

*Then $\mathcal{T}$ is called an **simplical mesh** of Q iff*

$$\overline{Q} = \bigcup_{\tau \in \mathcal{T}} \overline{\tau}.$$

Remark 3.22. *The index N refers to the number of elements in the triangulation $\mathcal{T}$. This can be made explicit by using the notation $\mathcal{T}_N$.*

Remark 3.23. *We will restrict ourselves to simplical meshes only. Therefore we will skip the term simplical mesh and use the term mesh henceforth.*

Definition 3.24 (Element characteristics)**.** *Given a triangulation $\mathcal{T}$ of Q. Then for each $\tau_l \in \mathcal{T}$ the **volume** is defined as*

$$\Delta_l := \int_{\tau_l} dq.$$

*The **local mesh-size** is defined as $h_l := \Delta_l^{\frac{1}{d_T}}$. Moreover the **diameter** is defined as*

$$d_l := \sup_{\boldsymbol{x}, \boldsymbol{y} \in \tau_l} |\boldsymbol{x} - \boldsymbol{y}|.$$

The radius of the inscribed circle is denoted by r_l. The ***global mesh-size*** *is defined as*

$$h := \max_{\tau_l \in \mathcal{T}} h_l.$$

Remark 3.25. *One may use the notation $\mathcal{T}_h$ for the triangulation $\mathcal{T}_N$ with N elements of Q with global mesh-size h.*

A key ingredient to discontinuous Galerkin methods are interior and boundary facets.

Definition 3.26 (Interior and boundary facets)**.** *Let $\mathcal{T}_N$ be a mesh. A subset $F \subset Q$ is called an* ***interior facet*** *if there are two distinct elements $\tau_k, \tau_l \in \mathcal{T}_N$ such that*

$$F = \partial\tau_k \cap \partial\tau_l.$$

In this case we will use the notation $\Gamma_{kl} := F$. The subset $F \subset Q$ is called an ***boundary facet*** *if there is a $\tau_l \in \mathcal{T}_N$ such that*

$$F = \partial\tau_l \cap \partial Q.$$

For boundary facets we will use the notation Γ_l. The set of all interior facets will be denoted by $\mathcal{I}_N$. The set of all boundary facets will be denoted by $\mathcal{B}_N$.

Definition 3.27 (Matching mesh)**.** *Let $\mathcal{T}_N$ be a triangulation of Q. Then $\mathcal{T}_N$ is called a* ***matching mesh*** *if for any two distinct $\tau_k, \tau_l \in \mathcal{T}_N$ there holds that the intersection $\overline{\tau}_l \cap \overline{\tau}_k$ is always a sub-simplex of dimension $\{d, d-1, \ldots, 0\}$.*

Remark 3.28. *If $d_T = 3$ this means, for example, that the intersection of two arbitrary simplex elements of a triangulation $\mathcal{T}_N$ is either a common vertex, a common edge or a common face of the elements.*

For the convergence proofs of discontinuous Galerkin Element Methods one needs to define families of triangulations, see also [47, Chapter 1] and [30, 58].

Definition 3.29 (Family of triangulations)**.** *A* ***family of triangulations*** *is a collection of triangulations*

$$\{\mathcal{T}_N\}_{N \in \mathcal{N}}$$

where $\mathcal{N} \subseteq \mathbb{N}$ denotes an sequence of natural numbers having ∞ as only accumulation point. The shorthand notation $\mathcal{T}_{\mathcal{N}}$ will be used.

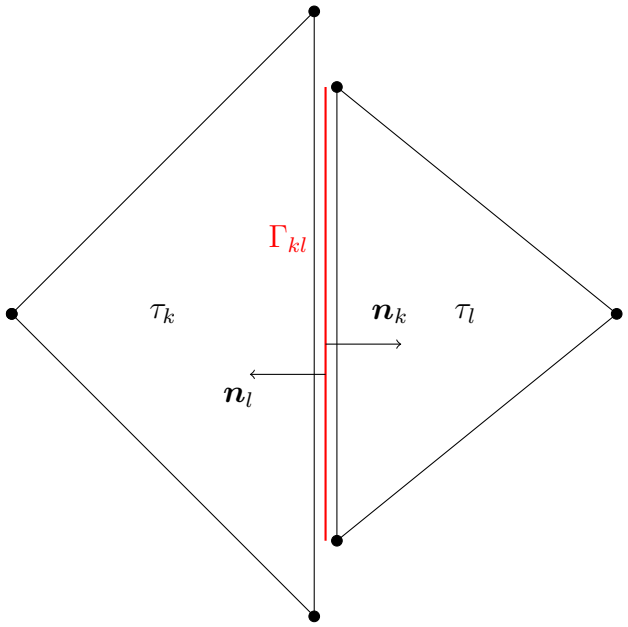

Figure 3.1: Illustration of an interior facet for $d_T = 2$.

In contrast to standard conforming Galerkin finite element methods hanging nodes are allowed within the mesh, see Figure 3.1 for an illustration of a typical interior facet. For applying the standard theory it is not possible to work with complete arbitrary meshes with arbitrary elements having hanging nodes. Instead it is necessary, that one can construct sub-meshes of a given mesh without hanging nodes. This is collected in the following definition, see [47, Definition 1.36] and also [30, Assumption 1].

Definition 3.30 (Mesh quality)**.** *Let $\mathcal{T}_N$ be a family of triangulations. The mesh family is said to be a* ***good family*** *if it satisfies the following mesh quality conditions*

(a) Shape regularity *There exists a parameter $c_F > 0$ such that for all $\tau_l \in \mathcal{T}_N$*

$$d_l \leq c_F r_l.$$

(b) Contact regularity *There exists a constant $c_1 > 0$ such that*

$$c_1 h_l^{d_T - 1} \leq |e| \qquad \text{for all } \tau_l \in \mathcal{T}_N,\ e \in \mathcal{I}_N \cup \mathcal{B}_N,\ \text{s.t. } e \subset \overline{\tau_l}.$$

(c) Locally quasi-uniform *Given any two elements $\tau_l, \tau_k \in \mathcal{T}_N$ there exist a constant $\tilde{c}_G \geq 1$ independent of h such that*

$$\tilde{c}_G^{-1} \leq \frac{h_k}{h_l} \leq \tilde{c}_G$$

(d) Sub-mesh condition *For each $\mathcal{T}_N \in \mathcal{T}_\mathcal{N}$ there exists a regular, conforming submesh $\widetilde{\mathcal{T}}_N$ having no hanging nodes such that*

1. *For each $\tilde{\tau} \in \widetilde{\mathcal{T}}_N$ there exists a $\tau \in \mathcal{T}_N$ such that $\tilde{\tau} \subset \tau$.*
2. *The family induced by $\widetilde{\mathcal{T}}_N$ fulfills (a), (b) and (c).*
3. *There exists a constant $\tilde{c}$ such that, whenever $\tilde{\tau}_p \subset \tau_l$ then $h_p \leq \tilde{c} h_l$.*

Remark 3.31. *The concept of matching sub-meshes was introduced in [28]*

Remark 3.32. *The contact regularity of $\mathcal{T}_\mathcal{N}$ implies the following bound on the measure of the boundaries of the elements: There exist $c_{R_1}, c_{R_2} > 0$ such that*

$$c_{R_1} h_l^{d_T - 1} \leq |\partial \tau_l| \leq c_{R_2} h_l^{d_T - 1}. \tag{3.12}$$

Given two neighboring elements τ_k, τ_l the local quasi-uniformity implies a bound on the average mesh size $\overline{h}_{kl} := \frac{1}{2}(h_k + h_l)$: There exists a constant $c_G \geq 1$ independent of the family $\mathcal{T}_\mathcal{N}$ such that

$$c_G^{-1} \leq \frac{\overline{h}_{kl}}{h_l} \leq c_G \qquad c_G^{-1} \leq \frac{\overline{h}_{kl}}{h_k} \leq c_G. \tag{3.13}$$

See [129, Section 2.2] and [47, Section 1.4] for details.

Remark 3.33 (Boundary Discretization)**.** *When assuming that Ω has a polygonal boundary one also has that Σ is polygonal. Furthermore a boundary discretization $\mathcal{E}_M = \mathcal{E}_0 \cup \mathcal{E}_T \cup \mathcal{E}_R$ such that $\overline{\mathcal{E}}_M = \Sigma$ is induced. Each element $e_j \in \mathcal{E}_M$ can then be uniquely associated to a d-dimensional sub-simplex of an element $\tau_l \in \mathcal{T}_h$. This means that for each $\tau_l \in \mathcal{T}_N$ with $\partial\tau_l \cap \Sigma \neq \emptyset$ there exists exactly one $e_{j(l)} \in \mathcal{E}_M$ and vice versa.*

For the proofs in the subsequent sections the following technical assumption is needed, see also [129].

Assumption 3.34 (Time Alignment)**.** *For all $\mathcal{T}_N \in \mathbb{T}_{\mathcal{N}}$ there holds:*

$$\min_{\Gamma_{kl} \in \mathcal{I}_N} \{|\boldsymbol{n}_{k,\boldsymbol{x}}| > 0 \colon \boldsymbol{n}_{k,\boldsymbol{x}} \text{ is normal vector of } \Gamma_{kl}\} \geq c_{\boldsymbol{n}} > 0. \tag{3.14}$$

Remark 3.35. *Condition* (3.14) *means that the minimum over all angles enclosed by the interior facets which are neither parallel nor normal to the time axis are large enough. Provided that the initial triangulation fulfills this condition and the family of meshes is obtained by successive red refinements the alignment condition holds also. See Figure 3.2 for an illustration.*

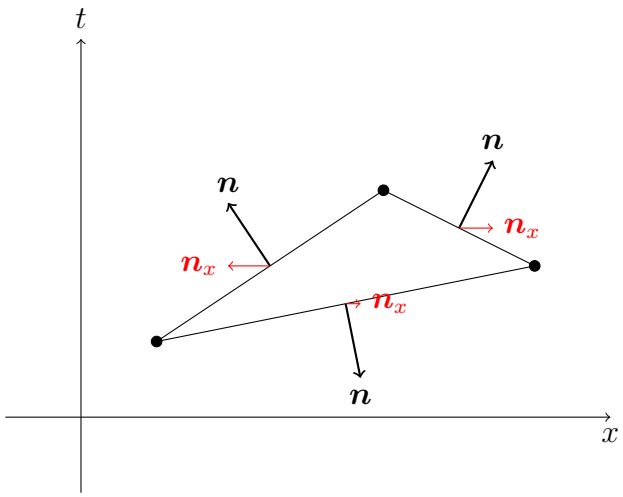

Figure 3.2: Illustration of the alignment condition

For the formulation of a discrete variational formulation the following standard definitions are used:

Definition 3.36. *Let $\Gamma_{kl} \in \mathcal{I}_N$ be an interior facet with outer normal $\boldsymbol{n}_k = (\boldsymbol{n}_{x,k}, n_{t,k})^\top \in \mathbb{R}^{d_T}$ for τ_k and $\boldsymbol{n}_l = -\boldsymbol{n}_k$ for τ_l. For a given function ϕ smooth enough restricted to either τ_k or τ_l one defines :*

- *The **jump** across Γ_{kl} as*

$$[\![\phi]\!]_{kl} := \phi|_{\tau_k} \boldsymbol{n}_k + \phi|_{\tau_l} \boldsymbol{n}_l.$$

- *The **space jump** across Γ_{kl} as*

$$[\![\phi]\!]_{\boldsymbol{x},kl} := \phi|_{\tau_k} \boldsymbol{n}_{\boldsymbol{x},k} + \phi|_{\tau_l} \boldsymbol{n}_{\boldsymbol{x},l}.$$

- *The **time jump** across Γ_{kl} as*

$$[\![\phi]\!]_{t,kl} := \phi|_{\tau_k} n_{t,k} + \phi|_{\tau_l} n_{t,l}.$$

- *The **average** of ϕ on Γ_{kl} as*

$$\langle\phi\rangle_{kl} := \frac{1}{2}\left(\phi|_{\tau_k} + \phi|_{\tau_l}\right).$$

- *Given $\omega_1, \omega_2 \in [0,1]$ with $\omega_1 + \omega_2 = 1$ the **weighted average** of ϕ on Γ_{kl} is defined as*

$$\langle\phi\rangle_{\omega,kl} := \omega_1\phi|_{\tau_k} + \omega_2\phi|_{\tau_l}.$$

- *The **upwind** in time direction of ϕ is defined as*

$$\{\phi\}^{\mathrm{up}}_{kl} := \begin{cases} \phi|_{\tau_k} & \text{if } n_{k,t} > 0 \\ 0 & \text{if } n_{k,t} = 0 \\ \phi|_{\tau_l} & \text{if } n_{k,t} < 0 \end{cases}$$

Remark 3.37. *With this definition the jump of a scalar-valued function is independent of the ordering of the finite elements τ_k, τ_l. It is a vector-valued function. Other definitions for these terms are possible see for example [47, Section 1.2.3]. Given that $\boldsymbol{\phi}$ is vector-valued one defines the tensor valued jump as*

$$\underline{[\![\phi]\!]}_{kl} := \boldsymbol{\phi}|_{\tau_k} \otimes \boldsymbol{n}_k + \boldsymbol{\phi}|_{\tau_l} \otimes \boldsymbol{n}_l.$$

In Section 3.4 it was discussed that the discontinuous Galerkin method is nonconforming. Next, the spaces that will be used for this method will be introduced.

Definition 3.38 (Broken Sobolev space)**.** *Let $\mathcal{T}_N \in \mathcal{T}_{\mathcal{N}}$ be an admissible triangulation of Q. For $s \geq 0$ we define the **broken Sobolev space** $\mathrm{H}^s(\mathcal{T}_N)$ as*

$$\mathrm{H}^s(\mathcal{T}_N) := \left\{v \in \mathrm{L}^2(Q) \colon v|_{\tau_l} \in \mathrm{H}^s(\tau_l) \text{ for all } \tau_l \in \mathcal{T}_N\right\}.$$

Remark 3.39. *It is easy to show, that provided $u \in \mathrm{H}^{r,s}(Q)$ one has that $u \in \mathrm{H}^{\min\{r,s\}}(Q)$.*

For a given discretization $\mathcal{T}_N \in \mathcal{T}_{\mathcal{N}}$ one defines the discrete test and trial spaces

$$S_h^p(\mathcal{T}_N) := \left\{ v_h \in \mathrm{L}^2(Q) \colon v_h|_{\tau_l} \in \mathbb{P}(\tau_l) \text{ for all } \tau_l \in \mathcal{T}_N \right\}$$

where $\mathbb{P}(\tau_l)$ is the space of polynomials with degree less or equal p on τ_l.

Remark 3.40. *In the case of Dirichlet boundary conditions one uses a slightly different definition*

$$S_h^p(\mathcal{T}_N) := \left\{ v_h \in \mathrm{L}^2(Q) \colon v_h|_{\tau_l} \in \mathbb{P}(\tau_l) \text{ for all } \tau_l \in \mathcal{T}_N \text{ and } v_h|_{\Sigma_D} = 0 \right\}.$$

It is possible to use different polynomial degrees on each element τ_l as well as different Sobolev spaces on each τ_l. For more on broken polynomial spaces we refer to [47, Section 1.2.4 and A.2].

For the broken polynomial spaces the following trace and inverse inequalities are valid:

Lemma 3.41 (Inverse and trace inequalities)**.** *Let $\mathcal{T}_N \in \mathcal{T}_{\mathcal{N}}$ be a shape and contact regular mesh sequence. Then, for all $v_h \in S_h^p(\mathcal{T}_N)$ there holds:*

$$\|v_h\|_{\mathrm{L}^2(\Gamma_{kl})} \leq c_I \, |\Gamma_{kl}|^{\frac{1}{2}} \, |\tau_l|^{-\frac{1}{2}} \, \|v_h\|_{\mathrm{L}^2(\tau_l)}, \tag{3.15}$$

$$\|v_h\|_{\mathrm{H}^1(\Gamma_{kl})} \leq c_I \overline{h}_{kl}^{-1} \|v_h\|_{\mathrm{L}^2(\Gamma_{kl})}, \tag{3.16}$$

$$\|v_h\|_{\mathrm{H}^1(\tau_l)} \leq c_I h_l^{-1} \|v_h\|_{\mathrm{L}^2(\tau_l)}. \tag{3.17}$$

Proof. See [47, Lemma 1.46] for a proof of (3.15). The proof for inequality (3.16) can be found in [191, Section 4.2.4] and the proof of inequality (3.17) can be looked up in [47, 171]. □

Remark 3.42. *From estimate* (3.15) *one obtains also the estimate*

$$\|\mathbf{A}\nabla_{\boldsymbol{x}} v_h\|_{[\mathrm{L}^2(\Gamma_{kl})]^d} \leq c_I \, |\Gamma_{kl}|^{\frac{1}{2}} \, |\tau_l|^{-\frac{1}{2}} \, \|\mathbf{A}\nabla_{\boldsymbol{x}} v_h\|_{[\mathrm{L}^2(\tau_l)]^d}, \tag{3.18}$$

for any symmetric positive definite piecewise constant matrix $\mathbf{A}$. This can be seen by observing that $\mathbf{A}\nabla_{\boldsymbol{x}} v_h \in [S_h^{p-1}(\mathcal{T}_N)]^d$ and applying estimate (3.15)

component-wise. In the case that $\mathbf{A}$ *is not constant but in* $[\mathrm{L}^\infty(\mathcal{T}_N)]^{d\times d}$ *one can prove the following:*

$$\begin{aligned}
\|\mathbf{A}\nabla_{\boldsymbol{x}} v_h\|_{[\mathrm{L}^2(\Gamma_{kl})]^d} &\leq \|\mathbf{A}\|_{[\mathrm{L}^\infty(\mathcal{T}_N)]^{d\times d}} \|\nabla_{\boldsymbol{x}} v_h\|_{[\mathrm{L}^2(\Gamma_{kl})]^d} \\
&\leq c_I \|\mathbf{A}\|_{[\mathrm{L}^\infty(\mathcal{T}_N)]^{d\times d}} |\Gamma_{kl}|^{\frac{1}{2}} |\tau_l|^{-\frac{1}{2}} \left\|\mathbf{A}^{-1}\mathbf{A}\nabla_{\boldsymbol{x}} v_h\right\|_{[\mathrm{L}^2(\tau_l)]^d} \\
&\leq c_I \max_{\boldsymbol{x}\in Q} \left|\frac{\lambda_{\max}(\mathbf{A}(\boldsymbol{x}))}{\lambda_{\min}(\mathbf{A}(\boldsymbol{x}))}\right| |\Gamma_{kl}|^{\frac{1}{2}} |\tau_l|^{-\frac{1}{2}} \|\mathbf{A}\nabla_{\boldsymbol{x}} v_h\|_{[\mathrm{L}^2(\tau_l)]^d}.
\end{aligned}$$

4 Space-Time Discontinuous Galerkin Finite Element Method for the Bidomain Equations

In this chapter a space-time discontinuous Galerkin finite element method for the Bidomain equations will be discussed. The first part of this chapter is devoted to existing results on unique solvability and regularity for the Bidomain equations. Subsequently, the discretization of the Bidomain equations will be presented. Proceeding, we will start our numerical considerations with a corresponding linear problem and then extend the results to the nonlinear case. This chapter will be closed with some convergence studies.

4.1 Unique Solvability and Regularity Results

In this section existence and uniqueness results for the Bidomain equations will be summarized which can be found in [25, 26, 38, 105, 182]. It is clear that the results can not be independent of the chosen ionic model. The Bidomain equations will be considered in the following form

$$\begin{aligned} \frac{\partial}{\partial t} V_{\mathrm{tm}} + \mathrm{I}_{\mathrm{ion}}(V_{\mathrm{tm}}, v) - \operatorname{div}(\mathbf{M}_i \operatorname{grad} V_{\mathrm{tm}}) - \operatorname{div}(\mathbf{M}_i \operatorname{grad} u_e) &= s_i, \\ - \operatorname{div}(\mathbf{M}_i \operatorname{grad} V_{\mathrm{tm}}) - \operatorname{div}((\mathbf{M}_i + \mathbf{M}_e) \operatorname{grad} u_e) &= 0, \\ \frac{\partial}{\partial t} v + H(V_{\mathrm{tm}}, v) &= 0, \end{aligned} \tag{4.1}$$

in $Q := \Omega \times (0,T)$. We will consider only phenomenological ionic models, i.e. with one additional variable. The following initial and boundary conditions will be considered

$$\begin{aligned} \boldsymbol{n} \cdot \mathbf{M}_i \operatorname{grad}(V_{\mathrm{tm}} + u_e) + \alpha_i (V_{\mathrm{tm}} + u_e) &= g_{i,R}, \\ \boldsymbol{n} \cdot \mathbf{M}_e \operatorname{grad} u_e + \alpha_e u_e &= g_{e,R}, \\ V_{\mathrm{tm}}(\boldsymbol{x}, 0) &= V_{\mathrm{tm}}^0(\boldsymbol{x}), \\ v(\boldsymbol{x}, 0) &= v^0(\boldsymbol{x}). \end{aligned} \tag{4.2}$$

For the case of non-phenomenological ionic models we refer to [182]. One has to be careful in the use of term "weak solutions" to the Bidomain equations as this term is ambiguous. In literature, there arise different notions of solutions to the Bidomain equations, each entitled "weak solution". For example the definitions of weak solutions in [25, 26, 105, 106, 182] are different and in general not equivalent to those found in [8, 9]. For a more general discussion on the various solution concepts in the context of time dependent partial differential equations we refer to [7, Chapter 3]. We will try to emphasize this by explicitly adding the first author to the various weak solution concepts. The most recent result concerning existence and regularity of solutions to the Bidomain equations can be found in [105, Theorems 2.5, 2.7, 2.8 and 3.3] and also [106]. The first concept of weak solutions is the one of Kunisch et al. To this end we fix the following spaces

$$\begin{aligned} X &:= \mathcal{C}(0,T;\mathrm{L}^2(\Omega)) \cap \mathrm{L}^2(0,T;\mathrm{H}^1(\Omega)) \cap \mathrm{L}^p(Q_T), \\ Y &:= \mathrm{L}^2(0,T;\mathrm{H}^2(\Omega)), \\ Z &:= \mathcal{C}(0,T;\mathrm{L}^2(\Omega)), \end{aligned}$$

where $p \geq 2$ when $\Omega \subset \mathbb{R}^2$ and $2 \leq p \leq 6$ in the case $\Omega \subset \mathbb{R}^3$. This are results for weak solutions in the sense of Kunisch et al. The formulation is depicted in Formulation 4.1.

Find $(V_{\mathrm{tm}}, u_e, v) \in X \times Y \times Z$ *such that*

$$\begin{aligned}\int_\Omega s_i\phi_1 \ \mathrm{d}\boldsymbol{x} = &\int_\Omega \frac{\partial V_{\mathrm{tm}}}{\partial t}\phi_1 \ \mathrm{d}\boldsymbol{x} + \int_\Omega \mathrm{I}_{\mathrm{ion}}(V_{\mathrm{tm}}, v)\phi_1 \ \mathrm{d}\boldsymbol{x} \\ &+ \int_\Omega \mathbf{M}_i \nabla_{\boldsymbol{x}} V_{\mathrm{tm}} \cdot \nabla_{\boldsymbol{x}}\phi \ \mathrm{d}\boldsymbol{x} + \int_\Omega \mathbf{M}_i \nabla_{\boldsymbol{x}} u_e \cdot \nabla_{\boldsymbol{x}}\phi \ \mathrm{d}\boldsymbol{x} \\ &+ \alpha_i \int_{\Gamma_R} (V_{\mathrm{tm}} + u_e)\phi_1 \ \mathrm{ds}_{\boldsymbol{x}}\end{aligned}$$

for all $\phi_1 \in \mathrm{H}^1(\Omega)$ *and almost all* $t \in (0, T)$,

$$\begin{aligned}\int_\Omega (s_i + s_e)\phi_2 \ \mathrm{d}\boldsymbol{x} = &\int_\Omega \mathbf{M}_i \nabla_{\boldsymbol{x}} V_{\mathrm{tm}} \nabla_{\boldsymbol{x}}\phi_2 \ \mathrm{d}\boldsymbol{x} + \int_\Omega \mathbf{M}_{i+e} \nabla_{\boldsymbol{x}} u_e \nabla_{\boldsymbol{x}}\phi_2 \ \mathrm{d}\boldsymbol{x} \\ &+ \alpha_i \int_{\Gamma_R} (V_{\mathrm{tm}} + u_e)\phi_2 \ \mathrm{ds}_{\boldsymbol{x}} + \alpha_e \int_{\Gamma_R} u_e\phi_2 \ \mathrm{ds}_{\boldsymbol{x}}\end{aligned}$$

for all $\phi_2 \in \mathrm{H}^1(\Omega)$ *and almost all* $t \in (0, T)$,

$$0 = \int_\Omega \frac{\partial v}{\partial t}\phi_3 \ \mathrm{d}\boldsymbol{x} + \int_\Omega G(V_{\mathrm{tm}}, v)\phi_3 \ \mathrm{d}\boldsymbol{x}$$

for all $\phi_3 \in \mathrm{L}^2(\Omega)$ *and almost all* $t \in (0, T)$.

Formulation 4.1: Weak formulation of the Bidomain equations as in [105, 106].

For the proof of existence, uniqueness and regularity of solutions to Formulation 4.1 one needs to rely on the following assumptions, cf. [105, Assumptions 2.3] and [106, Theorem 1.1].

Assumption 4.1 (Basic assumptions on the input data)**.**

1. *The space domain* $\Omega \subset \mathbb{R}^d$ *is a bounded Lipschitz domain.*

2. *For the conductivity tensors there holds:* $\mathbf{M}_i$, $\mathbf{M}_e \in [\mathrm{L}^\infty(\Omega)]^{d\times d}$, $\mathbf{M}_i$, $\mathbf{M}_e$ *are symmetric and positive definite obeying the following uniform ellipticity estimates*

$$0 \leq \mu_1 |\boldsymbol{v}|^2 \leq \left(\mathbf{M}_{\{i,e\}}\boldsymbol{v}, \boldsymbol{v}\right) \leq \mu_2 |\boldsymbol{v}|^2$$

with $\mu_1, \mu_2 > 0$.
3. *The initial values* V_{tm}^0, v^0 *belong to* $\mathrm{L}^2(\Omega)$.
4. *The input data* s_i, s_e *belong to* $\mathrm{L}^\infty(0,T;\widetilde{\mathrm{H}}^{-1}(\Omega))$. *The boundary data* $g_{R,i}, g_{R,e}$ *belongs to* $\mathrm{L}^\infty(0,T;H^{-1/2}(\Gamma))$

Furthermore we recite the growth conditions to be imposed on the nonlinearities, see also [26, Page 470,471].

Assumption 4.2 (Growth conditions)**.**

1. *The nonlinearity* $\mathrm{I}_{\mathrm{ion}}$ *can be written as*

$$\begin{aligned} \mathrm{I}_{\mathrm{ion}}(V_{\mathrm{tm}}, v) &= f_1(V_{\mathrm{tm}}) + f_2(V_{\mathrm{tm}})v, \\ G(V_{\mathrm{tm}}, v) &= g_1(V_{\mathrm{tm}}) + g_2 v \end{aligned}$$

where $f_1 \colon \mathbb{R} \to \mathbb{R}$, $f_2 \colon \mathbb{R} \to \mathbb{R}$ *and* $g_1 \colon \mathbb{R} \to \mathbb{R}$ *are continuous functions and* $g_2 \in \mathbb{R}$.
2. *There exist non-negative constants* $\{c_i\}_{i=1}^6$ *such that for any* $u \in \mathbb{R}$

$$\begin{aligned} |f_1(u)| &\leq c_1 + c_2 |u|^{p-1}, \\ |f_2(u)| &\leq c_3 + c_4 |u|^{p/2-1}, \\ |g_1(u)| &\leq c_5 + c_6 |u|^{p/2}. \end{aligned}$$

3. *There exist constants* $a, \lambda > 0, b, c \geq 0$ *such that for any* $(u, v) \in \mathbb{R}^2$

$$\lambda u \mathrm{I}_{\mathrm{ion}}(u, v) + v G(u, v) \geq a |u|^p - b(\lambda |u|^2 + |v|^2) - c.$$

Under these assumptions it is possible to show existence and uniqueness (see [106, Theorem 1.4] to the problem posed in Formulation 4.1. Further the authors were able to show the additional regularity results (see [106, Proposition 2.5,Proposition 2.6,Proposition 2.7,Proposition 2.8])

- $V_{\mathrm{tm}} \in \mathrm{L}^2(0,T;\mathrm{L}^6(\Omega)) \cap \mathrm{L}^q(0,T;\mathrm{L}^r(\Omega)) \cap \mathrm{L}^5(Q_T)$ where $1 < q < \infty$ and $4 \leq r < 6$,
- $u_e \in \mathrm{L}^2(0,T;\mathrm{H}^2(\Omega))$,
- $v \in \mathcal{C}^1([0,T],\mathrm{L}^1(\Omega))$,
- If $^{26}/_9 < r < 3$ and $v^0 \in W^{1,r/2}(\Omega)$ then $v \in \mathrm{L}^1(0,T;W^{1,r/2}(\Omega)) \cap \mathcal{C}(0,T;\mathrm{L}^{8/3}(\Omega))$.

The second concept of weak solutions we want to mention can be found in the works [8, 9]. For defining the weak solution concept one introduces the following spaces

$$\begin{aligned} X &:= \mathrm{L}^2(0,T;\mathrm{H}^1(\Omega)) \cap \mathrm{L}^4(Q), \\ X' &= \mathrm{L}^2(0,T;\widetilde{\mathrm{H}}^{-1}(\Omega)) + \mathrm{L}^{\frac{4}{3}}(Q), \\ Y &:= \mathrm{L}^2(0,T;\mathrm{H}^1(\Omega)), \\ Z &:= \mathcal{C}(0,T;\mathrm{L}^2(\Omega)), \\ W(Q) &:= \left\{ v \in X : \frac{\partial}{\partial t} v \in X' \right\}, \\ V(Q) &:= \left\{ v \in X : \frac{\partial}{\partial t} v \in \mathrm{L}^\infty(Q) \right\}. \end{aligned}$$

The weak formulation in the sense of Andreianov et al. is depicted in Formulation 4.2.

Find $(V_{\mathrm{tm}}, u_e, v) \in W(Q) \times Y \times Z$ *such that*

$$\begin{aligned} \int_Q s_i \phi_1 \, \mathrm{d}q + \int_{\Sigma_0} V_{\mathrm{tm}}^0 \phi_1 \, \mathrm{ds_q} &= -\int_Q V_{\mathrm{tm}} \frac{\partial \phi_1}{\partial t} \, \mathrm{d}q + \int_Q \mathrm{I}_{\mathrm{ion}}(V_{\mathrm{tm}}, v)\phi_1 \, \mathrm{d}q \\ &+ \int_Q \mathbf{M}_i \nabla_{\boldsymbol{x}} V_{\mathrm{tm}} \cdot \nabla_{\boldsymbol{x}} \phi_1 \, \mathrm{d}q + \int_Q \mathbf{M}_i \nabla_{\boldsymbol{x}} u_e \cdot \nabla_{\boldsymbol{x}} \phi_1 \, \mathrm{d}q \\ &+ \alpha_i \int_{\Sigma_R} (V_{\mathrm{tm}} + u_e)\phi_1 \, \mathrm{ds_q} \end{aligned}$$

for all $\phi_1 \in V(Q)$,

$$\int_Q (s_i + s_e)\phi_2 \, \mathrm{d}q = \int_Q \mathbf{M}_i \nabla_{\boldsymbol{x}} V_{\mathrm{tm}} \nabla_{\boldsymbol{x}} \phi_2 \, \mathrm{d}q + \int_Q \mathbf{M}_{i+e} \nabla_{\boldsymbol{x}} u_e \nabla_{\boldsymbol{x}} \phi_2 \, \mathrm{d}q + \alpha_i \int_{\Sigma_R} (V_{\mathrm{tm}} + u_e)\phi_2 \, \mathrm{d}s_{\mathrm{q}} + \alpha_e \int_{\Sigma_R} u_e \phi_2 \, \mathrm{d}s_{\mathrm{q}}$$

for all $\phi_2 \in \mathrm{L}^2(0,T;\mathrm{H}^1(\Omega))$,

$$\int_{\Sigma_0} v^0 \phi_3 \, \mathrm{d}s_{\mathrm{q}} = -\int_Q v \frac{\partial \phi_3}{\partial t} \, \mathrm{d}q + \int_Q G(V_{\mathrm{tm}}, v)\phi_3 \, \mathrm{d}q$$

for all $\phi_3 \in \mathrm{L}^2(Q)$.

Formulation 4.2: Weak formulation of the Bidomain equations as in [8, 9].

The existence of a unique weak solution in the sense of Formulation 4.2 is shown in [9, Section 3]. However higher regularity results for this formulation remain an open question, see [9, Section 4.2]. For defining the space-time discretization we will assume that $(V_{\mathrm{tm}}, u_e, v) \in [\mathrm{H}^{r,s}(Q)]^3$ with $\min\{r,s\} > \frac{3}{2}$.

4.2 Numerical Analysis

In this section we will derive a discrete space-time variational formulation of the Bidomain equations (4.1)-(4.2). Following ideas from [129] the entire space-time cylinder $Q = \Omega \times (0,T)$ will be used as computational domain. On top of the growth conditions 4.2 we will additionally pose the following assumptions:

Assumption 4.3 (Additional assumptions on nonlinearities)**.** *We will assume that:*

1. *There holds*

$$\mathrm{I}_{\mathrm{ion}}(V_{\mathrm{tm}}, v), G(V_{\mathrm{tm}}, v) \in \mathcal{C}^1(Q)$$

2. *Upon defining*

$$\mathbf{A}(u,w) := \begin{pmatrix} \frac{\partial \mathrm{I}_{\mathrm{ion}}}{\partial V_{\mathrm{tm}}}(u,w) & \frac{\partial \mathrm{I}_{\mathrm{ion}}}{\partial v}(u,w) \\ \frac{\partial G}{\partial V_{\mathrm{tm}}}(u,w) & \frac{\partial G}{\partial v}(u,w) \end{pmatrix}$$

there holds

$$\lambda_{\min}(\mathrm{sym}(\mathbf{A}(u_h,w_h))) \geq c_{nl} > 0 \quad \textit{for all } (u_h,v_h)^\top \in S_h^{p_1}(\mathcal{T}_N) \times S_h^{p_2}(\mathcal{T}_N)$$

3. *There holds* $\|\mathbf{A}(u_h,w_h))\|_F \leq c^{nl} < \infty$ *for all* $(u_h,v_h)^\top \in S_h^{p_1}(\mathcal{T}_N) \times S_h^{p_2}(\mathcal{T}_N)$
4. *There holds* $\frac{(c^{nl})^2}{4c_{nl}} < 1$.

The discrete variational problem reads: Find $(V_{\mathrm{tm}}^h, u_e^h, v^h) \in S_h^{p_1}(\mathcal{T}_N) \times S_h^{p_2}(\mathcal{T}_N) \times S_h^{p_3}(\mathcal{T}_N)$ such that :

$$\begin{aligned} b_T^{\mathrm{DG}}(V_{\mathrm{tm}}^h,\phi^h) + a_i^{\mathrm{DG}}(V_{\mathrm{tm}}^h,\phi^h) + a_i^{\mathrm{DG}}(u_e^h,\phi^h) + I^{\mathrm{DG}}(V_{\mathrm{tm}}^h,v^h;\phi^h) &= l_1(\phi^h), \\ a_i^{\mathrm{DG}}(V_{\mathrm{tm}}^h,\psi^h) + a_{i+e}^{\mathrm{DG}}(u_e^h,\psi^h) &= l_2(\psi^h), \\ b_T^{\mathrm{DG}}(v^h,\zeta^h) + G^{\mathrm{DG}}(V_{\mathrm{tm}}^h,v^h;\zeta^h) &= l_3(\zeta^h), \end{aligned} \tag{4.3}$$

for all $(\phi^h,\psi^h,\zeta^h) \in S_h^{p_1}(\mathcal{T}_N) \times S_h^{p_2}(\mathcal{T}_N) \times S_h^{p_3}(\mathcal{T}_N)$. The bilinear form $a_{\{i,e\}}^{\mathrm{DG}}(\bullet,\bullet)$ is defined as

$$\begin{aligned} a_{\{i,e\}}^{\mathrm{DG}}(u_h,v_h) := &\sum_{l=1}^{N} \int_{\tau_l} \mathbf{M}_{\{i,e\}} \nabla_{\boldsymbol{x}} u_h \cdot \nabla_{\boldsymbol{x}} v_h \, dq \\ &- \sum_{\Gamma_{kl} \in \mathcal{I}_N} \int_{\Gamma_{kl}} \left\langle \mathbf{M}_{\{i,e\}} \nabla_{\boldsymbol{x}} u_h \right\rangle_{kl,\omega} \cdot [\![v_h]\!]_{kl,\boldsymbol{x}} ds_q \\ &- \sum_{\Gamma_{kl} \in \mathcal{I}_N} \int_{\Gamma_{kl}} [\![u_h]\!]_{\boldsymbol{x},kl} \cdot \left\langle \mathbf{M}_{\{i,e\}} \nabla_{\boldsymbol{x}} v_h \right\rangle_{kl,\omega} ds_q \\ &+ \sum_{\Gamma_{kl} \in \mathcal{I}_N} \frac{\sigma \gamma_{kl}}{\overline{h}_{kl}} \int_{\Gamma_{kl}} [\![u_h]\!]_{\boldsymbol{x},kl} \cdot [\![v_h]\!]_{\boldsymbol{x},kl} ds_q \\ &+ \alpha_{\{i,e\}} \int_{\Sigma_R} u_h v_h ds_q. \end{aligned} \tag{4.4}$$

Bilinear form (4.4) is the **symmetric weighted interior penalty** discretization of an anisotropic Poisson operator see [47, Section 4.5 and Section 4.5.6]. The weights for the averages read:

$$\omega_1 := \frac{m_k}{m_l + m_k}, \tag{4.5}$$

$$\omega_2 := \frac{m_l}{m_l + m_k}, \tag{4.6}$$

$$\gamma_{kl} := \frac{2m_k m_l}{m_k + m_l}, \tag{4.7}$$

$$m_k := \left(\mathbf{M}_{\{i,e\}}|_{\tau_k} \boldsymbol{n}_{k,\boldsymbol{x}}, \boldsymbol{n}_{k,\boldsymbol{x}}\right), \tag{4.8}$$

$$m_l := \left(\mathbf{M}_{\{i,e\}}|_{\tau_l} \boldsymbol{n}_{l,\boldsymbol{x}}, \boldsymbol{n}_{l,\boldsymbol{x}}\right). \tag{4.9}$$

The bilinear form $b_T^{\mathrm{DG}}(\bullet, \bullet)$ is defined as

$$\begin{aligned} b_T^{\mathrm{DG}}(u_h, v_h) := \sum_{l=1}^{N} - \int_{\tau_l} u_h \frac{\partial}{\partial t} v_h dq + \int_{\Sigma_T} u_h v_h ds_q \\ + \sum_{\Gamma_{kl} \in \mathcal{I}_N} \int_{\Gamma_{kl}} \{u_h\}_{kl}^{\mathrm{up}} [\![v_h]\!]_{t,kl} ds_q. \end{aligned} \tag{4.10}$$

Bilinear form (4.10) results from an upwind discretization of the time derivative as used in [129, Section 2.1] and [47, Section 2.3].

Remark 4.4. *Using integration by parts one may observe that*

$$b_T^{\mathrm{DG}}(u_h, v_h) = \sum_{l=1}^{N} \int_{\tau_l} \frac{\partial}{\partial t} u_h v_h dq + \int_{\Sigma_0} u_h v_h ds_q - \sum_{\Gamma_{kl} \in \mathcal{I}_N} \int_{\Gamma_{kl}} [\![u_h]\!]_{t,kl} \{v_h\}_{kl}^{\mathrm{down}} ds_q \tag{4.11}$$

where the ***downwind*** *is defined as*

$$\{\phi\}_{kl}^{\mathrm{down}} := \begin{cases} \phi|_{\tau_l} & \text{if } n_{k,t} > 0, \\ 0 & \text{if } n_{k,t} = 0, \\ \phi|_{\tau_k} & \text{if } n_{k,t} < 0. \end{cases}$$

The nonlinear forms are defined as

$$I^{\mathrm{DG}}(V_{\mathrm{tm}}^h, v^h; \phi^h) := \sum_{l=1}^{N} \int_{\tau_l} \mathrm{I}_{\mathrm{ion}}(V_{\mathrm{tm}}^h, v^h)\phi^h dq,$$

$$G^{\mathrm{DG}}(V_{\mathrm{tm}}^h, v^h; \zeta^h) := \sum_{l=1}^{N} \int_{\tau_l} G(V_{\mathrm{tm}}^h, v^h)\zeta^h dq.$$

Finally the linear forms on the right hand side of (4.3) read as:

$$\begin{aligned} l_1(\phi^h) &:= \int_{\Sigma_0} V_{\mathrm{tm}}^0 \phi^h ds_q + \int_Q s_i \phi^h dq, \\ l_2(\psi^h) &:= \int_{\Sigma_R} g_R \psi^h ds_q, \\ l_3(\zeta^h) &:= \int_{\Sigma_0} v^0 \zeta^h ds_q. \end{aligned}$$

Henceforth we will assert that $p_1 = p_2 = p_3 = p \geq 1$. Starting point for the numerical analysis shall be the following linear problem: Find $(V_{\mathrm{tm}}^h, u_e^h) \in S_h^p(\mathcal{T}_N) \times S_h^p(\mathcal{T}_N)$ such that

$$\begin{aligned} b_T^{\mathrm{DG}}(V_{\mathrm{tm}}^h, \phi^h) + a_i^{\mathrm{DG}}(V_{\mathrm{tm}}^h, \phi^h) + a_i^{\mathrm{DG}}(u_e^h, \phi^h) &= l_1(\phi^h), \\ a_i^{\mathrm{DG}}(V_{\mathrm{tm}}^h, \psi^h) + a_{i+e}^{\mathrm{DG}}(u_e^h, \psi^h) &= l_2(\psi^h), \end{aligned} \tag{4.12}$$

for all $(\phi^h, \psi^h) \in S_h^p(\mathcal{T}_N) \times S_h^p(\mathcal{T}_N)$. For later use we will also consider the following form of Problem (4.12)

$$\begin{aligned} c^{\mathrm{DG}}((V_{\mathrm{tm}}^h, u_e^h), (\phi^h, \psi^h)) := \\ b_T^{\mathrm{DG}}(V_{\mathrm{tm}}^h, \phi^h) + a_i^{\mathrm{DG}}(V_{\mathrm{tm}}^h + u_e^h, \phi^h + \psi^h) + a_e^{\mathrm{DG}}(u_e^h, \psi^h) \\ = l_1(\phi^h) + l_2(\psi^h) \end{aligned} \tag{4.13}$$

for all $(\phi^h, \psi^h) \in S_h^p(\mathcal{T}_N) \times S_h^p(\mathcal{T}_N)$. For studying the bilinear form $b_T^{\mathrm{DG}}(\cdot,\cdot)$ we will introduce the following norms for functions $u \in \mathrm{H}^s(\mathcal{T}_N)$ with $s \geq 1$:

$$|\!|\!| u |\!|\!|_{\mathrm{time}}^2 := \sum_{l=1}^{N} h_l \left\| \frac{\partial}{\partial t} u \right\|_{\mathrm{L}^2(\tau_l)}^2 + \|u\|_{\mathrm{L}^2(\Sigma_0)}^2 + \|u\|_{\mathrm{L}^2(\Sigma_T)}^2 + \sum_{\Gamma_{kl} \in \mathcal{I}_N} \left\| [\![u]\!]_{kl,t} \right\|_{\mathrm{L}^2(\Gamma_{kl})}^2,$$

$$|\!|\!| u |\!|\!|_{\mathrm{time},*}^2 := \sum_{l=1}^{N} h_l^{-1} \|u\|_{\mathrm{L}^2(\tau_l)}^2 + \|u\|_{\mathrm{L}^2(\Sigma_T)}^2 + \sum_{\Gamma_{kl} \in \mathcal{I}_N} \|\{u\}_{kl}^{\mathrm{up}}\|_{\mathrm{L}^2(\Gamma_{kl})}^2.$$

Having defined these norms one is able to prove the following theorems.

Lemma 4.5. *The bilinear form $b_T^{\mathrm{DG}}(\cdot,\cdot)$ is bounded, i.e.:*

$$b_T^{\mathrm{DG}}(u, v_h) \leq c_2^B |\!|\!| u |\!|\!|_{time} |\!|\!| v_h |\!|\!|_{time,*}$$

for all $u \in u \in \mathrm{H}^s(\mathcal{T}_N)$ and $v_h \in S_h^p(\mathcal{T}_N)$.

Proof. See [129, Lemma 2.2.8]. □

Lemma 4.6. *Let $u_h \in S_h^p(\mathcal{T}_h)$. Then there holds*

$$b_T^{\mathrm{DG}}(u_h, u_h) \geq \frac{1}{2}\left(\|u_h\|^2_{\mathrm{L}^2(\Sigma_0)} + \|u_h\|^2_{\mathrm{L}^2(\Sigma_T)} + \sum_{\Gamma_{kl}\in\mathcal{I}_N} \left\| [\![u_h]\!]_{t,kl} \right\|^2_{\mathrm{L}^2(\Gamma_{kl})} \right).$$

Proof. See [129, Lemma 2.2.11]. □

Lemma 4.7. *For $u_h \in S_h^p(\mathcal{T}_N)$ let w_h be defined as*

$$w_h|_{\tau_l} := h_l \frac{\partial}{\partial t} u_h.$$

Then there exists a constant $c_1^b(\delta)$ independent of u_h such that

$$b_T^{\mathrm{DG}}(u_h, u_h + \delta w_h) \geq c_1^b(\delta) |\!|\!| u_h |\!|\!|^2_{time}. \tag{4.14}$$

The δ-dependent constant is given by

$$c_1^b(\delta) = \frac{1}{2} \min\left\{1, \delta, 1 - 2c_I^2 c_{R_2} \delta\right\}.$$

Proof. See [129, Lemma 2.2.14]. □

Further we need to define the following norms for studying the bilinear forms $a_{\{i,e\}}^{\mathrm{DG}}(\cdot,\cdot)$

$$\begin{aligned} |\!|\!| u |\!|\!|^2_{\mathrm{space},\{i,e\}} &:= \sum_{l=1}^{N} \left\| \mathbf{M}_{\{i,e\}}^{\frac{1}{2}} \nabla_{\boldsymbol{x}} u \right\|^2_{\mathrm{L}^2(\tau_l)} + \sum_{\Gamma_{kl}\in\mathcal{I}_N} \frac{\gamma_{kl}\sigma}{\overline{h}_{kl}} \left\| [\![u]\!]_{kl,\boldsymbol{x}} \right\|^2_{\mathrm{L}^2(\Gamma_{kl})} \\ &\quad + \alpha_{\{i,e\}} \int_{\Sigma_R} |u|^2 \, ds_q, \\ |\!|\!| u |\!|\!|^2_{\mathrm{space},\{i,e\},*} &:= |\!|\!| u |\!|\!|^2_{\mathrm{space},\{i,e\}} + \sum_{\Gamma_{kl}\in\mathcal{I}_N} \overline{h}_{kl} \left\| \left\langle \mathbf{M}_{\{i,e\}} \nabla_x u \right\rangle_{\omega,kl} \right\|^2_{\mathrm{L}^2(\Gamma_{kl})}. \end{aligned}$$

Remark 4.8. *Since $\mathbf{M}_i, \mathbf{M}_e$ are symmetric positive definite it holds*

$$|||u|||_{space,i} \leq \chi_i |||u|||_{space,e}, \tag{4.15}$$
$$|||u|||_{space,e} \leq \chi_e |||u|||_{space,i}, \tag{4.16}$$

where

$$\chi_i := \left(\max \left\{ \frac{\lambda_{\max}(\mathbf{M}_i)}{\lambda_{\min}(\mathbf{M}_e)}, \frac{\alpha_i}{\alpha_e} \right\} \right)^{\frac{1}{2}},$$
$$\chi_e := \left(\max \left\{ \frac{\lambda_{\max}(\mathbf{M}_e)}{\lambda_{\min}(\mathbf{M}_i)}, \frac{\alpha_e}{\alpha_i} \right\} \right)^{\frac{1}{2}}.$$

Lemma 4.9. *Let $\mathbf{S} \in [\mathrm{L}^\infty(Q)]^{d\times d}$ be a symmetric positive definite matrix. For all $u \in S_h^p(\mathcal{T}_N)$ there holds:*

$$\sum_{\Gamma_{kl}\in\mathcal{I}_N} \overline{h}_{kl} \left\| \langle \mathbf{S}\nabla_x u \rangle_{\omega,kl} \right\|^2_{\mathrm{L}^2(\Gamma_{kl})} \leq c_K \sum_{l=1}^{N} \left\| \mathbf{S}^{\frac{1}{2}} \nabla_{\boldsymbol{x}} u \right\|^2_{\mathrm{L}^2(\tau_l)} \tag{4.17}$$

where $c_K = c_K(\frac{\lambda_{max}(\mathbf{S})}{\lambda_{min}(\mathbf{S})}, c_I, c_G, c_{R_2})$.

Proof. Since $\mathbf{S}$ is symmetric and positive definite there exists a unique decomposition $\mathbf{S} = \mathbf{S}^{\frac{1}{2}}\mathbf{S}^{\frac{1}{2}}$ where $\mathbf{S}^{\frac{1}{2}}$ is again symmetric and positive definite. Recall the Definitions (4.5) and (4.6) of ω_1, ω_2. We first observe that due to positive definiteness

$$0 \leq \omega_1 = \frac{\left(\mathbf{S}|_{\tau_k}\boldsymbol{n}_k, \boldsymbol{n}_k\right)}{\left(\mathbf{S}|_{\tau_l}\boldsymbol{n}_l, \boldsymbol{n}_l\right) + \left(\mathbf{S}|_{\tau_k}\boldsymbol{n}_k, \boldsymbol{n}_k\right)} \leq \frac{\left(\mathbf{S}|_{\tau_k}\boldsymbol{n}_k, \boldsymbol{n}_k\right) + \left(\mathbf{S}|_{\tau_l}\boldsymbol{n}_l, \boldsymbol{n}_l\right)}{\left(\mathbf{S}|_{\tau_k}\boldsymbol{n}_k, \boldsymbol{n}_k\right) + \left(\mathbf{S}|_{\tau_l}\boldsymbol{n}_l, \boldsymbol{n}_l\right)} = 1.$$

The same holds for ω_2. Next by using the definition of the weighted average we obtain

$$\begin{aligned}
\sum_{\Gamma_{kl}\in\mathcal{I}_N} \overline{h}_{kl} \left\| \langle \mathbf{S}\nabla_x u_h \rangle_{\omega,kl} \right\|^2_{\mathrm{L}^2(\Gamma_{kl})} &= \sum_{\Gamma_{kl}\in\mathcal{I}_N} \overline{h}_{kl} \left\| \omega_1 \mathbf{S}|_{\tau_k}\nabla_x u_h|_{\tau_k} + \omega_2 \mathbf{S}|_{\tau_l}\nabla_x u_h|_{\tau_l} \right\|^2_{\mathrm{L}^2(\Gamma_{kl})} \\
&\leq \sum_{\Gamma_{kl}\in\mathcal{I}_N} \overline{h}_{kl} 2 \underbrace{\max\{\omega_1, \omega_2\}}_{\leq 1} \left(\left\| \mathbf{S}|_{\tau_k}\nabla_x u_h|_{\tau_k} \right\|^2_{\mathrm{L}^2(\Gamma_{kl})} + \left\| \mathbf{S}|_{\tau_l}\nabla_x u_h|_{\tau_l} \right\|^2_{\mathrm{L}^2(\Gamma_{kl})} \right) \\
&\leq 2 \sum_{\Gamma_{kl}\in\mathcal{I}_N} \overline{h}_{kl} \left(\underbrace{\left\| \mathbf{S}|_{\tau_k}\nabla_x u_h|_{\tau_k} \right\|^2_{\mathrm{L}^2(\Gamma_{kl})}}_{=:(a)} + \underbrace{\left\| \mathbf{S}|_{\tau_l}\nabla_x u_h|_{\tau_l} \right\|^2_{\mathrm{L}^2(\Gamma_{kl})}}_{=:(b)} \right) =: 2(\mathrm{I})
\end{aligned}$$

Now we apply inequality (3.18) to (a) and (b). Thus

$$(\mathrm{I}) \leq \sum_{\Gamma_{kl}\in\mathcal{I}_N} \underbrace{\overline{h}_{kl} c_I^2 \left|\Gamma_{kl}\right| \left(\left|\tau_k\right|^{-1} \left\| \mathbf{S}|_{\tau_k} \nabla_x u|_{\tau_k} \right\|^2_{\mathrm{L}^2(\tau_k)} + \left|\tau_l\right|^{-1} \left\| \mathbf{S}|_{\tau_l} \nabla_x u|_{\tau_l} \right\|^2_{\mathrm{L}^2(\tau_l)} \right)}_{=:(\mathrm{II})}.$$

Rewriting the above sum leads to

$$\begin{aligned}(\mathrm{II}) &= c_I^2 \sum_{l=1}^{N} \sum_{\substack{\Gamma_{kl}\in\mathcal{I}_N \\ \Gamma_{kl}\subset\partial\tau_l}} \overline{h}_{kl} \left|\Gamma_{kl}\right| \left|\tau_l\right|^{-1} \left\| \mathbf{S}|_{\tau_l} \nabla_x u|_{\tau_l} \right\|^2_{\mathrm{L}^2(\tau_l)} \\ &= c_I^2 \sum_{l=1}^{N} \left|\tau_l\right|^{-1} \left\| \mathbf{S}|_{\tau_l} \nabla_x u|_{\tau_l} \right\|^2_{\mathrm{L}^2(\tau_l)} \sum_{\substack{\Gamma_{kl}\in\mathcal{I}_N \\ \Gamma_{kl}\subset\partial\tau_l}} \overline{h}_{kl} \left|\Gamma_{kl}\right|.\end{aligned}$$

Using Assumption (3.13) we end up with

$$\begin{aligned}&c_I^2 \sum_{l=1}^{N} \left|\tau_l\right|^{-1} \left\| \mathbf{S}|_{\tau_l} \nabla_x u|_{\tau_l} \right\|^2_{\mathrm{L}^2(\tau_l)} \sum_{\substack{\Gamma_{kl}\in\mathcal{I}_N \\ \Gamma_{kl}\subset\partial\tau_l}} \overline{h}_{kl} \left|\Gamma_{kl}\right| \\ &\quad\leq c_I^2 \sum_{l=1}^{N} \left|\tau_l\right|^{-1} \left\| \mathbf{S}|_{\tau_l} \nabla_x u|_{\tau_l} \right\|^2_{\mathrm{L}^2(\tau_l)} c_G h_l \sum_{\substack{\Gamma_{kl}\in\mathcal{I}_N \\ \Gamma_{kl}\subset\partial\tau_l}} \left|\Gamma_{kl}\right| \\ &\quad\leq c_I^2 c_G \sum_{l=1}^{N} h_l \lambda_{\max}(\mathbf{S}|_{\tau_l})^{\frac{1}{2}} \left|\tau_l\right|^{-1} \left\| \mathbf{S}^{\frac{1}{2}}|_{\tau_l} \nabla_x u|_{\tau_l} \right\|^2_{\mathrm{L}^2(\tau_l)} \left|\partial\tau_l\right| =: (\mathrm{III})\end{aligned}$$

With Assumption (3.12) we can conclude that $\left|\tau_l\right|^{-1} \left|\partial\tau_l\right| h_l \leq c_{R_2}$. Thus we conclude

$$\begin{aligned}(\mathrm{III}) &\leq c_I^2 c_G c_{R_2} \max_{\boldsymbol{x}\in\Omega}(\lambda_{\max}(\mathbf{S})) \sum_{l=1}^{N} \left\| \mathbf{S}^{\frac{1}{2}}|_{\tau_l} \nabla_x u|_{\tau_l} \right\|^2_{\mathrm{L}^2(\tau_l)} \\ &= c_K \sum_{l=1}^{N} \left\| \mathbf{S}^{\frac{1}{2}}|_{\tau_l} \nabla_x u|_{\tau_l} \right\|^2_{\mathrm{L}^2(\tau_l)}\end{aligned}$$

□

Remark 4.10. *With the results of Lemma 4.9 we may also estimate*

$$\left|\!\left|\!\left| u \right|\!\right|\!\right|_{space,i,*} \leq (1 + c_K(\mathbf{M}_i))^{\frac{1}{2}} \left|\!\left|\!\left| u \right|\!\right|\!\right|_{space,i}, \tag{4.18}$$

$$\left|\!\left|\!\left| u \right|\!\right|\!\right|_{space,e,*} \leq (1 + c_K(\mathbf{M}_e))^{\frac{1}{2}} \left|\!\left|\!\left| u \right|\!\right|\!\right|_{space,e} \tag{4.19}$$

Remark 4.11. *From the results one sees, that the constants derived in the proofs depend on the quotient* $\lambda_{max}(\mathbf{M}_{\{i,e\}})/\lambda_{min}(\mathbf{M}_{\{i,e\}})$. *Hence, in the case of strongly anisotropic behavior, the constants will deteriorate. A remedy to this, is to use techniques for anisotropic finite elements, see [10].*

Now we are able to prove a boundedness result for the symmetric weighted interior penalty bilinear form. The techniques for proving such estimates are similar to those given in [129] and also [47].

Lemma 4.12. *Let* $\mathcal{T}_N \in \mathcal{T}_\mathcal{N}$ *with* $\mathcal{T}_\mathcal{N}$ *being an admissible good family of triangulations of* Q. *For* $u \in \mathrm{H}^s(\mathcal{T}_N)$ *with* $s > \frac{3}{2}$ *and* $v_h \in S_h^p(\mathcal{T}_N)$ *there holds:*

$$a^{\mathrm{DG}}_{\{i,e\}}(u, v_h) \leq c_2^{\{i,e\}} |\!|\!| u |\!|\!|_{space,\{i,e\},*} |\!|\!| v_h |\!|\!|_{space,\{i,e\}}$$

with h*-independent constant* $c_2^{\{i,e\}}$ *depending on* $\lambda_{max}(\mathbf{M}_{\{i,e\}})/\lambda_{min}(\mathbf{M}_{\{i,e\}})$, $c_{\boldsymbol{n}}$.

Proof. It suffices to prove the assertion for one bilinear form. For given $u \in \mathrm{H}^s(\mathcal{T}_N)$ with $s > \frac{3}{2}$ and $v_h \in S_h^p(\mathcal{T}_N)$ we can apply the Cauchy-Schwarz inequality and obtain

$$\begin{aligned}
a_i^{\mathrm{DG}}(u, v_h) \leq & \sum_{l=1}^{N} \left\| \mathbf{M}_i^{\frac{1}{2}} \nabla_{\boldsymbol{x}} u \right\|_{\mathrm{L}^2(\tau_l)} \left\| \mathbf{M}_i^{\frac{1}{2}} \nabla_{\boldsymbol{x}} v_h \right\|_{\mathrm{L}^2(\tau_l)} \\
& + \sum_{\Gamma_{kl} \in \mathcal{I}_N} \left\| \langle \mathbf{M}_i \nabla_{\boldsymbol{x}} u \rangle_{\omega,kl} \right\|_{\mathrm{L}^2(\Gamma_{kl})} \left\| [\![v_h]\!]_{\boldsymbol{x},kl} \right\|_{\mathrm{L}^2(\Gamma_{kl})} \\
& + \sum_{\Gamma_{kl} \in \mathcal{I}_N} \left\| [\![u]\!]_{\boldsymbol{x},kl} \right\|_{\mathrm{L}^2(\Gamma_{kl})} \left\| \langle \mathbf{M}_i \nabla_{\boldsymbol{x}} v_h \rangle_{\omega,kl} \right\|_{\mathrm{L}^2(\Gamma_{kl})} \\
& + \sum_{\Gamma_{kl} \in \mathcal{I}_N} \frac{\sigma \gamma_{kl}}{\overline{h}_{kl}} \left\| [\![u]\!]_{\boldsymbol{x},kl} \right\|_{\mathrm{L}^2(\Gamma_{kl})} \left\| [\![v_h]\!]_{\boldsymbol{x},kl} \right\|_{\mathrm{L}^2(\Gamma_{kl})} \\
& + \alpha_i \| u \|_{\mathrm{L}^2(\Sigma_R)} \| v_h \|_{\mathrm{L}^2(\Sigma_R)}.
\end{aligned}$$

We split the three summands over $\Gamma_{kl} \in \mathcal{I}_N$ into a part where $|\boldsymbol{n}_{\boldsymbol{x},k}| \neq 0$ and a part where $|\boldsymbol{n}_{\boldsymbol{x},k}| = 0$. The part with $|\boldsymbol{n}_{\boldsymbol{x},k}| = 0$ vanishes due to the definition of the space jump $[\![\cdot]\!]_{\boldsymbol{x},kl}$. This means that interior facets with $|\boldsymbol{n}_{k,\boldsymbol{x}}| = 0$ do not

contribute to the boundedness estimate. Next we use Hölder's inequality for sums and obtain

$$\begin{aligned}
a_i^{\mathrm{DG}}(u, v_h) \leq & \left[\sum_{l=1}^{N} \left\| \mathbf{M}_i^{\frac{1}{2}} \nabla_{\boldsymbol{x}} u \right\|_{\mathrm{L}^2(\tau_l)}^2\right]^{\frac{1}{2}} \left[\sum_{l=1}^{N} \left\| \mathbf{M}_i^{\frac{1}{2}} \nabla_{\boldsymbol{x}} v_h \right\|_{\mathrm{L}^2(\tau_l)}^2\right]^{\frac{1}{2}} \\
& + \left[\sum_{\Gamma_{kl} \in \mathcal{I}_N} \frac{\overline{h}_{kl}}{\sigma \gamma_{kl}} \left\| \langle \mathbf{M}_i \nabla_{\boldsymbol{x}} u \rangle_{\omega,kl} \right\|_{\mathrm{L}^2(\Gamma_{kl})}^2\right]^{\frac{1}{2}} \left[\sum_{\Gamma_{kl} \in \mathcal{I}_N} \frac{\gamma_{kl}\sigma}{\overline{h}_{kl}} \left\| [\![v_h]\!]_{\boldsymbol{x},kl} \right\|_{\mathrm{L}^2(\Gamma_{kl})}^2\right]^{\frac{1}{2}} \\
& + \left[\sum_{\Gamma_{kl} \in \mathcal{I}_N} \frac{\gamma_{kl}\sigma}{\overline{h}_{kl}} \left\| [\![u]\!]_{\boldsymbol{x},kl} \right\|_{\mathrm{L}^2(\Gamma_{kl})}^2\right]^{\frac{1}{2}} \left[\sum_{\Gamma_{kl} \in \mathcal{I}_N} \frac{\overline{h}_{kl}}{\sigma \gamma_{kl}} \left\| \langle \mathbf{M}_i \nabla_{\boldsymbol{x}} v_h \rangle_{\omega,kl} \right\|_{\mathrm{L}^2(\Gamma_{kl})}^2\right]^{\frac{1}{2}} \\
& + \left[\sum_{\Gamma_{kl} \in \mathcal{I}_N} \frac{\sigma \gamma_{kl}}{\overline{h}_{kl}} \left\| [\![u]\!]_{\boldsymbol{x},kl} \right\|_{\mathrm{L}^2(\Gamma_{kl})}^2\right]^{\frac{1}{2}} \left[\sum_{\Gamma_{kl} \in \mathcal{I}_N} \frac{\sigma \gamma_{kl}}{\overline{h}_{kl}} \left\| [\![v_h]\!]_{\boldsymbol{x},kl} \right\|_{\mathrm{L}^2(\Gamma_{kl})}^2\right]^{\frac{1}{2}} \\
& + \alpha_i \|u\|_{\mathrm{L}^2(\Sigma_R)} \|v_h\|_{\mathrm{L}^2(\Sigma_R)}.
\end{aligned}$$

Looking at this we see that we need to bound γ_{kl} from above and below. Recall the definition of γ_{kl} (4.7). It holds

$$\begin{aligned}
\gamma_{kl} &= 2 \frac{\left(\mathbf{M}_i|_{\tau_k} \boldsymbol{n}_{\boldsymbol{x},k}, \boldsymbol{n}_{\boldsymbol{x},k}\right)\left(\mathbf{M}_i|_{\tau_l} \boldsymbol{n}_{\boldsymbol{x},l}, \boldsymbol{n}_{\boldsymbol{x},l}\right)}{\left(\mathbf{M}_i|_{\tau_l} \boldsymbol{n}_{\boldsymbol{x},l}, \boldsymbol{n}_{\boldsymbol{x},l}\right) + \left(\mathbf{M}_i|_{\tau_l} \boldsymbol{n}_{\boldsymbol{x},k}, \boldsymbol{n}_{\boldsymbol{x},k}\right)} \\
&\leq 2 \max_{\boldsymbol{x} \in \Omega} (\lambda_{\max}(\mathbf{M}_i) \|\mathbf{M}_i\|_2^2) \, |\boldsymbol{n}_{\boldsymbol{x},k}|^2 \\
&\leq 2 \max_{\boldsymbol{x} \in \Omega} (\lambda_{\max}(\mathbf{M}_i) \|\mathbf{M}_i\|_2^2) =: c_\gamma^1.
\end{aligned} \tag{4.20}$$

For the lower part we obtain

$$\begin{aligned}
\gamma_{kl} &= 2 \frac{\left(\mathbf{M}_i|_{\tau_k} \boldsymbol{n}_{\boldsymbol{x},k}, \boldsymbol{n}_{\boldsymbol{x},k}\right)\left(\mathbf{M}_i|_{\tau_l} \boldsymbol{n}_{\boldsymbol{x},l}, \boldsymbol{n}_{\boldsymbol{x},l}\right)}{\left(\mathbf{M}_i|_{\tau_l} \boldsymbol{n}_{\boldsymbol{x},l}, \boldsymbol{n}_{\boldsymbol{x},l}\right) + \left(\mathbf{M}_i|_{\tau_l} \boldsymbol{n}_{\boldsymbol{x},k}, \boldsymbol{n}_{\boldsymbol{x},k}\right)} \\
&\geq 2 \min_{\boldsymbol{x} \in \Omega} (\lambda_{\min}(\mathbf{M}_i) \|\mathbf{M}_i\|_2^{-2}) \, |\boldsymbol{n}_{\boldsymbol{x},k}|^2 \\
&\geq 2 c_{\boldsymbol{n}}^2 \min_{\boldsymbol{x} \in \Omega} (\lambda_{\min}(\mathbf{M}_i) \|\mathbf{M}_i\|_2^{-2}) =: c_{\boldsymbol{n}}^2 c_\gamma^2.
\end{aligned} \tag{4.21}$$

Using these estimates and Lemma 4.9 we can conclude the boundedness with the constant

$$c_i^2 := 2 \max\{1 + \sigma^{-\frac{1}{2}} c_K^{\frac{1}{2}} c_{\boldsymbol{n}}^{-1} (c_\gamma^2)^{-\frac{1}{2}}, \sigma^{-\frac{1}{2}} c_{\boldsymbol{n}}^{-1} (c_\gamma^2)^{-\frac{1}{2}}\}.$$

□

Lemma 4.13. *Let $\mathcal{T}_N \in \mathcal{T}_{\mathcal{N}}$ with $\mathcal{T}_{\mathcal{N}}$ being an admissible good family of triangulations of Q. Further let $\sigma > \frac{c_K}{c_{\boldsymbol{n}}^2 c_\gamma^2}$. Then the bilinear forms $a^{\mathrm{DG}}_{\{i,e\}}(\cdot,\cdot)$ can be bounded from below*

$$a^{\mathrm{DG}}_{\{i,e\}}(u_h,u_h) \geq |\!|\!| u_h |\!|\!|^2_{space,\{i,e\}} \qquad \text{for all } u_h \in S_h^p(\mathcal{T}_N).$$

Proof. Let $u_h \in S_h^p(\mathcal{T}_N)$ be given. Again it suffices to prove the result only for one bilinear form. By the definition of the bilinear form $a_i^{\mathrm{DG}}(\cdot,\cdot)$ we have

$$\begin{aligned} a_i^{\mathrm{DG}}(u_h,u_h) = \sum_{l=1}^{N} \left\| \mathbf{M}_i^{\frac{1}{2}} \nabla_{\boldsymbol{x}} \right\|^2_{\mathrm{L}^2(\tau_l)} - 2 \sum_{\Gamma_{kl} \in \mathcal{I}_N} \int_{\Gamma_{kl}} \langle \mathbf{M}_i \nabla_{\boldsymbol{x}} u_h \rangle_{\omega,kl} [\![u_h]\!]_{\boldsymbol{x},kl} ds_q \\ + \sum_{\Gamma_{kl} \in \mathcal{I}_N} \frac{\sigma \gamma_{kl}}{\overline{h}_{kl}} \left\| [\![u_h]\!]_{\boldsymbol{x},kl} \right\|^2_{\mathrm{L}^2(\Gamma_{kl})}. \end{aligned}$$

We again observe that we can restrict ourselves to those interior facets where $|\boldsymbol{n}_{\boldsymbol{x},k}| > 0$. Next, we apply the Cauchy-Schwarz inequality followed by Hölder inequality and obtain

$$\begin{aligned} &\geq |\!|\!| u_h |\!|\!|^2_{\mathrm{space},i} - 2 \sum_{\Gamma_{kl} \in \mathcal{I}_N} \left\| \langle \mathbf{M}_i \nabla_{\boldsymbol{x}} u_h \rangle_{\omega,kl} \right\|_{\mathrm{L}^2(\Gamma_{kl})} \left\| [\![u_h]\!]_{\boldsymbol{x},kl} \right\|_{\mathrm{L}^2(\Gamma_{kl})} \\ &\geq |\!|\!| u_h |\!|\!|^2_{\mathrm{space},i} \\ &\quad - 2 \left[\sum_{\Gamma_{kl} \in \mathcal{I}_N} \frac{\overline{h}_{kl}}{\sigma \gamma_{kl}} \left\| \langle \mathbf{M}_i \nabla_{\boldsymbol{x}} u_h \rangle_{\omega,kl} \right\|^2_{\mathrm{L}^2(\Gamma_{kl})} \right]^{\frac{1}{2}} \left[\sum_{\Gamma_{kl} \in \mathcal{I}_N} \frac{\sigma \gamma_{kl}}{\overline{h}_{kl}} \left\| [\![u_h]\!]_{\boldsymbol{x},kl} \right\|^2_{\mathrm{L}^2(\Gamma_{kl})} \right]^{\frac{1}{2}}. \end{aligned}$$

Now we apply Lemma 4.9 together with the estimate (4.21). Hence

$$\begin{aligned} &\geq |\!|\!| u_h |\!|\!|^2_{\mathrm{space},i} \\ &\quad - 2 c_K^{\frac{1}{2}} \sigma^{-\frac{1}{2}} c_{\boldsymbol{n}}^{-1} c_\gamma^{-1} \left[\sum_{l=1}^{N} \left\| \mathbf{M}_i^{\frac{1}{2}} \nabla_{\boldsymbol{x}} \right\|^2_{\mathrm{L}^2(\tau_l)} \right]^{\frac{1}{2}} \left[\sum_{\Gamma_{kl} \in \mathcal{I}_N} \frac{\sigma \gamma_{kl}}{\overline{h}_{kl}} \left\| [\![u_h]\!]_{\boldsymbol{x},kl} \right\|^2_{\mathrm{L}^2(\Gamma_{kl})} \right]^{\frac{1}{2}} \\ &\geq |\!|\!| u_h |\!|\!|^2_{\mathrm{space},i} - c_K^{\frac{1}{2}} \sigma^{-\frac{1}{2}} c_{\boldsymbol{n}}^{-1} c_\gamma^{-1} \left[\sum_{l=1}^{N} \left\| \mathbf{M}_i^{\frac{1}{2}} \nabla_{\boldsymbol{x}} \right\|^2_{\mathrm{L}^2(\tau_l)} \right] \\ &\qquad - c_K^{\frac{1}{2}} \sigma^{-\frac{1}{2}} c_{\boldsymbol{n}}^{-1} c_\gamma^{-1} \left[\sum_{\Gamma_{kl} \in \mathcal{I}_N} \frac{\sigma \gamma_{kl}}{\overline{h}_{kl}} \left\| [\![u_h]\!]_{\boldsymbol{x},kl} \right\|^2_{\mathrm{L}^2(\Gamma_{kl})} \right]. \end{aligned}$$

With $\sigma > \frac{c_K}{c_{\boldsymbol{n}}^2 c_\gamma^2}$ we can conclude the assertion. □

Lemma 4.14. *Let $\mathcal{T}_N \in \mathcal{T}_{\mathcal{N}}$ with $\mathcal{T}_{\mathcal{N}}$ being an admissible good family of triangulations of Q. For $u_h \in S_h^p(\mathcal{T}_N)$ define the function $w_h \in S_h^p(\mathcal{T}_N)$ as*

$$w_h|_{\tau_l} := h_l \frac{\partial}{\partial t} u_h.$$

Then there holds

$$|||w_h|||_{space,e} \leq c_e |||u_h|||_{space,e}.$$

Proof. The main ideas for proving such an estimate were developed in [129, Lemma 2.2.19]. Exploiting the definition of the norm $|||\cdot|||_{\text{space},i}$ we see

$$\begin{aligned} |||w_h|||_{\text{space},e}^2 &= \sum_{l=1}^{N} \left\| \mathbf{M}_e^{\frac{1}{2}} \nabla_{\boldsymbol{x}} w_h \right\|_{\mathrm{L}^2(\tau_l)}^2 + \sum_{\Gamma_{kl} \in \mathcal{I}_N} \frac{\gamma_{kl}\sigma}{\overline{h}_{kl}} \left\| [\![w_h]\!]_{kl,\boldsymbol{x}} \right\|_{\mathrm{L}^2(\Gamma_{kl})}^2 + \alpha_e \|w_h\|_{\mathrm{L}^2(\Sigma_R)}^2 \\ &= \text{(I)} + \text{(II)} + \text{(III)} \end{aligned}$$

We will consider the terms (I), (II) and (III) separately. Beginning with (I) we see that

$$\begin{aligned} \text{(I)} \leq \sum_{l=1}^{N} h_l^2 \left\| \mathbf{M}_e^{\frac{1}{2}} \nabla_{\boldsymbol{x}} \left(\frac{\partial}{\partial t} u_h \right) \right\|_{\mathrm{L}^2(\tau_l)}^2 &\leq \sum_{l=1}^{N} h_l^2 \lambda_{\max}(\mathbf{M}_e|_{\tau_l}) \left\| \nabla_{\boldsymbol{x}} \left(\frac{\partial}{\partial t} u_h \right) \right\|_{\mathrm{L}^2(\tau_l)}^2 \\ &= \sum_{l=1}^{N} h_l^2 \lambda_{\max}(\mathbf{M}_e|_{\tau_l}) \left\| \frac{\partial}{\partial t} \nabla_{\boldsymbol{x}} u_h \right\|_{\mathrm{L}^2(\tau_l)}^2. \end{aligned}$$

Next, we use inverse inequality (3.17) and conclude

$$\begin{aligned} \sum_{l=1}^{N} h_l^2 \lambda_{\max}(\mathbf{M}_e|_{\tau_l}) \left\| \frac{\partial}{\partial t} \nabla_{\boldsymbol{x}} u_h \right\|_{\mathrm{L}^2(\tau_l)}^2 &\leq c_I^2 \sum_{l=1}^{N} h_l^2 \lambda_{\max}(\mathbf{M}_e|_{\tau_l}) h_l^{-2} \|\nabla_{\boldsymbol{x}} u_h\|_{\mathrm{L}^2(\tau_l)}^2 \\ &= c_I^2 \sum_{l=1}^{N} \lambda_{\max}(\mathbf{M}_e|_{\tau_l}) \left\| \mathbf{M}_e^{-\frac{1}{2}} \mathbf{M}_e^{\frac{1}{2}} \nabla_{\boldsymbol{x}} u_h \right\|_{\mathrm{L}^2(\tau_l)}^2. \end{aligned}$$

This can be estimated further as

$$\begin{aligned} &\leq c_I^2 \sum_{l=1}^{N} \frac{\lambda_{\max}(\mathbf{M}_e|_{\tau_l})}{\lambda_{\min}(\mathbf{M}_e|_{\tau_l})} \left\| \mathbf{M}_e^{\frac{1}{2}} \nabla_{\boldsymbol{x}} u_h \right\|_{\mathrm{L}^2(\tau_l)}^2 \\ &\leq \underbrace{c_I^2 \|\mathbf{M}_e\|_{[\mathrm{L}^\infty(Q)]^{d\times d}}}_{=:c_e^I} \sum_{l=1}^{N} \left\| \mathbf{M}_e^{\frac{1}{2}} \nabla_{\boldsymbol{x}} u_h \right\|_{\mathrm{L}^2(\tau_l)}^2. \end{aligned}$$

Secondly we will estimate (III). This term can be rewritten as

$$(\mathrm{III}) = \sum_{\substack{\tau_l \\ \partial\tau_l \cap \Sigma_R \neq \emptyset}} \int_{\partial\tau_l \cap \Sigma_R} |w_h|^2 \, ds_q.$$

Since we assumed that Q has a polygonal boundary we know that $\partial\tau_l \cap \Sigma_R = e_{j(l)} \in \mathcal{E}_R$. Therefore we can rewrite the sum as

$$\sum_{\substack{\tau_l \\ \partial\tau_l \cap \Sigma_R \neq \emptyset}} \int_{\partial\tau_l \cap \Sigma_R} |w_h|^2 \, ds_q = \sum_{e_j \in \mathcal{E}_R} h_{l(j)}^2 \int_{e_j} \left| \frac{\partial}{\partial t} u_h|_{\tau_{l(j)}} \right|^2 ds_q.$$

Next we use an inverse inequality of the form

$$|u_h|_{1,e_j} \leq \tilde{c}_I \, |e_j|^{-\frac{1}{d}} \, \|u_h\|_{\mathrm{L}^2(e_j)}$$

see [171, Lemma 10.7]. Due to shape regularity we know that there exists a constant c_{SR} such that

$$h_{l(j)} \, |e_j|^{-\frac{1}{d}} \leq c_{SR}.$$

Therefore we obtain

$$\begin{aligned}
\sum_{\substack{\tau_l \\ \partial\tau_l \cap \Sigma_R \neq \emptyset}} \int_{\partial\tau_l \cap \Sigma_R} |w_h|^2 \, ds_q &\leq \sum_{e_j \in \mathcal{E}_R} \tilde{c}_I^2 h_{l(j)}^2 \, |e_j|^{-\frac{2}{d}} \left\| \frac{\partial}{\partial t} u_h|_{\tau_{l(j)}} \right\|_{\mathrm{L}^2(e_j)}^2 \\
&\leq c_{SR}^2 \tilde{c}_I^2 \sum_{e_j \in \mathcal{E}_R} \left\| u_h|_{\tau_{l(j)}} \right\|_{\mathrm{L}^2(e_j)}^2 \\
&= c_{SR}^2 \tilde{c}_I^2 \|u_h\|_{\mathrm{L}^2(\Sigma_R)}^2.
\end{aligned}$$

It remains to estimate (II). We observe that

$$\begin{aligned}
[\![w_h]\!]_{\boldsymbol{x},kl} &= w_h|_{\tau_k} \boldsymbol{n}_{\boldsymbol{x},k} + w_h|_{\tau_l} \boldsymbol{n}_{\boldsymbol{x},l} = \left(h_k \frac{\partial}{\partial t} u_h|_{\tau_k} - h_l \frac{\partial}{\partial t} u_h|_{\tau_l} \right) \boldsymbol{n}_{\boldsymbol{x},k} \\
&= \frac{\partial}{\partial t} \left(h_k u_h|_{\tau_k} - h_l u_h|_{\tau_l} \right) \boldsymbol{n}_{x,k} \\
&= \overline{h}_{kl} \frac{\partial}{\partial t} (u_h|_{\tau_k} - u_h|_{\tau_l}) \boldsymbol{n}_{x,k} + \frac{1}{2} (h_k - h_l) \frac{\partial}{\partial t} (u_h|_{\tau_k} - u_h|_{\tau_l}) \boldsymbol{n}_{x,k}.
\end{aligned}$$

Thus we obtain by setting $z_h := u_h|_{\tau_k} - u_h|_{\tau_l}$

$$\begin{aligned}\left\|[\![w_h]\!]_{kl,\boldsymbol{x}}\right\|_{\mathrm{L}^2(\Gamma_{kl})} &= \left\|\overline{h}_{kl}\frac{\partial}{\partial t}z_h\boldsymbol{n}_{x,k} + \frac{1}{2}(h_k - h_l)\frac{\partial}{\partial t}z_h\boldsymbol{n}_{x,k}\right\|_{\mathrm{L}^2(\Gamma_{kl})} \\ &\leq \overline{h}_{kl}\left\|\frac{\partial}{\partial t}z_h\boldsymbol{n}_{\boldsymbol{x},k}\right\|_{\mathrm{L}^2(\Gamma_{kl})} + \frac{1}{2}\left|h_k - h_l\right|\left\|\frac{\partial}{\partial t}z_h\boldsymbol{n}_{\boldsymbol{x},k}\right\|_{\mathrm{L}^2(\Gamma_{kl})} \\ &\leq 2\overline{h}_{kl}\left\|\frac{\partial}{\partial t}z_h\boldsymbol{n}_{\boldsymbol{x},k}\right\|_{\mathrm{L}^2(\Gamma_{kl})}.\end{aligned}$$

We will distinguish three cases. First if $|\boldsymbol{n}_{\boldsymbol{x},k}| = 1$ (thus $n_{k,t} = 0$) we obtain with inverse inequality (3.17)

$$\left\|[\![w_h]\!]_{kl,\boldsymbol{x}}\right\|_{\mathrm{L}^2(\Gamma_{kl})} \leq 2\overline{h}_{kl}\left|\boldsymbol{n}_{\boldsymbol{x},k}\right|\left\|\frac{\partial}{\partial t}z_h\right\|_{\mathrm{L}^2(\Gamma_{kl})} \leq 2c_I\|z_h\|_{\mathrm{L}^2(\Gamma_{kl})} = 2c_I\left\|[\![u_h]\!]_{kl,\boldsymbol{x}}\right\|_{\mathrm{L}^2(\Gamma_{kl})}.$$

Second if $|\boldsymbol{n}_{\boldsymbol{x},k}| = 0$ we trivially conclude that

$$0 = \left\|[\![w_h]\!]_{kl,\boldsymbol{x}}\right\|_{\mathrm{L}^2(\Gamma_{kl})} = 2c_I\left\|[\![u_h]\!]_{kl,\boldsymbol{x}}\right\|_{\mathrm{L}^2(\Gamma_{kl})}.$$

The third case is the most challenging. For $0 < |\boldsymbol{n}_{\boldsymbol{x},k}| < 1$ we will decompose the derivative $\frac{\partial}{\partial t}z_h\boldsymbol{n}_{x,k}$ into a tangential part and a part containing only spatial derivatives. For a given normal vector $\boldsymbol{n}_k = (\boldsymbol{n}_{x,k}, n_{t,k})^\top$ we define tangential vectors $\boldsymbol{t}_i \in \mathbb{R}^{d_T}$ $i = 1, \ldots, d$ as

$$\boldsymbol{t}_i[s] := \begin{cases} n_{x_i,k} & \text{if } s = d_T \\ -n_{t,k} & \text{if } s = i \\ 0 & \text{else} \end{cases}.$$

Since $0 < |\boldsymbol{n}_{\boldsymbol{x},k}| < 1$ we know that $n_{k,t} \neq 0$ and thus we can define the normalized tangential vectors

$$\widetilde{\boldsymbol{t}}_i := \frac{1}{\sqrt{n_{x_i,k}^2 + n_{t,k}^2}}\boldsymbol{t}_i.$$

Now we can write the i-th tangential derivative of z_h as

$$(\nabla z_h, \boldsymbol{t}_i) = -n_{t,k}\frac{\partial}{\partial x_i}z_h + n_{x_i,k}\frac{\partial}{\partial t}z_h$$

and thus

$$n_{x_i,k}\frac{\partial}{\partial t}z_h = (\nabla z_h, \boldsymbol{t}_i) + n_{t,k}\frac{\partial}{\partial x_i}z_h \qquad \text{for all } i = 1,\dots,d.$$

With this relation we obtain

$$\begin{aligned}
\left\|[\![w_h]\!]_{kl,\boldsymbol{x}}\right\|^2_{\mathrm{L}^2(\Gamma_{kl})} &\leq 4\overline{h}^2_{kl}\left\|\frac{\partial}{\partial t}z_h\boldsymbol{n}_{k,\boldsymbol{x}}\right\|^2_{\mathrm{L}^2(\Gamma_{kl})} = \overline{h}^2_{kl}\sum_{i=1}^{d}\left\|n_{x_i,k}\frac{\partial}{\partial t}z_h\right\|^2_{\mathrm{L}^2(\Gamma_{kl})} \\
&= 4\overline{h}^2_{kl}\sum_{i=1}^{d}\left\|(\nabla z_h,\boldsymbol{t}_i) + n_{t,k}\frac{\partial}{\partial x_i}z_h\right\|^2_{\mathrm{L}^2(\Gamma_{kl})} \\
&\leq 8\overline{h}^2_{kl}\sum_{i=1}^{d}\left(\underbrace{\|(\nabla z_h,\boldsymbol{t}_i)\|^2_{\mathrm{L}^2(\Gamma_{kl})}}_{=:(a)} + \underbrace{\left\|n_{t,k}\frac{\partial}{\partial x_i}z_h\right\|^2_{\mathrm{L}^2(\Gamma_{kl})}}_{=:(b)}\right).
\end{aligned}$$

For part (a) we get with the normalized tangential vectors $\widetilde{\boldsymbol{t}}_i$ and the inverse inequality (3.17)

$$\begin{aligned}
(a) &\leq c_I^2\overline{h}_{kl}^{-2}(n^2_{k,x_i}+n^2_{k,t})\|z_h\|^2_{\mathrm{L}^2(\Gamma_{kl})} \\
&= c_I^2\overline{h}_{kl}^{-2}\frac{n^2_{k,x_i}+n^2_{k,t}}{|\boldsymbol{n}_{k,\boldsymbol{x}}|^2}\left\|[\![u_h]\!]_{k,\boldsymbol{x}}\right\|^2_{\mathrm{L}^2(\Gamma_{kl})}.
\end{aligned}$$

Hence by summing up we obtain for the first part

$$\begin{aligned}
8\overline{h}^2_{kl}\sum_{i=1}^{d}\|(\nabla z_h,\boldsymbol{t}_i)\|^2_{\mathrm{L}^2(\Gamma_{kl})} &\leq 8c_I^2\sum_{i=1}^{d}\frac{n^2_{k,x_i}+n^2_{k,t}}{|\boldsymbol{n}_{k,\boldsymbol{x}}|^2}\left\|[\![u_h]\!]_{k,\boldsymbol{x}}\right\|^2_{\mathrm{L}^2(\Gamma_{kl})} \\
&\leq 8c_I^2\left(1+\frac{d}{c_{\boldsymbol{n}}^2}\right)\left\|[\![u_h]\!]_{k,\boldsymbol{x}}\right\|^2_{\mathrm{L}^2(\Gamma_{kl})}
\end{aligned}$$

with the constant $c_{\boldsymbol{n}}$ from Assumption (3.14). We proceed by estimating (b). We observe that

$$\sum_{i=1}^{d}\left\|n_{t,k}\frac{\partial}{\partial x_i}z_h\right\|^2_{\mathrm{L}^2(\Gamma_{kl})} \leq \|\nabla_{\boldsymbol{x}}z_h\|^2_{\mathrm{L}^2(\Gamma_{kl})} \leq \lambda_{\min}(\mathbf{M}_e)^{-1}\left\|\mathbf{M}_e^{\frac{1}{2}}\nabla_{\boldsymbol{x}}z_h\right\|^2_{\mathrm{L}^2(\Gamma_{kl})}.$$

Hence collecting what has been proven so far we get for (II)

$$\sum_{\Gamma_{kl}\in\mathcal{I}_N}\frac{\gamma_{kl}\sigma}{\overline{h}_{kl}}\left\|[\![w_h]\!]_{kl,\boldsymbol{x}}\right\|^2_{\mathrm{L}^2(\Gamma_{kl})} \leq 8c_I^2\left(1+\frac{d}{c_{\boldsymbol{n}}^2}\right)\sum_{\Gamma_{kl}\in\mathcal{I}_N}\frac{\sigma\gamma_{kl}}{\overline{h}_{kl}}\left\|[\![u_h]\!]_{kl,\boldsymbol{x}}\right\|^2_{\mathrm{L}^2(\Gamma_{kl})} + 8\sigma\lambda_{\min}(\mathbf{M}_e)^{-1}\sum_{\Gamma_{kl}\in\mathcal{I}_N}\overline{h}_{kl}\left\|\mathbf{M}_e^{\frac{1}{2}}\nabla_{\boldsymbol{x}}z_h\right\|^2_{\mathrm{L}^2(\Gamma_{kl})}.$$

We still need to estimate

$$\sum_{\Gamma_{kl}\in\mathcal{I}_N}\overline{h}_{kl}\left\|\mathbf{M}_e^{\frac{1}{2}}\nabla_{\boldsymbol{x}}z_h\right\|^2_{\mathrm{L}^2(\Gamma_{kl})} \leq 2\sum_{\Gamma_{kl}\in\mathcal{I}_N}\overline{h}_{kl}\left(\left\|\mathbf{M}_e^{\frac{1}{2}}\nabla_{\boldsymbol{x}}u_h|_{\tau_k}\right\|^2_{\mathrm{L}^2(\Gamma_{kl})}+\left\|\mathbf{M}_e^{\frac{1}{2}}\nabla_{\boldsymbol{x}}u_h|_{\tau_l}\right\|^2_{\mathrm{L}^2(\Gamma_{kl})}\right).$$

With the same arguments as in the proof of Lemma 4.9 we obtain

$$\sum_{\Gamma_{kl}\in\mathcal{I}_N}\overline{h}_{kl}\left\|\mathbf{M}_e^{\frac{1}{2}}\nabla_{\boldsymbol{x}}z_h\right\|^2_{\mathrm{L}^2(\Gamma_{kl})} \leq c_K\sum_{i=1}^{N}\left\|\mathbf{M}_e^{\frac{1}{2}}\nabla_{\boldsymbol{x}}u_h\right\|^2_{\mathrm{L}^2(\tau_l)}.$$

Therefore we conclude

$$\begin{aligned}|\!|\!|w_h|\!|\!|^2_{\mathrm{space},i} &\leq 8\left(c_e^I+c_K\sigma\lambda_{\min}(\mathbf{M}_e)^{-1}\right)\sum_{i=1}^{N}\left\|\mathbf{M}_e^{\frac{1}{2}}\nabla_{\boldsymbol{x}}u_h\right\|^2_{\mathrm{L}^2(\tau_l)}\\ &\quad+8c_I^2\left(1+\frac{d}{c_{\boldsymbol{n}}^2}\right)\sum_{\Gamma_{kl}\in\mathcal{I}_N}\frac{\gamma_{kl}\sigma}{\overline{h}_{kl}}\left\|[\![u_h]\!]_{kl,\boldsymbol{x}}\right\|^2_{\mathrm{L}^2(\Gamma_{kl})}\\ &\quad+\tilde{c}_I^2c_{SR}^2\alpha_e\|u_h\|^2_{\mathrm{L}^2(\Sigma_R)}\\ &\leq c_e|\!|\!|u_h|\!|\!|^2_{\mathrm{space},i}\end{aligned}$$

with $c_e := 8\max\{c_e^I+c_K\sigma\lambda_{\min}(\mathbf{M}_e)^{-1}, c_I^2(1+\frac{d}{c_{\boldsymbol{n}}^2}), \frac{1}{8}\tilde{c}_I^2c_{SR}^2\alpha_e\}$. □

Before stating the stability result we define the following compound norms:

$$\begin{aligned}|\!|\!|(u_h,v_h)|\!|\!|^2_{\mathrm{DG}} &:= |\!|\!|u_h|\!|\!|^2_{\mathrm{time}}+|\!|\!|u_h|\!|\!|^2_{\mathrm{space},i}+|\!|\!|u_h|\!|\!|^2_{\mathrm{space},e},\\ |\!|\!|(u_h,v_h)|\!|\!|^2_{\mathrm{DG},*} &:= |\!|\!|u_h|\!|\!|^2_{\mathrm{time},*}+|\!|\!|u_h|\!|\!|^2_{\mathrm{space},i,*}+|\!|\!|u_h|\!|\!|^2_{\mathrm{space},e,*}.\end{aligned}$$

Theorem 4.15. *There holds:*

$$\left|c^{\mathrm{DG}}((u,v),(\phi_h,\psi_h))\right| \leq c_1^C \left|\!\left|\!\left|(u,v)\right|\!\right|\!\right|_{\mathrm{DG},*} \left|\!\left|\!\left|(\phi_h,\psi_h)\right|\!\right|\!\right|_{\mathrm{DG}}.$$

Proof. Using the boundedness of the individual components of the bilinear form $c^{\mathrm{DG}}((\cdot,\cdot),(\cdot,\cdot))$ we have

$$\begin{aligned}\left|c^{\mathrm{DG}}((u,v),(\phi_h,\psi_h))\right| &\leq c_2^B |\!|\!| u |\!|\!|_{\mathrm{time},*} \left|\!\left|\!\left|\phi_h\right|\!\right|\!\right|_{\mathrm{time}} \\ &\quad + c_2^i |\!|\!| u+v |\!|\!|_{\mathrm{space},i,*} \left|\!\left|\!\left|\phi_h+\psi_h\right|\!\right|\!\right|_{\mathrm{space},i} \\ &\quad + c_2^e |\!|\!| v |\!|\!|_{\mathrm{space},e,*} \left|\!\left|\!\left|\psi_h\right|\!\right|\!\right|_{\mathrm{space},e}.\end{aligned}$$

Next using triangle inequality we get

$$\begin{aligned}&\leq c_2^B |\!|\!| u |\!|\!|_{\mathrm{time},*} \left|\!\left|\!\left|\phi_h\right|\!\right|\!\right|_{\mathrm{time}} \\ &\quad + c_2^i \left(|\!|\!| u |\!|\!|_{\mathrm{space},i,*} + |\!|\!| v |\!|\!|_{\mathrm{space},i,*} \right) \left(\left|\!\left|\!\left|\phi_h\right|\!\right|\!\right|_{\mathrm{space},i} + \left|\!\left|\!\left|\psi_h\right|\!\right|\!\right|_{\mathrm{space},i} \right) \\ &\quad + c_2^e |\!|\!| v |\!|\!|_{\mathrm{space},e,*} \left|\!\left|\!\left|\psi_h\right|\!\right|\!\right|_{\mathrm{space},e}.\end{aligned}$$

Now using the relations (4.15)-(4.19) we conclude the result with

$$c_2^B := \max\left\{c_2^B, c_2^i(1+c_K(\mathbf{M}_i))^{\frac{1}{2}}\chi_i, c_2^e\right\}.$$

□

Eventually, we can prove a stability estimate similar to the one in [129].

Theorem 4.16. *Let $(u_h,v_h) \in S_h^p(\mathcal{T}_N) \times S_h^p(\mathcal{T}_N)$. Then there exists a constant $c_S^C > 0$ independent of $\mathcal{T}_N$ such that*

$$\sup_{\substack{(\phi_h,\psi_h)\in S_h^p(\mathcal{T}_N)\times S_h^p(\mathcal{T}_N) \\ (\phi_h,\psi_h)\neq \mathbf{0}}} \frac{c^{\mathrm{DG}}((u_h,v_h),(\phi_h,\psi_h))}{\left|\!\left|\!\left|(\phi_h,\psi_h)\right|\!\right|\!\right|_{\mathrm{DG}}} \geq c_S^C \left|\!\left|\!\left|(u_h,v_h)\right|\!\right|\!\right|_{\mathrm{DG}}$$

for all $(u_h,v_h) \in S_h^p(\mathcal{T}_N) \times S_h^p(\mathcal{T}_N)$.

Proof. The proof is based on a special choice for (ϕ_h,ψ_h) namely

$$\begin{aligned}\phi_h &:= u_h + \delta w_h, \\ \psi_h &:= v_h - \delta w_h\end{aligned}$$

for $\delta > 0$ to be defined later. Inserting this special test functions into the bilinear form $c^{\mathrm{DG}}((\cdot,\cdot),(\cdot,\cdot))$ we obtain

$$b_T^{\mathrm{DG}}(u_h, u_h + \delta w_h) + a_i^{\mathrm{DG}}(u_h + v_h, u_h + v_h) + a_e^{\mathrm{DG}}(v_h, v_h - \delta w_h).$$

Next, we use Lemma 4.7 together with Lemma 4.13 and obtain

$$\geq c_1^B(\delta)|\!|\!|u_h|\!|\!|_{\mathrm{time}}^2 + c_1^i|\!|\!|u_h + v_h|\!|\!|_{i,\mathrm{space}}^2 + c_1^e|\!|\!|v_h|\!|\!|_{e,\mathrm{space}} - \delta a_e^{\mathrm{DG}}(v_h, w_h).$$

Proceeding with Lemma 4.12 we get

$$\begin{aligned}\geq c_1^B(\delta)|\!|\!|u_h|\!|\!|_{\mathrm{time}}^2 + c_1^i|\!|\!|u_h + v_h|\!|\!|_{i,\mathrm{space}}^2 \\ + c_1^e|\!|\!|v_h|\!|\!|_{e,\mathrm{space}}^2 - \delta c_2^e|\!|\!|v_h|\!|\!|_{e,\mathrm{space},*}|\!|\!|w_h|\!|\!|_{e,\mathrm{space}}.\end{aligned}$$

This can be further estimated by

$$\begin{aligned}\geq c_1^B(\delta)|\!|\!|u_h|\!|\!|_{\mathrm{time}}^2 + \min\{c_1^i, c_1^e\}\left(|\!|\!|u_h + v_h|\!|\!|_{i,\mathrm{space}}^2 + |\!|\!|v_h|\!|\!|_{e,\mathrm{space}}^2\right) \\ - \delta c_2^e|\!|\!|v_h|\!|\!|_{e,\mathrm{space},*}|\!|\!|w_h|\!|\!|_{e,\mathrm{space}}.\end{aligned}$$

Now we use Young's inequality together with the relations (4.15), (4.16) and (4.18) to arrive at the estimate

$$\begin{aligned}\geq c_1^B(\delta)|\!|\!|u_h|\!|\!|_{\mathrm{time}}^2 + \min\{c_1^i, c_1^e\}\left(\chi_e^{-1}|\!|\!|u_h + v_h|\!|\!|_{e,\mathrm{space}}^2 + |\!|\!|v_h|\!|\!|_{e,\mathrm{space}}^2\right) \\ - \frac{\delta c_2^e(1+c_K)^{\frac{1}{2}}}{2}|\!|\!|v_h|\!|\!|_{e,\mathrm{space}}^2 - \frac{\delta c_2^e}{2}|\!|\!|w_h|\!|\!|_{e,\mathrm{space}}^2.\end{aligned}$$

Further estimates lead to

$$\begin{aligned}\geq c_1^B(\delta)|\!|\!|u_h|\!|\!|_{\mathrm{time}}^2 + \min\{c_1^i, c_1^e, \chi_e^{-1}\}\left(|\!|\!|u_h + v_h|\!|\!|_{e,\mathrm{space}}^2 + |\!|\!|v_h|\!|\!|_{e,\mathrm{space}}^2\right) \\ - \frac{\delta c_2^e(1+c_K)^{\frac{1}{2}}}{2}|\!|\!|v_h|\!|\!|_{e,\mathrm{space}}^2 - \frac{\delta c_2^e}{2}|\!|\!|w_h|\!|\!|_{e,\mathrm{space}}^2.\end{aligned}$$

Now we use Lemma 4.14 together with the fact that $\|u+v\|^2 + \|v\|^2 \geq \frac{1}{4}\|u\|^2 + \frac{1}{4}\|v\|^2$ and obtain

$$\begin{aligned}\geq c_1^B(\delta)|\!|\!|u_h|\!|\!|_{\mathrm{time}}^2 + \frac{1}{4}\min\{c_1^i, c_1^e, \chi_e^{-1}\}\left(|\!|\!|u_h|\!|\!|_{e,\mathrm{space}}^2 + |\!|\!|v_h|\!|\!|_{e,\mathrm{space}}^2\right) \\ - \frac{\delta c_2^e(1+c_K)^{\frac{1}{2}}}{2}|\!|\!|v_h|\!|\!|_{e,\mathrm{space}}^2 - \frac{\delta c_2^e c_e}{2}|\!|\!|u_h|\!|\!|_{e,\mathrm{space}}^2.\end{aligned}$$

This together with (4.15) finally leads to the estimate

$$\geq c_1^B(\delta)|||u_h|||^2_{\text{time}} + \underbrace{\left(\frac{\chi_i^{-1}}{4}\min\{c_1^i, c_1^e, \chi_e^{-1}\} - \frac{\delta\chi_i c_e c_2^e}{2}\right)}_{=:c_2(\delta)}|||u_h|||^2_{\text{space},i}$$
$$+ \underbrace{\left(\frac{1}{4}\min\{c_1^i, c_1^e, \chi_e^{-1}\} - \frac{\delta c_2^e(1+c_K)^{\frac{1}{2}}}{2}\right)}_{=:c_3(\delta)}|||v_h|||^2_{\text{space},e}.$$

Now we look at each of the constants. To get $c_1^B(\delta) > 0$ we need to choose

$$\delta \leq \frac{1}{1 + 2c_I^2 c_{R_2}} =: \delta_1^* > 0.$$

For having $c_2(\delta) > 0$ we need to choose

$$\delta \leq \frac{\min\{c_1^i, c_1^e, \chi_e^{-1}\}}{2\chi_i^2 c_e c_2^e} =: \delta_2^* > 0$$

Finally for getting $c_3(\delta) > 0$ we need to choose

$$\delta \leq \frac{\min\{c_1^i, c_1^e, \chi_e^{-1}\}}{2(1+c_K)^{\frac{1}{2}} c_2^e} =: \delta_3^* > 0.$$

Thus we choose $\delta^* := \min\{\delta_1^*, \delta_2^*, \delta_3^*\}$ and obtain

$$\geq \min\{c_1^B(\delta^*), c_2(\delta^*), c_3(\delta^*)\}\left(|||u_h|||^2_{\text{time}} + |||u_h|||^2_{\text{space},i} + |||v_h|||^2_{\text{space},e}\right),$$
$$= \min\{c_1^B(\delta^*), c_2(\delta^*), c_3(\delta^*)\}|||(u_h, v_h)|||^2_{\text{DG}}.$$

With this we conclude the stability estimate with the stability constant

$$c_S^C := \frac{\min\{c_1^B(\delta^*), c_2(\delta^*), c_3(\delta^*)\}}{\sqrt{\max\{1 + \delta^* c_I^B, 1 + \delta^*(c_i + \chi_i c_e), 1\}}} > 0.$$

□

With the stability and boundedness estimate we can prove an error estimate in the energy norm. The proof can be done analogously to the proof [129, Theorem 2.2.21] by replacing the isotropic estimates with the revised estimates for the anisotropic diffusion behavior.

Theorem 4.17. *Let $\mathcal{T}_N \in \mathcal{T}_{\mathcal{N}}$ be a good family of triangulations of Q. Let the exact solution $(V_{\mathrm{tm}}, u_e) \in H^{s_1,r_1}(Q) \times H^{s_2,r_2}(Q)$ for some s_1, s_2, r_1, r_2 with $\min\{s_1, r_1\} > \frac{3}{2}$ and, $\min\{s_2, r_2\} > \frac{3}{2}$. For $\sigma > 4c_K$ let $(u_h, v_h) \in S_h^p(\mathcal{T}_h) \times S_h^p(\mathcal{T}_h)$ be the solutions to the discrete linear variational problem (4.12). Then there holds:*

$$\begin{aligned}\left|\!\left|\!\left|(V_{\mathrm{tm}}, u_e) - (u_h, v_h)\right|\!\right|\!\right|_{\mathrm{DG}} \leq \inf_{(z_h,q_h)\in[S_h^p(\mathcal{T}_h)]^2} \Big[&\left|\!\left|\!\left|(V_{\mathrm{tm}}, u_e) - (z_h, q_h)\right|\!\right|\!\right|_{\mathrm{DG}} \\ &+ \frac{c_2^B}{c_S^C} \left|\!\left|\!\left|(V_{\mathrm{tm}}, u_e) - (z_h, q_h)\right|\!\right|\!\right|_{\mathrm{DG},*} \Big]\end{aligned}$$

For proving bounds on the error estimate appearing in Theorem 4.17 one can apply the same techniques as in See the proofs of [129, Lemmata 2.2.22, 2.2.23, 2.2.24, 2.2.26 and Theorem 2.2.27]. By introducing local L^2-projections and again replace the isotropic estimates with the revised anisotropic ones one can prove the following:

Theorem 4.18. *Let $\mathcal{T}_N \in \mathcal{T}_{\mathcal{N}}$ be a good family of triangulations of Q. Let the exact solution to the linear problem (4.12) $(V_{\mathrm{tm}}, u_e) \in H^{s_1,r_1}(Q) \times H^{s_2,r_2}(Q)$ with $\min\{s_1, r_1\} > 2$ and, $\min\{s_2, r_2\} > 2$. Assume $\sigma \geq 4c_K$. For the solution to the discrete linear problem $(u_h, v_h) \in [S_h^p(\mathcal{T}_h)]^2$ for an $\mathcal{T}_h \in \mathcal{T}_{\mathcal{H}}$ there holds*

$$\left|\!\left|\!\left|(V_{\mathrm{tm}}, u_e) - (u_h, v_h)\right|\!\right|\!\right|_{\mathrm{DG}} \leq c(\mathbf{M}_i, \mathbf{M}_e) \left[\sum_{l=1}^{N} h_l^{2\min\{s,p+1\}-2} |(V_{\mathrm{tm}}, u_e)|^2_{[\mathrm{H}^s(Q)]^2}\right]^{\frac{1}{2}}.$$

If $\mathcal{T}_{\mathcal{N}}$ is additionally quasi-uniform there holds

$$\left|\!\left|\!\left|(V_{\mathrm{tm}}, u_e) - (u_h, v_h)\right|\!\right|\!\right|_{\mathrm{DG}} \leq \widetilde{c}(\mathbf{M}_i, \mathbf{M}_e) h^{2\min\{s,p+1\}-1} |(V_{\mathrm{tm}}, u_e)|_{[\mathrm{H}^s(Q)]^2}.$$

4.3 Convergence Studies

In this section convergence studies will be presented to support the theoretical results given in Section 4.2. The approximation of two regular solutions V_{tm} and u_e in different space dimensions and different polynomial degrees for the

approximation space will be considered. The setup will be the same for all simulation studies. As space-time cylinder Q the unit hyper-cube

$$Q := (0,1)^{d_T}, \qquad d_T \geq 3,$$

will be considered. In all examples given subsequently we will consider solutions to the problem (4.12).

Example 4.19. As a first example we set $d_T = 3$. The diffusion tensors are chosen as

$$\mathbf{M}_i := \begin{pmatrix} \frac{3}{4} & \frac{3}{20} \\ \frac{3}{20} & \frac{3}{4} \end{pmatrix}, \qquad \mathbf{M}_e := \begin{pmatrix} \frac{5}{4} & \frac{1}{4} \\ \frac{1}{4} & \frac{5}{4} \end{pmatrix}.$$

On the boundary $\Sigma_R := \partial(0,1)^2 \times (0,1)$ we apply Robin boundary conditions with $\alpha_i = 1$ and $\alpha_e = 1$. The given data s_i,s_e,$g_{i,R}$, $g_{e,R}$ and V_{tm}^0 are chosen such that the exact solutions of the linear Bidomain equations are given as

$$\begin{aligned} V_{\text{tm}}(\boldsymbol{x},t) &= x(1-x)y(1-y)t(1-t), \\ u_e(\boldsymbol{x},t) &= \sin(\pi x)\sin(\pi y)\sin(\pi t). \end{aligned}$$

For the stabilization parameter we chose $\sigma_{kl} = 25$. The resulting linear systems are solved with a preconditioned GMRes method within Neshmet. As preconditioner the black-box algebraic multigrid BoomerAmg provided within the Hypre package was taken, see [64]. The results for the polynomial degrees $p = 1, 2$ are shown in Tables 4.1, 4.2, 4.3 and 4.4.

Example 4.20. In the second example we consider $d_T = 4$. Thus Q is the four dimensional unit cube. For the discretization of four dimensional objects we refer to [130]. The diffusion tensors are chosen as

$$\mathbf{M}_i := \begin{pmatrix} \frac{3}{4} & \frac{1}{10} & \frac{1}{20} \\ \frac{1}{10} & \frac{7}{10} & \frac{1}{10} \\ \frac{1}{20} & \frac{1}{10} & \frac{3}{4} \end{pmatrix} \qquad \mathbf{M}_e := \begin{pmatrix} \frac{23}{12} & \frac{1}{6} & -\frac{7}{12} \\ \frac{1}{6} & \frac{7}{6} & \frac{1}{6} \\ -\frac{7}{12} & \frac{1}{6} & \frac{23}{12} \end{pmatrix}.$$

Again we apply Robin boundary conditions on $\Sigma_R := \partial(0,1)^3 \times (0,1)$ with $\alpha_i = 1$ and $\alpha_e = 1$. The given data s_i,s_e,$g_{i,R}$, $g_{e,R}$ and V_{tm}^0 are chosen such that the exact solutions of the linear Bidomain equations are given as

$$\begin{aligned} V_{\text{tm}}(\boldsymbol{x},t) &= x(1-x)y(1-y)z(1-z)t(1-t), \\ u_e(\boldsymbol{x},t) &= \sin(\pi x)\sin(\pi y)\sin(\pi z)\sin(\pi t). \end{aligned}$$

level	elements	dof	$\|\|\|\boldsymbol{z}-\boldsymbol{z}_h\|\|\|_{\mathrm{DG}}$	eoc
0	6	48	1.3723E+0	–
1	48	384	1.0833E+0	0.34
2	384	3072	6.6351E−1	0.71
3	3072	24576	3.5900E−1	0.89
4	24576	196608	1.8443E−1	0.96
5	196608	1572864	9.3071E−2	0.99
6	1572864	12582912	4.6690E−2	1.00
Theory:				1.00

Table 4.1: Energy error $|||\boldsymbol{z}-\boldsymbol{z}_h|||_{DG}$ for $p=1$. For reasons of brevity we have defined $\boldsymbol{z}=(V_{\mathrm{tm}},u_e)$ and $\boldsymbol{z}_h=(V_{\mathrm{tm}}^h,u_e^h)$.

			Error V_{tm}		Error u_e	
level	elements	dof	error	eoc	error	eoc
0	6	24	9.2459E−2	–	1.3692E+0	–
1	48	192	4.7700E−2	0.95	1.0823E+0	0.34
2	384	1536	2.2604E−2	1.08	6.6313E−1	0.71
3	3072	12288	1.0229E−2	1.14	3.5886E−1	0.89
4	24576	98304	4.7466E−3	1.11	1.8436E−1	0.96
5	196608	786432	2.2789E−3	1.06	9.3043E−2	0.99
6	1572864	6291456	1.1135E−3	1.03	4.6677E−2	1.00
Observed:				1.00		1.00

Table 4.2: Individual error components for $p=1$.

level	elements	dof	$\|\|\|\boldsymbol{z}-\boldsymbol{z}_h\|\|\|_{\mathrm{DG}}$	eoc
0	6	120	8.9235E−1	–
1	48	960	3.9336E−1	1.18
2	384	7680	1.2610E−1	1.64
3	3072	61440	3.4188E−2	1.88
4	24576	491520	8.8077E−3	1.96
5	196608	3932160	2.2279E−3	1.98
Theory:				2.00

Table 4.3: Energy error $|||\boldsymbol{z}-\boldsymbol{z}_h|||_{DG}$ for $p=2$. For reasons of brevity we have defined $\boldsymbol{z}=(V_{\mathrm{tm}},u_e)$ and $\boldsymbol{z}_h=(V_{\mathrm{tm}}^h,u_e^h)$.

			Error V_{tm}		Error u_e	
level	elements	dof	error	eoc	error	eoc
0	6	60	2.7700E−2	–	8.9192E−1	–
1	48	480	1.2879E−2	1.10	3.9315E−2	1.18
2	384	3840	3.4286E−3	1.91	1.2605E−1	1.64
3	3072	30720	7.9743E−4	2.10	3.4179E−2	1.88
4	24576	245760	1.8905E−4	2.08	8.8056E−3	1.96
5	196608	1966080	4.5158E−5	2.07	2.2274E−3	1.98
Observed:				2.00		2.00

Table 4.4: Individual error components for $p=2$.

For the stabilization parameter we chose $\sigma_{kl} = 25$. The results are depicted in Table 4.5 and 4.6.

level	elements	dof	$\|\|\|\boldsymbol{z} - \boldsymbol{z}_h\|\|\|_{\mathrm{DG}}$	eoc
0	16	240	1.5223E+0	–
1	256	3840	1.3572E+0	0.17
2	4096	61440	9.5583E−1	0.51
3	65536	983040	6.0298E−1	0.66
4	1048576	15728640	3.2097E−1	0.91
Theory:				1.00

Table 4.5: Energy error $|||\boldsymbol{z} - \boldsymbol{z}_h|||_{DG}$ for $p = 1$. For reasons of brevity we have defined $\boldsymbol{z} = (V_{\mathrm{tm}}, u_e)$ and $\boldsymbol{z}_h = (V_{\mathrm{tm}}^h, u_e^h)$.

			Error V_{tm}		Error u_e	
level	elements	dof	error	eoc	error	eoc
0	16	240	1.5211E−1	–	1.5147E+0	–
1	256	3840	1.8473E−1	−0.28	1.3446E+0	0.17
2	4096	61440	1.3742E−1	0.43	9.4590E−1	0.51
3	65536	983040	8.2419E−2	0.74	5.9732E−1	0.66
4	1048576	15728640	4.1799E−2	0.98	3.1839E−1	0.91
Observed:				1.00		1.00

Table 4.6: Individual error components for $p = 1$.

4.4 Extension to Bidomain Equations

In this section we will consider the nonlinear case. As stated earlier it is assumed that the exact solution $(V_{\mathrm{tm}}, u_e, v) \in [\mathrm{H}^s(Q)]^3$ with $s > \frac{3}{2}$.

4.4.1 Numerical Analysis of the Linearized Problem

The linearized problem of (4.3) reads as: Given $(u_h, u_h^e, w_h) \in [S_h^p(\mathcal{T}_N)]^3$ find $(\delta_h^{\mathrm{tm}}, \delta_h^e, \delta_h^v) \in [S_h(\mathcal{T}_N)]^3$ such that

$$\begin{aligned} c^{\mathrm{DG}}((u_h, v_h); (\delta_h^{\mathrm{tm}}, \delta_h^e, \delta_h^v), (\phi_h, \psi_h, \zeta_h)) := \\ b_T^{\mathrm{DG}}(\delta_h^{\mathrm{tm}}, \phi_h) + b_T^{\mathrm{DG}}(\delta_h^v, \zeta_h) + a_{\boldsymbol{x},i}(\delta_h^{\mathrm{tm}} + \delta_h^e, \phi_h + \psi_h) + a_{\boldsymbol{x},e}(\delta_h^e, \psi_h) \\ + c_{nl}((u_h, w_h); (\delta_h^{\mathrm{tm}}, \delta_h^v), (\phi_h, \psi_h)) = rhs \end{aligned} \tag{4.22}$$

for all $(\phi_h, \psi_h, \zeta_h) \in [S_h(\mathcal{T}_N]^3$ where

$$c_{nl}((u_h, w_h); (\delta_h^{\mathrm{tm}}, \delta_h^v), (\phi_h, \psi_h)) := \sum_{l=1}^{N} \int_{\tau_l} \left(\mathbf{A}(u_h, w_h) \begin{pmatrix} \delta_h^{\mathrm{tm}} \\ \delta_h^v \end{pmatrix}, \begin{pmatrix} \phi_h \\ \psi_h \end{pmatrix} \right) dq.$$

For the numerical analysis we need to define appropriate norms :

$$\begin{aligned} |\!|\!| (u, v, w) |\!|\!|_{\mathrm{DG}}^2 &:= |\!|\!| u |\!|\!|_{\mathrm{time}}^2 + |\!|\!| w |\!|\!|_{\mathrm{time}}^2 + |\!|\!| u |\!|\!|_{\mathrm{space},i}^2 + |\!|\!| v |\!|\!|_{\mathrm{space},e}^2 \\ &\quad + \|u\|_{\mathrm{L}^2(Q)}^2 + \|w\|_{\mathrm{L}^2(Q)}^2, \end{aligned} \tag{4.23}$$

$$\begin{aligned} |\!|\!| (u, v, w) |\!|\!|_{\mathrm{DG},*}^2 &:= |\!|\!| u |\!|\!|_{\mathrm{time},*}^2 + |\!|\!| w |\!|\!|_{\mathrm{time},*}^2 + |\!|\!| u |\!|\!|_{\mathrm{space},i;*}^2 + |\!|\!| v |\!|\!|_{\mathrm{space},e,*}^2 \\ &\quad + \|u\|_{\mathrm{L}^2(Q)}^2 + \|w\|_{\mathrm{L}^2(Q)}^2. \end{aligned} \tag{4.24}$$

With the norms (4.23), (4.24) we can prove the following

Theorem 4.21 (Boundedness)**.** *Given $(u_h, v_h) \in [S_h^p(\mathcal{T}_N)]^2$. Under the assumptions 4.1:1, 4.1:2 and 4.3 there holds for all $(\delta_h^{tm}, \delta_h^e, \delta_h^v) \in [S_h^p(\mathcal{T}_N)]^3$ and $(\phi_h, \psi_h, \zeta_h) \in [S_h^p(\mathcal{T}_N)]^3$:*

$$\begin{aligned} &\left| c^{\mathrm{DG}}((u_h, v_h); (\delta_h^{tm}, \delta_h^e, \delta_h^v), (\phi_h, \psi_h, \zeta_h)) \right| \\ &\quad \leq c_2^{B,nl}(u_h, v_h) |\!|\!| (\delta_h^{tm}, \delta_h^e, \delta_h^v) |\!|\!|_{\mathrm{DG},*} |\!|\!| (\phi_h, \psi_h, \zeta_h) |\!|\!|_{\mathrm{DG}}. \end{aligned}$$

Proof. The proof can be done similarly to Theorem 4.15. The changes appear in the treatment of the term $c_{nl}(\cdot;\cdot,\cdot)$. Examining the definition of $c_{nl}(\cdot;\cdot,\cdot)$ we get

$$\begin{aligned}
&\left|\sum_{l=1}^{N}\int_{\tau_l}\left(\mathbf{A}(u_h,w_h)\begin{pmatrix}\delta_h^{\mathrm{tm}}\\ \delta_h^{v}\end{pmatrix},\begin{pmatrix}\phi_h\\ \psi_h\end{pmatrix}\right)dq\right| \\
&\qquad\le \sum_{l=1}^{N}\int_{\tau_l}\|\mathbf{A}(u_h,v_h)\|\left|\begin{pmatrix}\delta_h^{\mathrm{tm}}\\ \delta_h^{v}\end{pmatrix}\right|\left|\begin{pmatrix}\phi_h\\ \psi_h\end{pmatrix}\right|\,dq \\
&\qquad\le c^{nl}\left\|(\delta_h^{\mathrm{tm}},\delta_h^{v})\right\|_{\mathrm{L}^2(Q)}\left\|(\phi_h^{\mathrm{tm}},\psi_h^{v})\right\|_{\mathrm{L}^2(Q)}.
\end{aligned}$$

Therefore collecting the constants from the proof of Theorem 4.15 and c^{nl} we can conclude the result. □

Further we can prove the following stability result.

Theorem 4.22 (Stability)**.** *Given $(u_h,v_h)\in[S_h^p(\mathcal{T}_N)]^2$. Under the assumptions 4.1:1, 4.1:2 and 4.3 there holds: $\exists c_s>0$ not depending on h such that*

$$c_s\left|\!\left|\!\left|(\delta_h^{tm},\delta_h^{e},\delta_h^{v})\right|\!\right|\!\right|_{\mathrm{DG}}\le \sup_{\substack{(\phi_h,\psi_h,\zeta_h)\in[S_h^p(\mathcal{T}_h)]^3\\ |||(\phi_h,\psi_h,\zeta_h)|||_{\mathrm{DG}}\neq 0}}\frac{c^{\mathrm{DG}}((u_h,v_h);(\delta_h^{tm},\delta_h^{e},\delta_h^{v}),(\phi_h,\psi_h,\zeta_h))}{\left|\!\left|\!\left|(\phi_h,\psi_h,\zeta_h)\right|\!\right|\!\right|_{\mathrm{DG}}}$$

for all $(\delta_h^{tm},\delta_h^{e},\delta_h^{v})\in[S_h^p(\mathcal{T}_N)]^3$.

Proof. For ease of notation we will write $a_h=\delta_h^{\mathrm{tm}}$, $b_h=\delta_h^{e}$, $c_h=\delta_h^{v}$, $w_h:=h_l\frac{\partial}{\partial t}a_h$ and $q_h:=h_l\frac{\partial}{\partial t}c_h$. As in the proof of Theorem 4.16 we will use special test functions, namely

$$\begin{aligned}
\phi_h|_{\tau_l}&:=a_h|_{\tau_l}+\omega w_h|_{\tau_l},\\
\psi_h|_{\tau_l}&:=b_h|_{\tau_l}-\omega w_h|_{\tau_l},\\
\zeta_h|_{\tau_l}&:=c_h|_{\tau_l}+\omega q_h|_{\tau_l}
\end{aligned}$$

for a $\omega>0$ to be defined later. The crux of the proof is the estimation of

$$\begin{aligned}
&b_T^{\mathrm{DG}}(a_h,a_h+\omega w_h)+b_T^{\mathrm{DG}}(c_h,c_h+\omega q_h)\\
&\qquad+c_{nl}((u_h,v_h);(a_h,c_h),(a_h+\omega w_h,c_h+\omega q_h)).
\end{aligned}$$

The first step is to take a look at $b_T^{\mathrm{DG}}(a_h, w_h)$. We follow the lines of the proof of [129, Lemma 2.2.14]. Using the representation of $b_T^{\mathrm{DG}}(\cdot,\cdot)$ from Remark 4.4 we have

$$b_T^{\mathrm{DG}}(a_h, w_h) = \sum_{l=1}^{N} h_l \int_{\tau_l} \left| \frac{\partial}{\partial t} a_h \right|^2 dq + \int_{\Sigma_0} a_h w_h ds_q - \sum_{\Gamma_{kl} \in \mathcal{I}_N} \int_{\Gamma_{kl}} [\![a_h]\!]_{kl,t} \{ w_h \}_{kl}^{\mathrm{down}} ds_q.$$

Using the Cauchy-Schwarz-Inequality we get

$$\geq \sum_{l=1}^{N} h_l \left\| \frac{\partial}{\partial t} a_h \right\|^2_{\mathrm{L}^2(\tau_l)} - \|a_h\|_{\mathrm{L}^2(\Sigma_0)} \|w_h\|_{\mathrm{L}^2(\Sigma_0)} - \sum_{\Gamma_{kl} \in \mathcal{I}_N} \left\| [\![a_h]\!]_{kl,t} \right\|_{\mathrm{L}^2(\Gamma_{kl})} \left\| \{ w_h \}_{kl}^{\mathrm{down}} \right\|_{\mathrm{L}^2(\Gamma_{kl})}.$$

This can be estimated as

$$\geq \sum_{l=1}^{N} h_l \left\| \frac{\partial}{\partial t} a_h \right\|^2_{\mathrm{L}^2(\tau_l)} - \|a_h\|_{\mathrm{L}^2(\Sigma_0)} \|w_h\|_{\mathrm{L}^2(\Sigma_0)} - \left[\sum_{\Gamma_{kl} \in \mathcal{I}_N} \left\| [\![a_h]\!]_{kl,t} \right\|^2_{\mathrm{L}^2(\Gamma_{kl})} \right]^{\frac{1}{2}} \left[\sum_{\Gamma_{kl} \in \mathcal{I}_N} \left\| \{ w_h \}_{kl}^{\mathrm{down}} \right\|^2_{\mathrm{L}^2(\Gamma_{kl})} \right]^{\frac{1}{2}}.$$

Next we estimate w_h on Σ_0. Using the inverse and trace inequalities (3.15)-(3.17) this can be done as follows:

$$\|w_h\|^2_{\mathrm{L}^2(\Sigma_0)} = \sum_{\substack{\tau_l \in \mathcal{T}_h \\ \partial\tau_l \cap \Sigma_0 \neq \emptyset}} \|w_h\|^2_{\mathrm{L}^2(\partial\tau_l \cap \Sigma_0)} \leq c_I^2 \sum_{\substack{\tau_l \in \mathcal{T}_h \\ \partial\tau_l \cap \Sigma_0 \neq \emptyset}} |\partial\tau_l| \, |\tau_l|^{-1} \, \|w_h\|^2_{\mathrm{L}^2(\tau_l)} \leq c_I^2 \sum_{l=1}^{N} |\partial\tau_l| \, |\tau_l|^{-1} \, \|w_h\|^2_{\mathrm{L}^2(\tau_l)}$$

Plugging in the definition of w_h using shape regularity and $|\tau_l| = h_l^{d+1}$ we get

$$\leq c_I^2 c_{R_2} \sum_{l=1}^{N} h_l^{-1} \left\| h_l \frac{\partial}{\partial t} a_h \right\|^2_{\mathrm{L}^2(\tau_l)} = c_I^2 c_{R_2} \sum_{l=1}^{N} h_l \left\| \frac{\partial}{\partial t} a_h \right\|^2_{\mathrm{L}^2(\tau_l)}.$$

Second we will estimate the downwind of w_h:

$$\sum_{\Gamma_{kl}\in\mathcal{I}_N}\left\|\{w_h\}_{kl}^{\text{down}}\right\|^2_{\mathrm{L}^2(\Gamma_{kl})} \leq \sum_{\Gamma_{kl}\in\mathcal{I}_N}\left(\left\|w_h|_{\tau_l}\right\|^2_{\mathrm{L}^2(\Gamma_{kl})} + \left\|w_h|_{\tau_k}\right\|^2_{\mathrm{L}^2(\Gamma_{kl})}\right).$$

The last term can be rewritten as a sum over elements:

$$\sum_{\Gamma_{kl}\in\mathcal{I}_N}\left(\left\|w_h|_{\tau_l}\right\|^2_{\mathrm{L}^2(\Gamma_{kl})} + \left\|w_h|_{\tau_k}\right\|^2_{\mathrm{L}^2(\Gamma_{kl})}\right) = \sum_{l=1}^{N}\sum_{\substack{\Gamma_{kl}\in\mathcal{I}_N\\ \Gamma_{kl}\subset\partial\tau_l}}\|w_h\|^2_{\mathrm{L}^2(\Gamma_{kl})}.$$

Again using shape regularity and the inverse and trace inequalities (3.15)-(3.17) we can bound this by

$$\leq c_I^2 c_{R_2}\sum_{l=1}^{N} h_l\left\|\frac{\partial}{\partial t}a_h\right\|^2_{\mathrm{L}^2(\tau_l)}.$$

Combing all those estimates we have shown that

$$\begin{aligned} b_T^{\mathrm{DG}}(a_h,w_h) \geq \sum_{l=1}^{N} h_l\left\|\frac{\partial}{\partial t}a_h\right\|^2_{\mathrm{L}^2(\tau_l)} &- \|a_h\|_{\mathrm{L}^2(\Sigma_0)}\left[c_I^2c_{R_2}\sum_{l=1}^{N}h_l\left\|\frac{\partial}{\partial t}a_h\right\|^2_{\mathrm{L}^2(\tau_l)}\right]^{\frac{1}{2}}\\ &- \left[\sum_{\Gamma_{kl}\in\mathcal{I}_N}\left\|[\![a_h]\!]_{kl,t}\right\|^2_{\mathrm{L}^2(\Gamma_{kl})}\right]^{\frac{1}{2}}\left[c_I^2c_{R_2}\sum_{l=1}^{N}h_l\left\|\frac{\partial}{\partial t}a_h\right\|^2_{\mathrm{L}^2(\tau_l)}\right]^{\frac{1}{2}}. \end{aligned}$$

Now we use Young's inequality twice with $\epsilon_1,\epsilon_2>0$ and obtain

$$\begin{aligned} &\geq \left(1-c_I^2c_{R_2}\frac{\epsilon_1}{2}-c_I^2c_{R_2}\frac{\epsilon_2}{2}\right)\sum_{l=1}^{N}h_l\left\|\frac{\partial}{\partial t}a_h\right\|^2_{\mathrm{L}^2(\tau_l)} - \frac{1}{2\epsilon_1}\|a_h\|^2_{\mathrm{L}^2(\Sigma_0)}\\ &-\frac{1}{2\epsilon_2}\sum_{\Gamma_{kl}\in\mathcal{I}_N}\left\|[\![a_h]\!]_{kl,t}\right\|^2_{\mathrm{L}^2(\Gamma_{kl})}. \end{aligned}$$

The same estimate holds for $b_T^{\mathrm{DG}}(c_h, q_h)$. At this point we will start to estimate $c_{nl}((u_h, v_h); (a_h, c_h), (w_h, q_h))$. There holds

$$\begin{aligned}
&\left| \sum_{l=1}^{N} \int_{\tau_l} \left(\mathbf{A}(u_h, w_h) \begin{pmatrix} a_h \\ c_h \end{pmatrix}, \begin{pmatrix} w_h \\ q_h \end{pmatrix} \right) dq \right| \\
&\quad \geq -\sum_{l=1}^{N} \int_{\tau_l} \|\mathbf{A}(u_h, v_h)\| \left| \begin{pmatrix} a_h \\ c_h \end{pmatrix} \right| \left| \begin{pmatrix} w_h \\ q_h \end{pmatrix} \right| dq \\
&\quad \geq -c^{nl} \|(a_h, c_h)\|_{\mathrm{L}^2(Q)} \|(w_h, q_h)\|_{\mathrm{L}^2(Q)} \\
&\quad \geq -\frac{c^{nl}}{2\epsilon_3} \|(a_h, c_h)\|_{\mathrm{L}^2(Q)}^2 - \frac{\epsilon_3 c^{nl}}{2} \|(w_h, q_h)\|_{\mathrm{L}^2(Q)}^2
\end{aligned}$$

for a $\epsilon_3 > 0$ to be chosen later. If we now plug in the definitions of w_h and q_h and use the fact that $h_l^2 \leq h_l$ for $h_l \in (0, 1]$ we get that

$$\begin{aligned}
&\left| \sum_{l=1}^{N} \int_{\tau_l} \left(\mathbf{A}(u_h, w_h) \begin{pmatrix} a_h \\ c_h \end{pmatrix}, \begin{pmatrix} h_l \frac{\partial}{\partial t} a_h \\ h_l \frac{\partial}{\partial t} c_h \end{pmatrix} \right) dq \right| \\
&\quad \geq -\frac{c^{nl}}{2\epsilon_3} \|(a_h, c_h)\|_{\mathrm{L}^2(Q)}^2 - \frac{\epsilon_3 c^{nl}}{2} \sum_{l=1}^{N} h_l \left\| \left(\frac{\partial}{\partial t} a_h, \frac{\partial}{\partial t} c_h \right) \right\|_{\mathrm{L}^2(Q)}^2 \\
&\quad = -\frac{c^{nl}}{2\epsilon_3} \|a_h\|_{\mathrm{L}^2(Q)}^2 - \frac{c^{nl}}{2\epsilon_3} \|c_h\|_{\mathrm{L}^2(Q)}^2 - \frac{\epsilon_3 c^{nl}}{2} \sum_{l=1}^{N} h_l \left\| \frac{\partial}{\partial t} a_h \right\|_{\mathrm{L}^2(Q)}^2 \\
&\qquad - \frac{\epsilon_3 c^{nl}}{2} \sum_{l=1}^{N} h_l \left\| \frac{\partial}{\partial t} c_h \right\|_{\mathrm{L}^2(Q)}^2 .
\end{aligned}$$

Next we look at the same term but with the test functions being chosen as (a_h, c_h). Then using Assumptions 4.3 we get

$$\begin{aligned}
&\left| \sum_{l=1}^{N} \int_{\tau_l} \left(\mathbf{A}(u_h, w_h) \begin{pmatrix} a_h \\ c_h \end{pmatrix}, \begin{pmatrix} a_h \\ c_h \end{pmatrix} \right) dq \right| \\
&\quad = \left| \sum_{l=1}^{N} \int_{\tau_l} \left(\operatorname{sym} \left(\mathbf{A}(u_h, w_h) \right) \begin{pmatrix} a_h \\ c_h \end{pmatrix}, \begin{pmatrix} a_h \\ c_h \end{pmatrix} \right) dq \right| \\
&\quad \geq c_{nl} \|(a_h, c_h)\|_{\mathrm{L}^2(Q)}^2 = c_{nl} \|a_h\|_{\mathrm{L}^2(Q)}^2 + c_{nl} \|c_h\|_{\mathrm{L}^2(Q)}^2 .
\end{aligned}$$

Hence we see that

$$\begin{aligned}
&\left|\sum_{l=1}^{N}\int_{\tau_l}\left(\mathbf{A}(u_h,w_h)\begin{pmatrix}a_h\\c_h\end{pmatrix},\begin{pmatrix}a_h+\omega h_l\frac{\partial}{\partial t}a_h\\c_h+\omega h_l\frac{\partial}{\partial t}c_h\end{pmatrix}\right)dq\right| \\
&\qquad\geq\left(c_{nl}-\frac{c^{nl}}{2\epsilon_3}\right)\|a_h\|^2_{\mathrm{L}^2(Q)}+\left(c_{nl}-\frac{c^{nl}}{2\epsilon_3}\right)\|c_h\|^2_{\mathrm{L}^2(Q)} \\
&\qquad-\omega\frac{\epsilon_3 c^{nl}}{2}\sum_{l=1}^{N}h_l\left\|\frac{\partial}{\partial t}a_h\right\|^2_{\mathrm{L}^2(Q)}-\omega\frac{\epsilon_3 c^{nl}}{2}\sum_{l=1}^{N}h_l\left\|\frac{\partial}{\partial t}c_h\right\|^2_{\mathrm{L}^2(Q)}.
\end{aligned}$$

Collecting all estimates we have shown that

$$\begin{aligned}
&b_T^{\mathrm{DG}}(a_h,a_h+\omega w_h)+b_T^{\mathrm{DG}}(c_h,c_h+\omega q_h) \\
&\quad+c_{nl}((u_h,v_h);(a_h,c_h),(a_h+\omega w_h,c_h+\omega q_h)) \\
&\quad\geq\omega\left(1-c_I^2c_{R_2}\frac{\epsilon_1}{2}-c_I^2c_{R_2}\frac{\epsilon_2}{2}-c^{nl}\frac{\epsilon_3}{2}\right)\sum_{l=1}^{N}h_l\left\|\frac{\partial}{\partial t}a_h\right\|^2_{\mathrm{L}^2(\tau_l)} \\
&\quad+\left(\frac{1}{2}-\frac{\omega}{2\epsilon_1}\right)\|a_h\|^2_{\mathrm{L}^2(\Sigma_0)}+\left(\frac{1}{2}-\frac{\omega}{2\epsilon_2}\right)\sum_{\Gamma_{kl}\in\mathcal{I}_N}\left\|[\![a_h]\!]_{kl,t}\right\|^2_{\mathrm{L}^2(\Gamma_{kl})} \\
&\quad+\left(c_{nl}-\frac{c^{nl}}{2\epsilon_3}\right)\|a_h\|^2_{\mathrm{L}^2(Q)}+\left(\frac{1}{2}-\frac{\omega}{2\epsilon_1}\right)\|c_h\|^2_{\mathrm{L}^2(\Sigma_0)} \\
&\quad+\left(1-c_I^2c_{R_2}\frac{\epsilon_1}{2}-c_I^2c_{R_2}\frac{\epsilon_2}{2}-c^{nl}\frac{\epsilon_3}{2}\right)\sum_{l=1}^{N}h_l\left\|\frac{\partial}{\partial t}c_h\right\|^2_{\mathrm{L}^2(\tau_l)} \\
&\quad+\left(\frac{1}{2}-\frac{\omega}{2\epsilon_2}\right)\sum_{\Gamma_{kl}\in\mathcal{I}_N}\left\|[\![c_h]\!]_{kl,t}\right\|^2_{\mathrm{L}^2(\Gamma_{kl})}+\left(c_{nl}-\frac{c^{nl}}{2\epsilon_3}\right)\|c_h\|^2_{\mathrm{L}^2(Q)}.
\end{aligned}$$

It remains to define $\epsilon_1,\epsilon_2,\epsilon_3$ appropriately. We observe that for a given $\alpha\in(0,1)$ we can choose

$$\epsilon_1=\epsilon_2=\frac{1-\alpha}{c_I^2c_{R_2}}.$$

Thus

$$1-c_I^2c_{R_2}\frac{\epsilon_1}{2}-c_I^2c_{R_2}\frac{\epsilon_2}{2}=\alpha.$$

Next consider the choice

$$\epsilon_3 = \frac{c^{nl} + \varepsilon}{2c_{nl}}$$

for $\varepsilon > 0$. Then

$$c_{2,*}(\varepsilon) := c_{nl} - \frac{c^{nl}}{2\epsilon_3} = c_{nl}\left(1 - \frac{c^{nl}}{c^{nl} + \varepsilon}\right) > 0.$$

With this we get the restriction

$$\alpha - \frac{(c^{nl})^2}{4c_{nl}} - \frac{\varepsilon c^{nl}}{4c_{nl}} > 0.$$

From this we see that for any $\varepsilon_* \in (0, \frac{4(1-d)c_{nl}}{c^{nl}})$, where $d := \frac{(c^{nl})^2)}{4c_{nl}} \in (0,1)$ we can choose an $\alpha_*(\varepsilon_*)$ such that $\alpha_*(\varepsilon_*) \in (0,1)$ and

$$\alpha_*(\varepsilon_*) - \frac{(c^{nl})^2}{4c_{nl}} - \frac{\varepsilon_* c^{nl}}{4c_{nl}} \geq c_{1,*}(\varepsilon_*) > 0.$$

Thus we arrive at the estimate

$$\begin{aligned}
&b_T^{\mathrm{DG}}(a_h, a_h + \omega w_h) + b_T^{\mathrm{DG}}(c_h, c_h + \omega q_h) \\
&\quad + c_{nl}((u_h, v_h); (a_h, c_h), (a_h + \omega w_h, c_h + \omega q_h)) \\
&\quad \geq \omega c_{1,*}(\varepsilon_*) \sum_{l=1}^{N} h_l \left\| \frac{\partial}{\partial t} a_h \right\|^2_{\mathrm{L}^2(\tau_l)} + \left(\frac{1}{2} - \frac{\omega c_I^2 c_{R_2}}{2(1-\alpha_*(\varepsilon_*))}\right) \|a_h\|^2_{\mathrm{L}^2(\Sigma_0)} \\
&\quad + \left(\frac{1}{2} - \frac{\omega c_I^2 c_{R_2}}{2(1-\alpha_*(\varepsilon_*))}\right) \sum_{\Gamma_{kl} \in \mathcal{I}_N} \left\| [\![a_h]\!]_{kl,t} \right\|^2_{\mathrm{L}^2(\Gamma_{kl})} + c_{2,*}(\varepsilon_*) \|a_h\|^2_{\mathrm{L}^2(Q)} \\
&\quad + \omega c_{1,*}(\varepsilon_*) \sum_{l=1}^{N} h_l \left\| \frac{\partial}{\partial t} c_h \right\|^2_{\mathrm{L}^2(\tau_l)} + \left(\frac{1}{2} - \frac{\omega c_I^2 c_{R_2}}{2(1-\alpha_*(\varepsilon_*))}\right) \|c_h\|^2_{\mathrm{L}^2(\Sigma_0)} \\
&\quad + \left(\frac{1}{2} - \frac{\omega c_I^2 c_{R_2}}{2(1-\alpha_*(\varepsilon_*))}\right) \sum_{\Gamma_{kl} \in \mathcal{I}_N} \left\| [\![c_h]\!]_{kl,t} \right\|^2_{\mathrm{L}^2(\Gamma_{kl})} + c_{2,*}(\varepsilon_*) \|c_h\|^2_{\mathrm{L}^2(Q)}.
\end{aligned}$$

At this point we can proceed as in the proof of Theorem 4.16. This means that

$$
\begin{aligned}
&b_T^{\mathrm{DG}}(a_h, a_h+\omega w_h) + b_T^{\mathrm{DG}}(c_h, c_h+\omega q_h) + a_{\boldsymbol{x},i}(a_h+b_h, a_h+b_h)\\
&\quad + a_{\boldsymbol{x},e}(b_h, b_h-\omega w_h) + c_{nl}((u_h,v_h);(a_h,c_h),(a_h+\omega w_h, c_h+\omega q_h))\\
&\quad \geq \omega c_{1,*}(\varepsilon_*)\sum_{l=1}^{N} h_l \left\| \frac{\partial}{\partial t} a_h \right\|^2_{\mathrm{L}^2(\tau_l)} + \underbrace{\left(\frac{1}{2} - \frac{\omega c_I^2 c_{R_2}}{2(1-\alpha_*(\varepsilon_*))}\right)}_{=:c_1(\omega)} \|a_h\|^2_{\mathrm{L}^2(\Sigma_0)}\\
&\quad + \left(\frac{1}{2} - \frac{\omega c_I^2 c_{R_2}}{2(1-\alpha_*(\varepsilon_*))}\right) \sum_{\Gamma_{kl}\in\mathcal{I}_N} \left\| [\![a_h]\!]_{kl,t} \right\|^2_{\mathrm{L}^2(\Gamma_{kl})} + c_{2,*}(\varepsilon_*)\|a_h\|^2_{\mathrm{L}^2(Q)}\\
&\quad + \omega c_{1,*}(\varepsilon_*)\sum_{l=1}^{N} h_l \left\| \frac{\partial}{\partial t} c_h \right\|^2_{\mathrm{L}^2(\tau_l)} + \left(\frac{1}{2} - \frac{\omega c_I^2 c_{R_2}}{2(1-\alpha_*(\varepsilon_*))}\right) \|c_h\|^2_{\mathrm{L}^2(\Sigma_0)}\\
&\quad + \left(\frac{1}{2} - \frac{\omega c_I^2 c_{R_2}}{2(1-\alpha_*(\varepsilon_*))}\right) \sum_{\Gamma_{kl}\in\mathcal{I}_N} \left\| [\![c_h]\!]_{kl,t} \right\|^2_{\mathrm{L}^2(\Gamma_{kl})} + c_{2,*}(\varepsilon_*)\|c_h\|^2_{\mathrm{L}^2(Q)}\\
&\quad + \underbrace{\left(\frac{\chi_i^{-1}}{4}\min\{c_1^i, c_1^e, \chi_e^{-1}\} - \frac{\omega\chi_i c_e c_2^e}{2}\right)}_{=:c_2(\omega)} |\!|\!| a_h |\!|\!|^2_{\mathrm{space},i}\\
&\quad + \underbrace{\left(\frac{1}{4}\min\{c_1^i, c_1^e, \chi_e^{-1}\} - \frac{\omega c_2^e (1+c_K)^{\frac{1}{2}}}{2}\right)}_{=:c_3(\omega)} |\!|\!| v_h |\!|\!|^2_{\mathrm{space},e}.
\end{aligned}
$$

Now we need to find a suitable ω. For this purpose we will look at the constants $c_1(\omega), c_2(\omega), c_3(\omega)$. A suitable choice is

$$
0 < \omega_\dagger < \min\left\{ \frac{1-\alpha_*(\varepsilon_*)}{c_I^2 c_{R_2}}, \frac{\min\{c_1^i, c_1^e, \chi_e^{-1}\}}{2\chi_i^2 c_e, c_2^e}, \frac{\min\{c_1^i, c_1^e, \chi_e^{-1}\}}{2(1+c_K)^{\frac{1}{2}} c_2^e} \right\}.
$$

Hence

$$
\begin{aligned}
&b_T^{\mathrm{DG}}(a_h, a_h+\omega w_h) + b_T^{\mathrm{DG}}(c_h, c_h+\omega q_h) + a_{\boldsymbol{x},i}(a_h+b_h, a_h+b_h)\\
&\quad + a_{\boldsymbol{x},e}(b_h, b_h-\omega w_h) + c_{nl}((u_h,v_h);(a_h,c_h),(a_h+\omega w_h, c_h+\omega q_h))\\
&\quad \geq c_4(\omega_\dagger) |\!|\!| (a_h, b_h, c_h) |\!|\!|^2_{\mathrm{DG}}
\end{aligned}
$$

with

$$
c_4(\omega_\dagger) = \min\{\omega_\dagger c_{1,*}(\varepsilon_*), c_{2,*}(\varepsilon_*), c_1(\omega_\dagger), c_2(\omega_\dagger), c_3(\omega_\dagger),\} > 0.
$$

So we can conclude the proof and have found the stability constant

$$c_S := \frac{c_4(\omega_\dagger)}{\sqrt{\max\left\{1+\omega_\dagger c_1^B, 1+\omega_\dagger(c_i+\chi_i c_e), 1\right\}}}.$$

□

Remark 4.23. *Suppose that Assumption 4.3:(2) does not hold but there holds*

$$\lambda_{\min}(\mathrm{sym}(\mathbf{A})) \geq -\kappa^2 > -\infty.$$

Then the result still holds. To see this one needs to make a change of variables

$$\widetilde{u}(\boldsymbol{x},t) = \exp(-(\kappa^2+1)t)u(\boldsymbol{x},t).$$

Then one has that

$$\frac{\partial}{\partial t}u = \exp((\kappa^2+1)t)\frac{\partial}{\partial t}\widetilde{u} + (\kappa^2+1)\exp((\kappa^2+1)t)\widetilde{u}.$$

The additional mass term ensures the stability. The boundedness constant will be multiplied by a factor of $\exp((\kappa^2+1)T)$*. The boundedness constant influences the quality of the approximation error. Thus the approximation quality will deteriorate when* κ^2 *is big.*

4.5 Convergence Study for a Nonlinear Problem

In this section a convergence study for a nonlinear problem will be given. The space-time cylinder will be given again as $Q := (0,1)^3$. The diffusion tensors are chosen as

$$\mathbf{M}_i := \begin{pmatrix} \frac{3}{4} & \frac{3}{20} \\ \frac{3}{20} & \frac{3}{4} \end{pmatrix}, \qquad \mathbf{M}_e := \begin{pmatrix} \frac{5}{4} & \frac{1}{4} \\ \frac{1}{4} & \frac{5}{4} \end{pmatrix}.$$

As nonlinear model we choose the FitzHugh-Nagumo model (2.7), which fulfills the Assumptions 4.3. On the boundary $\Sigma_R := \partial(0,1)^2 \times (0,1)$ we apply Robin boundary conditions with $\alpha_i = 1$ and $\alpha_e = 1$. The given data s_i,s_e,$g_{i,R}$, $g_{e,R}$

and V_{tm}^0 are chosen such that the exact solutions of the Bidomain equations are given as

$$\begin{aligned} V_{\mathrm{tm}}(\boldsymbol{x},t) &= x(1-x)y(1-y)t(1-t), \\ u_e(\boldsymbol{x},t) &= \sin(\pi x)\sin(\pi y)\sin(\pi t), \\ v(\boldsymbol{x},t) &= \cos(\pi x)\cos(\pi y)\cos(\pi t). \end{aligned}$$

For the stabilization parameter we chose $\sigma_{kl} = 25$. We used the same solvers and preconditioners as for the convergence studies for the linear problem discussed in Section 4.3. The results which confirm our theoretical investigations can be looked up in Table 4.7 and Table 4.8. The convergence order of 1.50 for the approximation error of v is a well-known result for the approximation of pure convection problems, see for example [47, Corollary 2.38].

level	elements	dof	$\lvert\!\lvert\!\lvert \boldsymbol{z} - \boldsymbol{z}_h \rvert\!\rvert\!\rvert_{\mathrm{DG}}$	eoc
0	6	72	1.6486E+0	–
1	48	576	1.1599E+0	0.51
2	384	4608	6.8151E−1	0.77
3	3072	36864	3.6315E−1	0.91
4	24576	294912	1.8540E−1	0.97
5	196608	2359296	9.3307E−2	0.99
Theory:				1.00

Table 4.7: Energy error $\lvert\!\lvert\!\lvert \boldsymbol{z} - \boldsymbol{z}_h \rvert\!\rvert\!\rvert_{\mathrm{DG}}$ for $p = 1$. For reasons of brevity we have set $\boldsymbol{z} := (V_{\mathrm{tm}}, u_e, v)$ and $\boldsymbol{z}_h := (V_{\mathrm{tm}}^h, u_e^h, v^h)$.

			Error V_{tm}		Error u_e		Error v	
level	elements	dof	error	eoc	error	eoc	error	eoc
0	6	24	9.0116E−2	–	1.3691E+0	–	9.1390E−1	–
1	48	192	4.7239E−2	0.93	1.0823E+0	0.34	4.1441E−1	1.14
2	384	1536	2.2469E−2	1.07	6.6313E−1	0.71	1.5558E−1	1.41
3	3072	12288	1.0199E−2	1.14	3.5886E−1	0.89	5.4727E−2	1.51
4	24576	98304	4.7416E−3	1.10	1.8436E−1	0.96	1.8995E−2	1.53
5	196608	786432	2.2781E−3	1.06	9.3043E−2	0.99	6.6280E−3	1.52
Observed:				1.00		1.00		1.50

Table 4.8: Individual error components for $p = 1$.

5 Discontinous Galerkin Finite Element Method for Nonlinear Elasticity

In this chapter the results for the numerical treatment of nonlinear elasticity with the discontinuous Galerkin finite element method will be summarized. Due to the fact, that a discontinuous Galerkin method was already considered in the previous chapter the aim is to use such a method for the treatment of nonlinear elasticity, too. For a more complete treatment of discontinuous Galerkin methods for nonlinear elasticity we refer to [60, 61, 62, 63, 133, 138]. For general information on the treatment of nonlinear elasticity with the finite element method we refer to [11, 12, 24]. Finally we refer to [17, 85, 135, 180] for more general topics in the context of nonlinear elastic behavior.

5.1 Analytic Results

Recall the equilibrium equations of stationary hyper-elasticity in material coordinates given by

$$\begin{aligned} -\operatorname{Div}\left(\mathbf{F}(\boldsymbol{U})\mathbf{S}(\boldsymbol{U})\right) &= \mathbf{0} && \text{in } \Omega_r, \\ \boldsymbol{U} &= \boldsymbol{G}_D(\boldsymbol{X}) && \text{on } \Gamma_{D,r}, \\ \mathbf{F}(\boldsymbol{U})\mathbf{S}(\boldsymbol{U})\boldsymbol{N} &= \boldsymbol{G}_N(\boldsymbol{U}) && \text{on } \Gamma_{N,r}. \end{aligned} \tag{5.1}$$

The tensor $\mathbf{S}$ is given through the constitutive relation as $\mathbf{S} = 2\frac{\partial \Psi(\mathbf{C})}{\partial \mathbf{C}}$ with the Helmholtz free energy function $\Psi(\mathbf{C})$. In this section known results for this nonlinear system of partial differential equations will be recited. The weak

formulation of system (5.1) reads: Find $\boldsymbol{U}$ with $\boldsymbol{U}|_{\Gamma_{D,r}} = \boldsymbol{G}_D$ smooth enough such that

$$\int_{\Omega_r} \mathbf{F}(\boldsymbol{U})\mathbf{S}(\boldsymbol{U}) : \operatorname{Grad} \boldsymbol{V} \, \mathrm{d}\boldsymbol{X} - \int_{\Gamma_{N,r}} (\boldsymbol{G}_N(\boldsymbol{U}), \boldsymbol{V}) \, \mathrm{ds}_{\boldsymbol{X}} = 0$$

for all smooth enough $\boldsymbol{V}$ such that $\boldsymbol{V}|_{\Gamma_{D,r}} = \mathbf{0}$. This variational formulation is also known as the **principle of virtual work**, see [85, Chapter 8.2] and [35, Chapter 2.6] for more details. At this point no specification of the underlying function spaces for $\boldsymbol{U}, \boldsymbol{V}$ has been made. We will comment on this later. It is well known (see [35, Theorems 4.1-1 and 4.1-2]) that, for hyperelastic materials and conservative traction and body forces, the solution of the principle of virtual work is formally equivalent to find infimizers of the functional

$$I(\boldsymbol{U}) := \int_{\Omega_r} W(\mathbf{F}(\boldsymbol{U})) \; \mathrm{d}\boldsymbol{X} - \int_{\Gamma_{N,r}} (\boldsymbol{G}_N, \boldsymbol{U}) \; \mathrm{ds}_{\boldsymbol{X}} \, .$$

The infimum is taken over all smooth enough $\boldsymbol{\psi} \colon \overline{\Omega}_r \to \mathbb{R}^d$ such that $\boldsymbol{\psi}|_{\Gamma_{D,r}} = \boldsymbol{G}_D$. One of the major problems in studying the existence of infimizers is the lack of convexity of the energy function $W(\mathbf{F})$. Classical hyperelastic materials are however **polyconvex**. This means that

$$W(\mathbf{F}) = \widetilde{W}(\mathbf{F}, \operatorname{adj}(\mathbf{F}), \det(\mathbf{F}))$$

and $\widetilde{W}$ is convex in its arguments. For more details on the various convexity concepts in nonlinear elasticity we refer to [35, 42]. Concerning the existence and regularity of infimizers to the functional $I(\boldsymbol{U})$ a well known theorem from J. Ball will be cited:

Theorem 5.1 (J. Ball's Existence Theorem for pure displacements)**.** *Let Ω_r be a bounded domain with Lipschitz boundary and $\Gamma_{D,r} = \partial\Omega_r$. Let further $p \geq 2$, $q \geq \frac{p}{p-1}$ and $s > 1$. Assume that $W(\mathbf{F})$ is polyconvex and fulfills the conditions* (2.33)-(2.35)*. Let $\boldsymbol{G}_D \in W^{1,1-\frac{1}{p}}(\partial\Omega_r)$. Define the space*

$$X := \Big\{ \boldsymbol{V} \in W^{1,p}(\Omega_r) \colon \operatorname{adj}(\mathbf{F}(\boldsymbol{V})) \in L^q(\Omega_r), \; \det(\mathbf{F}(\boldsymbol{V})) \in L^s(\Omega_r) \\ \boldsymbol{V}|_{\partial\Omega_r} = \boldsymbol{G}_D \text{ and } \det(\mathbf{F}(\boldsymbol{V})) > 0 \text{ a.e. in } \Omega_r \Big\} .$$

Assume further that there exists a $\boldsymbol{U}_0 \in X$ *such that* $I(\boldsymbol{U}_0) < \infty$*. Then there exists at least one function* $\boldsymbol{U} \in X$ *such that*

$$I(\boldsymbol{U}) = \inf_{\boldsymbol{V} \in X} I(\boldsymbol{V}).$$

Proof. See [35, Theorem 7.7-1]. □

Remark 5.2. *A similar theorem holds in the case of mixed boundary conditions and pure Neumann boundary conditions, see [35, Theorem 7.7-2].*

Remark 5.3. *The theorem remains true in the case of almost incompressible materials, however the proofs need to be adapted. See [32] for details.*

The equivalence of the minimization problem and the principle of virtual work for hyperelastic materials together with the Theorem 5.1 justifies the following weak formulation. Given $\boldsymbol{G}_D \in W^{1,1-\frac{1}{p}}(\Gamma_{D,r})$ find $\boldsymbol{U} \in W^{1,p}_{\boldsymbol{G}_D,\Gamma_{D,r}}(\Omega_r)$ such that

$$\int_{\Omega_r} \mathsf{F}(\boldsymbol{U})\mathsf{S}(\boldsymbol{U}) : \operatorname{Grad} \boldsymbol{V} \, \mathrm{d}\boldsymbol{X} = 0 \tag{5.2}$$

for all $\boldsymbol{V} \in W^{1,p}_{\boldsymbol{0},\Gamma_{D,r}}(\Omega_r)$.

Remark 5.4. *The above concepts are only valid for hyperelastic materials. In general it is still an open problem whether the equivalence of the minimization of the strain energy function and the principle of virtual work holds. See [17] for more details.*

5.2 Discretization

In this section a discontinuous Galerkin discretization for the equations of stationary nonlinear elasticity with hyperelastic materials will be discussed. One may roughly distinguish two approaches. The first approach is based on a discontinuous Galerkin discretization of the energy functional and thus aims at minimizing a discrete energy functional. This approach is used for example in [62, 63, 133]. However the convergence of discrete energy minimizers to

minimizers of the continuous functional is, in general, still an open question, see [30]. In this thesis a different approach, first introduced in [138], will be considered. Given the system (5.1) and assume that the Neumann boundary conditions do not depend on the normal vector $\boldsymbol{N}$, e.g.: dead loads or traction forces. One multiplies the first equation with a test function $\boldsymbol{V} \in [\mathrm{H}_0^1(\mathcal{T}_N)]^d$ and integrates over Ω_r. This leads to

$$\sum_{l=1}^{N} \int_{\tau_l} -(\mathrm{Div}(\mathbf{F}(\boldsymbol{U})\mathbf{S}(\boldsymbol{U}))), \boldsymbol{V}) \ \mathrm{d}\boldsymbol{X} = \sum_{l=1}^{N} \int_{\tau_l} \mathbf{F}(\boldsymbol{U})\mathbf{S}(\boldsymbol{U}) : \mathrm{Grad}\, \boldsymbol{V} - \sum_{l=1}^{N} \int_{\partial\tau_l} (\mathbf{F}(\boldsymbol{U})\mathbf{S}(\boldsymbol{U}), \boldsymbol{V}) \ \mathrm{ds}_{\boldsymbol{X}} .$$

After rearranging the second sum one obtains

$$\begin{aligned} \sum_{l=1}^{N} \int_{\tau_l} -(\mathrm{Div}(\mathbf{F}(\boldsymbol{U})\mathbf{S}(\boldsymbol{U}))), \boldsymbol{V}) \ \mathrm{d}\boldsymbol{X} = &\sum_{l=1}^{N} \int_{\tau_l} \mathbf{F}(\boldsymbol{U})\mathbf{S}(\boldsymbol{U}) : \mathrm{Grad}\, \boldsymbol{V} \\ &- \sum_{\Gamma_{kl} \in \mathcal{I}_N} \int_{\Gamma_{kl}} \langle \mathbf{F}(\boldsymbol{U})\mathbf{S}(\boldsymbol{U}) \rangle : \underline{[\![\boldsymbol{V}]\!]}_{kl} \ \mathrm{ds}_{\boldsymbol{X}} \\ &- \int_{\Gamma_{N,r}} (\boldsymbol{G}_N, \boldsymbol{V}) \ \mathrm{ds}_{\boldsymbol{X}} . \end{aligned}$$

This motivates the definition of the following semi-linear form

$$b(\boldsymbol{U}, \boldsymbol{V}) := \sum_{l=1}^{N} \int_{\tau_l} \mathbf{F}(\boldsymbol{U})\mathbf{S}(\boldsymbol{U}) : \mathrm{Grad}\, \boldsymbol{V} - \sum_{\Gamma_{kl} \in \mathcal{I}_N} \int_{\Gamma_{kl}} \langle \mathbf{F}(\boldsymbol{U})\mathbf{S}(\boldsymbol{U}) \rangle : [\![\boldsymbol{V}]\!] \ \mathrm{ds}_{\boldsymbol{X}}$$

and the linear form

$$l(\boldsymbol{V}) := \int_{\Gamma_{N,r}} (\boldsymbol{G}_N, \boldsymbol{V}) \ \mathrm{ds}_{\boldsymbol{X}}$$

for $\boldsymbol{U} \in \mathcal{C}^1(\mathcal{T}_N)$ and $\boldsymbol{V} \in \mathrm{H}_0^1(\mathcal{T}_N)$. For ensuring stability one needs to add a stabilization bilinear form

$$s(\boldsymbol{U}, \boldsymbol{V}) := \sum_{\Gamma_{kl} \in \mathcal{I}_N} \frac{\sigma_{kl}}{\overline{h}_{kl}} \int_{\Gamma_{kl}} \underline{[\![\boldsymbol{U}]\!]}_{kl} : \underline{[\![\boldsymbol{V}]\!]}_{kl} \ \mathrm{ds}_{\boldsymbol{X}} .$$

The discontinuous Galerkin formulation reads: Find $\boldsymbol{U}_{\mathrm{DG}} \in [S_h^p(\mathcal{T}_N)]^d$ with $\boldsymbol{U}_{\mathrm{DG}}|_{\Gamma_{D,r}} = \boldsymbol{G}_D$ such that

$$b(\boldsymbol{U}_{\mathrm{DG}}, \boldsymbol{V}_h) + s(\boldsymbol{U}_{\mathrm{DG}}, \boldsymbol{V}) = l(\boldsymbol{V}_h) \tag{5.3}$$

for all $\boldsymbol{V}_h \in [S_h^p(\mathcal{T}_N)]^d$ such that $\boldsymbol{V}_h|_{\Gamma_{D,r}} = \boldsymbol{0}$. In the case of a linear problem this derivation resembles the **incomplete interior penalty method** see [47, Section 5.3] and [45]. This is still a nonlinear set of algebraic equations. The linearization is defined for $\boldsymbol{\phi} \in [\mathcal{C}^1(\mathcal{T}_N)]^d$ and $\boldsymbol{U}, \boldsymbol{V} \in \mathrm{H}_0^1(\mathcal{T}_N)$:

$$a^{\mathrm{DG}}(\boldsymbol{\phi}; \boldsymbol{U}, \boldsymbol{V}) := a_1^{\mathrm{DG}}(\boldsymbol{\phi}; \boldsymbol{U}, \boldsymbol{V}) + a_2^{\mathrm{DG}}(\boldsymbol{\phi}; \boldsymbol{U}, \boldsymbol{V}) + a_3^{\mathrm{DG}}(\boldsymbol{\phi}; \boldsymbol{U}, \boldsymbol{V})$$

where

$$\begin{aligned} a_1^{\mathrm{DG}}(\boldsymbol{\phi}; \boldsymbol{U}, \boldsymbol{V}) := \sum_{l=1} \Bigg(& \int_{\tau_l} \operatorname{Grad} \boldsymbol{U} \mathbf{S}(\boldsymbol{\phi}) : \operatorname{Grad} \boldsymbol{V} \ \mathrm{d}\boldsymbol{x} \\ & + \int_{\tau_l} \operatorname{sym}(\mathbf{F}^\top(\boldsymbol{\phi}) \operatorname{Grad} \boldsymbol{U}) : \mathbb{C}(\boldsymbol{\phi}) : \operatorname{sym}(\mathbf{F}^\top(\boldsymbol{\phi}) \operatorname{Grad} \boldsymbol{V}) \, \mathrm{d}\boldsymbol{x} \Bigg) \end{aligned}$$

and

$$\begin{aligned} a_2^{\mathrm{DG}}(\boldsymbol{\phi}; \boldsymbol{U}, \boldsymbol{V}) := & \\ & - \sum_{\Gamma_{kl} \in \mathcal{I}_N} \int_{\Gamma_{kl}} \left\langle \mathbf{F}(\boldsymbol{\phi}) \left(\mathbb{C}(\boldsymbol{\phi}) : \operatorname{sym}(\mathbf{F}^\top(\boldsymbol{\phi}) \operatorname{Grad} \boldsymbol{U}) \right) \right\rangle : \underline{[\![\boldsymbol{V}]\!]}_{kl} \, \mathrm{ds}_{\boldsymbol{x}} \\ & - \sum_{\Gamma_{kl} \in \mathcal{I}_N} \int_{\Gamma_{kl}} \langle \operatorname{Grad} \boldsymbol{U} \mathbf{S}(\boldsymbol{\phi}) \rangle : \underline{[\![\boldsymbol{V}]\!]}_{kl} \, \mathrm{ds}_{\boldsymbol{x}} \\ & + \sum_{\Gamma_{kl} \in \mathcal{I}_N} \frac{\sigma_{kl}}{\overline{h}_{kl}} \int_{\Gamma_{kl}} \underline{[\![\boldsymbol{U}]\!]}_{kl} : \underline{[\![\boldsymbol{V}]\!]}_{kl} \, \mathrm{ds}_{\boldsymbol{x}} \, . \end{aligned}$$

The occurring tensors are evaluated as

$$\begin{aligned} \mathbf{F}(\boldsymbol{\phi}) &= \mathbf{I} + \operatorname{Grad} \boldsymbol{\phi}, \\ \mathbf{S}(\boldsymbol{\phi}) &= 2 \frac{\partial \Psi(\mathbf{C})}{\partial \mathbf{C}} \Big|_{\mathbf{C} = \mathbf{F}^\top(\boldsymbol{\phi}) \mathbf{F}(\boldsymbol{\phi})}, \\ \mathbb{C}(\boldsymbol{\phi}) &= 4 \frac{\partial^2 \Psi(\mathbf{C})}{\partial \mathbf{C}^2} \Big|_{\mathbf{C} = \mathbf{F}^\top(\boldsymbol{\phi}) \mathbf{F}(\boldsymbol{\phi})}. \end{aligned}$$

For compatibility with the notation in [138] we want to mention that this formulation is equivalent to

$$b(\boldsymbol{U},\boldsymbol{V}) := \sum_{l=1}^{N} \int_{\tau_l} \mathbf{P}(\boldsymbol{U}) : \operatorname{Grad} \boldsymbol{V} \ \mathrm{d}\boldsymbol{X} - \sum_{\Gamma_{kl}\in\mathcal{I}_N} \int_{\Gamma_{kl}} \langle \mathbf{P}(\boldsymbol{U}) \rangle : \underline{[\![\boldsymbol{V}]\!]}_{kl} \ \mathrm{ds}_{\boldsymbol{X}}$$

and

$$a_1^{\mathrm{DG}}(\boldsymbol{\phi};\boldsymbol{U},\boldsymbol{V}) := \sum_{l=1} \int_{\tau_l} \operatorname{Grad} \boldsymbol{U} : \mathbb{A}(\boldsymbol{\phi}) : \operatorname{Grad} \boldsymbol{V} \, \mathrm{d}\boldsymbol{X}$$

as well as

$$\begin{aligned} a_2^{\mathrm{DG}}(\boldsymbol{\phi};\boldsymbol{U},\boldsymbol{V}) := &- \sum_{\Gamma_{kl}\in\mathcal{I}_N} \int_{\Gamma_{kl}} \langle \mathbb{A}(\boldsymbol{\phi}) : \operatorname{Grad} \boldsymbol{U} \rangle : \underline{[\![\boldsymbol{V}]\!]}_{kl} \ \mathrm{ds}_{\boldsymbol{X}} \\ &+ \sum_{\Gamma_{kl}\in\mathcal{I}_N} \frac{\sigma_{kl}}{\overline{h}_{kl}} \int_{\Gamma_{kl}} \underline{[\![\boldsymbol{U}]\!]}_{kl} : \underline{[\![\boldsymbol{V}]\!]}_{kl} \, \mathrm{ds}_{\boldsymbol{X}} \, . \end{aligned}$$

where the **first Piola-Kirchoff stress tensor** is defined as

$$\mathbf{P} := \mathbf{F}\mathbf{S} = \frac{\partial W(\mathbf{F})}{\partial \mathbf{F}}$$

and the elasticity tensor $\mathbb{A}$ is defined as

$$\mathbb{A} := \frac{\partial^2 W(\mathbf{F})}{\partial \mathbf{F} \partial \mathbf{F}}.$$

The elasticity tensor $\mathbb{A}$ has only major symmetries.

5.3 Numerical Analysis

In this section the main convergence result to be found in [138] will be given. Throughout this section it is assumed that the problem (5.2) has a solution

$$\boldsymbol{U} \in [W^{1,p}(\Omega_r)]^d \cap [\mathrm{H}^{m+1}(\Omega_r)]^d \cap [\mathrm{H}^1_{\Gamma_{D,r},\boldsymbol{G}_D}(\Omega_r)]^d$$

with $m > \frac{d}{2}$. With this regularity one has that $\operatorname{Grad} \boldsymbol{U} \in [\mathrm{L}^\infty(\Omega_r)]^{d\times d}$. One further needs to assume that $W(\mathbf{F}) \in \mathcal{C}^4(\mathbb{R}^{d\times d};\mathbb{R})$. Further one assumes that

$\mathbf{P}$ and $\mathbb{A}$ are locally Lipschitz-continuous. For the error analysis the following norm will be used:

$$|||\boldsymbol{U}|||_{1,h}^2 := \sum_{l=1}^{N} \|\operatorname{Grad} \boldsymbol{U}\|_{\mathrm{L}^2(\tau_l)}^2 + \sum_{\Gamma_{kl} \in \mathcal{I}_N} \frac{\sigma_{kl}}{\overline{h}_{kl}} \left\| \underline{[\![\boldsymbol{U}]\!]}_{kl} \right\|_{\mathrm{L}^2(\Gamma_{kl})}^2.$$

With the assumptions made above one can show, that the discrete problem has a unique solution $\boldsymbol{U}_{\mathrm{DG}}$ provided σ_{kl} is large enough and for a quasi-uniform triangulation with mesh size h fine enough there holds

$$|||\boldsymbol{U} - \boldsymbol{U}_{\mathrm{DG}}|||_{1,h} \leq c h^s \|\boldsymbol{U}\|_{\mathrm{H}^{s+1}(\Omega_r)} \tag{5.4}$$

for $\frac{d}{2} < s \leq \min\{p, m\}$. We refer to [138, Section 5] for the proofs.

5.4 Additional Topics

In this section some additional technical topics which are of relevance in the implementation of discontinuous Galerkin methods for nonlinear elasticity will be discussed.

5.4.1 Treatment of Pressure Boundary Conditions

It was shown, that for a pressure boundary condition of the form

$$\boldsymbol{\sigma}(\boldsymbol{u})\boldsymbol{n} = -p\boldsymbol{n}$$

in spatial coordinates one obtains a nonlinear boundary condition in material coordinates

$$\mathbf{F}(\boldsymbol{U})\mathbf{S}(\boldsymbol{U}) = -pJ(\boldsymbol{U})\mathbf{F}^{-\top}(\boldsymbol{U})\boldsymbol{N}.$$

The linearization corresponding to such a boundary condition can be calculated as

$$a_3^{\mathrm{DG}}(\boldsymbol{\phi}; \boldsymbol{U}, \boldsymbol{V}) := p \left(\int_{\Gamma_{N,r}} J(\boldsymbol{\phi}) \Big(\mathbf{F}^{-\top}(\boldsymbol{\phi}) (\operatorname{Grad} \boldsymbol{U})^{\top} \mathbf{F}^{-\top}(\boldsymbol{\phi}) \boldsymbol{N}, \boldsymbol{V} \Big) \, \mathrm{ds}_{\boldsymbol{X}} \right.$$
$$\left. - \int_{\Gamma_{N,r}} J(\boldsymbol{\phi}) \Big((\mathbf{F}^{-\top}(\boldsymbol{\phi}) : \operatorname{Grad} \boldsymbol{U}) \mathbf{F}^{-\top} \boldsymbol{N}, \boldsymbol{V} \Big) \, \mathrm{ds}_{\boldsymbol{X}} \right).$$

There are different approaches how to include pressure boundary conditions, see for example [24, Section 6.5.2].

5.4.2 Static Condensation for Almost Incompressible Materials

Recall that for almost incompressible materials one has to solve a block system of the form

$$
\begin{aligned}
-\operatorname{Div}\left(\mathbf{F}(\boldsymbol{U})\left(\mathbf{S}_{\text{iso}}(\boldsymbol{U}, J)+\mathbf{S}_{\text{vol}}(\boldsymbol{U}, P, J)\right)\right)&=0, && \text{in } \Omega_r, && (5.5)\\
\frac{\mathrm{d}U(D)}{\mathrm{d}D}\Big|_{D=J}-P&=0 && \text{in } \Omega_r, && (5.6)\\
J-\det\mathbf{F}(\boldsymbol{U})&=0 && \text{in } \Omega_r. && (5.7)
\end{aligned}
$$

In the context of almost incompressible linear elasticity one encounters similar saddle point problems as a remedy to prevent locking effects. See for example [27, Chapter VI §4]. When using a discontinuous Galerkin finite element method for discretizing the equations of almost incompressible linear elasticity one can construct locking-free methods without the need to solve a block system, see [48, 187] for details. This may serve as a motivation to achieve the same for almost incompressible nonlinear elasticity. As a motivation consider the conformal discretized variational formulation of the pure Dirichlet problem. Find $(\boldsymbol{U}_h, P_h, J_h) \in X_h \times \Pi_h \times \Sigma_h$ with $\boldsymbol{U}_h|_{\partial\Omega_r} = \boldsymbol{g}_D$ such that

$$
\begin{aligned}
0 = &\int_{\Omega_r} \mathbf{F}(\boldsymbol{U}_h)\mathbf{S}_{\text{iso}}(\boldsymbol{U}_h, J_h) : \operatorname{Grad}\boldsymbol{V}_h \ \mathrm{d}\boldsymbol{X} + \\
&\int_{\Omega_r} \mathbf{F}(\boldsymbol{U}_h)\mathbf{S}_{\text{vol}}(\boldsymbol{U}_h, P_h, J_h) : \operatorname{Grad}\boldsymbol{V}_h \ \mathrm{d}\boldsymbol{X}\Big)',\\
0 = &\int_{\Omega_r} \frac{\mathrm{d}U(D)}{\mathrm{d}D}\Big|_{D=J_h} Q_h \ \mathrm{d}\boldsymbol{x} - \int_{\Omega_r} P_h Q_h \ \mathrm{d}\boldsymbol{X},\\
0 = &\int_{\Omega_r} J_h Z_h \ \mathrm{d}\boldsymbol{X} - \int_{\Omega_r} \det\mathbf{F}(\boldsymbol{U}_h) Z_h \ \mathrm{d}\boldsymbol{X}\,.
\end{aligned}
$$

In conforming finite element methods one usually uses globally continuous ansatz spaces for discretizing the variable $\boldsymbol{U}$. For the variables P, J however,

one may use globally discontinuous ansatz functions, thus one may interpret this as a coupling of a continuous Galerkin method coupled with a discontinuous Galerkin method. In the literature one usually uses piecewise constant functions for discretizing (P, J). To solve such a nonlinear block system one would apply for example Newton's method. The solution of a three by three nonlinear saddle point problem can be a demanding task. Therefore one uses an additional approximation and treats the variable J_h explicitly, e.g.

$$\int_{\Omega_r} J_h^{k+1} Z_h \ \mathrm{d}\boldsymbol{X} - \int_{\Omega_r} \det \mathbf{F}(\boldsymbol{U}_h^k) Z_h \ \mathrm{d}\boldsymbol{X} = 0.$$

Thus, in the case of piecewise constant test and ansatz functions one may deduce

$$J_h^{k+1}|_{\tau_l} = \frac{\int_{\tau_l} \det \mathbf{F}(\boldsymbol{U}_h^k) \ \mathrm{d}\boldsymbol{X}}{|\tau_l|}.$$

Hence one can also calculate the next iterate P_h^{k+1} as

$$P_h^{k+1}|_{\tau_l} = \left(\frac{\mathrm{d}U(D)}{\mathrm{d}D}|_{D=J_h^{k+1}} \right) |_{\tau_l}.$$

This procedure is called **mean dilatation technique** see [86, 122, 167, 168] and [100] for more details.

5.4.3 Assembling of the Element Matrices

In this section the assembling of the stiffness matrices for the discontinuous Galerkin method for nonlinear elasticity will be briefly discussed. To this end, consider the calculation of the local element matrices. For more details on assembling global matrices in the context of finite element methods in general we refer to [171, Chapter 11], [47, Appendix A] and [29]. The first element matrix to be investigated is given by

$$a_h^1(\boldsymbol{W}; \boldsymbol{U}_h, \boldsymbol{V}_h) := \int_{\tau_l} \operatorname{Grad} \boldsymbol{U}_h \mathbf{S}(\boldsymbol{W}) : \operatorname{Grad} \boldsymbol{V}_h \ \mathrm{d}\boldsymbol{X} \,. \tag{5.8}$$

On the element $\tau_l \in \mathcal{T}_N$ one has a set of scalar basis functions $\{\phi_j\}_{j=0}^{\text{ndofs}-1}$ where ndofs are the degrees of freedom on the element τ_l. With this one has

$$\boldsymbol{U}_h|_{\tau_l} = \sum_{s=0}^{d-1} \sum_{t=0}^{\text{ndofs}-1} U_s^t \phi_t(\boldsymbol{X}) \boldsymbol{e}_s.$$

This can be rewritten in a more compact form as

$$\boldsymbol{U}_h|_{\tau_l} = \boldsymbol{\Phi} \boldsymbol{U}$$

where

$$\begin{aligned}
\boldsymbol{\Phi} &:= \mathbf{I} \otimes \boldsymbol{\phi}, \\
\boldsymbol{\phi} &:= (\phi_0, \phi_1, \dots, \phi_{\text{ndofs}-1}), \\
\boldsymbol{U} &:= (U_0^0, U_0^1, \dots, U_0^{\text{ndofs}-1}, U_1^0, U_1^1, \dots, U_1^{\text{ndofs}-1}, \dots, U_{d-1}^0, U_{d-1}^1, \dots, U_{d-1}^{\text{ndofs}-1}).
\end{aligned}$$

Here "$\otimes$" denotes the **Kronecker product**. One can obtain a similar representation for the vectorized gradient $\text{vec}(\text{Grad}\, \boldsymbol{U}_h)$. There holds:

$$\text{vec}(\text{Grad}\, \boldsymbol{U}_h)|_{\tau_l} = \partial\boldsymbol{\Phi} \boldsymbol{U}$$

where

$$\begin{aligned}
\partial\boldsymbol{\Phi} &:= \mathbf{I} \otimes \partial\boldsymbol{\phi}, \\
\partial\boldsymbol{\phi}[i,j] &:= \frac{\partial \phi_j}{\partial X_i}, \qquad i = 0, \dots, d-1,\ j = 0, \dots, \text{ndofs}.
\end{aligned}$$

Remark 5.5. *The vectorization of a matrix* $\mathbf{A} \in \mathbb{R}^{n \times m}$, $\text{vec}(\mathbf{A}) \in \mathbb{R}^{nm}$ *is defined as*

$$\begin{aligned}
\text{vec}(\mathbf{A}) := (&A[0,0], A[0,1], \dots, A[0,m-1], A[1,0], A[1,1], \dots A[1,m-1], \dots, \\
&A[n-1,0], A[n-1,1], \dots, A[n-1,m-1])^\top.
\end{aligned}$$

For two matrices $\mathbf{A}, \mathbf{B} \in \mathbb{R}^{m \times n}$ *there holds:*

$$(\text{vec}(\mathbf{A}), \text{vec}(\mathbf{B})) = \mathbf{A} : \mathbf{B}. \tag{5.9}$$

The goal is to apply these techniques to derive a representation of the element matrix corresponding to the bilinear form (5.8). It can be shown that

$$\operatorname{vec}(\operatorname{Grad} \boldsymbol{U}_h \mathbf{S}(\boldsymbol{W}))|_{\tau_l} = (\mathbf{I} \otimes \mathbf{S}(\boldsymbol{W}) \partial \boldsymbol{\phi}) \boldsymbol{U}.$$

Therefore using (5.9), the symmetry $\mathbf{S}^\top = \mathbf{S}$ and the rule

$$(\mathbf{A} \otimes \mathbf{B})^\top = \mathbf{A}^\top \otimes \mathbf{B}^\top,$$

one deduces that the element matrix $\mathbf{A}^l_{1,h} \in \mathbb{R}^{d\text{ndofs} \times d\text{ndofs}}$ can be represented as

$$\begin{aligned} \mathbf{A}^l_h(\boldsymbol{W}) &= \int_{\tau_l} (\mathbf{I} \otimes (\partial \boldsymbol{\phi})^\top \mathbf{S}(\boldsymbol{W}) \partial \boldsymbol{\phi}) \ \mathrm{d}\boldsymbol{X}, \\ &= \int_{\tau_l} (\partial \boldsymbol{\Phi})^\top (\mathbf{I} \otimes \mathbf{S}(\boldsymbol{W})) \partial \boldsymbol{\Phi} \ \mathrm{d}\boldsymbol{X}\,. \end{aligned}$$

Due to the symmetry of $\mathbf{S}$, the element matrix is also symmetric. In the engineering community this representation is called a **$\mathbf{B}^\top\mathbf{DB}$ -integrator**. The second bilinear form to be investigated is given as

$$a^2_h(\boldsymbol{W}; \boldsymbol{U}_h, \boldsymbol{V}_h) := \int_{\tau_l} \operatorname{sym}(\mathbf{F}^\top(\boldsymbol{W}) \operatorname{Grad} \boldsymbol{U}_h) : \mathbb{C}(\boldsymbol{W}) : \operatorname{sym}(\mathbf{F}^\top(\boldsymbol{W}) \operatorname{Grad} \boldsymbol{V}_h) \ \mathrm{d}\boldsymbol{X}\,. \quad (5.10)$$

Again one is interested in a representation with the help of a $\mathbf{B}^\top\mathbf{DB}$-integrator. First take note that with the Mandel notation from Remark 2.16 one has

$$a^2_h(\boldsymbol{W}; \boldsymbol{U}_h, \boldsymbol{V}_h) = \int_{\tau_l} \left(\underline{\operatorname{sym}}^M(\mathbf{F}^\top(\boldsymbol{W}) \operatorname{Grad} \boldsymbol{U}_h), \mathbf{C}^M(\boldsymbol{W}) \underline{\operatorname{sym}}^M(\mathbf{F}^\top(\boldsymbol{W}) \operatorname{Grad} \boldsymbol{V}_h) \right) \ \mathrm{d}\boldsymbol{X}$$

where $\underline{\operatorname{sym}}^M(\mathbf{F}^\top \operatorname{Grad} \boldsymbol{U}_h)$ denotes the Mandel notation of $\operatorname{sym}(\mathbf{F}^\top \operatorname{Grad} \boldsymbol{U}_h)$. After some tedious calculations one can show that

$$\underline{\operatorname{sym}}^M(\mathbf{F}^\top \operatorname{Grad} \boldsymbol{U}_h) = \begin{pmatrix} \mathbf{F}^\top D_1 \boldsymbol{\Phi} \\ \mathbf{F} D_2 \boldsymbol{\Phi} \end{pmatrix} \boldsymbol{U}$$

where

$$D_1\mathbf{\Phi} = \begin{pmatrix} \frac{\partial\phi_0}{\partial X_0} & \frac{\partial\phi_1}{\partial X_0} & \dots & \frac{\partial\phi_{\text{ndofs}-1}}{\partial X_0} & & & 0 & & & & 0 & \\ & 0 & & & \frac{\partial\phi_0}{\partial X_1} & \frac{\partial\phi_1}{\partial X_1} & \dots & \frac{\partial\phi_{\text{ndofs}-1}}{\partial X_1} & & & 0 & \\ & 0 & & & & 0 & & & \frac{\partial\phi_0}{\partial X_2} & \frac{\partial\phi_1}{\partial X_2} & \dots & \frac{\partial\phi_{\text{ndofs}-1}}{\partial X_2} \end{pmatrix}$$

and

$$D_2\mathbf{\Phi} = \frac{\sqrt{2}}{2}\begin{pmatrix} \frac{\partial\phi_0}{\partial X_1} & \frac{\partial\phi_1}{\partial X_1} & \dots & \frac{\partial\phi_{\text{ndofs}-1}}{\partial X_1} & & & 0 & & \frac{\partial\phi_0}{\partial X_2} & \frac{\partial\phi_1}{\partial X_2} & \dots & \frac{\partial\phi_{\text{ndofs}-1}}{\partial X_2} \\ \frac{\partial\phi_0}{\partial X_0} & \frac{\partial\phi_1}{\partial X_0} & \dots & \frac{\partial\phi_{\text{ndofs}-1}}{\partial X_0} & \frac{\partial\phi_0}{\partial X_2} & \frac{\partial\phi_1}{\partial X_2} & \dots & \frac{\partial\phi_{\text{ndofs}-1}}{\partial X_2} & & & 0 & \\ & 0 & & & \frac{\partial\phi_0}{\partial X_1} & \frac{\partial\phi_1}{\partial X_1} & \dots & \frac{\partial\phi_{\text{ndofs}-1}}{\partial X_1} & \frac{\partial\phi_0}{\partial X_2} & \frac{\partial\phi_1}{\partial X_2} & \dots & \frac{\partial\phi_{\text{ndofs}-1}}{\partial X_2} \end{pmatrix}$$

in the case of $d = 3$. Thus again one can write the element matrix $\mathbf{A}^l_{2,h} \in \mathbb{R}^{d\text{ndofs}\times d\text{ndofs}}$ as

$$\mathbf{A}^l_{2,h} = \int_{\tau_l} \begin{pmatrix} (D_1\mathbf{\Phi})^\top \mathbf{F}(\boldsymbol{W}) & (D_2\mathbf{\Phi})^\top \mathbf{F}^\top(\boldsymbol{W}) \end{pmatrix} \mathbf{C}^M(\boldsymbol{W}) \begin{pmatrix} \mathbf{F}^\top(\boldsymbol{W}) D_1\mathbf{\Phi} \\ \mathbf{F}(\boldsymbol{W}) D_2\mathbf{\Phi} \end{pmatrix} \mathrm{d}\boldsymbol{X} \,. \tag{5.11}$$

Due to the symmetry properties of the elasticity tensor $\mathbb{C}$ one obtains a symmetric element matrix.

Remark 5.6. *With similar considerations one can derive representations for the bilinear forms*

$$a^3_h(\boldsymbol{W}; \boldsymbol{U}_h, \boldsymbol{V}_h) = \int_{\Gamma_{kl}} \left\langle \mathbf{F}(\boldsymbol{W}) \left(\mathbb{C}(\boldsymbol{W}) : \operatorname{sym}(\mathbf{F}^\top(\boldsymbol{W}) \operatorname{Grad} \boldsymbol{U}) \right) \right\rangle : [\![\boldsymbol{V}]\!]_{kl} \, \mathrm{ds}_{\boldsymbol{X}}$$

and

$$a^4_h(\boldsymbol{W}; \boldsymbol{U}_h, \boldsymbol{V}_h) = \int_{\Gamma_{kl}} \langle \operatorname{Grad} \boldsymbol{U} \mathbf{S}(\boldsymbol{W}) \rangle : [\![\boldsymbol{V}]\!]_{kl} \, \mathrm{ds}_{\boldsymbol{X}} \,.$$

For the first bilinear form one observes that

$$\begin{aligned} a^3_h(\boldsymbol{W}; \boldsymbol{U}_h, \boldsymbol{V}_h) = \frac{1}{2} \Bigg[& \int_{\Gamma_{kl}} \boldsymbol{A}_k : \mathbf{C}^M|_{\tau_k} : \boldsymbol{B}_{k,k} \, \mathrm{ds}_{\boldsymbol{X}} + \int_{\Gamma_{kl}} \boldsymbol{A}_l : \mathbf{C}^M|_{\tau_l} : \boldsymbol{B}_{l,k} \, \mathrm{ds}_{\boldsymbol{X}} \\ & - \int_{\Gamma_{kl}} \boldsymbol{A}_k : \mathbf{C}^M|_{\tau_k} : \boldsymbol{B}_{k,l} \, \mathrm{ds}_{\boldsymbol{X}} - \int_{\Gamma_{kl}} \boldsymbol{A}_l : \mathbf{C}^M|_{\tau_l} : \boldsymbol{B}_{l,l} \, \mathrm{ds}_{\boldsymbol{X}} \Bigg] \end{aligned}$$

where

$$\boldsymbol{A}_k := \underline{\mathrm{sym}^M}\left(\mathbf{F}^\top(\boldsymbol{W})_{|\tau_k}\,\mathrm{Grad}\,\boldsymbol{U}_{h|\tau_k}\right),$$
$$\boldsymbol{B}_{k,l} := \underline{\mathrm{sym}^M}\left(\mathbf{F}^\top(\boldsymbol{W})_{|\tau_k}(\boldsymbol{V}_{h|\tau_l}\otimes\boldsymbol{N})\right).$$

Using this one can derive a similar representation as for (5.11)*. However the resulting element matrices* $\mathbf{A}_h^3$ *and* $\mathbf{A}_h^4$ *are not symmetric. Thus the resulting global system matrix* $\mathbf{A}_h$ *will be non symmetric. For a deeper discussion about the advantages and disadvantages of this non symmetric formulation we refer to [113].*

5.5 Convergence Studies

In this section convergence studies for the discontinuous Galerkin finite element method for nonlinear elasticity for $d = 2, 3$ will be presented. The reference geometry for the convergence study is chosen as $\Omega_r = (0,1)^d$. As nonlinear material models the modified Saint-Venant Kirchoff model, see [85, p. 251], and the compressible neo-Hookean model are chosen. The corresponding free energy functions are given as

$$\Psi^{\mathrm{SV}}(\mathbf{C}) := \frac{\kappa}{2}(\ln(J))^2 + \frac{\mu}{4}\,\mathrm{tr}\left(\mathbf{C}^2 - 2\mathbf{C} + \mathbf{I}\right),$$
$$\Psi^{\mathrm{NH}}(\mathbf{C}) := \frac{\mu}{2}\left(\mathrm{tr}(\mathbf{C}) - 3 - 2\ln(J)\right) + \frac{\kappa}{2}(J-1)^2,$$

Dirichlet boundary conditions are posed on $\partial\Omega_r$. The input data are chosen in such a way that the exact solution to the equilibrium equations is given as

$$\boldsymbol{U}_{\mathrm{ex}}^{3D}(\boldsymbol{X}) := \frac{1}{2}\begin{pmatrix} 0 \\ 0 \\ z^2 x(1-x)y(1-y) \end{pmatrix},$$
$$\boldsymbol{U}_{\mathrm{ex}}^{2D}(\boldsymbol{X}) := \frac{1}{2}\begin{pmatrix} 0 \\ y^2 x(1-x) \end{pmatrix}.$$

We used Newton's method and take the element-wise $\mathrm{L}^2(\Omega_r)$-projection onto $[S_h^p(\mathcal{T}_N)]^d$ of $\boldsymbol{U}_{\mathrm{ex}}^{2D}$ or $\boldsymbol{U}_{\mathrm{ex}}^{3D}$ as initial guess. The error is measured in the norm $|||\boldsymbol{U}|||_{1,h}$ and in the $\mathrm{L}^2(\Omega)$-norm.

Results for 2D

Here we present the numerical results for the two dimensional example. We note that the plane strain approach discussed in Section 2.3.7 has been used. The numeric examples were performed with the help of NESHMET and the arising linear systems were solved with PARDISO, see [1, 160, 161].

Modified Saint-Venant Kirchoff Material

Our first example uses the Saint-Venant Kirchoff material. The material parameters were chosen as $\mu = 50$ and $\kappa = 71.43$. The stabilization parameter σ_{kl} was chosen as $\sigma_{kl} = 1000p^2$ where p is the polynomial degree. The results for $p = 1, 2$ are depicted in Table 5.1 and 5.2. For the polynomial degree $p = 3$ the results are depicted in Table 5.3. The sup-optimal convergence order in the $L^2(\Omega)$-norm for odd polynomial degrees is a well-known behavior for non-symmetric discontinuous Galerkin discretizations of linear partial differential equations, see [155, Theorem 2.14]. It should be mentioned, that the theory developed in [138] does not cover the case of polynomials with order less or equal $\frac{d}{2}$. However the results suggest, that the results are still valid for this case.

		$p=1$			$p=2$		
level	elements	dof	$\left\|\boldsymbol{U}_{\text{ex}}^{2D} - \boldsymbol{U}_h\right\|_{1,h}$	eoc	dof	$\left\|\boldsymbol{U}_{\text{ex}}^{2D} - \boldsymbol{U}_h\right\|_{1,h}$	eoc
0	8	48	7.0349E−1	–	96	2.7602E−2	–
1	32	192	3.1882E−1	1.14	384	7.4107E−3	1.90
2	128	768	1.6791E−1	0.93	1536	1.9250E−3	1.94
3	512	3072	8.8748E−2	0.92	6144	4.9159E−4	1.97
4	2048	12288	4.5888E−2	0.95	24576	1.2431E−4	1.98
5	8192	49152	2.3360E−2	0.97	98304	3.1261E−5	1.99
6	32768	196608	1.1789E−2	0.99	393216	7.8389E−6	2.00
7	131072	786432	5.9223E−3	1.00	1572864	1.9627E−6	2.00
Observed:				1.00			2.00

Table 5.1: Energy error $\left\|\boldsymbol{U}_{\text{ex}}^{2D} - \boldsymbol{U}_h\right\|_{1,h}$ for $p = 1, 2$

		$p=1$			$p=2$		
level	elements	dof	$\left\|\boldsymbol{U}_{\text{ex}}^{2D}-\boldsymbol{U}_h\right\|_{\text{L}^2(\Omega)}$	eoc	dof	$\left\|\boldsymbol{U}_{\text{ex}}^{2D}-\boldsymbol{U}_h\right\|_{\text{L}^2(\Omega)}$	eoc
0	8	48	9.2693E−3	–	96	1.7082E−3	–
1	32	192	2.5774E−3	1.85	384	2.0733E−4	3.04
2	128	768	6.1948E−4	2.06	1536	2.5019E−5	3.05
3	512	3072	1.4619E−4	2.08	6144	3.0989E−6	3.01
4	2048	12288	3.5113E−5	2.06	24576	3.9818E−7	2.96
5	8192	49152	8.5806E−6	2.03	98304	5.6068E−8	2.83
6	32768	196608	2.1179E−6	2.02	393216	9.6063E−9	2.55
7	131072	786432	5.2506E−7	2.01	1572864	2.0424E−9	2.23
Observed:				2.00			2.00

Table 5.2: $\text{L}^2(\Omega)$-error $\left\|\boldsymbol{U}_{\text{ex}}^{2D}-\boldsymbol{U}_h\right\|_{\text{L}^2(\Omega)}$ for $p=1,2$

			$p=3$		$p=3$	
level	elements	dof	$\left\|\boldsymbol{U}_{\text{ex}}^{2D}-\boldsymbol{U}_h\right\|_{1,h}$	eoc	$\left\|\boldsymbol{U}_{\text{ex}}^{2D}-\boldsymbol{U}_h\right\|_{\text{L}^2(\Omega)}$	eoc
0	8	160	2.5844E−3	–	1.2594E−04	–
1	32	640	3.1438E−4	3.04	7.2017E−06	4.13
2	128	2560	3.8495E−5	3.03	4.2444E−07	4.08
3	512	10240	4.7534E−6	3.02	2.5658E−08	4.05
4	2048	40960	5.9025E−7	3.01	1.5754E−09	4.03
5	8192	163840	7.3527E−8	3.00	9.7558E−11	4.01
Observed:				3.00		4.00

Table 5.3: Errors for $p=3$

Compressible Neo-Hooke Material

In the second example we use the compressible neo-Hooke material. The material parameters were chosen as $\mu = 50$ and $\kappa = 333.3$. The stabilization parameter σ_{kl} was again chosen as $\sigma_{kl} = 1000p^2$ where p is the polynomial degree. The results for $p = 1, 2$ are depicted in Table 5.4 and 5.5. For the polynomial degree $p = 3$ the results are depicted in Table 5.6.

		$p=1$			$p=2$		
level	elements	dof	$\left\|\boldsymbol{U}_{\text{ex}}^{2D} - \boldsymbol{U}_h\right\|_{1,h}$	eoc	dof	$\left\|\boldsymbol{U}_{\text{ex}}^{2D} - \boldsymbol{U}_h\right\|_{1,h}$	eoc
0	8	48	8.6254E−1	–	96	6.4544E−2	–
1	32	192	4.1814E−1	1.04	384	2.1383E−2	1.59
2	128	768	2.1725E−1	0.94	1536	6.0322E−3	1.83
3	512	3072	1.1297E−1	0.94	6144	1.5892E−3	1.92
4	2048	12288	5.7916E−2	0.96	24576	4.0686E−4	1.97
5	8192	49152	2.9364E−2	0.98	98304	1.0287E−4	1.98
6	32768	196608	1.4790E−2	0.99	393216	2.5858E−5	1.99
Observed:				1.00			2.00

Table 5.4: Energy error $\left\|\boldsymbol{U}_{\text{ex}}^{2D} - \boldsymbol{U}_h\right\|_{1,h}$ for $p = 1, 2$

		$p=1$			$p=2$		
level	elements	dof	$\left\|\boldsymbol{U}_{\text{ex}}^{2D} - \boldsymbol{U}_h\right\|_{\text{L}^2(\Omega)}$	eoc	dof	$\left\|\boldsymbol{U}_{\text{ex}}^{2D} - \boldsymbol{U}_h\right\|_{\text{L}^2(\Omega)}$	eoc
0	8	48	8.8312E−3	–	96	1.6559E−3	–
1	32	192	2.2734E−3	1.96	384	2.0597E−4	3.01
2	128	768	5.3146E−4	2.10	1536	2.8883E−5	2.83
3	512	3072	1.3061E−4	2.02	6144	5.3651E−6	2.43
4	2048	12288	3.3171E−5	1.98	24576	1.2403E−6	2.11
5	8192	49152	8.4487E−6	1.97	98304	3.0806E−7	2.01
6	32768	196608	2.1398E−6	1.98	393216	7.7441E−8	1.99
Observed:				2.00			2.00

Table 5.5: $\text{L}^2(\Omega)$-error $\left\|\boldsymbol{U}_{\text{ex}}^{2D} - \boldsymbol{U}_h\right\|_{\text{L}^2(\Omega)}$ for $p = 1, 2$

			$p=3$		$p=3$	
level	elements	dof	$\left\|\boldsymbol{U}_{\text{ex}}^{2D}-\boldsymbol{U}_h\right\|_{\text{L}^2(\Omega)}$	eoc	$\left\|\!\left\|\!\left\|\boldsymbol{U}_{\text{ex}}^{2D}-\boldsymbol{U}_h\right\|\!\right\|\!\right\|_{1,h}$	eoc
0	8	160	1.2643E−04	–	4.1520E−3	–
1	32	640	7.2299E−06	4.13	5.5930E−4	2.89
2	128	2560	4.2640E−07	4.08	7.2006E−5	2.96
3	512	10240	2.5802E−08	4.05	9.1199E−6	2.98
4	2048	40960	1.5853E−09	4.02	1.1471E−6	2.99
5	8192	163840	9.8215E−11	4.01	1.4382E−7	3.00
Observed:				4.00		3.00

Table 5.6: Errors for $p=3$

Results for 3D

In this section we present the convergence results for three-dimensional examples. The resulting linear system were solved with a ILU(0) precondtioned GMRes method within NESHMET.

Modified Saint-Venant Kirchoff material

As first example we use again the modified Saint-Venant Kirchoff material. The material parameters were chosen as $\mu = 50$ and $\kappa = 71.43$. The stabilization parameter σ_{kl} was chosen as $\sigma_{kl} = 1000p^2$ where p is the polynomial degree. The results for $p = 1, 2$ are depicted in Table 5.7 and 5.8.

Comparing the results for the behavior of the $\text{L}^2(\Omega_r)$-error in Table 5.8 with the two dimensional case in Table 5.2, we see that in the three dimensional case we can not observe a clear convergence order of two for $p = 2$.

Compressible Neo-Hooke material

In the second example we used the compressible neo-Hooke material. For this example we used a different initial discretization of Ω_r. The material parameters were chosen as $\mu = 50$ and $\kappa = 71.43$. The stabilization parameter σ_{kl} was

		$p=1$			$p=2$		
level	elements	dof	$\left\|\left\|\left\| \boldsymbol{U}_{\text{ex}}^{3D} - \boldsymbol{U}_h \right\|\right\|\right\|_{1,h}$	eoc	dof	$\left\|\left\|\left\| \boldsymbol{U}_{\text{ex}}^{3D} - \boldsymbol{U}_h \right\|\right\|\right\|_{1,h}$	eoc
0	6	72	5.0490E−1	–	360	1.3927E−1	–
1	48	576	3.2654E−1	0.63	2880	3.6689E−2	1.92
2	384	4608	1.1957E−1	1.45	23040	7.7106E−3	2.25
3	768	36864	4.9867E−2	1.27	184320	1.6456E−3	2.23
4	6144	294912	2.2945E−2	1.11	1474560	3.6784E−4	2.16
5	49152	2359296	1.1077E−2	1.05	11796480	8.5969E−5	2.10
Observed:				1.00			2.00

Table 5.7: Energy error $\left\|\left\|\left\| \boldsymbol{U}_{\text{ex}}^{3D} - \boldsymbol{U}_h \right\|\right\|\right\|_{1,h}$ for $p = 1, 2$

		$p=1$			$p=2$		
level	elements	dof	$\left\| \boldsymbol{U}_{\text{ex}}^{3D} - \boldsymbol{U}_h \right\|_{\text{L}^2(\Omega_r)}$	eoc	dof	$\left\| \boldsymbol{U}_{\text{ex}}^{3D} - \boldsymbol{U}_h \right\|_{\text{L}^2(\Omega_r)}$	eoc
0	6	72	4.1493E−3	–	360	8.7706E−4	–
1	48	576	2.2901E−3	0.86	2880	3.0963E−4	1.50
2	384	4608	1.0848E−3	1.08	23040	4.7439E−5	2.71
3	768	36864	3.4612E−4	1.65	184320	6.1847E−6	2.94
4	6144	294912	9.4153E−5	1.88	1474560	7.9445E−7	2.96
5	49152	2359296	2.4040E−5	1.97	11796480	1.1161E−7	2.83
Observed:				2.00			–

Table 5.8: $\text{L}^2(\Omega_r)$-error $\left\| \boldsymbol{U}_{\text{ex}}^{3D} - \boldsymbol{U}_h \right\|_{\text{L}^2(\Omega_r)}$ for $p = 1, 2$

again chosen as $\sigma_{kl} = 1000p^2$ where p is the polynomial degree. The results for $p = 1, 2$ are depicted in Table 5.9 and 5.5.

		$p=1$			$p=2$		
level	elements	dof	$\left\|\boldsymbol{U}_{\text{ex}}^{3D} - \boldsymbol{U}_h\right\|_{1,h}$	eoc	dof	$\left\|\boldsymbol{U}_{\text{ex}}^{3D} - \boldsymbol{U}_h\right\|_{1,h}$	eoc
0	6	72	5.0494E−1	–	180	1.3055E−1	–
1	48	576	3.3506E−1	0.59	1440	4.3122E−2	1.60
2	384	4608	1.3274E−1	1.34	11520	1.0797E−2	2.00
3	768	36864	6.0195E−2	1.14	92160	2.6582E−3	2.02
4	6144	294912	2.9173E−2	1.04	737280	6.6578E−4	2.00
5	49152	2359296	1.4377E−2	1.02	5898240	1.6736E−4	1.99
Observed:				1.00			2.00

Table 5.9: Energy error $\left\|\boldsymbol{U}_{\text{ex}}^{3D} - \boldsymbol{U}_h\right\|_{1,h}$ for $p = 1, 2$

		$p=1$			$p=2$		
level	elements	dof	$\left\|\boldsymbol{U}_{\text{ex}}^{3D} - \boldsymbol{U}_h\right\|_{\mathrm{L}^2(\Omega_r)}$	eoc	dof	$\left\|\boldsymbol{U}_{\text{ex}}^{3D} - \boldsymbol{U}_h\right\|_{\mathrm{L}^2(\Omega_r)}$	eoc
0	6	72	4.1523E−3	–	180	2.7040E−3	–
1	48	576	2.2726E−3	0.87	1440	9.9930E−4	1.44
2	384	4608	1.1157E−3	1.03	11520	1.4182E−4	2.82
3	768	36864	3.7026E−4	1.59	92160	1.6524E−5	3.10
4	6144	294912	1.0290E−4	1.85	737280	1.9582E−6	3.08
5	49152	2359296	2.6502E−5	1.96	5898240	2.7602E−7	2.83
Observed:				2.00			—

Table 5.10: $\mathrm{L}^2(\Omega_r)$-error $\left\|\boldsymbol{U}_{\text{ex}}^{3D} - \boldsymbol{U}_h\right\|_{\mathrm{L}^2(\Omega_r)}$ for $p = 1, 2$

Again, by comparison of the two dimensional error behavior in Table 5.5 with the one in Table 5.10 we see, that a clear convergence order of two can not be observed.

6 Coupled Electro-Mechanics

In this chapter the application of the previously developed methods to the system of coupled electro mechanics will be described. Recall the coupled system summarized in Formulation 2.1. Find $(V_{\mathrm{tm}}, u_e, \boldsymbol{v}, T_a, \boldsymbol{U})$ such that

$$\begin{aligned}
\frac{\partial}{\partial t}(JV_{\mathrm{tm}}) + J\overline{\mathrm{I_{ion}}} - J\,\mathrm{Div}(J\mathbf{M}_i\,\mathrm{Grad}\,V_{\mathrm{tm}}) - J\,\mathrm{Div}(J\mathbf{M}_i\,\mathrm{Grad}\,u_e) &= Js_i,\\
-J\,\mathrm{Div}(J\mathbf{M}_i\,\mathrm{Grad}\,V_{\mathrm{tm}}) - J\,\mathrm{Div}(J\mathbf{M}_{i+e}\,\mathrm{Grad}\,u_e) &= 0,\\
\frac{\partial}{\partial t}(J\boldsymbol{v}) + J\boldsymbol{H}(V_{\mathrm{tm}}, \boldsymbol{v}) &= \mathbf{0},\\
\frac{\partial}{\partial t}(JT_a) + J\epsilon(V_{\mathrm{tm}})\,(T_a - k_a(V_{\mathrm{tm}} - V_r)) &= 0,\\
-\,\mathrm{Div}(\mathbf{F}\,(\mathbf{S}_{\mathrm{pas}} + \mathbf{S}_{\mathrm{act}})) &= 0
\end{aligned}$$

in $\Omega_r \times (0,T)$ and the boundary and initial conditions

$$\begin{aligned}
\boldsymbol{N}\cdot(\mathbf{M}_i\,\mathrm{Grad}\,V_{\mathrm{tm}} + \mathbf{M}_i\,\mathrm{Grad}\,u_e) + \alpha_i(V_{\mathrm{tm}} + u_e) &= G_{R,i},\\
\boldsymbol{N}\cdot(\mathbf{M}_e\,\mathrm{Grad}\,u_e) + \alpha_e u_e &= G_{R,e},\\
\mathbf{F}(\mathbf{S}_{\mathrm{pas}} + \mathbf{S}_{\mathrm{act}})\boldsymbol{N} &= \mathbf{0},\\
V_{\mathrm{tm}}(0,\boldsymbol{X}) &= V^0_{\mathrm{tm}}(\boldsymbol{X}),\\
\boldsymbol{v}(0,\boldsymbol{X}) &= \boldsymbol{v}^0(\boldsymbol{X}),\\
T_a(0,\boldsymbol{X}) &= T^0_a(\boldsymbol{X}),
\end{aligned}$$

on $\partial\Omega_r \times (0,T)$ and $\Omega_r \times \{0\}$. The following additional simplifications are made:

- From the almost incompressibility one has that $J \approx 1$, hence one may drop this dependence from the equations.
- It is assumed that $\frac{\partial}{\partial t}J \approx 0$. Hence one may neglect also those terms in the equations.

Using these assumptions one obtains the simplified, yet still coupled, system Find $(V_{\mathrm{tm}}, u_e, \boldsymbol{v}, T_a, \boldsymbol{U})$ such that

$$\frac{\partial}{\partial t} V_{\mathrm{tm}} + \overline{\mathrm{I_{ion}}}(V_{\mathrm{tm}}, \boldsymbol{v}, \boldsymbol{U}) - \mathrm{Div}(\mathbf{M}_i \,\mathrm{Grad}\, V_{\mathrm{tm}}) - \mathrm{Div}(\mathbf{M}_i \,\mathrm{Grad}\, u_e) = s_i, \tag{6.1}$$

$$- \mathrm{Div}(\mathbf{M}_i \,\mathrm{Grad}\, V_{\mathrm{tm}}) - \mathrm{Div}(\mathbf{M}_{i+e} \,\mathrm{Grad}\, u_e) = 0, \tag{6.2}$$

$$\frac{\partial}{\partial t} \boldsymbol{v} + \boldsymbol{H}(V_{\mathrm{tm}}, \boldsymbol{v}) = \mathbf{0}, \tag{6.3}$$

$$\frac{\partial}{\partial t} T_a + \epsilon(V_{\mathrm{tm}}) \left(T_a - k_a(V_{\mathrm{tm}} - V_r)\right) = 0, \tag{6.4}$$

$$- \mathrm{Div}(\mathbf{F}\,(\mathbf{S}_{\mathrm{pas}} + \mathbf{S}_{\mathrm{act}})) = 0, \tag{6.5}$$

in $Q := \Omega_r \times (0, T)$ with the boundary and initial conditions

$$\boldsymbol{N} \cdot (\mathbf{M}_i \,\mathrm{Grad}\, V_{\mathrm{tm}} + \mathbf{M}_i \,\mathrm{Grad}\, u_e) + \alpha_i (V_{\mathrm{tm}} + u_e) = G_{R,i}, \tag{6.6}$$

$$\boldsymbol{N} \cdot (\mathbf{M}_e \,\mathrm{Grad}\, u_e) + \alpha_e u_e = G_{R,e}, \tag{6.7}$$

$$\mathbf{F}(\mathbf{S}_{\mathrm{pas}} + \mathbf{S}_{\mathrm{act}})\boldsymbol{N} = \mathbf{0}, \tag{6.8}$$

$$V_{\mathrm{tm}}(0, \boldsymbol{X}) = V_{\mathrm{tm}}^0(\boldsymbol{X}), \tag{6.9}$$

$$\boldsymbol{v}(0, \boldsymbol{X}) = \boldsymbol{v}^0(\boldsymbol{X}), \tag{6.10}$$

$$T_a(0, \boldsymbol{X}) = T_a^0(\boldsymbol{X}). \tag{6.11}$$

on $\Sigma := \partial\Omega_r \times (0, T)$ and Σ_0.

Remark 6.1. *It is also possible to include Robin type boundary conditions for the equations of nonlinear elasticity reading as*

$$\mathbf{F}(\mathbf{S}_{pas} + \mathbf{S}_{act})\boldsymbol{N} + \alpha \boldsymbol{U} = \boldsymbol{G}_R \tag{6.12}$$

on Σ.

6.1 Space-Time Discretization

We will apply the tools developed in Section 4.2 and Chapter 5. To this end we will define the following discrete spaces: Fix $p \in \mathbb{N}_0$

$$S_h^p(\mathcal{T}_N) := \left\{ v_h \in \mathrm{L}^2(Q) \colon v_h|_{\tau_l} \in \mathbb{P}^p(\tau_l) \text{ for all } \tau_l \in \mathcal{T}_N \right\},$$

$$V_h^p(\mathcal{T}_N) := \left\{ \boldsymbol{v}_h \in [\mathrm{L}^2(Q)]^d \colon \boldsymbol{v}_h|_{\tau_l} \in [\mathbb{P}^p(\tau_l)]^d \text{ for all } \tau_l \in \mathcal{T}_N \right\}.$$

For the equations (6.1)-(6.4) we use the space-time discontinuous Galerkin discretization derived in Section 4.2. Thus we get the following system

$$\begin{aligned} b_T^{\mathrm{DG}}(V_{\mathrm{tm}}^h, \phi^h) + a_i^{\mathrm{DG}}(V_{\mathrm{tm}}^h, \phi^h) + a_i^{\mathrm{DG}}(u_e^h, \phi^h) + \overline{I}^{\mathrm{DG}}(V_{\mathrm{tm}}^h, v^h, \boldsymbol{U}^h; \phi^h) &= l_1^{\mathrm{DG}}(\phi^h), \\ a_i^{\mathrm{DG}}(V_{\mathrm{tm}}^h, \psi^h) + a_{i+e}^{\mathrm{DG}}(u_e^h, \psi^h) &= l_2^{\mathrm{DG}}(\psi^h), \\ b_T^{\mathrm{DG}}(v^h, \xi^h) + H^{\mathrm{DG}}(V_{\mathrm{tm}}^h, v^h; \xi^h) &= l_3^{\mathrm{DG}}(\xi^h), \\ b_T^{\mathrm{DG}}(T_a^h, \theta^h) + T^{\mathrm{DG}}(V_{\mathrm{tm}}^h, T_a^h; \theta^h) &= l_4^{\mathrm{DG}}(\theta^h), \end{aligned}$$

for all $(\phi^h, \psi^h, \xi^h, \theta^h) \in S_h^p(\mathcal{T}_N) \times S_h^p(\mathcal{T}_N) \times S_h^p(\mathcal{T}_N) \times S_h^p(\mathcal{T}_N)$. The bilinear form $b_T^{\mathrm{DG}}(\cdot,\cdot)$ is taken as in (4.10). The bilinear forms $a_i^{\mathrm{DG}}(\cdot,\cdot)$, $a_{i+e}^{\mathrm{DG}}(\cdot,\cdot)$ are defined as in (4.4). The nonlinear forms are treated in the most simple way and are defined as

$$\begin{aligned} \overline{I}^{\mathrm{DG}}(V_{\mathrm{tm}}^h, v^h, \boldsymbol{U}^h; \phi^h) &:= \sum_{l=1}^{N} \int_{\tau_l} \mathrm{I}_{\mathrm{ion}}(V_{\mathrm{tm}}^h, v^h)\phi^h \, dq + \int_{\tau_l} \mathrm{I}_{\mathrm{MEF}}(V_{\mathrm{tm}}^h, \boldsymbol{U}^h)\phi^h \, dq, \\ H^{\mathrm{DG}}(V_{\mathrm{tm}}^h, v^h; \xi^h) &:= \sum_{l=1}^{N} \int_{\tau_l} H(V_{\mathrm{tm}}^h, v^h)\xi^h \, dq, \\ T^{\mathrm{DG}}(V_{\mathrm{tm}}^h, T_a^h; \theta^h) &:= \sum_{l=1}^{N} \int_{\tau_l} T(V_{\mathrm{tm}}^h, T_a^h)\theta^h \, dq. \end{aligned}$$

The linear forms on the right hand side are defined as

$$\begin{aligned} l_1^{\mathrm{DG}}(\phi^h) &:= \int_Q s_i\phi^h \, dq + \int_{\Sigma_0} V_{\mathrm{tm}}^0\phi^h \, ds_q + \int_{\Sigma_r} G_{R,i}\phi^h \, ds_q, \\ l_2^{\mathrm{DG}}(\psi^h) &:= \int_{\Sigma_r} (G_{R,i} + G_{R,e})\psi^h \, ds_q, \\ l_3^{\mathrm{DG}}(\xi^h) &:= \int_{\Sigma_0} v^0\xi^h \, ds_q, \\ l_4^{\mathrm{DG}}(\theta^h) &:= \int_{\Sigma_0} T_a^0\theta^h \, ds_q. \end{aligned}$$

For the discretization of the equations of nonlinear elasticity (6.5) we will adapt the bilinear form from (5.3) to the space-time setting. Thus we arrive at

$$a_{\mathrm{elast}}^{\mathrm{DG}}(T_a^h, \boldsymbol{U}^h; \boldsymbol{V}^h) = l_5(\boldsymbol{V}^h).$$

where

$$a^{\mathrm{DG}}_{\mathrm{elast}}(T^h_a, \boldsymbol{U}^h; \boldsymbol{V}^h) := \sum_{l=1}^{N} \int_{\tau_l} \mathbf{F}(\boldsymbol{U}^h) \left(\mathbf{S}_{\mathrm{pas}}(\boldsymbol{U}^h) + \mathbf{S}_{\mathrm{act}}(T^h_a, \boldsymbol{U}^h) \right) : \operatorname{Grad} \boldsymbol{V}^h \, dq$$
$$- \sum_{\Gamma_{kl} \in \mathcal{I}_N} \int_{\Gamma_{kl}} \left\langle \mathbf{F}(\boldsymbol{U}^h) \left(\mathbf{S}_{\mathrm{pas}}(\boldsymbol{U}^h) + \mathbf{S}_{\mathrm{act}}(T^h_a, \boldsymbol{U}^h) \right) \right\rangle : [\![\boldsymbol{V}_h]\!]_{\boldsymbol{X},kl} \, ds_q,$$
$$+ \sum_{\Gamma_{kl} \in \mathcal{I}_N} \frac{\sigma^{\mathrm{elast}}_{kl}}{\overline{h}_{kl}} \int_{\Gamma_{kl}} [\![\boldsymbol{U}_h]\!]_{\boldsymbol{X},kl} : [\![\boldsymbol{V}_h]\!]_{\boldsymbol{X},kl} \, ds_q.$$

and

$$l^{\mathrm{DG}}_5(\boldsymbol{V}^h) = 0.$$

Remark 6.2. *In the case of Robin type boundary conditions we may add the term*

$$\alpha \int_{\Sigma_r} \left(\boldsymbol{U}^h, \boldsymbol{V}^h \right) \, ds_q$$

to the nonlinear form $a^{\mathrm{DG}}_{elast}(T^h_a, \boldsymbol{U}^h; \boldsymbol{V}^h)$ *and*

$$\int_{\Sigma_r} \left(\boldsymbol{G}_R, \boldsymbol{V}^h \right) \, ds_q$$

to the right hand side.

Remark 6.3. *For almost incompressible materials we will use the mean dilatation technique described in Section* (5.4.2)*. Thus the incompressibility constraint is eliminated locally on each element.*

Collecting the two building blocks together we arrive at the following nonlinear discretized system: Find $(V^h_{\mathrm{tm}}, u^h_e, v^h, T^h_a, \boldsymbol{U}^h)$ such that

$$\begin{aligned}
b^{\mathrm{DG}}_T(V^h_{\mathrm{tm}}, \phi^h) + a^{\mathrm{DG}}_i(V^h_{\mathrm{tm}}, \phi^h) + a^{\mathrm{DG}}_i(u^h_e, \phi^h) + \overline{I}^{\mathrm{DG}}(V^h_{\mathrm{tm}}, v^h, \boldsymbol{U}^h; \phi^h) &= l^{\mathrm{DG}}_1(\phi^h), \\
a^{\mathrm{DG}}_i(V^h_{\mathrm{tm}}, \psi^h) + a^{\mathrm{DG}}_{i+e}(u^h_e, \psi^h) &= l^{\mathrm{DG}}_2(\psi^h), \\
b^{\mathrm{DG}}_T(v^h, \xi^h) + H^{\mathrm{DG}}(V^h_{\mathrm{tm}}, v^h; \xi^h) &= l^{\mathrm{DG}}_3(\xi^h), \\
b^{\mathrm{DG}}_T(T^h_a, \theta^h) + T^{\mathrm{DG}}(V^h_{\mathrm{tm}}, T^h_a; \theta^h) &= l^{\mathrm{DG}}_4(\theta^h), \\
a^{\mathrm{DG}}_{\mathrm{elast}}(T^h_a, \boldsymbol{U}^h; \boldsymbol{V}^h) &:= l^{\mathrm{DG}}_5(\boldsymbol{V}^h)
\end{aligned}$$

for all $(\phi^h, \psi^h, \xi^h, \theta^h, \boldsymbol{V}^h)$. As the derived system is nonlinear we will apply Newton's method to solve it. To this end we need the linearization around given solutions $(V_{\mathrm{tm}}^{k,h}, u_e^{k,h}, v^{k,h}, T_a^{k,h}, \boldsymbol{U}^{k,h})$. After performing the linearization and using the Galerkin isomorphism we can write the resulting Jacobian for Newton's method in the form

$$\mathbf{DF} := \begin{array}{c} \begin{matrix} V_{\mathrm{tm}} & u_e & v & T_a & \boldsymbol{U} \end{matrix} \\ \begin{pmatrix} \mathbf{F}_{11} & \mathbf{F}_{12} & \mathbf{F}_{13} & \mathbf{0} & \mathbf{F}_{15} \\ \mathbf{F}_{21} & \mathbf{F}_{22} & \mathbf{0} & \mathbf{0} & \mathbf{0} \\ \mathbf{F}_{31} & \mathbf{0} & \mathbf{F}_{33} & \mathbf{0} & \mathbf{0} \\ \mathbf{F}_{41} & \mathbf{0} & \mathbf{0} & \mathbf{F}_{44} & \mathbf{0} \\ \mathbf{0} & \mathbf{0} & \mathbf{0} & \mathbf{F}_{54} & \mathbf{F}_{55} \end{pmatrix} \end{array}$$

Above the matrix definition we indicated the variables to which the derivatives correspond. The individual blocks of the Jacobian are described in the following.

$\mathbf{F}_{11}$ corresponds to

$$b_T^{\mathrm{DG}}(\delta^h, \phi^h) + a_i^{\mathrm{DG}}(\delta^h, \phi^h) + \sum_{l=1}^{N} \int_{\tau_l} \frac{\partial \mathrm{I}_{\mathrm{ion}}}{\partial V_{\mathrm{tm}}}(V_{\mathrm{tm}}^{k,h}, v^{k,h}) \delta^h \phi^h \, dq + \sum_{l=1}^{N} \int_{\tau_l} \frac{\partial \mathrm{I}_{\mathrm{MEF}}}{\partial V_{\mathrm{tm}}}(V_{\mathrm{tm}}^{k,h}, \boldsymbol{U}^{k,h}) \delta^h \phi^h \, dq.$$

$\mathbf{F}_{12}$ corresponds to

$$a_i^{\mathrm{DG}}(\delta^h, \phi^h).$$

$\mathbf{F}_{13}$ corresponds to

$$\sum_{l=1}^{N} \int_{\tau_l} \frac{\partial \mathrm{I}_{\mathrm{ion}}}{\partial v}(V_{\mathrm{tm}}^{k,h}, v^{k,h}) \delta^h \phi^h \, dq$$

$\mathbf{F}_{15}$ corresponds to

$$\sum_{l=1}^{N} \int_{\tau_l} \frac{\partial \mathrm{I}_{\mathrm{MEF}}}{\partial \lambda_f}(V_{\mathrm{tm}}^{k,h}, \boldsymbol{U}^{k,h}) (2(\boldsymbol{f}_0 \otimes \boldsymbol{f}_0) : \mathrm{sym}(\mathbf{F}(\boldsymbol{U}^{k,h})^\top \operatorname{Grad} \boldsymbol{\delta}^h) \phi^h \, dq.$$

$\mathbf{F}_{21}$ corresponds to

$$a_i^{\mathrm{DG}}(\delta^h, \psi^h),$$

$\mathbf{F}_{22}$ corresponds to

$$a_{i+e}^{\mathrm{DG}}(\delta^h, \psi^h).$$

$\mathbf{F}_{31}$ corresponds to

$$\sum_{l=1}^{N} \int_{\tau_l} \frac{\partial H}{\partial V_{\mathrm{tm}}}(V_{\mathrm{tm}}^{h,k}, v^{h,k}) \delta^h \xi^h \, dq$$

$\mathbf{F}_{33}$ corresponds to

$$b_T^{\mathrm{DG}}(\delta^h, \xi^h) + \sum_{l=1}^{N} \int_{\tau_l} \frac{\partial H}{\partial v}(V_{\mathrm{tm}}^{h,k}, v^{h,k}) \delta^h \xi^h \, dq$$

$\mathbf{F}_{41}$ corresponds to

$$\sum_{l=1}^{N} \int_{\tau_l} \frac{\partial T}{\partial V_{\mathrm{tm}}}(V_{\mathrm{tm}}^{h,k}, T_a^{h,k}) \delta^h \theta^h \, dq$$

$\mathbf{F}_{44}$ corresponds to

$$b_T^{\mathrm{DG}}(\delta^h, \theta^h) + \sum_{l=1}^{N} \int_{\tau_l} \frac{\partial T}{\partial T_a}(V_{\mathrm{tm}}^{h,k}, T_a^{h,k}) \delta^h \theta^h \, dq$$

$\mathbf{F}_{54}$ corresponds to

$$\begin{aligned} &\sum_{l=1}^{N} \int_{\tau_l} \delta_h \left(\mathbf{F}(\boldsymbol{U}^{k,h}) \frac{\partial \mathbf{S}_{\mathrm{act}}}{\partial T_a}(T_a^{h,k}, \boldsymbol{U}^{h,k}) : \operatorname{Grad} \boldsymbol{V}^h \right) \, dq \\ &\qquad - \sum_{\Gamma_{kl} \in \mathcal{I}_N} \int_{\Gamma_{kl}} \left\langle \delta^h \left(\mathbf{F}(\boldsymbol{U}^{k,h}) \frac{\partial \mathbf{S}_{\mathrm{act}}}{\partial T_a}(T_a^{h,k}, \boldsymbol{U}^{h,k}) \right) \right\rangle : \left[\!\left[\boldsymbol{V}^h \right]\!\right]_{\boldsymbol{X},kl} \, ds_q \end{aligned}$$

$\mathbf{F}_{55}$ corresponds to

$$a_1^{\mathrm{DG}}(T_a^{h,k}, \boldsymbol{U}^{h,k}; \boldsymbol{\delta}^h, \boldsymbol{V}^h) + a_2^{\mathrm{DG}}(T_a^{h,k}, \boldsymbol{U}^{h,k}; \boldsymbol{\delta}^h, \boldsymbol{V}^h)$$

where

$$\begin{aligned} a_1^{\mathrm{DG}}(T_a^{h,k}, \boldsymbol{U}^{h,k}; \boldsymbol{\delta}^h, \boldsymbol{V}^h) := \\ \sum_{l=1} \int_{\tau_l} \operatorname{Grad} \boldsymbol{\delta}^h \underline{\mathbf{S}}_{h,k} : \operatorname{Grad} \boldsymbol{V}^h \, \mathrm{d}q \\ + \int_{\tau_l} \operatorname{sym}(\underline{\mathbf{F}}_{h,k}^\top \operatorname{Grad} \boldsymbol{\delta}^h) : \underline{\mathbb{C}}_{h,k} : \operatorname{sym}(\underline{\mathbf{F}}_{h,k}^\top \operatorname{Grad} \boldsymbol{V}^h) \mathrm{d}q \end{aligned}$$

with

$$\begin{aligned} \underline{\mathbf{F}}_{h,k} &:= \mathbf{F}(\boldsymbol{U}^{h,k}), \\ \underline{\mathbf{S}}_{h,k} &:= \mathbf{S}_{\mathrm{pass}}(\boldsymbol{U}^{h,k}) + \mathbf{S}_{\mathrm{act}}(T_a^{h,k}, \boldsymbol{U}^{h,k}), \\ \underline{\mathbb{C}}_{h,k} &:= \mathbb{C}_{\mathrm{pas}}(\boldsymbol{U}^{h,k}) + \mathbb{C}_{\mathrm{act}}(T_a^{h,k}, \boldsymbol{U}^{h,k}). \end{aligned}$$

The other bilinear forms are defined as

$$\begin{aligned} a_2^{\mathrm{DG}}(\boldsymbol{\phi}; \boldsymbol{U}, \boldsymbol{V}) := \\ - \sum_{\Gamma_{kl} \in \mathcal{I}_N} \int_{\Gamma_{kl}} \left\langle \underline{\mathbf{F}}_{h,k} \left(\underline{\mathbb{C}}_{h,k} : \operatorname{sym}(\underline{\mathbf{F}}_{h,k}^\top \operatorname{Grad} \boldsymbol{\delta}^h) \right) \right\rangle : [\![\boldsymbol{V}^h]\!]_{\boldsymbol{X},kl} \, \mathrm{ds_q} \\ - \sum_{\Gamma_{kl} \in \mathcal{I}_N} \int_{\Gamma_{kl}} \left\langle \operatorname{Grad} \boldsymbol{\delta}^h \underline{\mathbf{S}}_{h,k} \right\rangle : [\![\boldsymbol{V}^h]\!]_{\boldsymbol{X},kl} \, \mathrm{ds_q} \\ + \sum_{\Gamma_{kl} \in \mathcal{I}_N} \frac{\sigma_{kl}^{\mathrm{elast}}}{\overline{h}_{kl}} \int_{\Gamma_{kl}} [\![\boldsymbol{U}]\!]_{\boldsymbol{X},kl} : [\![\boldsymbol{V}]\!]_{\boldsymbol{X},kl} \, \mathrm{ds_q} \, . \end{aligned}$$

Remark 6.4. *For the special choice of* $\mathbf{S}_{act}$ *as in* (2.46) *we can calculate*

$$\frac{\partial \mathbf{S}_{act}}{\partial T_a} = I_{4f}^{-\frac{1}{2}} \boldsymbol{f}_0 \otimes \boldsymbol{f}_0.$$

For Newton's method we also need to define the residual

$$\boldsymbol{F} := \begin{pmatrix} \boldsymbol{R}_1 \\ \boldsymbol{R}_2 \\ \boldsymbol{R}_3 \\ \boldsymbol{R}_4 \\ \boldsymbol{R}_5 \end{pmatrix}$$

where the vectors $\boldsymbol{R}_1, \ldots, \boldsymbol{R}_5$ are induced by the following linear forms:

$\boldsymbol{R}_1$ corresponds to

$$b_T^{\mathrm{DG}}(V_{\mathrm{tm}}^{h,k}, \phi^h) + a_i^{\mathrm{DG}}(V_{\mathrm{tm}}^{h,k}, \phi^h) + a_i^{\mathrm{DG}}(u_e^{h,k}, \phi^h) + \overline{I}^{\mathrm{DG}}(V_{\mathrm{tm}}^{h,k}, v^{h,k}, \boldsymbol{U}^{h,k}; \phi^h) - l_1^{\mathrm{DG}}(\phi^h).$$

$\boldsymbol{R}_2$ corresponds to

$$a_i^{\mathrm{DG}}(V_{\mathrm{tm}}^{h,k}, \psi^h) + a_{i+e}^{\mathrm{DG}}(u_e^{h,k}, \psi^h) - l_2^{\mathrm{DG}}(\psi^h).$$

$\boldsymbol{R}_3$ corresponds to

$$b_T^{\mathrm{DG}}(v^{h,k}, \xi^h) + H^{\mathrm{DG}}(V_{\mathrm{tm}}^{h,k}, v^{h,k}; \xi^h) - l_3^{\mathrm{DG}}(\xi^h).$$

$\boldsymbol{R}_4$ corresponds to

$$b_T^{\mathrm{DG}}(T_a^{h,k}, \theta^h) + T^{\mathrm{DG}}(V_{\mathrm{tm}}^{h,k}, T_a^{h,k}; \theta^h) - l_3^{\mathrm{DG}}(\theta^h).$$

$\boldsymbol{R}_5$ corresponds to

$$a_{\mathrm{elast}}^{\mathrm{DG}}(T_a^{h,k}, \boldsymbol{U}^{h,k}; \boldsymbol{V}^h) - l_5(\boldsymbol{V}^h).$$

Collecting all things we can write Newton's method in our case as find $\boldsymbol{\Delta}$ such that

$$\mathbf{DF}(\boldsymbol{X}^k)\boldsymbol{\Delta} = -\boldsymbol{F}(\boldsymbol{X}^k), \boldsymbol{X}^{k+1} = \boldsymbol{X}^k + \boldsymbol{\Delta}.$$

6.2 Globalized Newton's Method and Load-stepping

In the previous section we presented all building blocks for applying Newton's method to the system of cardiac electromechanics. However, for the convergence of Newton's method one needs to provide a good initial guess $\boldsymbol{X}^0$. In the case of time dependent nonlinear problems which are discretized with time-stepping schemes one can always use the solution from the previous time step as initial guess for Newton's method. In a full space-time setting one can no longer use

this. Hence one needs to construct a good initial guess with other techniques, such as **globalization techniques**. Furthermore, since the linear systems in such problem are large one may also use inexact Newton methods. For more on this topic we refer to [46, Chapter 3] and [49, 50]. For solving our nonlinear systems we will rely on the **inexact Newton backtracking method** proposed in [50, Section 6]. The algorithm is depicted in Algorithm 1.

Algorithm 1 Inexact Newton Backtracking Method, [50]

1: Let $\boldsymbol{X}^0$, $\eta_{\max} \in [0,1)$, $t \in (0,1)$, $0 < \theta_{\min} < \theta_{\max} < 1$, $\epsilon > 0$, $n_{\max} > 0$ and $k_{\max} > 0$ be given
2: **for** $k = 0, \dots, k_{\max}$ **do**
3: $\quad n_{\text{bt}} = 0$
4: $\quad$ Choose $\eta_k \in [0, \eta_{\max}]$
5: $\quad$ Find $\boldsymbol{s}^k$ such that
6: $\quad \left\| \mathbf{DF}(\boldsymbol{X}^k)\boldsymbol{s}^k + \boldsymbol{F}(\boldsymbol{X}^k) \right\| \leq \eta_k \left\| \boldsymbol{F}(\boldsymbol{X}^k) \right\|$
7: $\quad$ **while** $\left\| \boldsymbol{F}(\boldsymbol{X}^k + \boldsymbol{s}^k) \right\| > (1 - t(1-\eta_k)) \left\| \boldsymbol{F}(\boldsymbol{X}^k) \right\|$ **and** $n_{\text{bt}} < n_{\max}$ **do**
8: $\quad\quad$ Choose $\theta \in [\theta_{\min}, \theta_{\max}]$
9: $\quad\quad \boldsymbol{s}^k = \theta \boldsymbol{s}^k$
10: $\quad\quad \eta_k = 1 - \theta(1 - \eta_k)$
11: $\quad\quad n_{\text{bt}} = n_{\text{bt}} + 1$
12: $\quad$ **end while**
13: $\quad \boldsymbol{X}^{k+1} = \boldsymbol{X}^k + \boldsymbol{s}^k$
14: $\quad$ **if** $\left\| \boldsymbol{F}(\boldsymbol{X}^{k+1}) \right\| < \epsilon \left\| \boldsymbol{F}(\boldsymbol{X}^0) \right\|$ **then**
15: $\quad\quad$ **break**
16: $\quad$ **end if**
17: **end for**

For choosing η_k (Line 4 in Algorithm 1) we will use the following criterion proposed in [49, (2.6)]: Given $\gamma \in (0,1)$, $\alpha \in (1,2]$ and $\eta_0 \in (0,1)$ we set

$$\eta_k := \gamma \left(\frac{\left\| \boldsymbol{F}(\boldsymbol{X}^k) \right\|}{\left\| \boldsymbol{F}(\boldsymbol{X}^{k-1}) \right\|} \right)^{\alpha}.$$

Furthermore, as suggested in [49, Section 2.1] we will apply the following safeguarding rule: If $\gamma \eta_{k-1}^{\alpha} > 0.1$ we set

$$\eta_k = \min(\eta_{\max}, \max(\eta_k, \gamma \eta_{k-1}^{\alpha})).$$

It remains to choose θ (Line 8 in Algorithm 1). Here we will follow the suggestion made in [22, Section 4.2] and also [96, 142]. We define the function

$$g(t) := \frac{1}{2}\left\|\boldsymbol{F}(\boldsymbol{X}^k + t\boldsymbol{s}^k)\right\|^2$$

Next we define a quadratic interpolant $p(t)$ of $g(t)$ such that

$$\begin{aligned} p(0) = g(0) &= \frac{1}{2}\left\|\boldsymbol{F}(\boldsymbol{X}^k)\right\|^2, \\ p(1) = g(1) &= \frac{1}{2}\left\|\boldsymbol{F}(\boldsymbol{X}^k + \boldsymbol{s}^k)\right\|^2, \\ p'(0) = g'(0) &= \Big(\mathbf{DF}(\boldsymbol{X}^k)\boldsymbol{s}^k, \boldsymbol{F}(\boldsymbol{X}^k)\Big). \end{aligned}$$

Having $p(t)$ we choose θ as $\min_{t\in[\theta_{\min},\theta_{\max}]} p(t)$. Further, for our numerical examples we will apply a load-stepping strategy. That means take a sequence $\{\tau_k\} \in (0, 1]$ converging to one and multiply each nonlinear contribution to our system by the factor τ_k.

6.3 Schur Complement

We have seen that in the course of Newton's method we need to solve the system

$$\mathbf{DF}(\boldsymbol{X}^k)\boldsymbol{\Delta} = -\boldsymbol{F}(\boldsymbol{X}^k)$$

with the help of an iterative method, like the GMRes. Recalling the block structure of the Jacobian this means that in each Newton step we need to solve

$$\begin{pmatrix} \mathbf{F}_{11} & \mathbf{F}_{12} & \mathbf{F}_{13} & \mathbf{0} & \mathbf{F}_{15} \\ \mathbf{F}_{21} & \mathbf{F}_{22} & \mathbf{0} & \mathbf{0} & \mathbf{0} \\ \mathbf{F}_{31} & \mathbf{0} & \mathbf{F}_{33} & \mathbf{0} & \mathbf{0} \\ \mathbf{F}_{41} & \mathbf{0} & \mathbf{0} & \mathbf{F}_{44} & \mathbf{0} \\ \mathbf{0} & \mathbf{0} & \mathbf{0} & \mathbf{F}_{54} & \mathbf{F}_{55} \end{pmatrix} \begin{pmatrix} \boldsymbol{\delta}V_{\mathrm{tm}} \\ \boldsymbol{\delta}u_e \\ \boldsymbol{\delta}v \\ \boldsymbol{\delta}T_a \\ \boldsymbol{\delta}\boldsymbol{U} \end{pmatrix} = \begin{pmatrix} \boldsymbol{R}_1 \\ \boldsymbol{R}_2 \\ \boldsymbol{R}_3 \\ \boldsymbol{R}_4 \\ \boldsymbol{R}_5 \end{pmatrix}.$$

Instead of solving the whole block system we will solve the following Schur complement system

$$\mathbf{SC} := \begin{pmatrix} \mathbf{SC}_1 & \mathbf{F}_{12} \\ \mathbf{F}_{21} & \mathbf{F}_{22} \end{pmatrix} \begin{pmatrix} \boldsymbol{\delta} V_{\mathrm{tm}} \\ \boldsymbol{\delta} u_e \end{pmatrix} = \begin{pmatrix} \widetilde{\boldsymbol{R}_1} \\ \boldsymbol{R}_2 \end{pmatrix}$$

where

$$\begin{aligned} \mathbf{SC}_1 &:= \mathbf{F}_{11} - \mathbf{F}_{13}\mathbf{F}_{33}^{-1}\mathbf{F}_{31} + \mathbf{F}_{15}\mathbf{F}_{55}^{-1}\mathbf{F}_{54}\mathbf{F}_{44}^{-1}\mathbf{F}_{41}, \\ \widetilde{\boldsymbol{R}_1} &:= \boldsymbol{R}_1 - \mathbf{F}_{13}\mathbf{F}_{33}^{-1}\boldsymbol{R}_3 - \mathbf{F}_{15}\mathbf{F}_{55}^{-1}\boldsymbol{R}_5 + \mathbf{F}_{15}\mathbf{F}_{55}^{-1}\mathbf{F}_{54}\mathbf{F}_{44}^{-1}\boldsymbol{R}_4. \end{aligned}$$

6.4 Numerical Examples

In this section we will present numeric examples for the coupled problem. In all the presented examples we used the **Aliev-Panfilov model** for the ionic currents, see [4]. The values of $c_1, c_2, c_3, \epsilon_0, \mu_1, \mu_2$ can be looked up in Table 6.2.

$$\begin{aligned} \mathrm{I}_{\mathrm{ion}}(V_{\mathrm{tm}}, v) &:= c_2 V_{\mathrm{tm}} v - c_1 V_{\mathrm{tm}}(1 - V_{\mathrm{tm}})(V_{\mathrm{tm}} - c_3), \\ H(V_{\mathrm{tm}}, v) &:= \left(\epsilon_0 + \frac{\mu_1 v}{\mu_2 + V_{\mathrm{tm}}}\right)(c_1 V_{\mathrm{tm}}(1 + b - V_{\mathrm{tm}}) - v) \end{aligned}$$

Further in all numerical examples we use the globalized inexact Newton backtracking algorithm combined with twenty load-steps. The parameters can be looked up in Table 6.1. The resulting linear systems were solved with Neshmet. The meshes were generated with the help of Gmsh [71].

Example One

In our first example we consider the following space-time domain:

$$Q := (-2.5, 2.5)^2 \times (0, 12).$$

Parameter	Value
$\eta_{\max}$	0.9
$\theta_{\min}$	0.1
$\theta_{\max}$	0.5
ϵ	1E−4
$n_{\max}$	5
$k_{\max}$	100

Table 6.1: Values of the parameters for Newton's method.

Parameter	Value
c_1	12.000
c_2	1.000
c_3	0.050
b	0.314
ϵ_0	0.016
μ_1	0.476
μ_2	0.654

Table 6.2: Values of the parameters for the Aliev Panfilov model.

For the anisotropic tensors $\mathbf{M}_i, \mathbf{M}_e$ we choose the following values:

$$\begin{aligned} \boldsymbol{f}_0 &:= \left(\frac{3}{\sqrt{10}}, \frac{1}{\sqrt{10}}\right)^\top, \\ \boldsymbol{s}_0 &:= \left(-\frac{1}{\sqrt{10}}, \frac{3}{\sqrt{10}}\right)^\top, \\ m_i^f &:= 0.2, \quad m_i^s := 0.3, \\ m_e^f &:= 1.1, \quad m_e^s := 1.3. \end{aligned}$$

On $\partial(-2.5, 2.5)^2$ we set Robin boundary conditions for V_{tm}, u_e with $\alpha_i = \alpha_e = 1\text{E}{-6}$. For the deformation we use homogeneous Dirichlet boundary conditions on $X = -2.5$ and homogeneous Neumann boundary conditions elsewhere. The initial conditions were set to

$$\begin{aligned} V_{\mathrm{tm}}^0(\boldsymbol{X}) &:= (X - 2.5)(X + 2.5)(Y - 2.5)(Y + 2.5), \\ v^0(\boldsymbol{X}) &:= 0, \\ T_a^0(\boldsymbol{X}) &:= 0. \end{aligned}$$

We needed an average of 14.2 Newton steps per load-step for this example. The results are depicted in Figures 6.1, 6.2, 6.3, 6.4 and 6.5. We can also calculate the resulting variables at different times t_k by slicing the space-time domain. The results are depicted in Figures 6.6 and 6.7.

Example Two

In the second example we consider the same geometry, conductivities and parameters for the nonlinearities. The initial values are set to

$$\begin{aligned} V_{\mathrm{tm}}^0(\boldsymbol{X}) &:= 0, \\ v^0(\boldsymbol{X}) &:= 0, \\ T_a^0(\boldsymbol{X}) &:= 0. \end{aligned}$$

The boundary conditions for V_{tm}, u_e are chosen in the same way as for example one. For the deformation $\boldsymbol{U}$ we choose again homogeneous Dirichlet data on

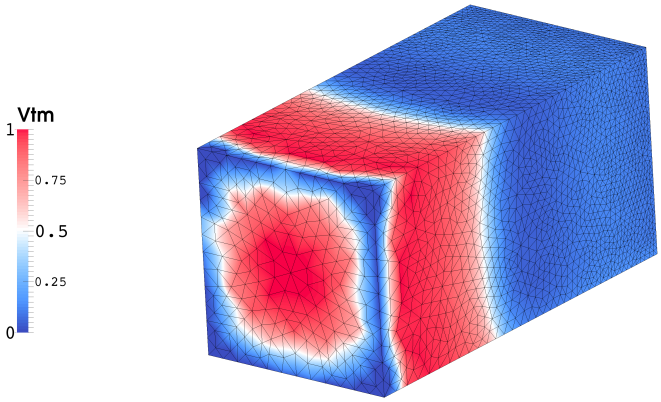

Figure 6.1: The potential V_{tm}.

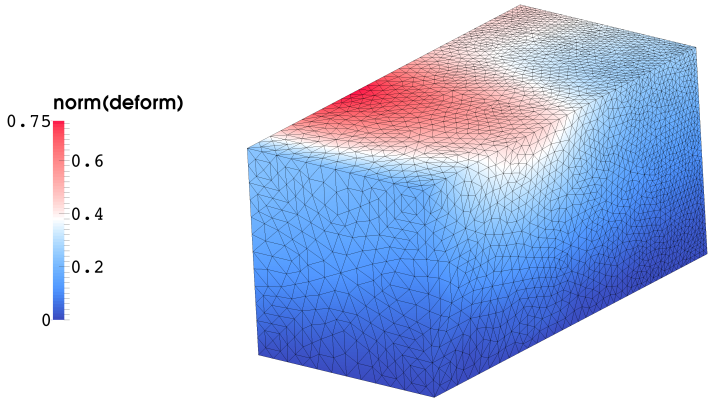

Figure 6.2: The absolute value of the deformation $\boldsymbol{U}$.

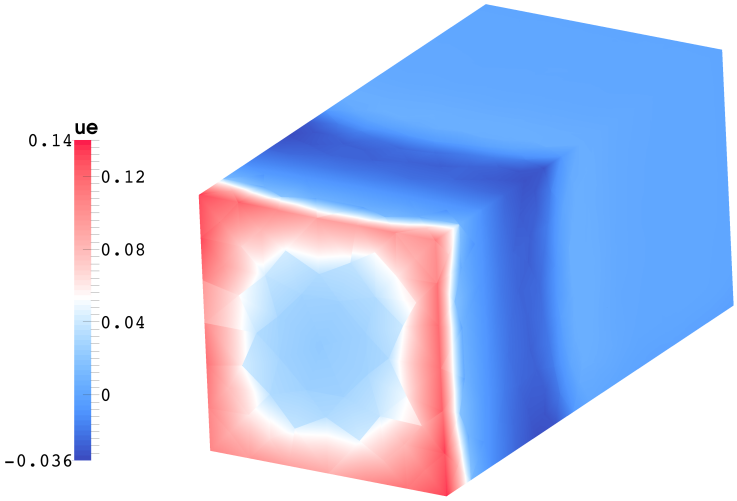

Figure 6.3: The potential u_e.

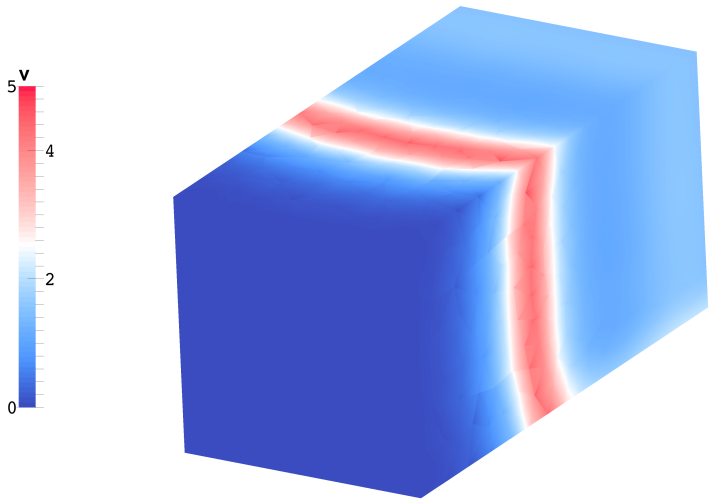

Figure 6.4: The ionic variable v.

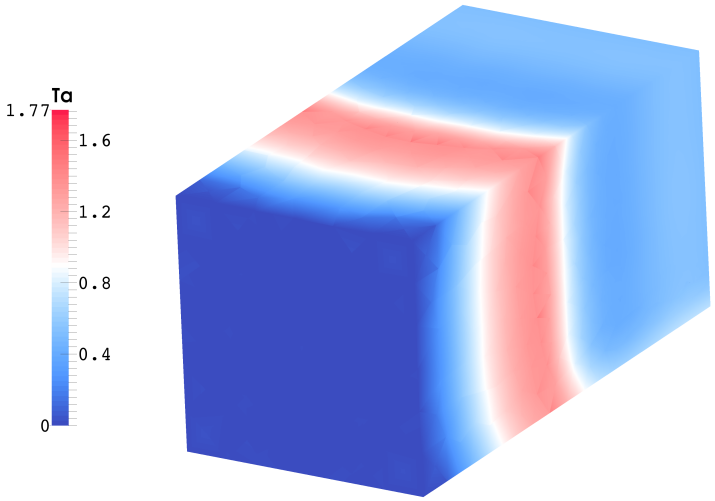

Figure 6.5: The active stress variable T_a.

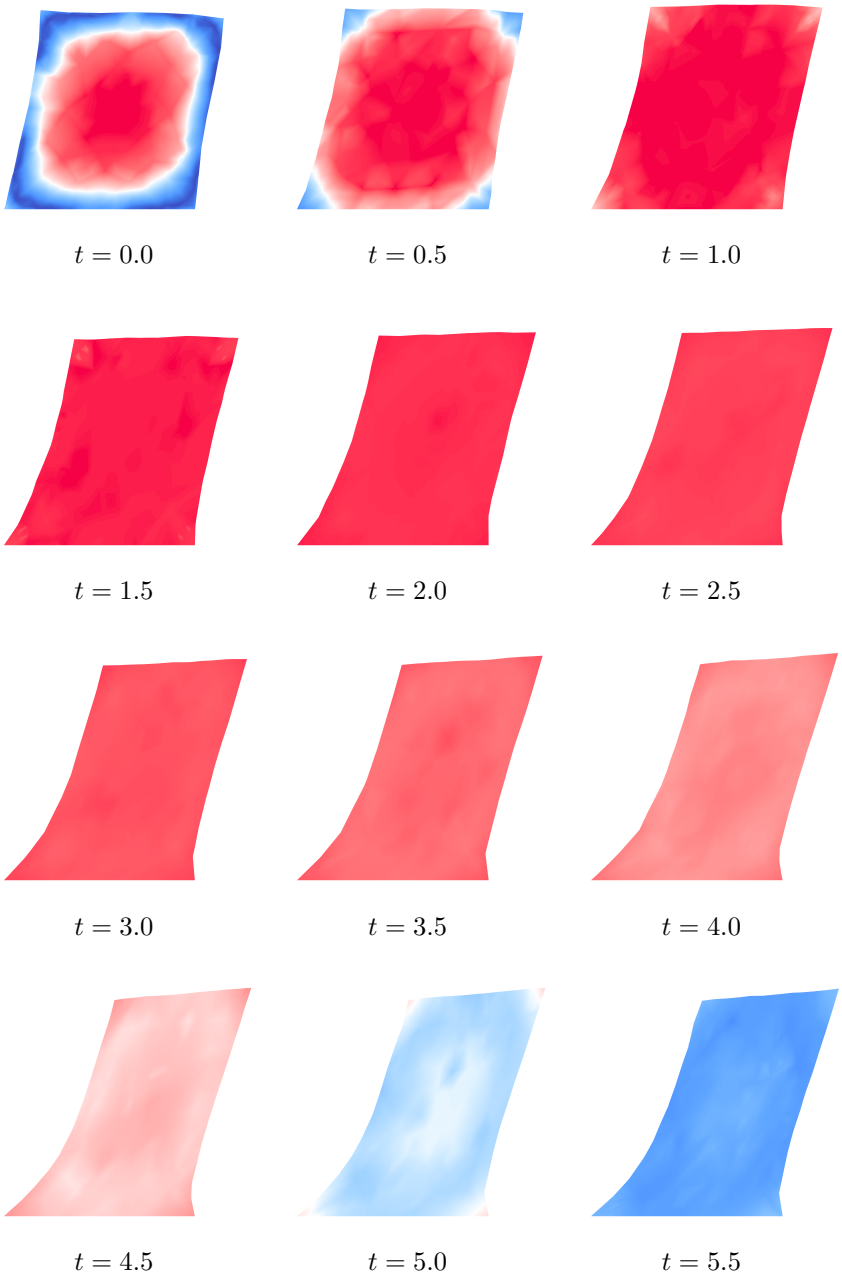

Figure 6.6: Time evolution of V_{tm}. The geometry Ω is wrapped by $2\boldsymbol{U}$.

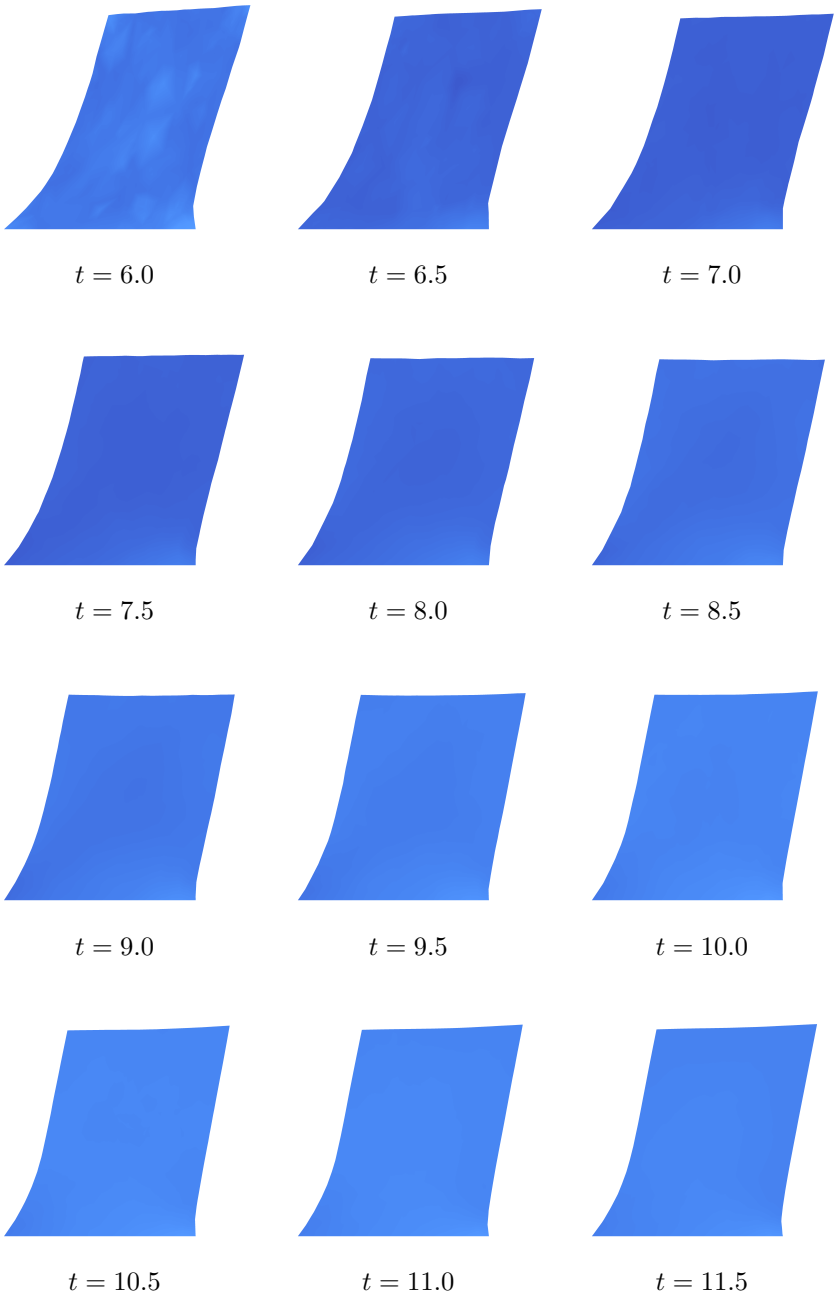

Figure 6.7: Time evolution of V_{tm}. The geometry Ω is wrapped by $2\boldsymbol{U}$.

$X = -2.5$. However on the boundary $X = 2.5$ we choose the following Neumann boundary condition

$$\boldsymbol{G}_N(\boldsymbol{X}, t) := \begin{cases} (0,0)^\top & \text{if } t \notin [2,4] \\ \frac{1}{2}(t-2)(0,1)^\top & \text{if } t \in [2,3) \\ \frac{1}{2}(4-t)(0,1)^\top & \text{if } t \in [3,4] \end{cases}$$

We needed an average of 18.1 Newton steps per load-step for this example. The results are depicted in Figures 6.8, 6.9, 6.10, 6.11 and 6.12. The results for the time evolution are depicted in Figures 6.13 and 6.14.

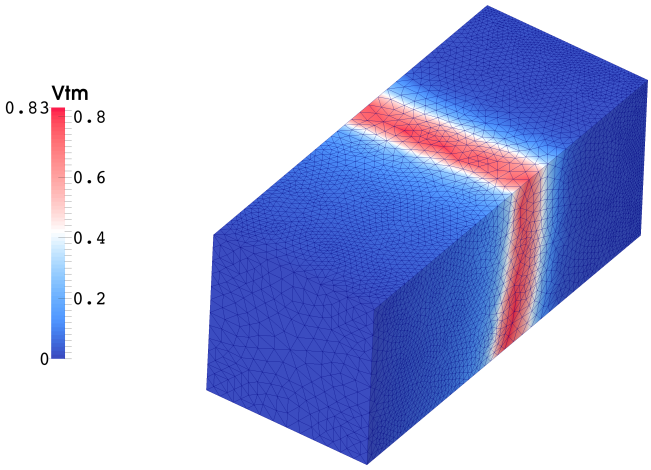

Figure 6.8: The potential V_{tm}.

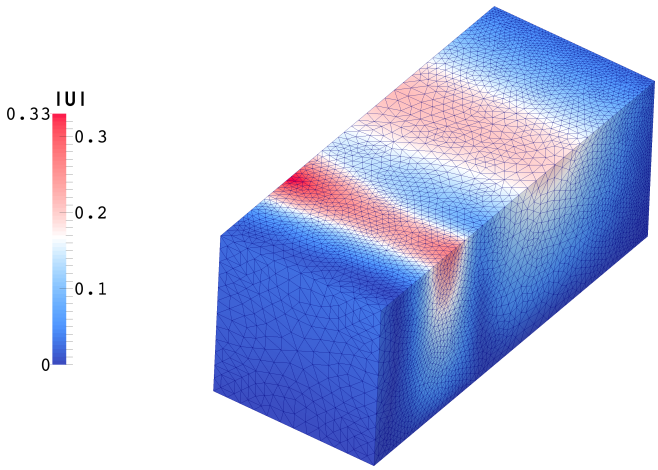

Figure 6.9: The absolute value of the deformation $\boldsymbol{U}$.

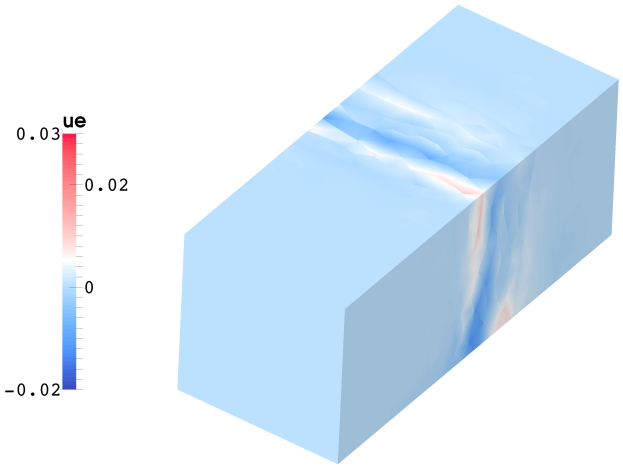

Figure 6.10: The potential u_e.

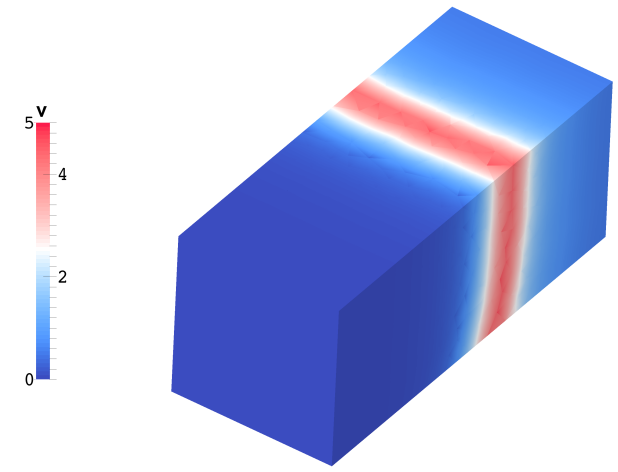

Figure 6.11: The ionic variable v.

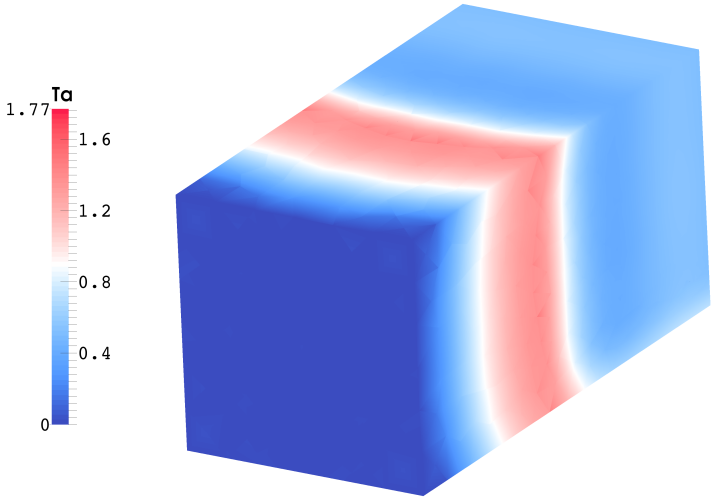

Figure 6.12: The active stress variable T_a.

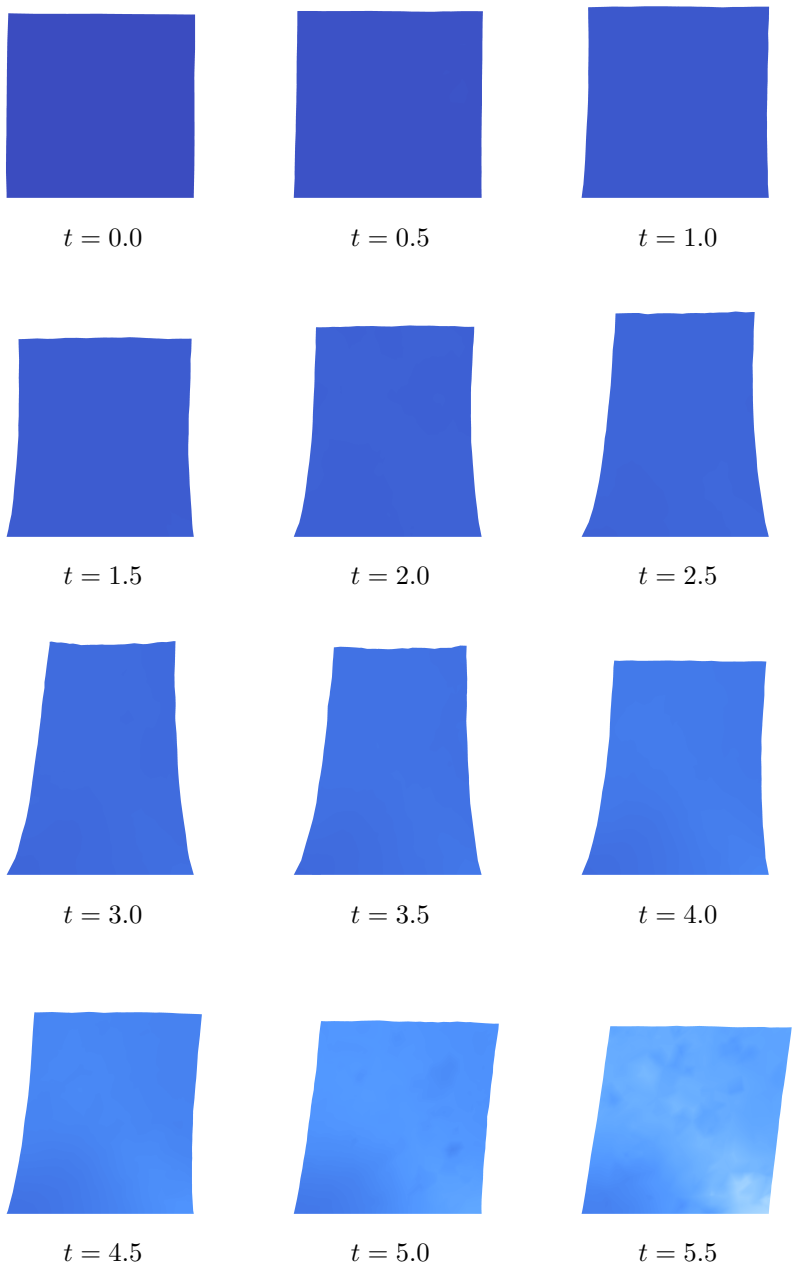

Figure 6.13: Time evolution of V_{tm}. The geometry Ω is wrapped by $2\boldsymbol{U}$.

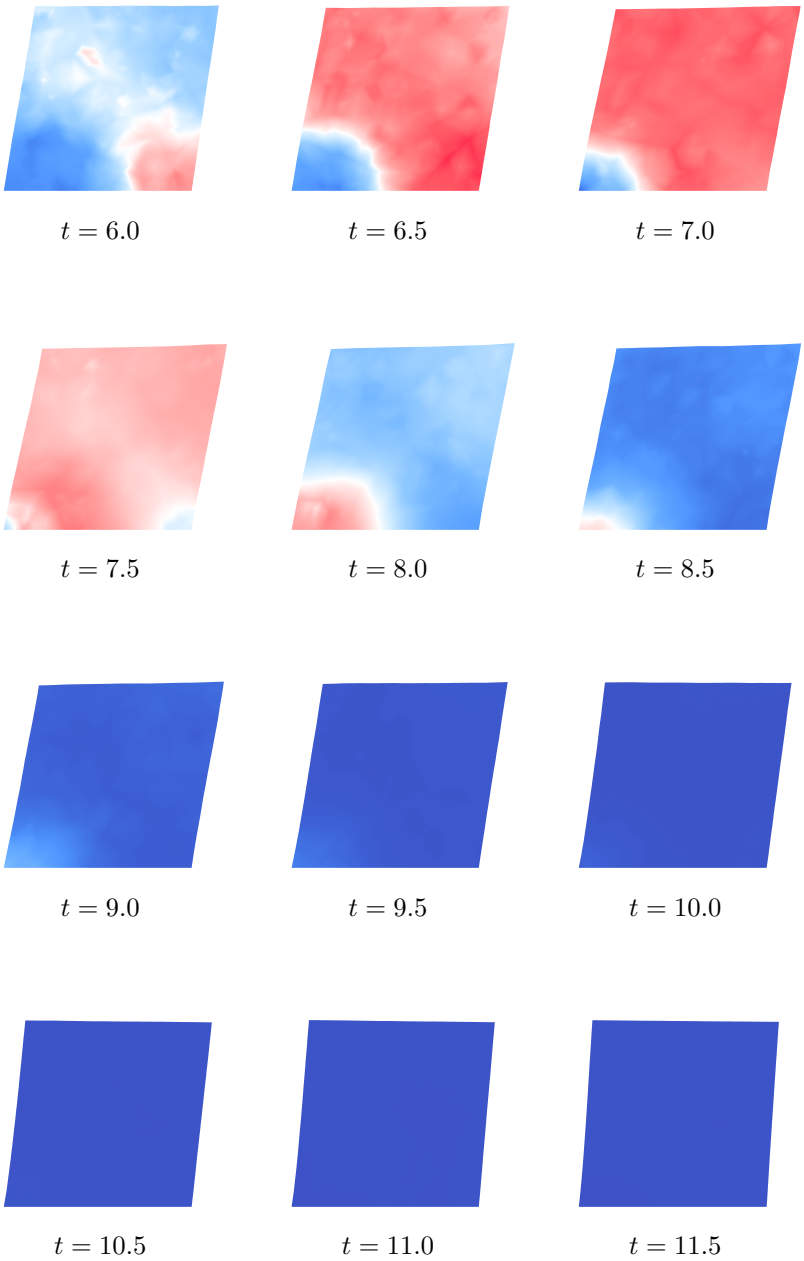

Figure 6.14: Time evolution of V_{tm}. The geometry Ω is wrapped by $2\boldsymbol{U}$.

Example Three

In our third example we consider a different spatial geometry. The geometry Ω is given by the following ellipsoidal annulus: given $a_1 > a_2$ and $b_1 > b_2$ we define

$$\begin{aligned}
\Omega &:= \left\{ \boldsymbol{X} \in \mathbb{R}^2 \colon \frac{X^2}{a_1^2} + \frac{Y^2}{b_1^2} < 1 \text{ and } \frac{X^2}{a_2^2} + \frac{Y^2}{b_2^2} > 1 \right\}, \\
\Gamma_1 &:= \left\{ \boldsymbol{X} \in \mathbb{R}^2 \colon \frac{X^2}{a_1^2} + \frac{Y^2}{b_1^2} = 1 \right\}, \\
\Gamma_2 &:= \left\{ \boldsymbol{X} \in \mathbb{R}^2 \colon \frac{X^2}{a_2^2} + \frac{Y^2}{b_2^2} = 1 \right\}, \\
\Gamma_{D,\text{elast}} &:= \left\{ \boldsymbol{X} \in \mathbb{R}^2 \colon \frac{X^2}{a_1^2} + \frac{Y^2}{b_1^2} = 1 \text{ and } X > 0 \text{ and } Y < 0 \right\}, \\
\Gamma_{N,\text{elast}} &:= \Gamma_1 \backslash \overline{\Gamma_{D,\text{elast}}}.
\end{aligned}$$

An example for Ω is depicted in Figure 6.15. The input parameters as well

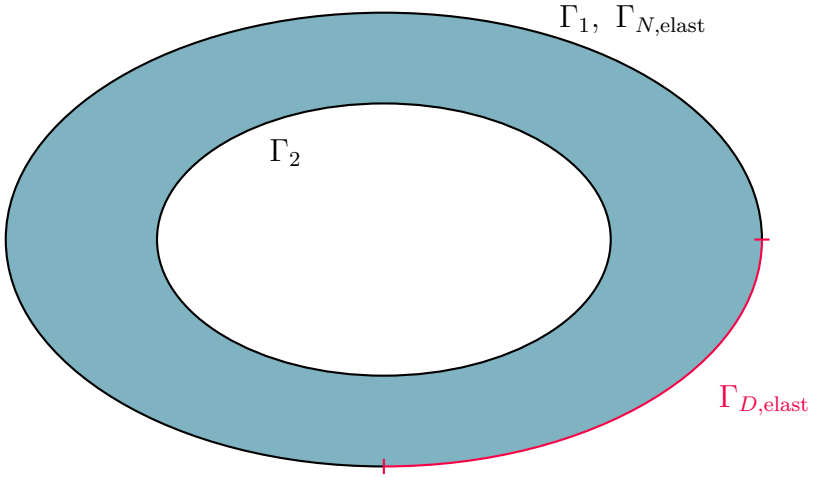

Figure 6.15: The domain Ω for example three, $a_1 = 5$, $b_1 = 3$, $a_2 = 3$, $b_2 = \frac{9}{5}$

as the initial data are chosen as in examples one and two. On the boundary Γ_1 and Γ_2 we chose Robin type boundary conditions with $\alpha_i = \alpha_e = 1\text{E}{-6}$ for V_{tm}, u_e. For the deformation we chose homogeneous Neumann boundary

conditions on Γ_2 and $\Gamma_{N,\text{elast}}$. On $\Gamma_{D,\text{elast}}$ we imposed homogeneous Dirichlet boundary conditions. For this example we needed an average of 16.4 Newton steps per load step. The results are depicted in Figures 6.16, 6.17, 6.18 and 6.19. The results for the time evolution are depicted in Figures 6.20 and 6.21.

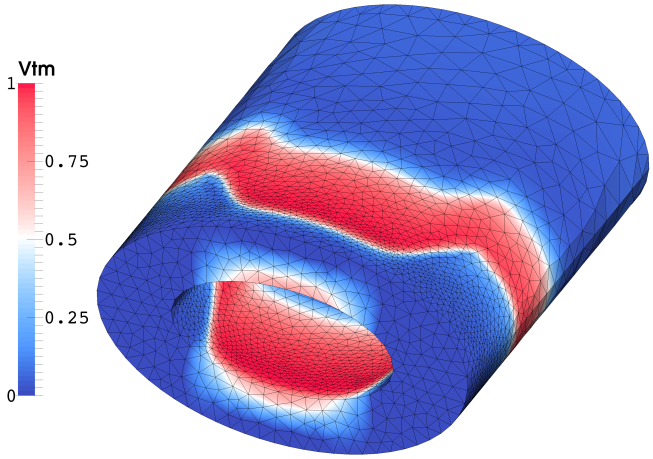

Figure 6.16: The potential V_{tm}.

Example Four

In this example we consider the same geometry as in example three, as well as the input parameters. The boundary conditions for V_{tm}, u_e as well as the initial conditions for V_{tm}, v, T_a are the same. For the deformation $\boldsymbol{U}$ we chose homogeneous Robin boundary conditions on Γ_1 and Γ_2. Furthermore we used non-constant fields for $\boldsymbol{f}_0, \boldsymbol{s}_0$. For the direction $\boldsymbol{s}_0$ we chose

$$\boldsymbol{s}_0(\boldsymbol{X}) := \operatorname{Grad} \phi(\boldsymbol{X})$$

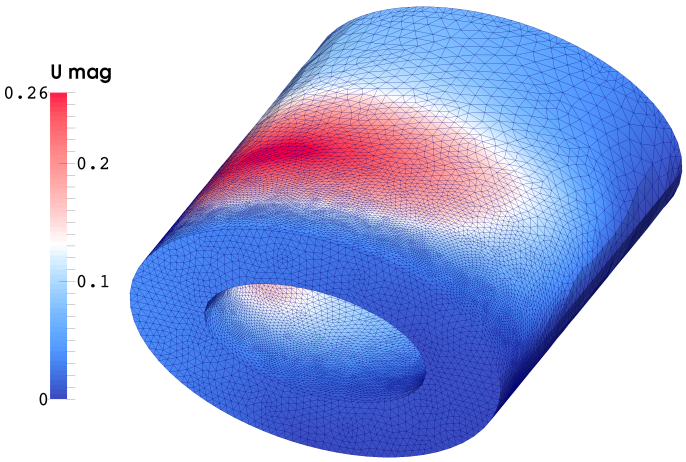

Figure 6.17: The absolute value of the deformation $\boldsymbol{U}$.

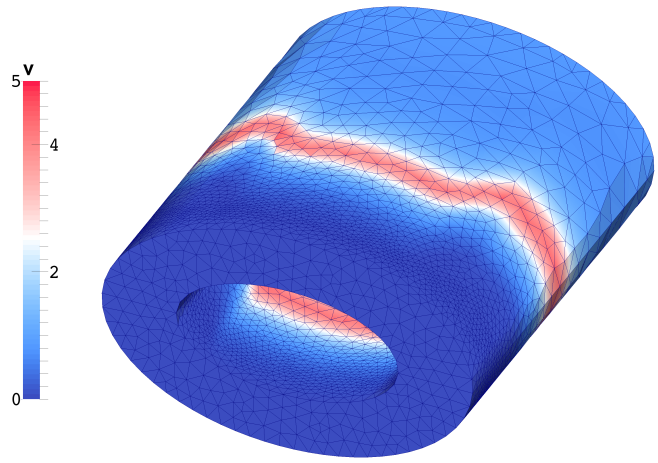

Figure 6.18: The ionic variable v.

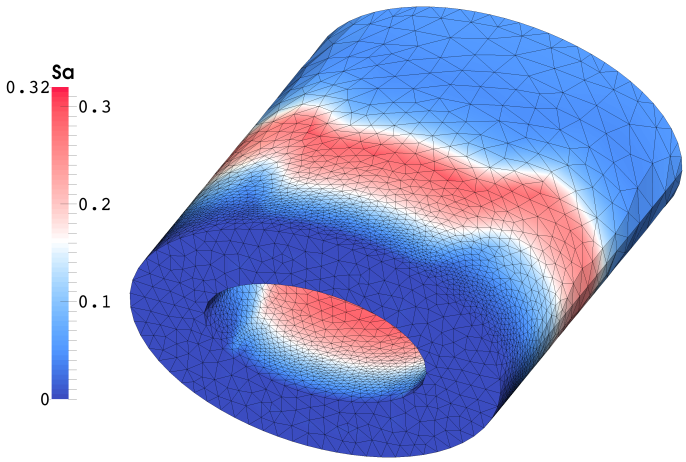

Figure 6.19: The active stress variable T_a.

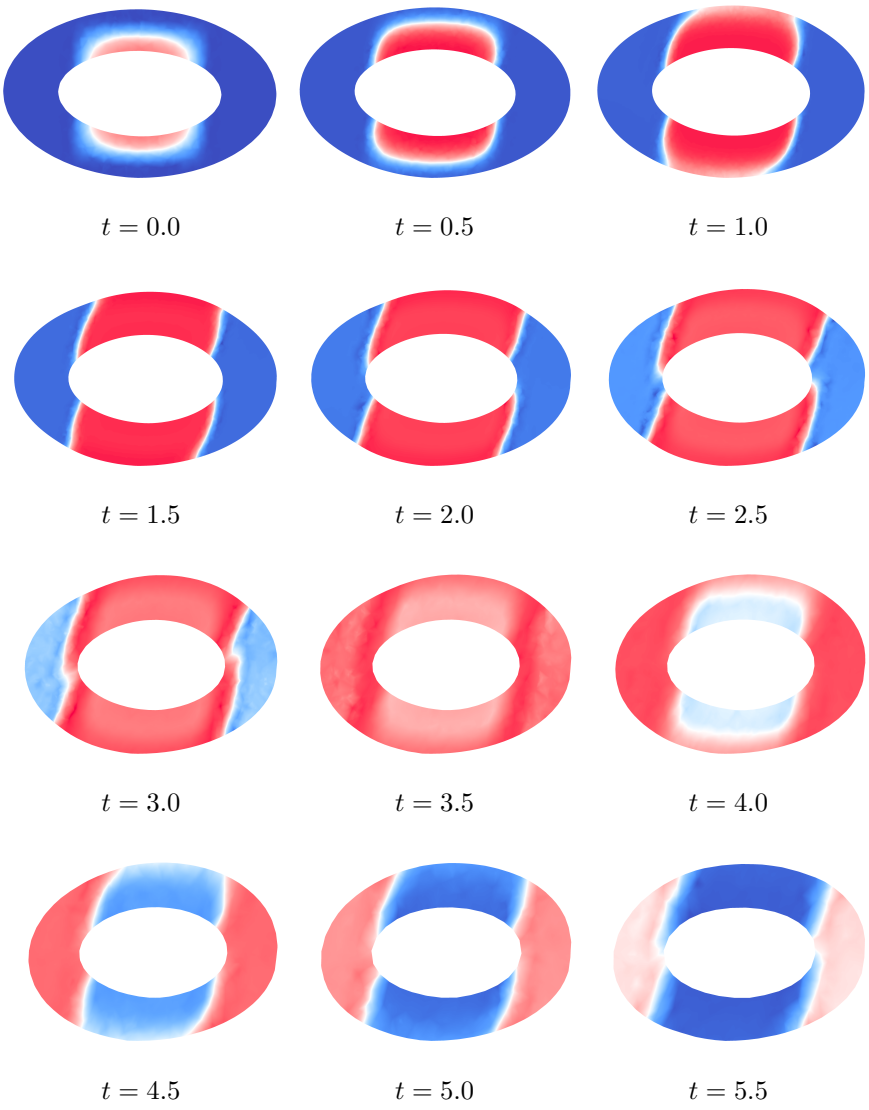

Figure 6.20: Time evolution of V_{tm}. The geometry Ω is wrapped by $2\boldsymbol{U}$.

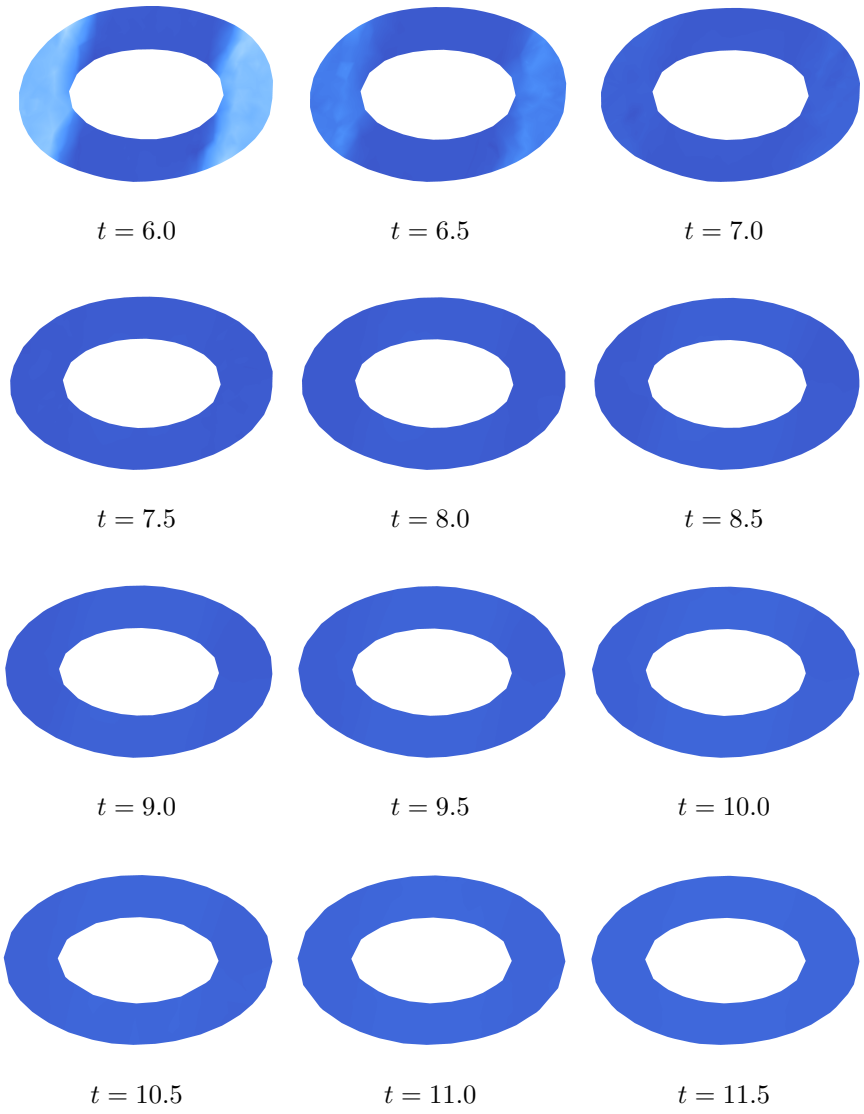

Figure 6.21: Time evolution of V_{tm}. The geometry Ω is wrapped by $2\boldsymbol{U}$.

where $\phi(\boldsymbol{X})$ solves the following partial differential equation

$$\begin{aligned} -\Delta\phi &= 0 && \text{in } \Omega, \\ \phi &= 1 && \text{on } \Gamma_1, \\ \phi &= 0 && \text{on } \Gamma_2. \end{aligned}$$

The direction $\boldsymbol{f}_0$ was chosen orthogonal to $\boldsymbol{s}_0$. A schematic view of $\boldsymbol{f}_0$ is depicted in Figure 6.22. For this example we used twenty load steps. We needed

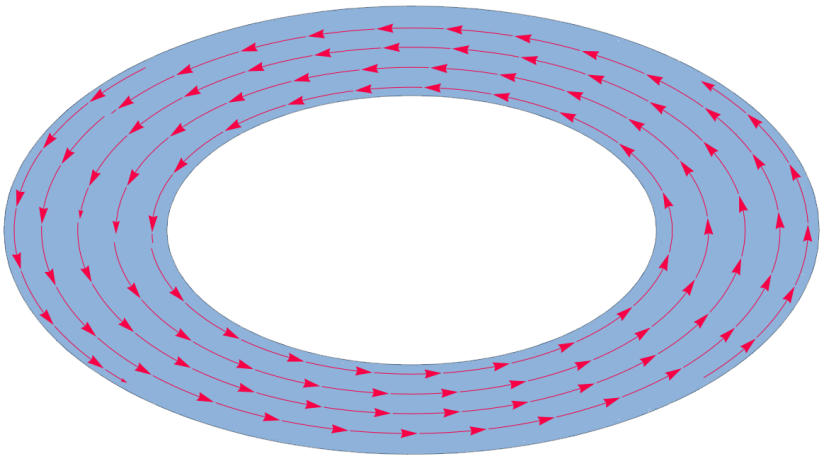

Figure 6.22: Schematic view of the direction $\boldsymbol{f}_0$ used in example four.

an average of 19.3 Newton steps per load step. The results are depicted in Figures 6.23, 6.24, 6.25 and 6.26. The results for the time evolution are depicted in Figures 6.27 and 6.28.

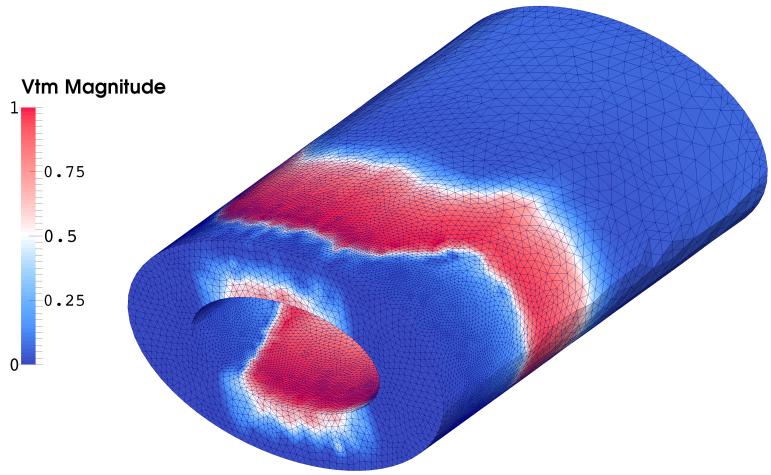

Figure 6.23: The potential V_{tm}.

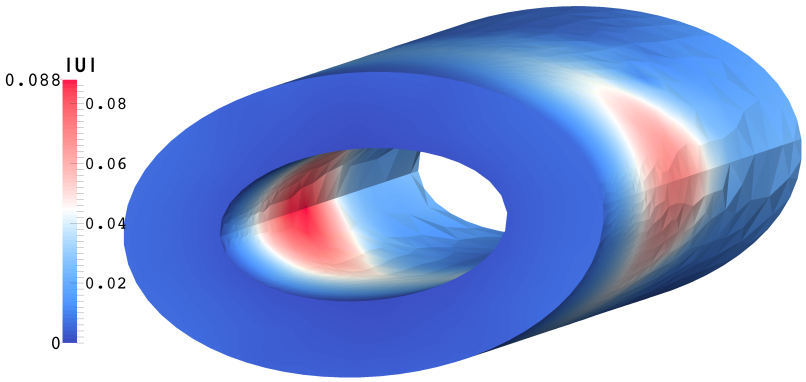

Figure 6.24: The absolute value of the deformation $\boldsymbol{U}$.

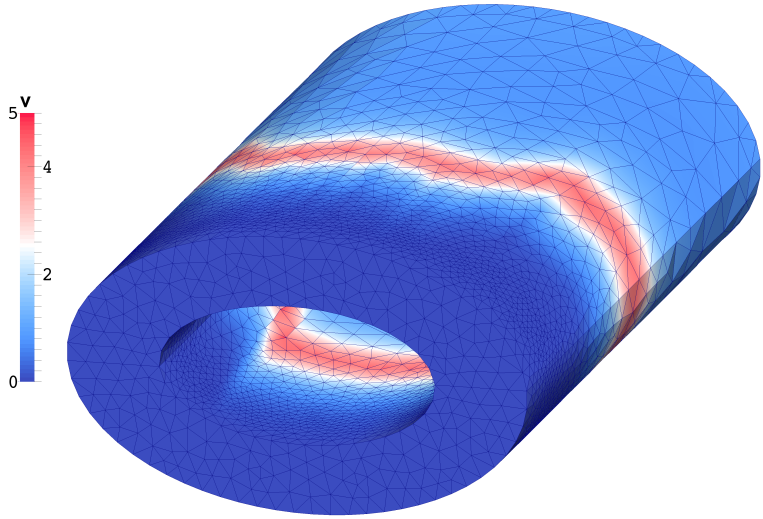

Figure 6.25: The ionic variable v.

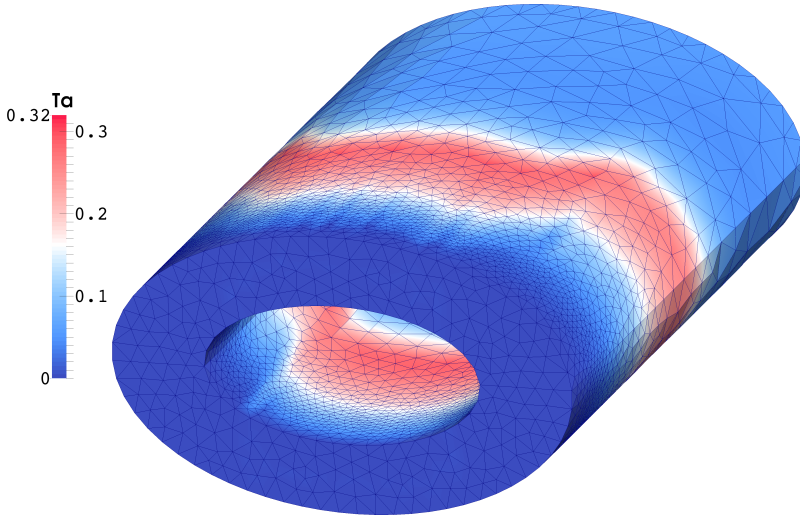

Figure 6.26: The active stress variable T_a.

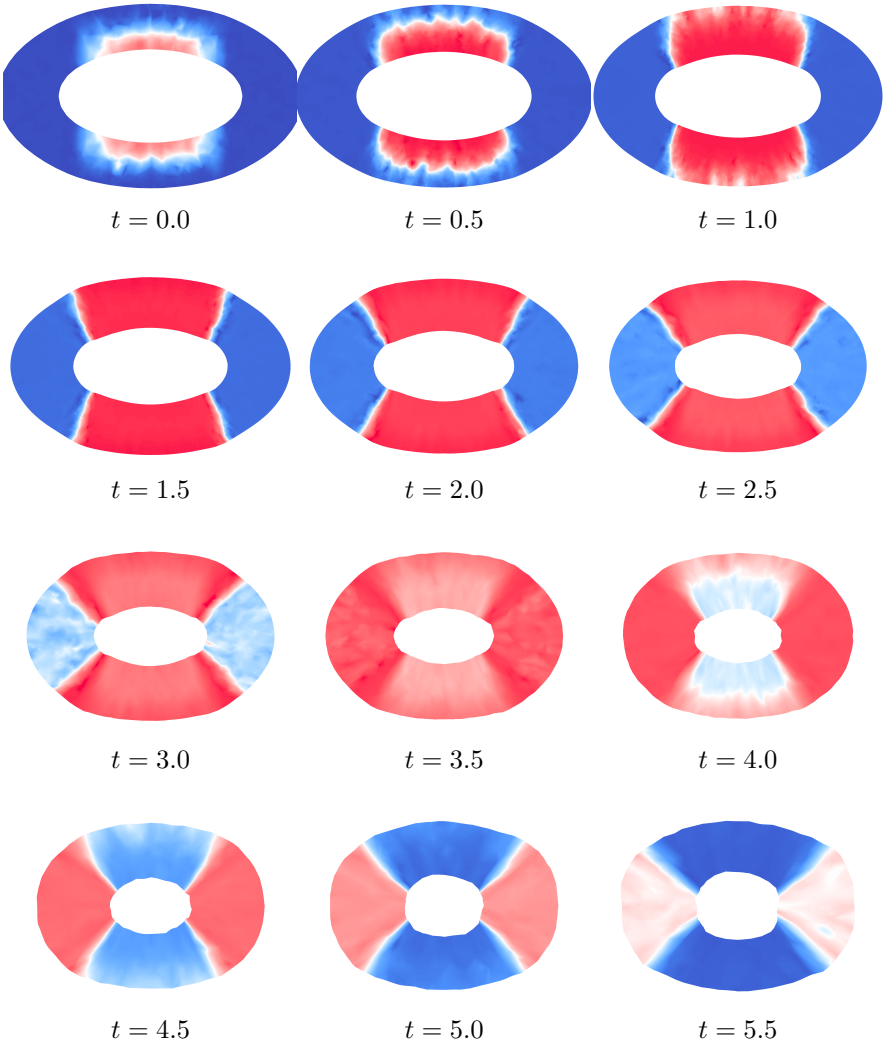

Figure 6.27: Time evolution of V_{tm}. The geometry Ω is wrapped by $2\boldsymbol{U}$.

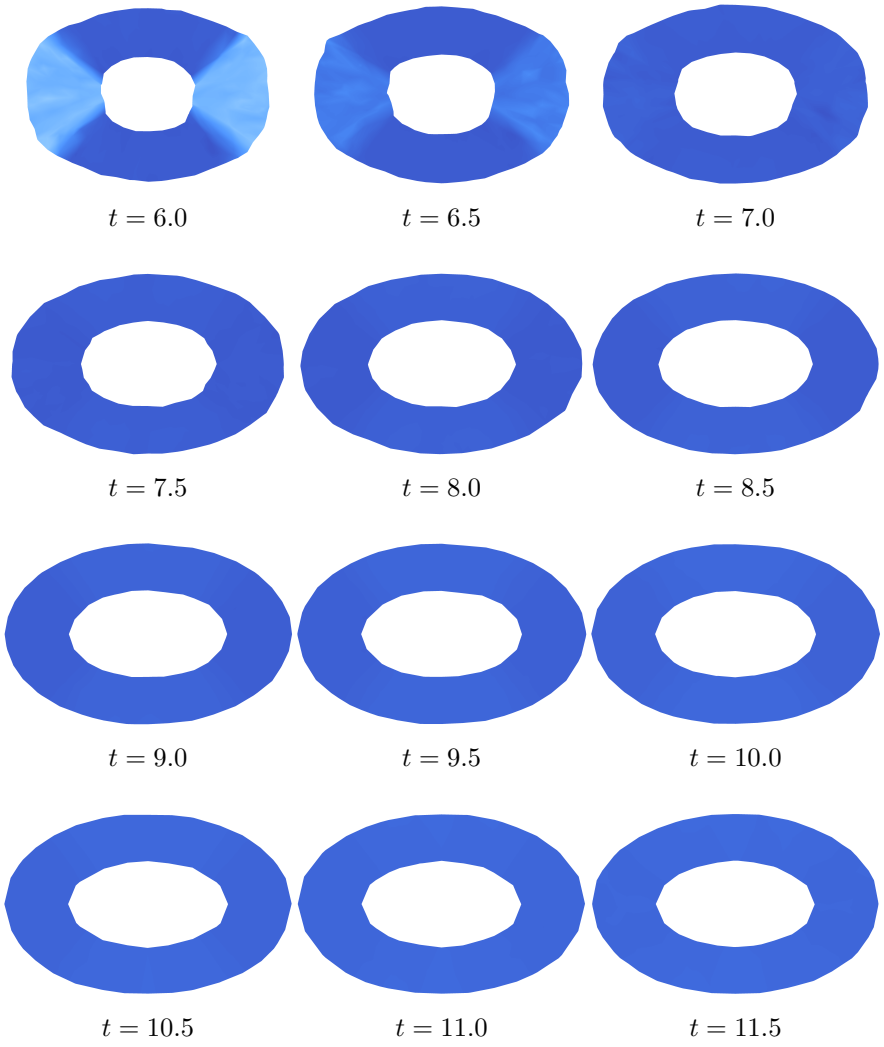

Figure 6.28: Time evolution of V_{tm}. The geometry Ω is wrapped by $10\boldsymbol{U}$.

7 Conclusions and Outlook

In this thesis we presented a novel approach to solve the governing equations of cardiac electro-mechanics. The main difference to other approaches is, that we considered the whole space-time cylinder Q as computational domain and we also allowed for rather general discretizations of those domains.

Starting in Chapter 2 we recalled the main modeling aspects for deriving the governing equations of cardiac electro-mechanics.

In particular, for discretizing the Bidomain equations in Chapter 4 we used a space-time symmetric weighted interior penalty discontinuous Galerkin finite element method to account for the anisotropic nature of conductivities in biological materials. This was combined with an upwind discretization for the time derivative. Subsequently, we analyzed the corresponding linear problem and extended the results under some assumptions to the nonlinear case. Finally we gave some convergence studies which support our theoretical results.

In the Chapter 5 we presented an existing, see [138], discontinuous Galerkin discretization for the equations of nonlinear quasi-stationary hyper-elasticity. We recalled the existing results and discussed some aspects worth mentioning for implementation. We supported the theoretical results developed in [138] with convergence studies.

Eventually, in Chapter 6 we presented a full space-time discontinuous Galerkin approach for solving the coupled system of cardiac electro-mechanics. We gave the discretized system of equations, discussed the use of globalized Newton's method and presented four numerical examples.

Outlook and Open Problems

With this thesis we have just scratched on the surface of possibilities such space-time methods may offer. It is clear, that with the use of unstructured discretizations of space-time domains one has the possibility to apply standard adaptive mesh refinement techniques to resolve complex phenomena in space and time simultaneously. For example, the sharp upstroke of the transmembrane potential V_{tm} could be resolved much more accurate with such techniques. Still, the development of reliable and efficient error estimators for the proposed space-time setting remains an open question. Since in the case of cardiac electro-mechanics one has to deal with systems of nonlinear time-dependent equations one may also think about the use of different error estimators for each variable and also the use of different meshes for each variable of interest.

Furthermore, for being able to handle more realistic problems one needs to think about unstructured triangulations for arbitrary four dimensional objects. First steps towards this have been made in [21, 121, 130, 179].

Going hand in hand with this topic one needs to think about a parallelization of such space-time methods as the degrees of freedom in four dimensional discretizations grow rather rapid. The use of unstructured grids suggests to use ideas from domain decomposition methods. First steps towards this have already been investigated for the Navier-Stokes equations in [129, Chapter 5]. One may also think of hybrid discontinuous Galerkin methods as well as the use of the Mortar finite element method or the finite element tearing and interconnecting approach discussed for example in [11, 12, 13].

Nevertheless, the constructions of suitable preconditioners in the fully unstructured space-time setting remains an open question. For more structured discretizations a space-time multigrid was developed in [129].

Finally, for being able to solve nonlinear time-dependent problems one needs to construct good initial guesses for Newton's method. It would be interesting, whether it is possible to do so and not being bound to the use of globalization techniques.

There are also a lot of open questions concerning the existence and regularity of solutions to the fully coupled system of cardiac electro-mechanics. Especially, the interplay and influence of the spatial and material formulation of the

individual governing equations, and here in particular the relation between the conductivity tensors $\mathbf{M}_i, \mathbf{M}_e$ from the Bidomain equations in material and spatial description.

Bibliography

[1] A. Kuzmin, M. Luisier, and O. Schenk. "Fast Methods for Computing Selected Elements of the Greens Function in Massively Parallel Nanoelectronic Device Simulations." In: **Euro-Par 2013 Parallel Processing**. Ed. by F. Wolf, B. Mohr, and D. Mey. Vol. 8097. Lecture Notes in Computer Science. Springer Berlin Heidelberg, 2013, pp. 533–544.

[2] J. M. Alam, N. K.-R. Kevlahan, and O. V. Vasilyev. "Simultaneous space–time adaptive wavelet solution of nonlinear parabolic differential equations." In: **Journal of Computational Physics** 214.2 (2006), pp. 829–857.

[3] R. Alexander. "Theoretical study of the effect of stress-dependent remodeling on arterial geometry under hypertensive conditions." In: **Journal of Biomechanics** 30 (1997), pp. 819–827.

[4] R. R. Aliev and A. V. Panfilov. "A simple two-variable model of cardiac excitation." In: **Chaos, Solitons & Fractals** 7.3 (1996), pp. 293–301.

[5] D. Ambrosi et al. "Electromechanical coupling in cardiac dynamics: the active strain approach." In: **SIAM Journal of Applied Mathematics** 71 (2011), pp. 605–621.

[6] D. Ambrosi and S. Pezzuto. "Active stress vs. active strain in mechanobiology: constitutive issues." In: **Journal of Elasticity** 107.2 (2012), pp. 199–212.

[7] R. Andreev. "Stability of space-time Petrov-Galerkin discretizations for parabolic evolution equations." PhD thesis. Eidgenössische Technische Hochschule ETH Zürich, 2012.

[8] B. Andreianov et al. "Convergence of discrete duality finite volume schemes for the cardiac bidomain model." In: **Netw. Heterog. Media** 6.2 (2011), pp. 195–240.

[9] B. Andreianov et al. “Weak solutions and numerical approximation of a coupled system modeling cardiac electromechanics.” In: **HAL Preprint hal-00865585** (2013). preprint available at `http://hal.archives-ouvertes.fr/hal-00865585`.

[10] T. Apel, S. Nicaise, and D. Sirch. “A posteriori error estimation of residual type for anisotropic diffusion–convection–reaction problems.” In: **Journal of Computational and Applied Mathematics** 235.8 (2011), pp. 2805 –2820.

[11] C. M. Augustin. “Classical and All-floating FETI Methods with Applications to Biomechanical Models.” PhD thesis. Graz University of Technology, 2012.

[12] C. M. Augustin, G. A. Holzapfel, and O. Steinbach. “Classical and all-floating FETI methods for the simulation of arterial tissues.” In: **International Journal for Numerical Methods in Engineering** 99.4 (2014), pp. 290–312.

[13] C. M. Augustin and O. Steinbach. “FETI Methods for the Simulation of Biological Tissues.” English. In: **Domain Decomposition Methods in Science and Engineering XX**. Ed. by R. Bank et al. Vol. 91. Lecture Notes in Computational Science and Engineering. Springer Berlin Heidelberg, 2013, pp. 503–510.

[14] I. Babuška. “Error-bounds for finite element method.” In: **Numer. Math.** 16 (1970/1971), pp. 322–333.

[15] I. Babuška and A. K. Aziz. “Survey lectures on the mathematical foundations of the finite element method.” In: **The mathematical foundations of the finite element method with applications to partial differential equations (Proc. Sympos., Univ. Maryland, Baltimore, Md., 1972)**. With the collaboration of G. Fix and R. B. Kellogg. Academic Press, New York, 1972, pp. 1–359.

[16] E. Bacry, S. Mallat, and G. Papanicolaou. “A wavelet based space-time adaptive numerical method for partial differential equations.” In: **RAIRO Modél. Math. Anal. Numér.** 26.7 (1992), pp. 793–834.

[17] J. M. Ball. “Some open problems in elasticity.” In: **Geometry, mechanics, and dynamics**. Springer, 2002, pp. 3–59.

[18] G. I. Barenblatt and D. D. Joseph, eds. **Collected Papers of R.S. Rivlin**. Springer New York, 1997.

[19] S. S. Barold. "Willem Einthoven and the Birth of Clinical Electrocardiography a Hundred Years Ago." In: **Cardiac Electrophysiology Review** 7 (1 2003), pp. 99–104.

[20] F. Bassi and S. Rebay. "A high-order accurate discontinuous finite element method for the numerical solution of the compressible Navier-Stokes equations." In: **J. Comput. Phys.** 131.2 (1997), pp. 267–279.

[21] M. Behr. "Simplex space-time meshes in finite element simulations." In: **Internat. J. Numer. Methods Fluids** 57.9 (2008), pp. 1421–1434.

[22] S. Bellavia and S. Berrone. "Globalization strategies for Newton-Krylov methods for stabilized FEM discretization of Navier-Stokes equations." In: **J. Comput. Phys.** 226.2 (2007), pp. 2317–2340.

[23] E. Berberoğlu, H. O. Solmaz, and S. Göktepe. "Computational modeling of coupled cardiac electromechanics incorporating cardiac dysfunctions." In: **European Journal of Mechanics-A/Solids** (2014).

[24] J. Bonet and R. D. Wood. **Nonlinear continuum mechanics for finite element analysis**. Second. Cambridge University Press, Cambridge, 2008, pp. xx+318.

[25] M. Boulakia et al. "A coupled system of PDEs and ODEs arising in electrocardiograms modeling." In: **Appl. Math. Res. Express. AMRX** 2 (2008), Art. ID abn002, 28.

[26] Y. Bourgault, Y. Coudière, and C. Pierre. "Existence and uniqeness of the solution for the bidomain model used in cardiac electrophysiology." In: **Nonlinear Anal. Real World Appl.** 10.1 (2009), pp. 458–482.

[27] D. Braess. **Finite elements**. Third. Theory, fast solvers, and applications in elasticity theory, Translated from the German by Larry L. Schumaker. Cambridge University Press, Cambridge, 2007, pp. xviii+365.

[28] S. C. Brenner. "Poincaré-Friedrichs inequalities for piecewise H^1 functions." In: **SIAM J. Numer. Anal.** 41.1 (2003), pp. 306–324.

[29] S. C. Brenner and L. R. Scott. **The mathematical theory of finite element methods**. Third. Vol. 15. Texts in Applied Mathematics. Springer, New York, 2008, pp. xviii+397.

[30] A. Buffa and C. Ortner. “Compact embeddings of broken Sobolev spaces and applications.” In: **IMA J. Numer. Anal.** 29.4 (2009), pp. 827–855.

[31] J. Česenek and M. Feistauer. “Theory of the space-time discontinuous Galerkin method for nonstationary parabolic problems with nonlinear convection and diffusion.” In: **SIAM J. Numer. Anal.** 50.3 (2012), pp. 1181–1206.

[32] P. Charrier et al. “An existence theorem for slightly compressible materials in nonlinear elasticity.” In: **SIAM Journal on Mathematical Analysis** 19.1 (1988), pp. 70–85.

[33] C. Cherubini et al. “An electromechanical model of cardiac tissue: Constitutive issues and electrophysiological effects.” In: **Progress in Biophysics and Molecular Biology** 97.2–3 (2008). Life and Mechanosensitivity, pp. 562 –573.

[34] K. Chrysafinos, S. P. Filopoulos, and T. K. Papathanasiou. “Error estimates for a Fitzhugh-Nagumo parameter-dependent reaction-diffusion system.” In: **ESAIM Math. Model. Numer. Anal.** 47.1 (2013), pp. 281–304.

[35] P. G. Ciarlet. **Mathematical elasticity. Vol. I**. Vol. 20. Studies in Mathematics and its Applications. Three-dimensional elasticity. North-Holland Publishing Co., Amsterdam, 1988, pp. xlii+451.

[36] P. G. Ciarlet. **The finite element method for elliptic problems**. Vol. 40. Classics in Applied Mathematics. Reprint of the 1978 original [North-Holland, Amsterdam; MR0520174 (58 #25001)]. Society for Industrial and Applied Mathematics (SIAM), Philadelphia, PA, 2002, pp. xxviii+530.

[37] B. Cockburn and C.-W. Shu. “The local discontinuous Galerkin method for time-dependent convection-diffusion systems.” In: **SIAM J. Numer. Anal.** 35.6 (1998), 2440–2463 (electronic).

[38] P. Colli Franzone and G. Savaré. “Degenerate evolution systems modeling the cardiac electric field at micro- and macroscopic level.” In: **Evolution equations, semigroups and functional analysis (Milano, 2000)**. Vol. 50. Progr. Nonlinear Differential Equations Appl. Birkhäuser, Basel, 2002, pp. 49–78.

[39] M. Costabel. “Boundary integral operators for the heat equation.” In: **Integral Equations Operator Theory** 13.4 (1990), pp. 498–552.

[40] K. D. Costa et al. “Three-dimensional residual strain in midanterior canine left ventricle.” In: **American Journal of Physiology - Heart and Circulatory Physiology** 273.4 (1997).

[41] K. D. Costa, J. W. Holmes, and A. D. McCulloch. “Modelling cardiac mechanical properties in three dimensions.” In: **Philosophical transactions of the Royal Society of London. Series A: Mathematical, physical and engineering sciences** 359.1783 (2001), pp. 1233–1250.

[42] B. Dacorogna. **Direct methods in the calculus of variations**. Vol. 78. Springer, 2007.

[43] H. Dal et al. “A fully implicit finite element method for bidomain models of cardiac electrom-echanics.” In: **Computer Methods in Applied Mechanics and Engineering** 253 (2013), pp. 323–336.

[44] H. Dal et al. “A fully implicit finite element method for bidomain models of cardiac electromechanics.” In: **Computer methods in applied mechanics and engineering** 253 (2013), pp. 323–336.

[45] C. Dawson, S. Sun, and M. F. Wheeler. “Compatible algorithms for coupled flow and transport.” In: **Comput. Methods Appl. Mech. Engrg.** 193.23-26 (2004), pp. 2565–2580.

[46] P. Deuflhard. **Newton methods for nonlinear problems**. Vol. 35. Springer Series in Computational Mathematics. Affine invariance and adaptive algorithms, First softcover printing of the 2006 corrected printing. Springer, Heidelberg, 2011, pp. xii+424.

[47] D. A. Di Pietro and A. Ern. **Mathematical aspects of discontinuous Galerkin methods**. Vol. 69. Mathématiques & Applications (Berlin) [Mathematics & Applications]. Springer, Heidelberg, 2012, pp. xviii+384.

[48] D. A. Di Pietro and S. Nicaise. “A locking-free discontinuous Galerkin method for linear elasticity in locally nearly incompressible heterogeneous media.” In: **Applied Numerical Mathematics** 63 (2013), pp. 105 –116.

[49] S. C. Eisenstat and H. F. Walker. “Choosing the forcing terms in an inexact Newton method.” In: **SIAM J. Sci. Comput.** 17.1 (1996). Special issue on iterative methods in numerical linear algebra (Breckenridge, CO, 1994), pp. 16–32.

[50] S. C. Eisenstat and H. F. Walker. “Globally convergent inexact Newton methods.” In: **SIAM J. Optim.** 4.2 (1994), pp. 393–422.

[51] K. Eriksson and C. Johnson. “Adaptive finite element methods for parabolic problems. I. A linear model problem.” In: **SIAM J. Numer. Anal.** 28.1 (1991), pp. 43–77.

[52] K. Eriksson and C. Johnson. “Adaptive finite element methods for parabolic problems. II. Optimal error estimates in $L_\infty L_2$ and $L_\infty L_\infty$.” In: **SIAM J. Numer. Anal.** 32.3 (1995), pp. 706–740.

[53] K. Eriksson, C. Johnson, and A. Logg. **Adaptive computational methods for parabolic problems**. Wiley Online Library, 2004.

[54] K. Eriksson, C. Johnson, and V. Thomée. “Time discretization of parabolic problems by the discontinuous Galerkin method.” In: **RAIRO Modél. Math. Anal. Numér.** 19.4 (1985), pp. 611–643.

[55] T. S. E. Eriksson. **Cardiovascular Mechanics : The Biomechanics of Arteries and the Human Heart**. Computation in Engineering and Science (CES). Graz, Austria: Verlag der Technischen Universität Graz, 2013.

[56] T. Eriksson et al. “Influence of myocardial fiber/sheet orientations on left ventricular mechanical contraction.” In: **Mathematics and Mechanics of Solids** (2013).

[57] A. Ern and J.-L. Guermond. **Theory and practice of finite elements**. Vol. 159. Applied Mathematical Sciences. Springer-Verlag, New York, 2004, pp. xiv+524.

[58] A. Ern and M. Vohralík. “Flux reconstruction and a posteriori error estimation for discontinuous Galerkin methods on general nonmatching grids.” In: **C. R. Math. Acad. Sci. Paris** 347.7-8 (2009), pp. 441–444.

[59] I. Ershler. “Willem Einthoven–The Man: The String Galvanometer Electrocardiograph.” In: **Arch Intern Med** 148.2 (1988), pp. 453–455.

[60] A. T. Eyck, F. Celiker, and A. Lew. "Adaptive stabilization of discontinuous Galerkin methods for nonlinear elasticity: analytical estimates." In: **Comput. Methods Appl. Mech. Engrg.** 197.33-40 (2008), pp. 2989–3000.

[61] A. T. Eyck, F. Celiker, and A. Lew. "Adaptive stabilization of discontinuous Galerkin methods for nonlinear elasticity: motivation, formulation, and numerical examples." In: **Comput. Methods Appl. Mech. Engrg.** 197.45-48 (2008), pp. 3605–3622.

[62] A. T. Eyck and A. Lew. "An adaptive stabilization strategy for enhanced strain methods in non-linear elasticity." In: **Internat. J. Numer. Methods Engrg.** 81.11 (2010), pp. 1387–1416.

[63] A. T. Eyck and A. Lew. "Discontinuous Galerkin methods for non-linear elasticity." In: **Internat. J. Numer. Methods Engrg.** 67.9 (2006), pp. 1204–1243.

[64] R. Falgout et al. **HYPRE: High performance preconditioners**. URL: `http://www.llnl.gov/casc/hypre/` (visited on 05/22/2014).

[65] F. Fenton and A. Karma. "Vortex dynamics in three-dimensional continuous myocardium with fiber rotation: filament instability and fibrillation." In: **Chaos: An Interdisciplinary Journal of Nonlinear Science** 8.1 (1998), pp. 20–47.

[66] R. FitzHugh. "Impulses and physiological states in theoretical models of nerve membrane." In: **Biophysical journal** 1.6 (1961), pp. 445–466.

[67] P. J. Flory. "Thermodynamic relations for high elastic materials." In: **Trans. Faraday Soc.** 57 (1961), pp. 829–838.

[68] J. S. Frank and G. A. Langer. "THE MYOCARDIAL INTERSTITIUM: ITS STRUCTURE AND ITS ROLE IN IONIC EXCHANGE." In: **The Journal of Cell Biology** 60.3 (1974), pp. 586–601.

[69] Y. C. Fung. **Biomechanics: Mechanical Properties of Living Tissues**. Springer, 1993.

[70] Y. C. Fung. **Foundation of solid mechanics**. Prentice–Hall, 1965.

[71] C. Geuzaine and J.-F. Remacle. “Gmsh: A 3-D finite element mesh generator with built-in pre-and post-processing facilities.” In: **International Journal for Numerical Methods in Engineering** 79.11 (2009), pp. 1309–1331.

[72] S. H. Gilbert et al. “Regional localisation of left ventricular sheet structure: integration with current models of cardiac fibre, sheet and band structure.” In: **European Journal of Cardio-Thoracic Surgery** 32.2 (2007), pp. 231–249.

[73] S. Göktepe and E. Kuhl. “Electromechanics of the heart: a unified approach to the strongly coupled excitation-contraction problem.” In: **Comput. Mech.** 45.2-3 (2010), pp. 227–243.

[74] A. Greenleaf, M. Lassas, and G. Uhlmann. “Anisotropic conductivities that cannot be detected by EIT.” In: **Physiological Measurement** 24.2 (2003), p. 413.

[75] M. Griebel and D. Oeltz. “A sparse grid space-time discretization scheme for parabolic problems.” In: **Computing** 81.1 (2007), pp. 1–34.

[76] J. M. Guccione, A. D. McCulloch, and L. K. Waldman. “Passive Material Properties of Intact Ventricular Myocardium Determined From a Cylindrical Model.” In: **Journal of Biomechanical Engineering** 113.1 (1991), pp. 42–55.

[77] J. M. Guccione, K. D. Costa, and A. D. McCulloch. “Finite element stress analysis of left ventricular mechanics in the beating dog heart.” In: **Journal of Biomechanics** 28.10 (1995), pp. 1167 –1177.

[78] M. Gurtin. **An Introduction to Continuum Mechanics**. Mathematics in Science and Engineering. Elsevier Science, 1982.

[79] K. Hayashi. “Biomechanics of Soft Tissues in Cardiovascular Systems.” In: **Mechanical properties of soft tissues and arterial walls**. Ed. by G. A. Holzapfel and R. W. Ogden. Vol. 441. CISM Courses and Lectures. Springer, 2003, pp. 15–64.

[80] P. Helnwein. “Some remarks on the compressed matrix representation of symmetric second-order and fourth-order tensors.” In: **Computer Methods in Applied Mechanics and Engineering** 190.22-23 (2001), pp. 2753–2770.

[81] C. S. Henriquez, A. L. Muzikant, and K. Smoak. "Anisotropy, fibre curvature and bath loading effects on activation in thin and thick cardiac tissue preparations." In: **Journal of Cardiovascular Physiology** 7 (1996), pp. 424–444.

[82] B. Hille. **Ion Channels of Excitable Membranes**. Sinauer Associates, 2001.

[83] A. L. Hodgkin and A. F. Huxley. "A quantitative description of membrane current and its application to conduction and excitation in nerve." In: **The Journal of Physiology** 117.4 (1952), pp. 500–544.

[84] G. A. Holzapfel and R. W. Ogden. "Constitutive modelling of passive myocardium. A structurally-based framework for material characterization." In: **Philosophical Transactions of the Royal Society A** 367 (2009), pp. 3445–3475.

[85] G. A. Holzapfel. **Nonlinear solid mechanics**. A continuum approach for engineering. John Wiley & Sons, Ltd., Chichester, 2000, pp. xiv+455.

[86] G. Holzapfel. "Structural and Numerical Models for the (Visco)elastic Response of Arterial Walls with Residual Stresses." English. In: **Biomechanics of Soft Tissue in Cardiovascular Systems**. Ed. by G. A. Holzapfel and R. W. Ogden. Vol. 441. International Centre for Mechanical Sciences. Springer Vienna, 2003, pp. 109–184.

[87] T. J. R. Hughes and G. M. Hulbert. "Space-time finite element methods for elastodynamics: formulations and error estimates." In: **Comput. Methods Appl. Mech. Engrg.** 66.3 (1988), pp. 339–363.

[88] J. D. Humphrey. **Cardiovascular Solid Mechanics. Cells, Tissues, and Organs**. Springer, 2002.

[89] J. D. Humphrey and F. C. Yin. "On constitutive relations and finite deformations of passive cardiac tissue: I. A pseudostrain-energy function." In: **J Biomech Eng** 109.4 (Nov. 1987), pp. 298–304.

[90] S. C. Hunter. **Mechanics of continuous media**. Ellis Horwood Ltd., 1983.

[91] S. Hussain, F. Schieweck, and S. Turek. "A note on accurate and efficient higher order Galerkin time stepping schemes for the nonstationary Stokes equations." In: **Open Numer. Methods J.** 4 (2012), pp. 35–45.

[92] J. D. Jackson. **Classical Electrodynamics**. Vol. 2010. 28 October 2010. Wiley, 1998.

[93] J. Keener and J. Sneyd. **Mathematical physiology. Vol. I: Cellular physiology**. Second. Vol. 8/. Interdisciplinary Applied Mathematics. Springer, New York, 2009, xxvi+470+A2+R45+I29.

[94] J. Keener and J. Sneyd. **Mathematical physiology. Vol. II: Systems physiology**. Second. Vol. 8/. Interdisciplinary Applied Mathematics. Springer, New York, 2009, i–xxvi, 471–974, A1–A2, A1–A2.

[95] R. Keldermann, M. Nash, and A. Panfilov. "Pacemakers in a reaction-diffusion mechanics system." In: **Journal of Statistical Physics** 128.1-2 (2007), pp. 375–392.

[96] C. T. Kelley. **Iterative methods for linear and nonlinear equations**. Vol. 16. Frontiers in Applied Mathematics. With separately available software. Society for Industrial and Applied Mathematics (SIAM), Philadelphia, PA, 1995, pp. iv+165.

[97] P. B. Kingsley. "Introduction to diffusion tensor imaging mathematics: Part III. Tensor calculation, noise, simulations, and optimization." In: **Concepts in Magnetic Resonance Part A** 28A.2 (2006), pp. 155–179.

[98] R. Klabunde. **Cardiovascular physiology concepts**. Lippincott Williams and Wilkins, 2011.

[99] C. M. Klaij, J. J. W. van der Vegt, and H. van der Ven. "Space-time discontinuous Galerkin method for the compressible Navier-Stokes equations." In: **J. Comput. Phys.** 217.2 (2006), pp. 589–611.

[100] A. Klawonn and O. Rheinbach. "Highly scalable parallel domain decomposition methods with an application to biomechanics." In: **ZAMM Z. Angew. Math. Mech.** 90.1 (2010), pp. 5–32.

[101] R. N. Klepfer, C. R. Johnson, and R. S. MacLeod. "The effects of inhomogeneities and anisotropies on electrocardiographic fields: a 3-D finite-element study." In: **IEEE Transactions on Biomedical Engineering** 44.8 (1997), pp. 706 –719.

[102] J. R. Knowles. "Enzyme-Catalyzed Phosphoryl Transfer Reactions." In: **Annual Review of Biochemistry** 49.1 (1980), pp. 877–919.

[103] P. Kohl, P. Hunter, and D. Noble. "Stretch-induced changes in heart rate and rhythm: clinical observations, experiments and mathematical models." In: **Progress in Biophysics and Molecular Biology** 71.1 (1999), pp. 91 –138.

[104] P. Kohl and F. Sachs. "Mechanoelectric feedback in cardiac cells." In: **Philosophical Transactions of the Royal Society of London. Series A: Mathematical, Physical and Engineering Sciences** 359.1783 (2001), pp. 1173–1185.

[105] K. Kunisch and M. Wagner. "Optimal control of the bidomain system (II): uniqueness and regularity theorems for weak solutions." In: **Ann. Mat. Pura Appl. (4)** 192.6 (2013), pp. 951–986.

[106] K. Kunisch and M. Wagner. "Optimal control of the bidomain system (IV): Corrected proofs of the stability and regularity theorems." In: **arXiv preprint arXiv:1409.6904** (2014).

[107] P. D. Lax and A. N. Milgram. "Parabolic equations." In: **Contributions to the theory of partial differential equations**. Annals of Mathematics Studies, no. 33. Princeton University Press, Princeton, N. J., 1954, pp. 167–190.

[108] I. J. LeGrice, P. J. Hunter, and B. H. Smaill. "Laminar structure of the heart: a mathematical model." In: **The American Journal of Physiology** 272 (1997), pp. 2466–2476.

[109] I. J. LeGrice and B. H. Smaill. "Extended confocal microscopy of myocardial laminae and collagen network." In: **Journal of Microscopy** 192.2 (1998), pp. 139–150.

[110] I. J. LeGrice et al. "Laminar structure of the heart: ventricular myocyte arrangement and connective tissue architecture in the dog." In: **The American Journal of Physiology** 269 (1995), pp. 571–582.

[111] J.-L. Lions and E. Magenes. **Non-homogeneous boundary value problems and applications. Vol. I**. Translated from the French by P. Kenneth, Die Grundlehren der mathematischen Wissenschaften, Band 182. Springer-Verlag, New York-Heidelberg, 1972.

[112] J.-L. Lions and E. Magenes. **Non-homogeneous boundary value problems and applications. Vol. II**. Translated from the French by P. Kenneth, Die Grundlehren der mathematischen Wissenschaften, Band 182. Springer-Verlag, New York-Heidelberg, 1972.

[113] R. Liu, M. F. Wheeler, and I. Yotov. "On the spatial formulation of discontinuous Galerkin methods for finite elastoplasticity." In: **Computer Methods in Applied Mechanics and Engineering** 253 (2013), pp. 219 –236.

[114] J. Malmivuo and R. Plonsey. **Bioelectromagnetism : Principles and Applications of Bioelectric and Biomagnetic Fields**. Oxford University Press, USA, 1995.

[115] J. Marsden and T. Hughes. **Mathematical Foundations of Elasticity**. Dover Civil and Mechanical Engineering Series. Dover, 1994.

[116] P. Medicine. **Cardiac Action Potential - Cellular Basis**. URL: `http://www.pathwaymedicine.org/Cardiac-Action-Potential-Cellular-Basis` (visited on 07/02/2014).

[117] D. Meidner and B. Vexler. "Adaptive space-time finite element methods for parabolic optimization problems." In: **SIAM J. Control Optim.** 46.1 (2007), 116–142 (electronic).

[118] A. Miller et al. "An overview of the CellML API and its implementation." In: **BMC Bioinformatics** 11.1 (2010), p. 178.

[119] C. C. Mitchell and D. G. Schaeffer. "A two-current model for the dynamics of cardiac membrane." In: **Bulletin of mathematical biology** 65.5 (2003), pp. 767–793.

[120] R. M. Miura. "Analysis of excitable cell models." In: **J. Comput. Appl. Math.** 144 (1-2 July 2002), pp. 29–47.

[121] A. D. Mont. "ADAPTIVE UNSTRUCTURED SPACETIME MESHING FOR FOUR-DIMENSIONAL SPACETIME DISCONTINUOUS GALERKIN FINITE ELEMENT METHODS." PhD thesis. University of Illinois, 2011.

[122] J. C. Nagtegaal, D. M. Parks, and J. R. Rice. "On numerically accurate finite element solutions in the fully plastic range." In: **Comput. Methods Appl. Mech. Engrg.** 4.2 (1974), pp. 153–177.

[123] J. Nagumo, S. Arimoto, and S. Yoshizawa. “An active pulse transmission line simulating nerve axon.” In: **Proceedings of the IRE** 50.10 (1962), pp. 2061–2070.

[124] P. Nardinocchi and L. Teresi. “On the active response of soft living tissues.” In: **Journal of Elasticity** 88.1 (2007), pp. 27–39.

[125] P. Nardinocchi, L. Teresi, and V. Varano. “Myocardial Contractions and the Ventricular Pressure–Volume Relationship.” In: **arXiv preprint arXiv:1005.5292** (2010).

[126] M. P. Nash and A. V. Panfilov. “Electromechanical model of excitable tissue to study reentrant cardiac arrhythmias.” In: **Progress in biophysics and molecular biology** 85.2 (2004), pp. 501–522.

[127] J. Nečas. “Sur une méthode pour résoudre les équations aux dérivées partielles du type elliptique, voisine de la variationnelle.” In: **Ann. Scuola Norm. Sup. Pisa (3)** 16 (1962), pp. 305–326.

[128] J. Neu and W. Krassowska. “Homogenization of syncytial tissues.” In: **Critical reviews in biomedical engineering** 21.2 (1992), pp. 137–199.

[129] M. Neumüller. **Space-Time Methods: Fast Solvers and Applications**. Computation in Engineering and Science (CES). Graz, Austria: Verlag der Technischen Universität Graz, 2013.

[130] M. Neumüller and O. Steinbach. “Refinement of flexible space–time finite element meshes and discontinuous Galerkin methods.” English. In: **Computing and Visualization in Science** 14.5 (2011), pp. 189–205.

[131] S. A. Niederer and N. P. Smith. “An improved numerical method for strong coupling of excitation and contraction models in the heart.” In: **Progress in Biophysics and Molecular Biology** 96.1–3 (2008). Cardiovascular Physiome, pp. 90 –111.

[132] D. Noble. **The Music of Life: Biology Beyond the Genome**. Oxford University Press, 2006.

[133] L. Noels and R. Radovitzky. “A general discontinuous Galerkin method for finite hyperelasticity. Formulation and numerical applications.” In: **International Journal for Numerical Methods in Engineering** 68.1 (2006), pp. 64–97.

[134] D. Nordsletten et al. “Coupling multi-physics models to cardiac mechanics.” In: **Progress in biophysics and molecular biology** 104.1 (2011), pp. 77–88.

[135] R. W. Ogden. **Nonlinear elastic deformations**. Ellis Horwood Series: Mathematics and its Applications. Ellis Horwood Ltd., Chichester; Halsted Press [John Wiley & Sons, Inc.], New York, 1984, pp. xv+532.

[136] J. H. Omens and Y. C. Fung. “Residual strain in rat left ventricle.” In: **Circ Res** 66.1 (1990), pp. 37–45.

[137] W. H. Organization. **The top 10 causes of death**. URL: `http://www.who.int/mediacentre/factsheets/fs310/en/` (visited on 07/02/2014).

[138] C. Ortner and E. Süli. “Discontinuous Galerkin finite element approximation of nonlinear second-order elliptic and hyperbolic systems.” In: **SIAM J. Numer. Anal.** 45.4 (2007), pp. 1370–1397.

[139] P. Pathmanathan and J. Whiteley. “A Numerical Method for Cardiac Mechanoelectric Simulations.” In: **Annals of Biomedical Engineering** 37 (5 2009), pp. 860–873.

[140] P. Pathmanathan and J. Whiteley. “A Numerical Method for Cardiac Mechanoelectric Simulations.” In: **Annals of Biomedical Engineering** 37(5) (2009), pp. 860–873.

[141] P. Pathmanathan et al. “Cardiac electromechanics: the effect of contraction model on the mathematical problem and accuracy of the numerical scheme.” In: **Quarterly Journal of Mechanics and Applied Mathematics** 3 (2010), pp. 375–399.

[142] R. P. Pawlowski et al. “Globalization techniques for Newton-Krylov methods and applications to the fully coupled solution of the Navier-Stokes equations.” In: **SIAM review** 48.4 (2006), pp. 700–721.

[143] M. Pennacchio, G. Savaré, and P. C. Franzone. “Multiscale Modeling for the Bioelectric Activity of the Heart.” In: **SIAM Journal on Mathematical Analysis** 37.4 (2005), pp. 1333–1370.

[144] S. Pezzuto, D. Ambrosi, and A. Quarteroni. “An orthotropic active strain model for the myocardium mechanics and its numerical approximation.” In: **European Journal of Mechanics - A/Solids** (2014),

[145] G. Plank et al. “Generation of histo-anatomically representative models of the individual heart: tools and application.” In: **Philosophical Transactions of the Royal Society A: Mathematical, Physical and Engineering Sciences** 367.1896 (2009), pp. 2257–2292.

[146] R. Plonsey, R. C. Barr, and A. Bioelectricity. **Bioelectricity — A Quantitative Approach**. Springer, 2007.

[147] A. E. Pollard, N. Hooke, and C. S. Henriquez. “Cardiac propagation simulation.” In: **Crit. Rev. in Biomed. Eng.** 20 (1992), pp. 171–200.

[148] W. H. Reed and T. Hill. “TRIANGULAR MESH METHODS FOR THE NEUTRON TRANSPORT EQUATION.” In: **Los Alamos Report LA-UR-73-479** (1973).

[149] O. Reichmann. “Optimal space-time adaptive wavelet methods for degenerate parabolic PDEs.” In: **Numer. Math.** 121.2 (2012), pp. 337–365.

[150] J. J. Rice et al. “Approximate Model of Cooperative Activation and Crossbridge Cycling in Cardiac Muscle Using Ordinary Differential Equations.” In: **Biophysical Journal** 95.5 (2008), pp. 2368 –2390.

[151] G. Richardson and S. J. Chapman. “Derivation of the bidomain equations for a beating heart with a general microstructure.” In: **SIAM J. Appl. Math.** 71.3 (2011), pp. 657–675.

[152] G. Richardson. “A multiscale approach to modelling electrochemical processes occurring across the cell membrane with application to transmission of action potentials.” In: **Mathematical Medicine and Biology** 26.3 (2009), pp. 201–224.

[153] T. Richter. “Discontinuous Galerkin as Time-Stepping Scheme for the Navier–Stokes Equations.” English. In: **Modeling, Simulation and Optimization of Complex Processes**. Ed. by H. G. Bock et al. Springer Berlin Heidelberg, 2012, pp. 271–281.

[154] T. Richter, A. Springer, and B. Vexler. “Efficient numerical realization of discontinuous Galerkin methods for temporal discretization of parabolic problems.” In: **Numer. Math.** 124.1 (2013), pp. 151–182.

[155] B. Rivière. **Discontinuous Galerkin methods for solving elliptic and parabolic equations**. Vol. 35. Frontiers in Applied Mathematics. Theory and implementation. Society for Industrial and Applied Mathematics (SIAM), Philadelphia, PA, 2008, pp. xxii+190.

[156] E. K. Rodriguez, A. Hoger, and A. D. McCulloch. "Stress-dependent finite growth in soft elastic tissues." In: **Journal of Biomechanics** 27.4 (1994), pp. 455 –467.

[157] J. M. Rogers and A. D. McCulloch. "A collocation-Galerkin finite element model of cardiac action potential propagation." In: **Biomedical Engineering, IEEE Transactions on** 41.8 (1994), pp. 743–757.

[158] G. B. Sands et al. "Automated imaging of extended tissue volumes using confocal microscopy." In: **Microscopy Research and Technique** 67.5 (2005), pp. 227–239.

[159] F. J. Sayas. "Infimum-supremum." In: **Bol. Soc. Esp. Mat. Apl. SeMA** 41 (2007), pp. 19–40.

[160] O. Schenk, M. Bollhöfer, and R. A. Römer. "On Large-Scale Diagonalization Techniques for the Anderson Model of Localization." In: **SIAM Rev.** 50.1 (Feb. 2008), pp. 91–112.

[161] O. Schenk, A. Wächter, and M. Hagemann. "Matching-based preprocessing algorithms to the solution of saddle-point problems in large-scale nonconvex interior-point optimization." English. In: **Computational Optimization and Applications** 36.2-3 (2007), pp. 321–341.

[162] H. Schmid et al. "Myocardial material parameter estimation." In: **Biomechanics and modeling in mechanobiology** 7.3 (2008), pp. 161–173.

[163] H. Schmid et al. "Myocardial material parameter estimation - a comparative study for simple shear." In: **Journal of biomechanical engineering** 128.5 (2006), pp. 742–750.

[164] C. Schwab and R. Stevenson. "Space-time adaptive wavelet methods for parabolic evolution problems." In: **Math. Comp.** 78.267 (2009), pp. 1293–1318.

[165] K. Schwlizerhof and E. Ramm. "Displacement dependent pressure loads in nonlinear finite element analyses." In: **Computers & Structures** 18.6 (1984), pp. 1099–1114.

[166] S. Silbernagl and A. Despopoulos. **Color Atlas of Physiology**. Thieme, 2009.

[167] J. C. Simo. "Numerical analysis and simulation of plasticity." In: **Handbook of numerical analysis, Vol. VI**. Handb. Numer. Anal., VI. North-Holland, Amsterdam, 1998, pp. 183–499.

[168] J. C. Simo, R. L. Taylor, and K. S. Pister. "Variational and projection methods for the volume constraint in finite deformation elasto-plasticity." In: **Comput. Methods Appl. Mech. Engrg.** 51.1-3 (1985), pp. 177–208.

[169] N. Smith et al. "Multiscale computational modelling of the heart." In: **Acta Numerica** 13 (2004), pp. 371–431.

[170] A. Spencer. "Theory of invariants." In: **Continuum Phys.** 1 (1971), pp. 239–353.

[171] O. Steinbach. **Numerical approximation methods for elliptic boundary value problems**. Finite and boundary elements, Translated from the 2003 German original. Springer, New York, 2008, pp. xii+386.

[172] G. Strang. "Variational crimes in the finite element method." In: **The mathematical foundations of the finite element method with applications to partial differential equations (Proc. Sympos., Univ. Maryland, Baltimore, Md., 1972)**. Academic Press, New York, 1972, pp. 689–710.

[173] J. Sudirham, J. van der Vegt, and R. van Damme. "Space–time discontinuous Galerkin method for advection–diffusion problems on time-dependent domains." In: **Applied Numerical Mathematics** 56.12 (2006), pp. 1491 –1518.

[174] J. Sundnes et al. **Computing the electrical activity in the heart**. Vol. 1. Monographs in Computational Science and Engineering. Springer-Verlag, Berlin, 2006, pp. xii+311.

[175] L. A. Taber and R. Perucchio. "Modeling heart development." In: **Journal of elasticity and the physical science of solids** 61.1-3 (2000), pp. 165–197.

[176] V. Thomée. **Galerkin finite element methods for parabolic problems**. Second. Vol. 25. Springer Series in Computational Mathematics. Springer-Verlag, Berlin, 2006, pp. xii+370.

[177] C. Truesdell and W. Noll. **The non-linear field theories of mechanics**. Third. Edited and with a preface by Stuart S. Antman. Springer-Verlag, Berlin, 2004, pp. xxx+602.

[178] L. Tung. "A bi–domain model for describing ischemic myocardial D–C potentials." PhD thesis. MIT, 1978.

[179] A. Üngör and A. Sheffer. "Tent-Pitcher: A meshing algorithm for space-time discontinuous Galerkin methods." In: **In proc. 9th int'l. meshing roundtable**. 2000.

[180] T. Valent. **Boundary value problems of finite elasticity**. Vol. 31. Springer Tracts in Natural Philosophy. Local theorems on existence, uniqueness, and analytic dependence on data. Springer-Verlag, New York, 1988, pp. xii+191.

[181] J. van der Vegt and H. van der Ven. "Space–Time Discontinuous Galerkin Finite Element Method with Dynamic Grid Motion for Inviscid Compressible Flows: I. General Formulation." In: **Journal of Computational Physics** 182.2 (2002), pp. 546 –585.

[182] M. Veneroni. "Reaction-diffusion systems for the macroscopic bidomain model of the cardiac electric field." In: **Nonlinear Anal. Real World Appl.** 10.2 (2009), pp. 849–868.

[183] J. Vossoughi, R. N. Vaishnav, and D. J. Patel. "Compressibility of the myocardial tissue." In: **Advances in bioengineering Mow VC** (1980), pp. 45–48.

[184] N. J. Walkington. "Compactness properties of the DG and CG time stepping schemes for parabolic equations." In: **SIAM J. Numer. Anal.** 47.6 (2010), pp. 4680–4710.

[185] P. J. Wang and N. A. M. Estes. **Supraventricular Tachycardia**. URL: `http://circ.ahajournals.org/content/106/25/e206.figures-only` (visited on 07/02/2014).

[186] J. P. Whiteley, M. J. Bishop, and D. J. Gavaghan. "Soft tissue modelling of cardiac fibres for use in coupled mechano-electric simulations." In: **Bull. Math. Biol.** 69.7 (2007), pp. 2199–2225.

[187] T. P. Wihler. "Locking-free adaptive discontinuous Galerkin FEM for linear elasticity problems." In: **Math. Comp.** 75.255 (2006), pp. 1087–1102.

[188] Wikipedia. **Cell Membrane**. URL: http://en.wikipedia.org/wiki/Cell_membrane (visited on 07/02/2014).

[189] Wikipedia. **Right Ventricle**. URL: http://en.wikipedia.org/wiki/Right_ventricle (visited on 07/02/2014).

[190] Wikipedia. **Sinus Rhythm**. URL: http://en.wikipedia.org/wiki/Sinus_rhythm (visited on 07/02/2014).

[191] J. Xu and J. Zou. "Some nonoverlapping domain decomposition methods." In: **SIAM Rev.** 40.4 (1998), pp. 857–914.

[192] F. C. Yin. "Ventricular wall stress." In: **Circulation Research** 49.4 (1981), pp. 829–842.